

Molecular nanostructures based on polyfunctional clathrochelate complexes

Thèse N° 9362

Présentée le 17 mai 2019

à la Faculté des sciences de base

Laboratoire de chimie supramoléculaire

Programme doctoral en chimie et génie chimique

pour l'obtention du grade de Docteur ès Sciences

par

Suzanne Maria JANSZE

Acceptée sur proposition du jury

Prof. S. Gerber, présidente du jury

Prof. K. Severin, directeur de thèse

Prof. M. H. Hardie, rapporteuse

Prof. K. Tiefenbacher, rapporteur

Prof. W. L. Queen, rapporteuse

2019

Acknowledgements

These four years in Switzerland could never have been such a valuable experience if it was not for the support I have received, in all its different forms. Everyone I have encountered over the years has left some sort of impression and unfortunately, I can't specifically name everyone, but please know that I am grateful.

First of all, of course, Prof. Kay Severin. Thank you very much for the constructive support over the years. You were always available for a discussion and were open to new ideas, whether it being in chemistry or for example Twitter. Your way of leading a research group and your sophisticated writing skills have been great lessons to experience. I hope our paths will continue to cross in the future.

Prof. Konrad Tiefenbacher, Prof. Michael Hardie, Prof. Wendy Queen and Prof. Sandrine Gerber are thanked for taking time of their schedules to be part of the jury for my thesis defence, the interesting discussions and comments on the written thesis.

Marie Curie Initial Training Networks *ReAd*, *Dynamol* and *ResMoSys* funded by the European Commission, the Swiss National Science Foundation, and the Ecole Polytechnique Fédérale de Lausanne (EPFL) are acknowledged for the financial support of the research presented in this thesis.

All the great technical support personal at the EPFL, thanks for all the discussions we had. No question was too far, and if the method for my "weird molecules" didn't exist, we were always able to adapt to make something work. Many thanks to: NMR: Dr. Pascal Miévielle (later more), Dr. Aurélien Bernet, Emilie Baudet, Anto Barisic and Vlado Jankovic; MS: Dr. Laure Menin, Dr. Daniel Ortiz. Dr. Konstantin Zhurov and Francisco Sepulveda; X-ray: Dr. Rosario Scopelliti, Dr. Euro Solari, Dr. Farzaneh Fadaei Tirani and Dr. Pascal Schouwink, and we are grateful to the Swiss-Norwegian Beamline Consortium for providing access to synchrotron radiation. Last but not least, for IT (and mental) support, the nice coffees and lunches: Dr. Daniel Jana and Thibault Roulet, many thanks.

For administrative support and running the magasin I am particularly grateful to: Christina Zamanos-Epremian, Anne Lene Odegard, Annelise Carrupt, Benjamin Kronenberg and Gladys Pache.

Then everyone in the LCS lab, including our great fish Rambo, thanks for the good years! A few people I would like to thank in specific: Matt, your guidance made for a flying start and a good couple of first months. Stephanie, for the administrative support when I arrived. Nicolas, for helping me buy my first motorcycle. Leo, Loïc, Ophélie, José and Giacomo, always available for some silly discussion and good conversation. The PostDocs: Albert, Marcus, Yizhu, Mark and Alex, thanks for the great advice and proofreading. Then of course my fellow Dutchies, Tim and Iris, it has been great having you around both inside and outside of the lab. Iris our adventures were a blast, hope there are many more to come. My fellow BCH.3407 trouble makers, for the first three and a bit years Florian, Flops, thanks for all you must have endured with me and Carl Thomas took over your duties in a great manner.

Beyond the EPFL, I had support of members of my previous research group BioNT at Wageningen UR. Specifically Prof. Aldrik Velders, Dr. Jan Bart ten Hove and Dr. Vittorio Saggiomo, thanks for encouraging me to continue on with a PhD and even while I was far away, the advice and support thankfully never stopped. Then there was the rest of the European Network, *ResMoSys*. I enjoyed every meeting and all interactions with the professors, other students and collaborators within the network.

I was lucky to meet some amazing people while in Switzerland, most of them I spent quite some hours riding motorcycles with and sharing many great experiences. A special thanks to Christina, Thierry (and Poulette), Philip (Flipje), Lorinz, Naomi, Pascal and Yann. All the amazing Chucharitas, in specific Pascal and Sibyl Miéville, Pascal thanks a million for the interesting discussions both scientifically and in any other way, your constructive advice and endless support has changed me for the better.

Then there are some people that make me feel at home wherever in the world I meet them. Marieke and Maxime, the other two of the “three musketeers” as I always see us, you guys are beyond amazing and you know it. My IBA friends, making me realize the world is a small place and no road is too far, special thanks to: Michiel (Giel), John and John. Also Gert-Jan, meeting you here in Lausanne even though we grew up so close was an interesting experience. Your unbelievable persistence and optimism can only be admired, seeing you walk again was a life changing experience.

Last but not least my family and extended family, specifically Pap, Mam, Jeroen, Anouk, Myrthe, Tim, Wendy and Eelke, you were there for me and supporting me every single step of the way, wish I could have been there more often, to be as much of a support to you as you have been to me. My grandparents, Opa’s and Oma’s, you didn’t always understand why I needed to go so far away for work, or have any clue what I am actually doing on a daily basis, but I hope the four of you realize that with the combined ~350 years of life-experience you possess, you are the smart ones.

Lausanne, 14th of December 2018

Abstract

This thesis describes the design and synthesis of clathrochelate metalloligands for the construction of molecular nanostructures. The low synthetic effort, versatility and stability of the clathrochelate metalloligands makes them particularly suited to the construction of coordination structures.

Chapter 2 shows it is possible to control the geometry and the composition of metallasupramolecular assemblies *via* the aspect ratio of their ligands. Functionalized clathrochelate complexes with variable aspect ratios were used as rod-like metalloligands. Cubic $\text{Fe}^{\text{II}}_8\text{L}_{12}$ cages were obtained from a metalloligand with an intermediate aspect ratio. By increasing the length or by decreasing the width of the ligand, the self-assembly process resulted in the clean formation of tetrahedral $\text{Fe}^{\text{II}}_4\text{L}_6$ cages instead of cubic cages.

Chapter 3 describes a simple one-step protocol, which allows large bipyridyl functionalized double clathrochelate metalloligands with an overall bent shape to be synthesized from easily accessible and/or commercially available starting materials. The ligands were used to construct $\text{Pd}^{\text{II}}_2\text{L}_4$ -type coordination cages of unprecedented size. Furthermore, evidence is provided that these cages may be stabilized by close intramolecular packing of lipophilic ligand side chains.

In Chapter 4, even larger triple clathrochelate metalloligands were used to form two $\text{Pd}^{\text{II}}_6\text{L}_8$ -type coordination cages. With molecular weights of more than 15 kDa and Pd...Pd distances of up to 4.2 nm, these complexes are among the largest palladium cages described to date.

In the 5th chapter, the stability of five different $[\text{Pd}_n(\text{N-donor})_m]^{2n+}$ assemblies was examined by performing disassembly experiments with pyridine and with trifluoroacetic acid. Pyridine-induced disassembly was found to be most pronounced for Pd complexes containing N-donor ligands of low basicity. At the same time, these assemblies displayed high acid resistance. The contrasting stability in the presence of acid or pyridine can be used for the pH-controlled switching between different metallosupramolecular structures.

The final research section (Chapter 6) shows that the addition of a metastable-state photoacid to solutions containing metal-ligand assemblies renders the systems light responsive. Upon irradiation, proton transfer from the photoacid to the ligand is observed, resulting in disassembly of the metallasupramolecular structure. In the dark, the process is fully reversed. Light-induced switching was demonstrated for six different metal-ligand assemblies containing Pd^{II} , Pt^{II} or Ru^{II} complexes and bridging polypyridyl ligands. The methodology allows the liberation of guest molecules using light as a stimulus.

Key words: Clathrochelate complexes, metalloligands, self-assembly, thermodynamic stability, photoacid, supramolecular chemistry

Résumé

Cette thèse décrit la conception et la synthèse de métallo-ligands clathrochélate pour la construction de nanostructures moléculaires. Le faible effort synthétique, la versatilité et la stabilité des métallo-ligands clathrochélate les rend particulièrement intéressant pour la construction de structures de coordination.

Le chapitre 2 montre qu'il est possible de contrôler la géométrie et la composition d'assemblages métallo-supramoléculaires *via* le ratio et l'aspect de leurs ligands. Les complexes de clathrochélate fonctionnalisés avec divers ratios et aspects ont été utilisés comme métallo-ligands semblable à des barres. Des cages cubiques de type $\text{Fe}^{\text{II}}_8\text{L}_{12}$ ont été obtenues à partir d'un métallo-ligand avec un aspect et un ratio intermédiaire. En augmentant la longueur ou en diminuant la largeur des ligands, le processus d'auto-assemblage résulta dans la formation de cages tétraédriques de type $\text{Fe}^{\text{II}}_4\text{L}_6$ au lieu de cages cubiques.

Le chapitre 3 décrit un protocole simple en une étape qui permet à de large double métallo-ligands bipyridyl clathrochélate avec une forme globale courbée d'être synthétisés à partir de matériaux de départ facilement accessible ou/et commercialement disponibles. Les ligands ont été utilisés pour construire des cages de coordination de type $\text{Pd}^{\text{II}}_2\text{L}_4$ de taille sans précédent. En outre, la preuve est fournie que ces cages peuvent être stabilisées par un empaquetage intramoléculaire aidé par des ligands à chaîne latérale lipophile.

Dans le chapitre 4, des métallo-ligands de type triple clathrochélate encore plus large ont été utilisés pour former deux cages de coordination de type Pd_6L_8 . Avec des poids moléculaires de plus de 15 kDa et des distances Pd...Pd allant jusqu'à 4.2 nm, ces complexes comptent parmi les plus large cages au palladium décrites à ce jour.

Dans le 5ème chapitre, la stabilité des cinq différents assemblages $[\text{Pd}_n(\text{N-donor})_m]^{2n+}$ a été examinée par des expériences de désassemblage avec de la pyridine et de l'acide trifluoroacétique. L'assemblage le plus prononcé induit par la pyridine a été trouvé pour les complexes de Pd avec des ligands N-donneur de faible basicité. Dans le même temps, ces assemblages ont montré une haute résistance aux acides. La stabilité contrastante en présence d'acide ou de pyridine peut être utilisée pour la commutation de différentes structures metallosupramoléculaires contrôlée par le pH.

La section de recherche finale (chapitre 6) montre que l'addition de photo-acides dans un état métastable à des solutions contenant des assemblages de métaux-ligands rend le système sensible à la lumière. Sur irradiation, le transfert du proton du photo-acide au ligand est observé, résultant dans le désassemblage de la structure métallo-supramoléculaire. Dans le noir, le processus est complètement inversé. La commutation induite par la lumière a été démontrée pour six assemblages métal-ligand différent contenant des complexes de Pd^{II} , Pt^{II} ou Ru^{II} et des ligands poly-pyridyl servant de pont.

Mots clés: Complexes clathrochélate, métallo-ligands, auto-assemblage, stabilité thermodynamique, photo-acide, chimie supramoléculaire

Contents

Acknowledgements	i
Abstract	iii
Résumé	iv
List of abbreviations and symbols	vii
Chapter 1 Introduction.....	1
1.1 Discrete molecular nanostructures by coordination-driven self-assembly.....	2
1.1.1 Metal-ligand assemblies based on $[\text{Pd}^{\text{II}}(\text{N-donor})_4]^{2+}$ complexes.....	3
1.1.2 Molecular nanostructures based on subcomponent self-assembly	5
1.2 Clathrochelate metalloligands as building blocks in supramolecular chemistry	7
1.2.1 Clathrochelate complexes.....	7
1.2.2 Clathrochelate metalloligands for construction of discrete molecular nanostructures.....	10
Chapter 2 Ligand aspect ratio as a decisive factor for the self-assembly of coordination cages	13
2.1 Introduction.....	14
2.2 Results and discussion	15
2.3 Conclusion.....	21
Chapter 3 $\text{Pd}^{\text{II}}_2\text{L}_4$ -type coordination cages up to three nanometers in size	23
3.1 Introduction.....	24
3.2 Results and discussion	25
3.3 Conclusion.....	32
Chapter 4 Inflating face-capped $\text{Pd}^{\text{II}}_6\text{L}_8$ coordination cages	33
4.1 Introduction.....	34
4.2 Results and discussion	35
4.3 Conclusion.....	41
Chapter 5 Palladium-based metal-ligand assemblies: the contrasting behavior upon addition of pyridine or acid	43
5.1 Introduction.....	44
5.2 Results and discussion	45
5.3 Conclusion.....	53

Chapter 6	Reversible disassembly of metallosupramolecular structures mediated by a metastable-state photoacid.....	55
6.1	Introduction.....	56
6.2	Results and Discussion.....	57
6.3	Conclusion.....	64
Chapter 7	Conclusions and outlook.....	65
Experimental section	67
References	105
Curriculum Vitae	113

List of abbreviations and symbols

°	degree
Å	Ångström
BA	boronic acid
°C	degree Celsius
CC	clathrochelate
d	doublet
DCM	dichloromethane
DOSY	diffusion-ordered NMR spectroscopy
DMSO	dimethylsulfoxide
δ	chemical shift
<i>e.g.</i>	exempla gratia
ESI-MS	electrospray ionisation mass spectrometry
Et	ethyl
g	gram
h	hour
HRMS	high-resolution mass spectrometry
Hz	Hertz (s ⁻¹)
<i>J</i>	coupling constant
K	Kelvin
K _a	association constant
m	multiplet
<i>m</i>	meta
M	molar (mol.L ⁻¹)
m/z	mass:charge ratio
Me	methyl
mg	milligram

MHz	megahertz
min	minutes
mL	millilitre
mM	millimolar (mmol.L ⁻¹)
mmol	millimole
MOF	metal–organic framework
mol	mole
μmol	micromole
MW	molecular weight
nm	nanometer
NMR	nuclear magnetic resonance
NTf ₂	triflimide, bis(trifluoromethane)sulfonimide
<i>o</i>	ortho
OTf	triflate, trifluoromethanesulfonate
<i>p</i>	para
ppm	parts per million
q	quartet
ref.	reference
r.t.	room temperature
s	singlet
sat.	saturated
t	triplet, or time
T	temperature

Note: additional abbreviations for specific compounds are defined within the thesis.

Chapter 1 Introduction

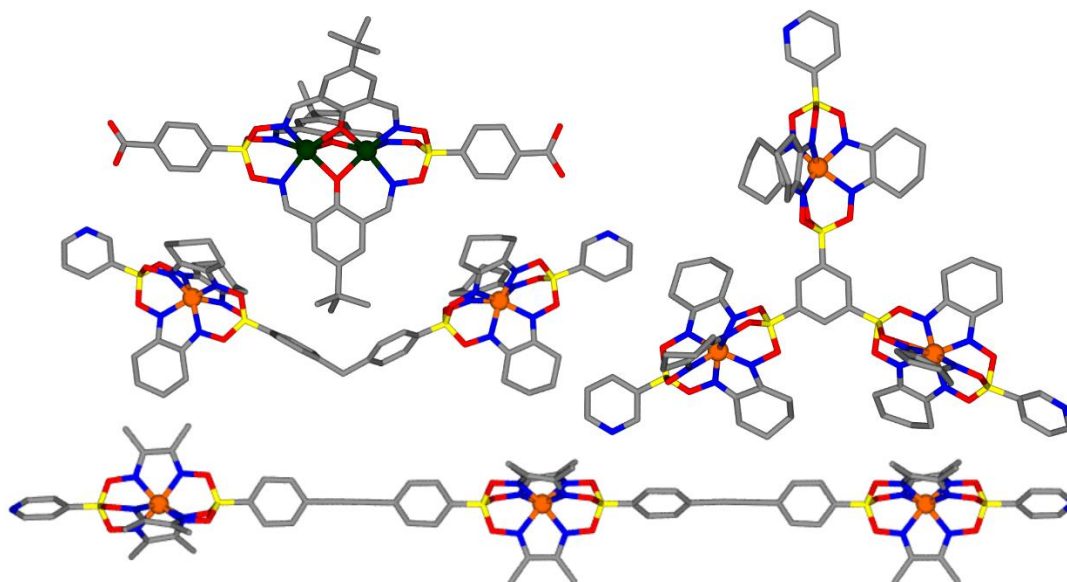
Part of this chapter (1.2) is based on published work:

“Clathrochelate Metalloligands in Supramolecular Chemistry and Materials Science”^[1]

S. M. Jansze, K. Severin, *Acc. Chem. Res.*, **2018**, 51, 2139–2147

Reprinted in an adapted version with permission from the American Chemical Society and all authors.

S. M. Jansze has contributed by writing text and by constructing figures for this publication.



1.1 Discrete molecular nanostructures by coordination-driven self-assembly

The construction of complex structures from simple building blocks is something everyone can relate to, as we remember our childhood days when we were building complex systems with our toy building blocks. Supramolecular chemistry is a subject area based on self-assembly to build complex nanostructures from easily accessible building blocks.

Supramolecular chemistry has recently gained novel general attention with the awarding of the 2016 Nobel prize for chemistry to professors Sauvage, Stoddart and Feringa. Their work on “the design and synthesis of molecular machines” employs supramolecular chemistry to construct complex systems where motion can be controlled on a molecular-level.^[2] Nobel prize winner professor Lehn described supramolecular chemistry in 1987 as the “chemistry beyond the molecule”.^[3] The formation of most supramolecular complexes is based on self-assembly. Self-assembly processes require the design of an unmediated system that under certain conditions forms a predefined supramolecular structure.^[4] This self-assembly method facilitates the construction of complex and tunable systems.^[5] The meticulous design of the individual molecular building blocks and comprehensive insight into the self-assembly processes are crucial to develop elaborate supramolecular complexes with a manifold of functions.

The self-assembly process can be driven by a multitude of chemical interactions, including van der Waals forces, hydrogen-bonding, π - π stacking and metal-ligand coordination.^[6] Although different combinations of these interactions can play a role in self-assembly, this thesis will focus on coordinative metal-ligand bonds. Coordination-driven self-assembly requires two types of molecular building blocks: an acceptor, often a metal ion with available coordination sites, and a donor, which can be any functional group possessing Lewis basicity. In this thesis, the focus will lie on two specific types of metal-ligand assemblies, mainly the systems based on $[\text{Pd}^{\text{II}}(\text{N-donor})_4]^{2+}$ complexes are introduced (Chapter 1.1.1) and then molecular nanostructures based on subcomponent self-assembly are also briefly discussed (Chapter 1.1.2).

An interesting feature of the metal-ligand bond is that they are non-covalent and reversible, which is of great importance for the self-assembly process. The reversibility of the bond allows for the organization of the building blocks into the thermodynamically most favorable state. Based on the conformation and angle of the donor and acceptors, the final architecture of the coordination complex becomes predictable. The meticulous design of individual building blocks plays an important role here. The ligands containing the donor-groups can have a wide-variety of shapes and sizes,^[7] and can be selected to suit the desired properties of the supramolecular complex.^[8] The research in this thesis describes a multitude of N-donor ligands, but the focus will lie on clathrochelate metalloligands, which will be further introduced in Chapter 1.2.

Generally, supramolecular complexes can be divided into two main classes, namely discrete structures,^[9] like cages,^[10] macrocycles^[11] and knots,^[12] or polymeric structures, like MOFs^[13] and gels.^[14] Considering the research described in this thesis, the focus will mainly lie on the description of discrete supramolecular structures, also referred to as molecular nanostructures.

1.1.1 Metal-ligand assemblies based on $[\text{Pd}^{\text{II}}(\text{N-donor})_4]^{2+}$ complexes

The $\text{Pd}(\text{II})$ ion is a square-planar metal-center, meaning it has a total of four available coordination sites, of which the directionality is on the corners of a square on the same plane. This is a typical geometry for metal complexes with the d^8 configuration. *Cis* or *trans* blocking of the square planar $\text{Pd}(\text{II})$ results in 90° and 180° acceptor-angles, respectively. Molecular structures based on these *cis*- or *trans*-blocked $\text{Pd}(\text{II})$ metal-acceptors have also been widely studied,^[15] but will not be the focus of this thesis.

Particularly suitable donors for coordination to the $\text{Pd}(\text{II})$ ion are neutral N-donors, like pyridyl and imidazole groups. Due to unfavorable hard-soft interactions between the ligand and the metal, oxygen-based donors are less suitable for the formation of supramolecular structures from $\text{Pd}(\text{II})$, although they have been employed before.^[16] The vast majority of discrete supramolecular structures from $\text{Pd}(\text{II})$ ions are based on ditopic and tritopic ligands with specific angles between the donors. This sub-chapter will therefore describe the recent advances in the construction of discrete supramolecular structures based on ditopic and tritopic N-donor ligands and square-planar $\text{Pd}(\text{II})$ metal centers.

When combining ditopic N-donor ligands with square planar $\text{Pd}(\text{II})$, generally Pd_nL_{2n} -type molecular nanostructures are formed (**Figure 1.1**). The assemblies with the lowest nuclearity are the Pd_2L_4 cages, which are based on ditopic ligands with an overall bent shape.^[17] Due to the relatively large cavity in these molecular complexes, shaped like an oval capsule, they have been studied for a multitude of applications. Examples are host-guest chemistry,^[17a, 18] medicinal inorganic chemistry,^[19] improved catalysis of a Diels-Alder reaction,^[20] and a light-switchable version of this complex has been developed.^[21] The group of Crowley has shown that the 1,2,3-triazole unit, known for the CuAAC "click reaction, could be used as the N-donor ligand, giving rise to a wide variety of functional ligands that form coordination complexes with $\text{Pd}(\text{II})$.^[22] The functionality of the complexes can be adjusted by changing the shape, size or functional groups within the linkers.^[8b, 23] Further details about these Pd_2L_4 -type coordination cages are discussed in Chapter 3 of this thesis.

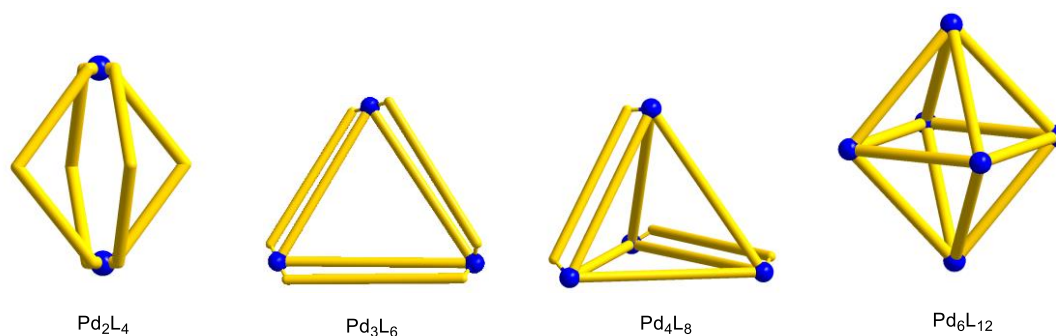


Figure 1.1. Examples of Pd_nL_{2n} structures that can form from ditopic N-donor ligands.

The molecular nanostructures that contain ditopic ligands and either three or four Pd^{II} ions most commonly are double triangle macrocycles or double walled tetrahedrons, respectively.^[24] The mechanism to form either the Pd_3L_6 macrocycle or the Pd_4L_8 tetrahedron seem closely related, and have been studied for these complexes quite extensively.^[25] The formation of one or the other architecture are for example the solvent or environment in which the building blocks are present.^[26]

There are, to the best of my knowledge, only two examples of molecular nanostructures containing five Pd^{II} and ditopic ligands known to date, and the geometry is like a ring,^[27] or a star^[28] from a combination of two different ditopic ligands.

For molecular nanostructures based on ditopic ligands and six or more Pd^{II} ions, Fujita and coworkers have shown that the angle between the N-donors of the ligands plays an important role in which type of assemblies will be formed.^[29] His work describes the utilization of 4-pyridyl functionalized ditopic ligands to form approximately spherical complexes. (**Figure 1.2.**) The smallest of these structures, is a Pd^{II}₆L₁₂ octahedron, which forms when there is an approximately 90° angle between the N-donors of the ligands.^[30] The group of Fujita then went on to show that if this angle between the donors is increased towards ~120°, the assembly that forms will be the cuboctahedron Pd^{II}₁₂L₂₄.^[31] Further increasing the angle between the donors to approximately 135° resulted in the even larger rhombicuboctahedron with a stoichiometry of Pd^{II}₂₄L₄₈.^[32] Last but not least, the group of Fujita recently demonstrated the synthesis and characterization of the icosidodecahedron Pd^{II}₃₀L₆₀, which is, with a maximum Pd...Pd distance of 7.4 nm, by far the largest structurally characterized Pd(II) containing supramolecular complex known to date.^[33] An interesting design feature that was shown with these spherical complexes, was the construction of double-layered spheres from covalently linked dual ditopic ligands, to make a smaller Pd^{II}₁₂L₂₄ cage within a larger Pd^{II}₁₂L₂₄ cage.^[34]

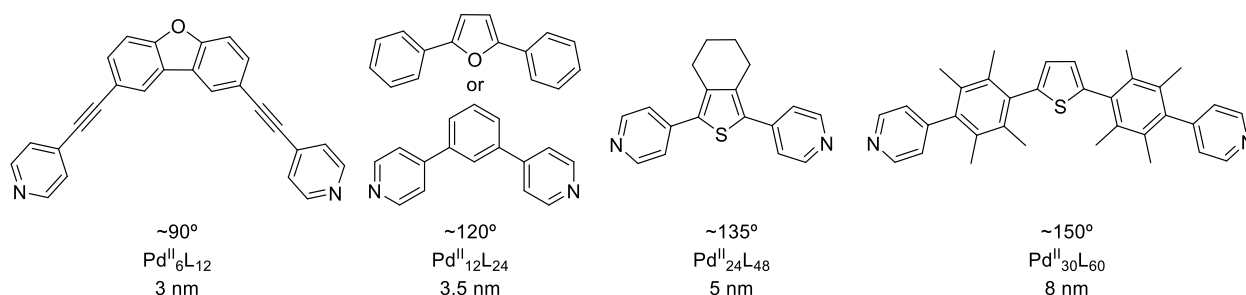


Figure 1.2. Examples of the ligands utilized by the group of Fujita, displayed below the structures are the optimal angle of the ligand, the stoichiometry of the formed complexes and estimated diameter of the assemblies they form when combined with square-planer Pd(II).

To make their large structures adopt functionality, Fujita and coworkers studied the introduction of for example guest-binding groups to the Pd^{II}₁₂L₂₄ cages.^[31] By simply functionalizing the ligands used for the self-assembly of these complexes they could introduce 24 groups on both the interior or the exterior of the cage complexes. They showed examples where the exterior of the cages are functionalized with sugars,^[35] which can aggregate upon addition of lectin or functionalized with oligonucleotides,^[36] which could lead to selective complexation with the complementary oligonucleotides.

The interior functionalization of their complexes led, for example, to light-induced control over the hydrophobicity of the cavity,^[37] endohedral radical polymerization of MMA,^[38] and template synthesis of monodisperse silica nanoparticles.^[39]

The molecular structures can also interlock to form higher nuclearity cage structures.^[40] Extensive studies on interlocked structures have mainly been performed on a range of Pd^{II}₂L₄ cages which can be triggered to interlock^[40a, 41] to create dimers or trimers that possess new cavities and functionalities.^[42] For example, interlocking can be triggered by the addition of halides, and the new cavity that forms can encapsulate neutral small-molecule guests.^[43]

A final set of structures based on square-planar Pd(II) that is particularly interesting are the Pd^{II}₆L₈-type coordination cages. They are formed from tritopic N-donor ligands that are divergently organized. Coordination of these ligands to Pd(II) gives relatively large coordination structures from a low number of building blocks (**Figure 1.3**). An early example by the group of professor Hardie showed tritopic cyclotrivenatrylene-based ligands which are used to form a structure of around 3 nm in size.^[44] More recent examples have been an assembly from imidazole-based ligands by Mukherjee and coworkers.^[45] The same group has shown the synthesis of a redox active water soluble Pd^{II}₆L₈ coordination cage.^[46] The host-guest chemistry of a large Pd^{II}₆L₈ structures was studied by Crowley and coworkers and they showed the size selective encapsulation of anionic guests.^[47] A more extensive discussion on Pd^{II}₆L₈-type coordination complexes can be found in Chapter 4 of this thesis.

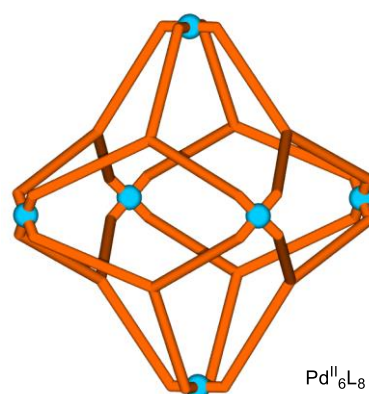


Figure 1.3. Graphical representation of Pd^{II}₆L₈ cage structure based on tritopic ligands. Blue: Pd(II) ions and orange: ligands.

1.1.2 Molecular nanostructures based on subcomponent self-assembly

Imines are known to form from a primary amine and aldehydes or ketones. They are generally unstable under aqueous conditions. In 2004 the research group of professor Nitschke showed that imines can be stabilized in aqueous conditions upon the coordination of a metal ion.^[48] Multiple of these imine units will self-assemble around one metal center. This method of subcomponent self-assembly has been developed into an extensive set of functional supramolecular structures.^[10a, 10e] For the design of molecular nanostructures from subcomponent self-assembly, the most commonly used conformation is when a M²⁺ ion, an aromatic primary amine and a formylpyridine are combined, and three of these imine units coordinate to the metal center, as is depicted in **Figure 1.4**.

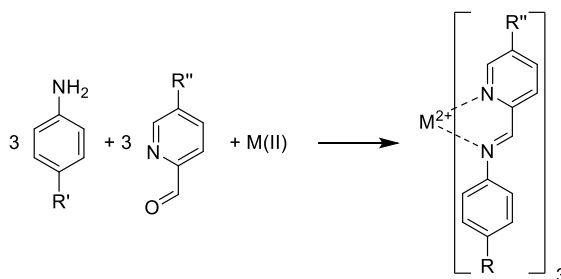
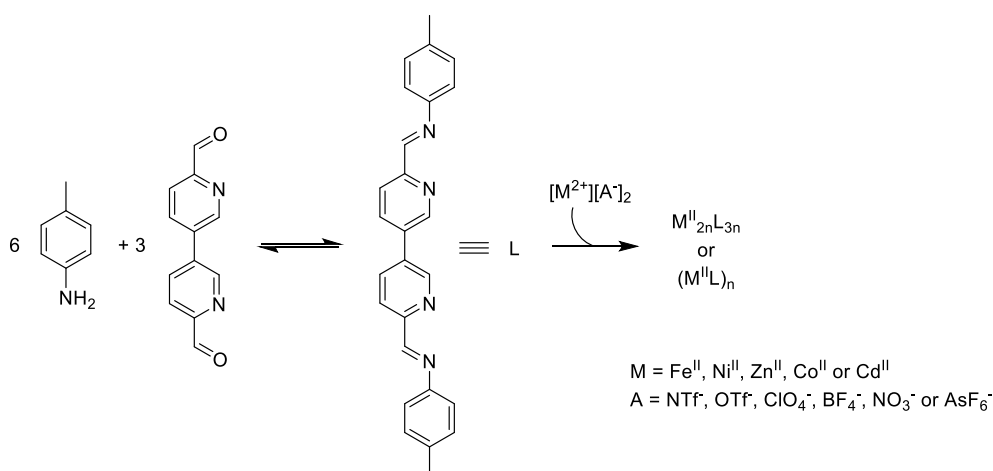


Figure 1.4. The coordination motif of three stabilized imines around one M(II) metal centre.

In 2008, the Nitschke group reported a water-soluble tetrahedral structure from commercially available 2-formylpyridine and 4,4'-diaminobiphenyl-2,2'-disulfonic acid using Fe(II) as the metal center.^[49] Later, it was demonstrated this cage structure is able to encapsulate and stabilize white phosphorus^[50] and selectively encapsulate greenhouse gas SF₆.^[51]

It was shown that the self-assembly of *p*-toluidine and 6,6'-diformyl-3,3'-bipyridine can result in a range of discrete supramolecular structures of the general formula M^{II}_{2n}L_{3n} or polymer (M^{II}L)_n, depending on the metal (M²⁺) or anion (A⁻) that are used for the subcomponent self-assembly (**Scheme 1.1**).^[52] For example, supramolecular cages were formed with the formula M^{II}_{2n}L_{3n} with *n* = 2, 3, 4, 5 and 6. It was reasoned that the anions acted as a template during the self-assembly process, thereby thermodynamically favoring one assembly over the other. In case of the Cd^{II} assemblies, some other templates, like F⁻, Cl⁻, Br⁻, N₃⁻, OCN⁻ and HF₂⁻ were additionally employed.^[52b]



Scheme 1.1. The self-assembly of a range of M^{II}_{2n}L_{3n} coordination structures from one ligand (L) by using different metal ions (M²⁺) and different anions (A⁻).

This method of subcomponent self-assembly is further discussed in Chapter 2 of this thesis.

1.2 Clathrochelate metalloligands as building blocks in supramolecular chemistry

Metalloligands are ligands which are based on a coordination complex. They often offer an ease of synthesis and the possibility to adapt the functional groups present on the ligands. The predetermined and well-defined electronic and structural preferences of the coordination complexes within the ligand facilitate rational design of the metalloligands to construct supramolecular structures.^[53]

1.2.1 Clathrochelate complexes

Coordinationally saturated complexes can be formed by encapsulation of metal ions within macropolycyclic ligands. Busch suggested the term 'clathrochelate' to describe complexes of this kind.^[54] Alternatively, they are sometimes referred to as 'cage complexes'.^[55] If the encapsulated ions are alkali or alkaline earth metal ions, the term 'cryptate' is commonly employed.^[56] Early examples of transition metal clathrochelates were reported by the groups of Rose,^[57] Holm,^[58] Goedken,^[59] and Sargeson^[60] (**Figure 1.4**).

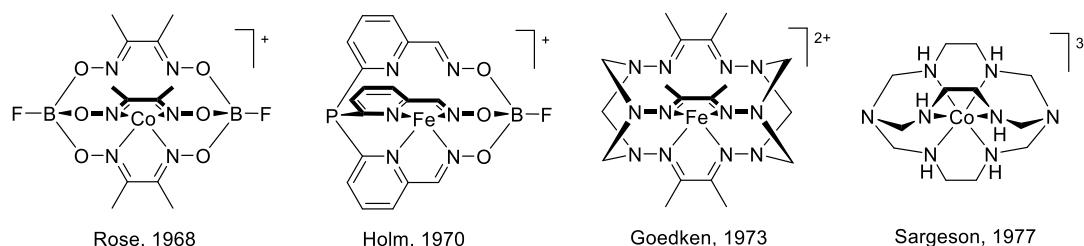
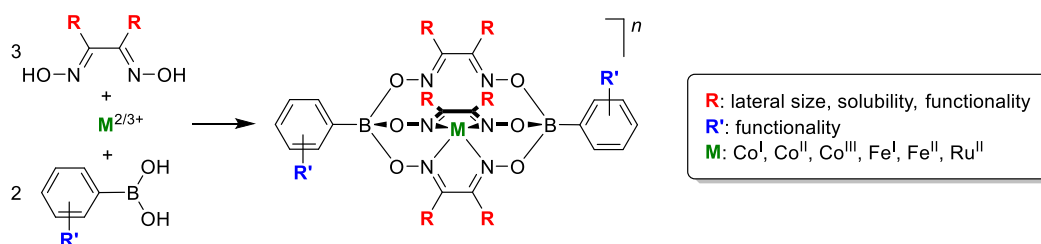


Figure 1.4. Early examples of transition metal clathrochelate complexes.

Following these initial reports, clathrochelate complexes have been studied extensively over the last decades. A comprehensive summary of the chemistry of clathrochelates, can be found in two books published in 2002^[61] and in 2017.^[55] Biological applications of clathrochelates are discussed in a recent review article.^[62]

In the following chapter the focus lies in particular on arylboron-capped clathrochelates. A convenient way to prepare these complexes is *via* a metal-templated condensation reaction of a dioxime and an arylboronic acid (**Scheme 1.2**). It is worth noting that alkylboronic acids can be incorporated as well.^[55, 61] However, for the applications described below, arylboronic acids are more relevant. Fe^{2+} and Co^{2+} ions can be used to template these reactions. The Co^{2+} ion is a less efficient template, and the yields tend to be lower compared to what is observed for reactions with Fe^{II} salts. The 4d transition metal ruthenium can be incorporated by employing Ru^{II} or Ru^{III} salts. In the latter case, *in situ* reduction to Ru^{II} is performed before complex formation.^[63]



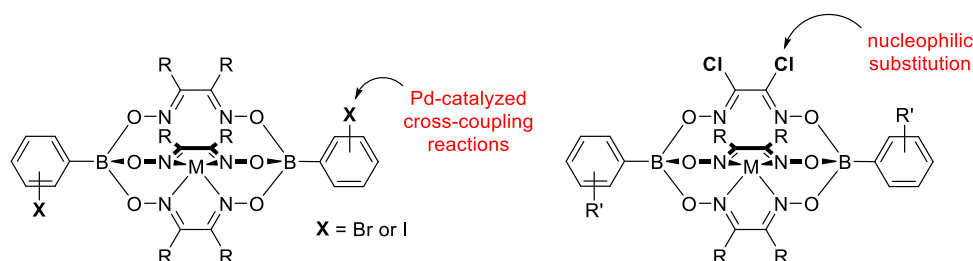
Scheme 1.2. Synthesis of mononuclear, arylboron-capped clathrochelate complexes.

Cobalt clathrochelates have been isolated in the +1, the +2, and the +3 oxidation state.^[64] In contrast, the chemistry of clathrochelates containing iron and ruthenium is largely limited to the +2 oxidation state, even though one can observe a quasi-reversible oxidation to the +3 state by electrochemistry. Using a dioxime with electron-withdrawing chloro substituents, the isolation of an Fe^I clathrochelate was recently accomplished.^[65]

Clathrochelate complexes can be decorated with functional groups in apical position (**Scheme 1.2**, R') by using the corresponding arylboronic acid. Notably, donor groups such as pyridine or carboxylic acids can be employed without compromising the metal-templated reaction. The lateral groups (**Scheme 1.2**, R) attached to the clathrochelate can be modified via the dioxime. In several projects, we have used nioxime (dioxime with a cyclohexyl group). This dioxime is commercially available, and it gives rise to complexes, which tend to be well-soluble in organic solvents.

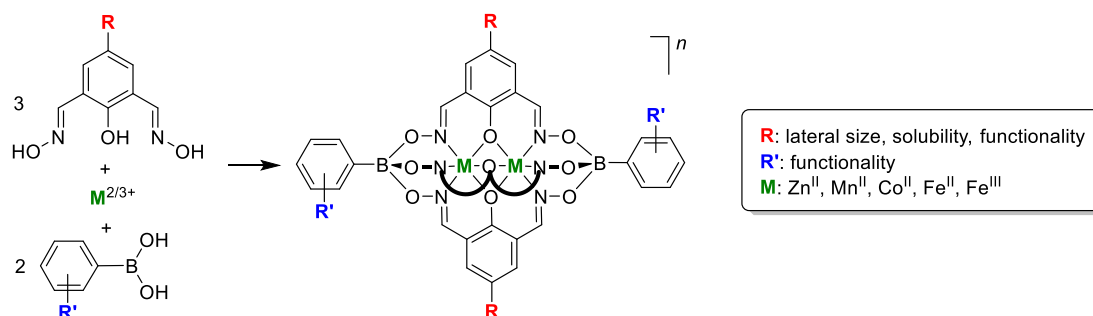
Clathrochelate complexes are often very stable, and arylboron-capped complexes are no exception. The boronate ester groups are not susceptible to hydrolysis, and ligand exchange reactions are only observed under very forcing conditions. Considering the handling of these complexes, it is worth mentioning that Fe^{II} clathrochelates are not air and moisture sensitive.

The inert character of boron-capped clathrochelates offers the opportunity to perform post-synthetic modifications. For example, clathrochelates can be used in palladium-catalyzed cross-coupling reactions (**Scheme 1.3**, left).^[66] For modifications in lateral position, substitution reactions are an interesting option. It is possible to prepare clathrochelate complexes containing between one and six chloro atoms in lateral position. These complexes are amenable to substitution reactions using N-, O-, and S-nucleophiles (**Scheme 1.3**, right).^[55, 61] There are other possibilities for the post-synthetic functionalization of clathrochelates, and a comprehensive discussion is provided in reference 55.



Scheme 1.3. Post-synthetic modification of clathrochelate complexes.

When metal-templated reactions are performed with phenoldioximes instead of simple 1,2-dioximes, dinuclear clathrochelate complexes are obtained (**Scheme 1.4**). The first example of such a complex featuring a methylboron cap was reported by Chaudhuri and co-workers.^[67] Subsequently it was shown that arylboron-capped complexes can be prepared in a similar fashion.^[68] Suited metal templates are Mn²⁺, Fe²⁺, Co²⁺ or Zn²⁺ ions. The resulting M^{II}/M^{II} clathrochelates have an overall charge of minus one. This feature is of importance for the applications in material science, which is not further discussed in this thesis. Dinuclear iron clathrochelates stand out because they are thermodynamically more stable than the corresponding cobalt or zinc complexes.^[69] Furthermore, they are accessible as anionic Fe^{II}/Fe^{II} complexes or as neutral Fe^{II}/Fe^{III} complexes.



Scheme 1.4. Synthesis of dinuclear, arylboron-capped clathrochelate complexes.

As in the case of mononuclear clathrochelates, it is possible to introduce functional groups such as pyridines,^[68] carboxylic acids,^[70] or amines^[71] in apical position by using the corresponding boronic acid during the synthesis. The post-synthetic introduction of functional groups is also possible via Pd-catalyzed cross-coupling reactions.^[72]

The lateral size of clathrochelates can be varied substantially by changing the groups R attached to the dioxime. **Figure 1.3** shows the cores of two mononuclear and one dinuclear clathrochelate as determined by crystallography (apical aryl groups are removed for clarity). By comparing the space-filling representations of the structures, it is apparent that the clathrochelate with lateral phenyl groups (**Figure 1.3b**) is significantly wider than the clathrochelate based on glyoxime (**Figure 1.3a**). Even wider complexes can be obtained with dinuclear clathrochelates (**Figure 1.3c**). As discussed in the next section, the lateral size can be a decisive parameter for controlling the architecture of supramolecular assemblies. Generally, clathrochelates are well soluble in polar organic solvents due to their three-dimensional shape, which disfavors π -stacking interactions. It is possible to tune the solubility by modifying the lateral and apical groups R and R'.

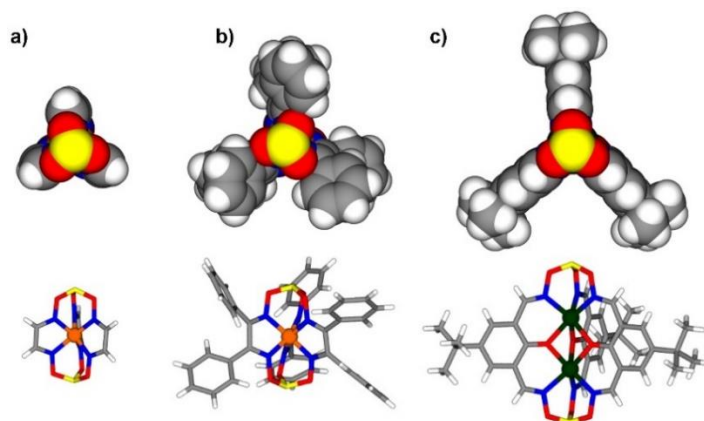


Figure 1.3. The molecular structures of mono- and dinuclear clathrochelate complexes with hydrogen atoms (a), phenyl groups (b), and *t*-butyl groups in lateral position (c). The aryl groups attached to the boron atoms are not shown for clarity. White: H, grey: C, blue: N, yellow: B, red: O, dark green: Co, orange: Fe.

1.2.2 Clathrochelate metalloligands for construction of discrete molecular nanostructures

As described in the last section, boron-capped clathrochelates can be obtained in one-pot reactions from easily accessible starting materials. Furthermore, they are very robust compounds, and it is possible to decorate clathrochelates with a variety functional groups. These features make boron-capped clathrochelates interesting structural elements for the construction of metalloligands.^[7, 53c]

In the area of coordination-driven supramolecular chemistry, ligands with pyridyl donor groups are of special importance.^[9b, 17a, 29] Iron clathrochelate complexes with terminal 4-pyridyl groups can be prepared in high yield by reaction of three commercially available compounds, namely nioxime, 4-pyridylboronic acid, and FeCl_2 .^[66a] The two terminal N-donor atoms are 1.5 nm apart from each other (**Figure 1.4**, left side). This value is similar to what is found for pyridyl-functionalized porphyrins, which have been used extensively as metalloligands.^[73] The dipyridyl clathrochelate was employed for the construction of heterometallic macrocycles containing iridium^[74] or rhenium.^[66a] A structurally related Co^{II} clathrochelate was used to bridge two zinc tetraphenylporphyrin complexes.^[75] In the presence of a sacrificial electron donor, light-induced reduction of the cobalt complex was observed.

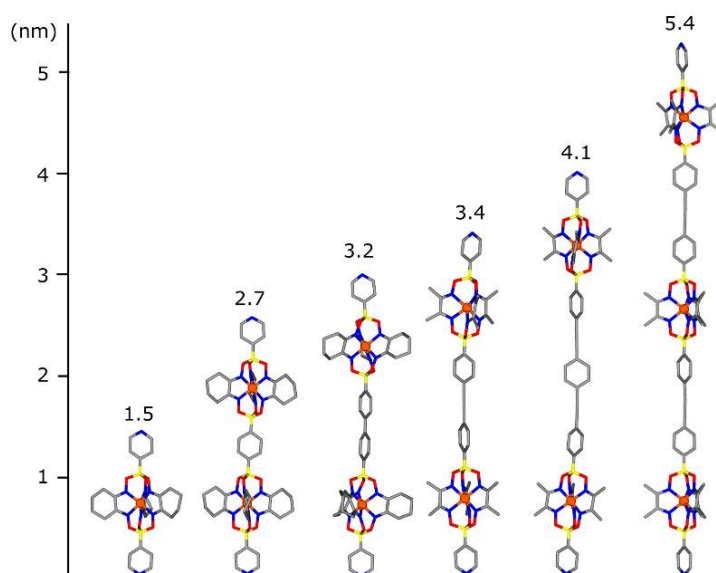
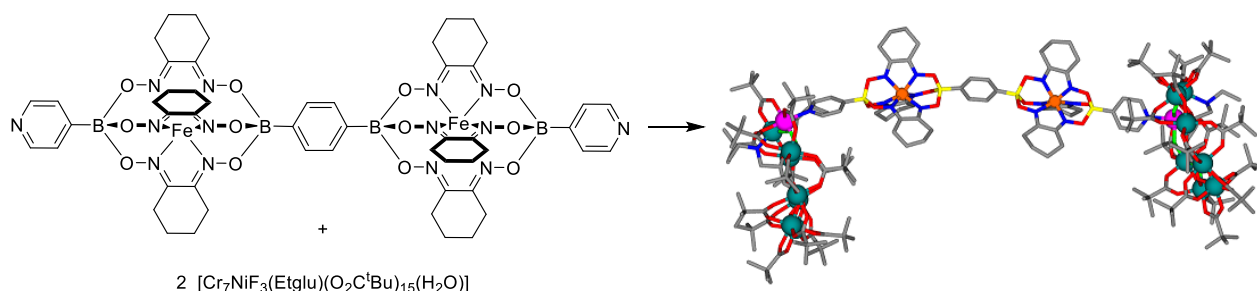


Figure 1.4. Clathrochelate-based metalloligands with terminal 4-pyridyl groups. The structures of the two shorter ligands are based on X-ray crystallography, whereas the structures of the other ligands were obtained by molecular modeling. The three longest ligands have octyl side chains, which are substituted by methyl groups for the clarity of this figure.

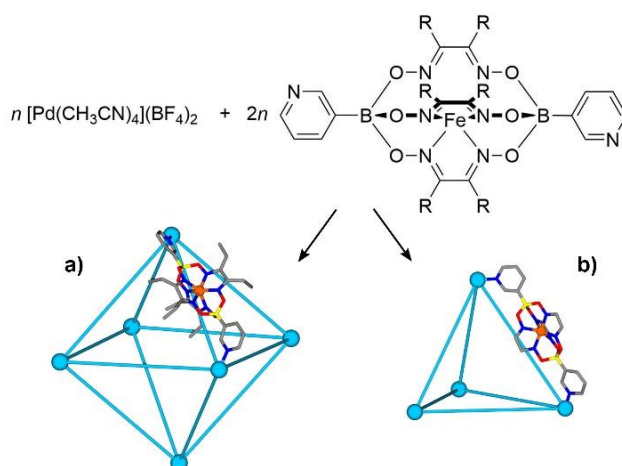
It is straightforward to extend the length of clathrochelate-based dipyridyl ligands. One possibility is to use a mixture of a diboronic acid and 4-pyridylboronic acid during the synthesis. This kind of statistical reaction will lead to a mixture of products, from which a metalloligand with two clathrochelate cores can be isolated by selective precipitation or chromatography. Pyridyl-terminated metalloligands with lengths of 2.7 and 3.2 nm (**Figure 1.4**) were prepared in this fashion. A second possibility to extend the lengths of these ligands is to connect pre-formed clathrochelate complexes with iodo or alkynyl functions via Sonogashira coupling reactions. Using this strategy, ligands with lengths of up to 5.4 nm were prepared (**Figure 1.4**).^[66a]

Pyridyl-terminated clathrochelate ligands were used by Ardavan and co-workers as linkers for heterometallic Cr_7Ni rings (**Scheme 1.5**).^[76] These paramagnetic rings with a well-defined $S = \frac{1}{2}$ ground state are of interest as molecular spin qubits. By variation of the metalloligand, they were able to change the minimum distance between the paramagnetic rings in the range of 1.9–3.1 nm, thereby providing control over the inter-qubit quantum interactions.



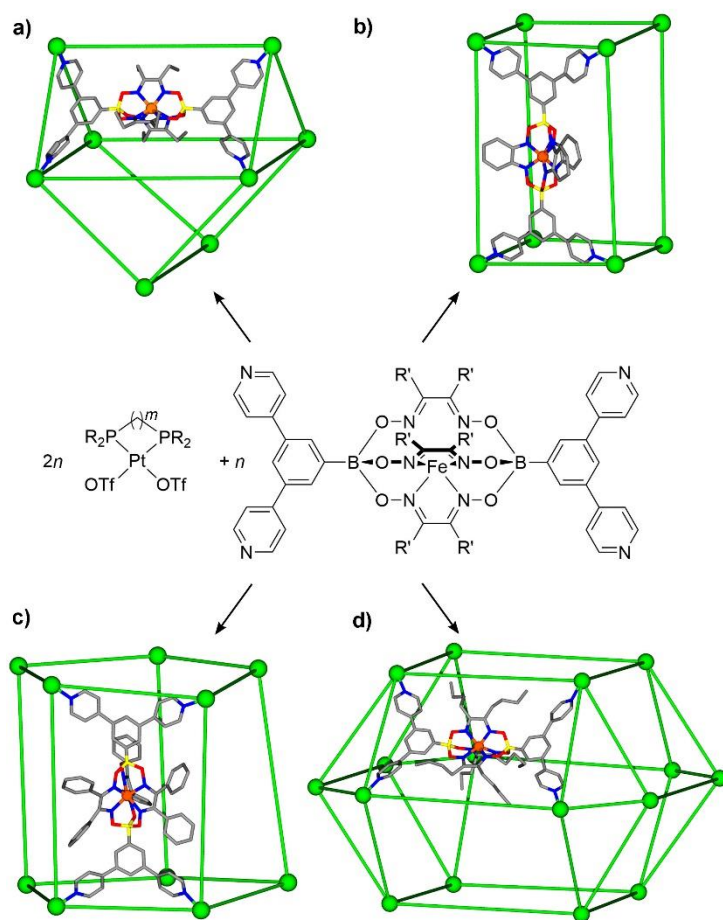
Scheme 1.5. A clathrochelate-based dipyrindyl ligand as a nanoscale spacer for heterometallic Cr-Ni rings (Cr: dark green balls, Ni: pink balls).

As described in Chapter 1.1.1, the combination of ditopic ligands with terminal pyridyl groups and Pd^{2+} ions is expected to give metal-ligand assemblies of the general formula $\text{Pd}^{\text{II}}_n\text{L}_{2n}$. For ligands with a linear geometry and 3-pyridyl groups at the end, assemblies of type $\text{Pd}^{\text{II}}_3\text{L}_6$ and $\text{Pd}^{\text{II}}_4\text{L}_8$ had been reported.^[77] Larger assemblies of type $\text{Pd}^{\text{II}}_6\text{L}_{12}$ were obtained when clathrochelates with terminal 3-pyridyl groups were employed (**Scheme 1.6a**; the graphic of the cage is based on crystallographic data, and only one ligand is shown for clarity).^[78] Most likely, assemblies with less than six palladium ions are disfavored due to steric interaction between the clathrochelate side chains. This hypothesis was corroborated by the following observation: when the reaction was carried out with a metalloligand containing a ‘thin’ clathrochelate core ($\text{R} = \text{H}$), the quantitative formation of a Pd_4L_8 tetrahedron instead of a Pd_6L_{12} octahedron was observed (**Scheme 1.6b**).^[79] Furthermore, it was found that the thermodynamic stability of $\text{Pd}^{\text{II}}_6\text{L}_{12}$ cages is strongly influenced by the lateral size of the clathrochelate side chains.



Scheme 1.6. Synthesis of octahedral or tetrahedral palladium coordination cages (Pd: cyan balls).

The importance of the lateral size of the metalloligands was also noted in investigations using tetrapyridyl ligands. These ligands were synthesized by cross-coupling reactions using tetrabrominated clathrochelate complexes and 4-pyridylboronic acid. Subsequently, reactions with *cis*-blocked Pt^{II} complexes were studied. A first unexpected result was the formation of a Pt^{II}₈L₄ coordination cage with a gyrobifastigium-like geometry (**Scheme 1.7a**).^[66b] The rectangular faces of the polyhedron are paneled by the tetratopic metalloligands. Later, we found that by varying the clathrochelate core of the ligand, we could also obtain Pt^{II}₈L₄ assemblies with a tetragonal barrel structure (**Scheme 1.7b**), pentagonal Pt^{II}₁₀L₅ barrels (**Scheme 1.7c**), and a Pt^{II}₁₆L₈ cage with an unprecedented square orthobicupola-like structure (**Scheme 1.7d**).^[80] The latter assembly has a molecular weight of more than 23 kDa and a diameter of 4.5 nm, making it one of the largest, structurally characterized Pt^{II} cages in the CCDC data base.



Scheme 1.7. Synthesis of platinum coordination cages using tetratopic metalloligands (Pt: green balls)

In the previous section, we have shown that clathrochelate-based metalloligands are useful building blocks for the construction of molecularly defined nanostructures. They have also been used for polymeric materials and other functional materials,^[68-70, 72, 81] but since this is beyond the scope of this thesis it will not be further addressed.

Chapter 2 Ligand aspect ratio as a decisive factor for the self-assembly of coordination cages

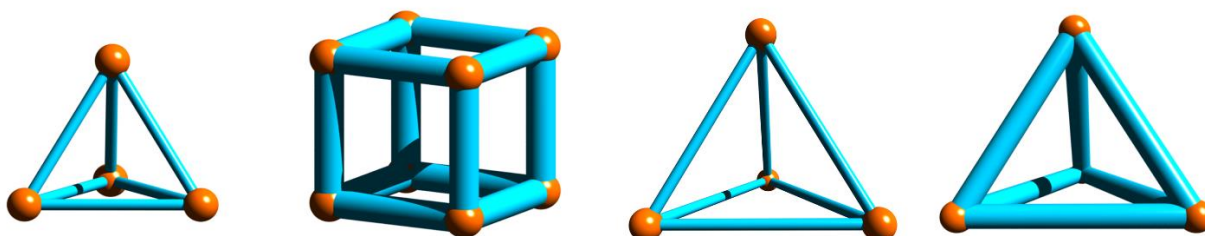
This chapter is based on published work:

"The Ligand Aspect Ratio as a Decisive Factor for the Self-Assembly of Coordination Cages"^[79]

S. M. Jansze, G. Cecot, M. D. Wise, K. O. Zhurov, T. K. Ronson, A. M. Castilla, A. Finelli, P. Pattison, E. Solari, R. Scopelliti, G. E. Zelinskii, A. V. Vologzhanina, Y. Z. Voloshin, J. R. Nitschke, K. Severin, *J. Am. Chem. Soc.* **2016**, *138*, 2046-2054.

Reprinted in an adapted version with permission from the American Chemical Society and all authors.

S. M. Jansze has contributed by designing and performing experiments, writing text and constructing figures for this publication. The work of Giacomo Cecot (shared first-author to this publication) was focused on palladium-based coordination cages. His work is briefly mentioned in Chapter 1.2.2, but not further discussed in this chapter.



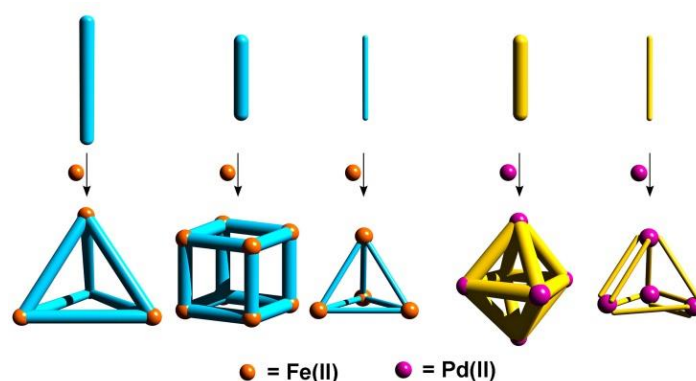
2.1 Introduction

The structural outcomes of metallasupramolecular self-assembly processes are largely controlled by the nature of the building blocks, i.e. metal ions, ligands, and possibly templates.^[9a, 9b, 82] From a design perspective, the ligand is arguably the most important building block, because chemists can use the repertoire of synthetic chemistry to make a vast collection of ligands with diverse structures and properties.

As mentioned in Chapter 1, by choosing an appropriate ligand, it is possible to influence the size, the geometry, and the functionality of the resulting metallasupramolecular assembly. Several factors are known to be of importance in this context. Structural rigidity of the ligand is a prerequisite for the assembly of polynuclear assemblies, because flexible ligands tend to favor complexes of low nuclearity. For rigid ligands, the distance and the relative orientation of the donor atoms are key parameters, allowing control of the size and geometry of the final assembly. This point is nicely illustrated by work from the Fujita group, on the assembly of spherical coordination cages from different bent dipyridyl ligands and Pd(II) ions (Chapter 1).^[29] The nature of the donor atom (e.g. oxygen vs. nitrogen) and the charge of the ligand are likewise important parameters. For example, it is possible to make heteroleptic assemblies by mixing cis-blocked L_2MX_2 complexes ($M = Pd^{II}$ or Pt^{II} ; $X =$ weakly coordinating anion) with neutral N-donor ligands and anionic carboxylate ligands.^[9b, 15] Taken together, the homoleptic $[L_2M(N\text{-donor})_2]^{2+}$ and $L_2M(O_2CR)_2$ complexes are thermodynamically less stable than the mixed $[L_2M(N\text{-donor})(O_2CR)]^+$ complex, resulting in the clean formation of heteroleptic assemblies.

Strategic functionalization of ligands with bulky groups can also be used to control the self-assembly behavior. For example, it is possible to favor heteroleptic complexes over homoleptic complexes by using two ligands, one of which has bulky groups in the vicinity of the donor atom(s).^[83] In this case, the coordination of two bulky ligands to the same metal center is thermodynamically disfavored, pushing the system towards the formation of heteroleptic complexes. Steric interactions that are remote from the metal binding site have also been employed as an element of control,^[84] but this strategy is less explored.

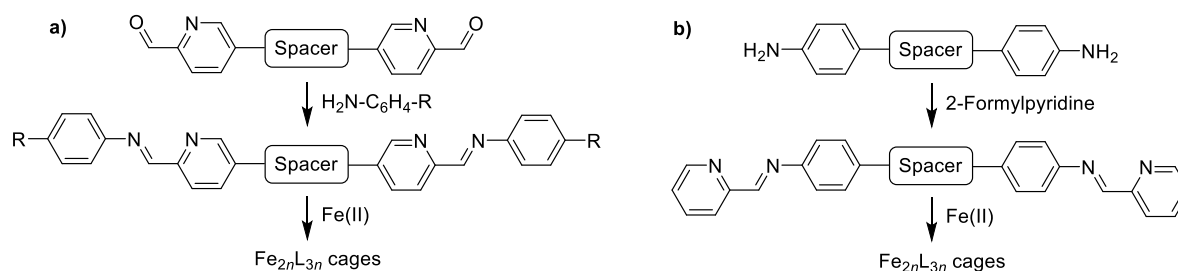
The investigation described in this chapter deals with an underappreciated parameter in ligand design: the aspect ratio of a rigid rod-type ligand. We show that the length-to-width ratio of a ligand can be used to control the geometries of coordination cages. In particular, we demonstrate that entropically disfavored cubic cages are formed instead of tetrahedra if the aspect ratio of the ligand is reduced (**Scheme 2.1**).



Scheme 2.1. Rigid rod-type ligands with different aspect ratios give rise to different coordination cages.

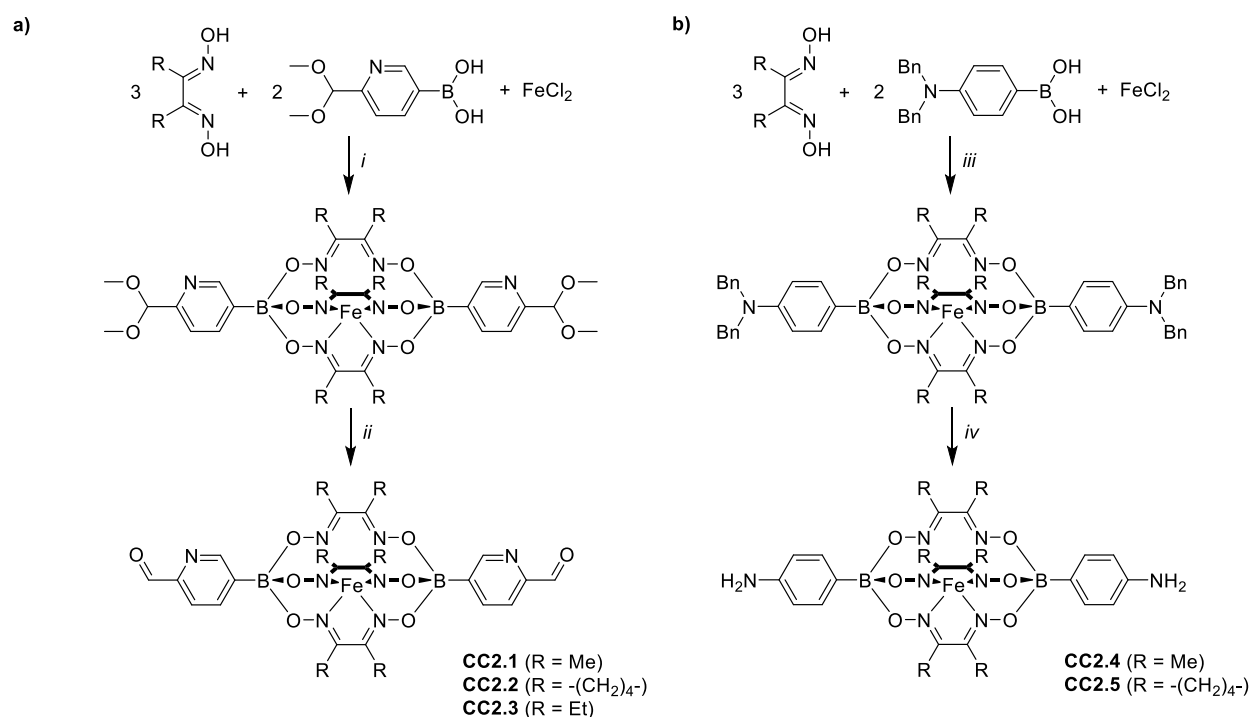
2.2 Results and discussion

Clathrochelate-based metalloligands appear to be ideally suited to investigate the influence of the aspect ratio on self-assembly behavior. The length of the ligands can be modulated via the boronate ester cap, and the lateral size of the ligand can be varied by choosing an appropriate dioxime ligand. Functionalized clathrochelate complexes are thus intrinsically 3-dimensional metalloligands with rigid rod geometry.



Scheme 2.2. Fe^{II} -based coordination cages with rigid rod-type ligands.

For this investigation, we have focused on two types of coordination cages, which are known to form with rigid rod ligands. Fe^{II} -based cages of type $\text{Fe}_{2n}\text{L}_{3n}$ can be obtained from ligands with two terminal formylpyridine groups upon reaction with aminobenzene derivatives and an Fe^{II} salt (**Scheme 2.2a**).^[10a, 10b, 85] In similar fashion, $\text{Fe}^{\text{II}}\text{L}_{3n}$ cages are formed when ligands bearing terminal aniline groups react with 2-formylpyridine in the presence of Fe^{II} salts (**Scheme 2.2b**).^[10a, 10b, 85d, 86]



Scheme 2.3. a) Synthesis of the clathrochelates **CC2.1**, **CC2.2** and **CC2.3**. Reagents and conditions: (i) MeOH, reflux, 4 h; (ii) TsOH (0.1 eq.), $\text{CHCl}_3/t\text{-BuOH}$ (4:1), 140 °C, 4 h. b) Synthesis of the clathrochelates **CC2.4** and **CC2.5**. Reagents and conditions: (iii) MeOH, reflux, 4 h; (iv) H_2 , Pd/C, MeOH/ CHCl_3 (1.5:1), 50 °C, 4 h.

In order to synthesize a clathrochelate ligand with apical formylpyridine groups, we used an acetal-protected boronic acid, the synthesis of which has been reported previously.^[87] Reaction with dimethylglyoxime, nioxime or diethylglyoxime and FeCl_2 in methanol gave protected clathrochelates. The yield for these reactions is modest (21, 33 and 29%, respectively), because side-products are formed by a protodeboronation reaction. Clean deprotection of the acetal was achieved by reaction with *p*-toluenesulfonic acid using microwave heating to give the desired clathrochelates **CC2.1**, **CC2.2** and **CC2.3** (**Scheme 2.3**).

For the syntheses of 4-aminophenyl-terminated clathrochelates, we also employed a protecting group strategy. Starting from (4-(dibenzylamino)phenyl)boronic acid,^[88] we first synthesized the Fe^{II} clathrochelate complexes, which were subsequently deprotected through hydrogenation to give complexes **CC2.4** and **CC2.5** with overall yields of 53% and 73%, respectively (**Scheme 2.3**).

The new clathrochelates **CC2.1–CC2.5** were characterized in solution by NMR spectroscopy and high resolution mass spectrometry.^[79] In addition, we have analyzed the molecular structure of **CC2.1** and of the HCl adducts of **CC2.4** and **CC2.5** in the solid state by single crystal X-ray crystallography. The structures are shown in **Figure 2.1**. The view along the B...B axis reveals the pseudo C_3 -symmetry of the complexes. Furthermore, it is evident that the lateral size of the nioxime-based complex **CC2.5** is significantly larger than that of the dimethylglyoxime-based complexes **CC2.1** and **CC2.4**.

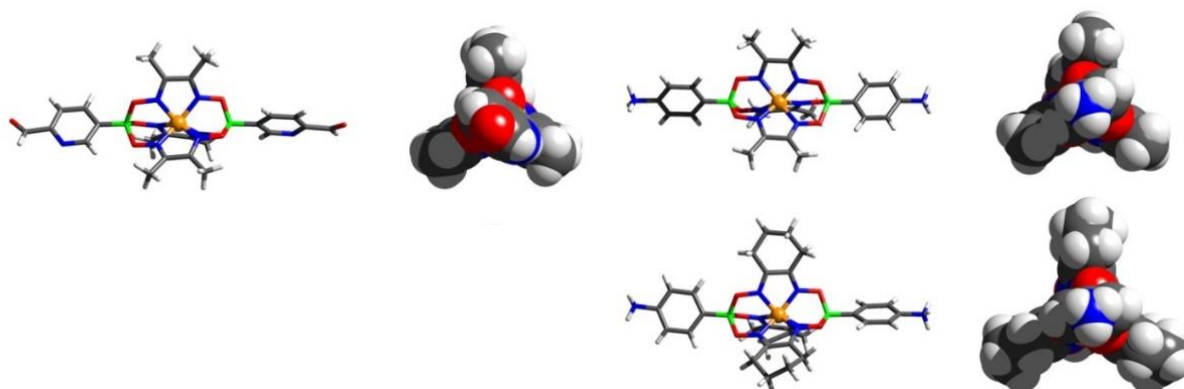
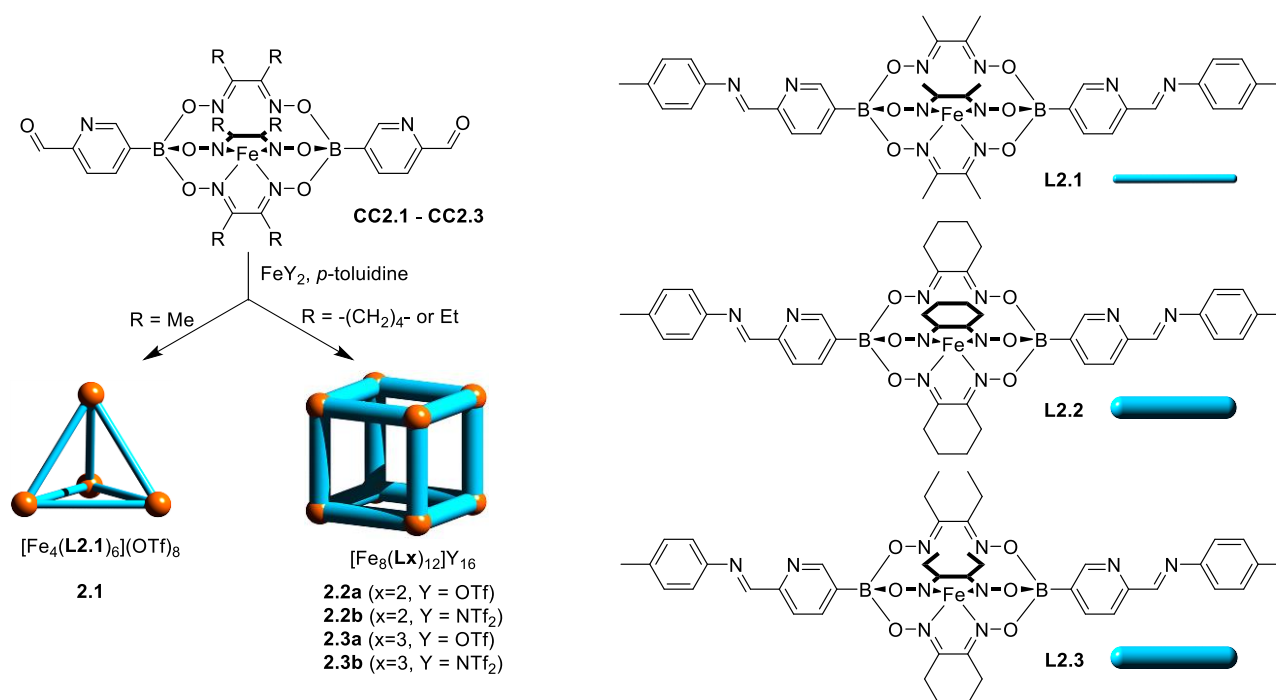


Figure 2.1. Molecular structures of the clathrochelates **CC2.1** (left), **CC2.4·HCl** (top right), and **CC2.5·HCl** (bottom right) in the crystal. A stick representation (side view, left) and a space filling representation (view along the B...B axis, right) is given for each complex. Chloride anions are omitted for clarity. Gray: C, white: H, dark blue: N, green: B, red: O and orange: Fe.

The coordination cages **2.1–2.3** were formed by heating an acetonitrile solution containing **CC2.1**, **CC2.2** or **CC2.3** (3 eq.), *p*-toluidine (6 eq.) and $\text{Fe}(\text{OTf})_2$ or $\text{Fe}(\text{NTf}_2)_2$ (2 eq.) at 50 °C for 18 h (**Scheme 2.4**). Workup allowed isolation of the cages in high yield (> 90%). The ^1H NMR spectra of the products were very complex, in particular those of cages **2.2** and **2.3**, which showed broad and ill-resolved peaks.^[79] Such behavior is not unexpected because this type of cage is often observed as a mixture of diastereoisomers with different relative stereo chemistries of the iron centers at the corners.^[10a, 10b, 85d, 89] Furthermore, the cages may not provide sufficient space for free rotation of the clathrochelate core. Restricted ligand rotation on the NMR time scale would lead to further reduction of the apparent symmetry.

The DOSY NMR spectra of **2.1–2.3** revealed the presence of large assemblies with a uniform diffusion constant.^[79] However, the diffusion constant of **2.1** ($4.43 \times 10^{-6} \text{ cm}^2/\text{s}$) was larger than that of **2.2** (**2.2a**: $2.89 \times 10^{-6} \text{ cm}^2/\text{s}$; **2.2b**: $2.85 \times 10^{-6} \text{ cm}^2/\text{s}$) and **2.3** (**2.3a**: $2.36 \times 10^{-6} \text{ cm}^2/\text{s}$; **2.3b**: $2.62 \times 10^{-6} \text{ cm}^2/\text{s}$), even though ligands of the same lengths were employed (**2.1–2.3**). This result provides evidence that complexes **2.2** and **2.3** are not typical tetrahedral coordination cages, but larger assemblies.



Scheme 2.4. Synthesis of coordination cages **2.1–2.3** from **L2.1 – L2.3**. Conditions: **CC2.1**, **CC2.2**, or **CC2.3** (3 eq.), $\text{Fe}(\text{OTf})_2$ or $\text{Fe}(\text{NTf}_2)_2$ (2 eq.), *p*-toluidine (6 eq.), CH_3CN , 50°C , 18 h.

High resolution ESI mass spectrometry revealed that **2.1** has the composition $[\text{Fe}^{\text{II}}_4(\text{L2.1})_6]^{8+}$ (**Figure 2.2**). The tetrahedral geometry is in line with what has been observed for other assemblies based on linear, rigid rod-type ligands with terminal formylpyridine groups.^[10a, 10b, 85] The cages **2.2** and **2.3**, on the other hand, have the composition $[\text{Fe}^{\text{II}}_8(\text{L2.2/2.3})_{12}]^{8+}$ (**Figure 2.3** for **2.3b**).

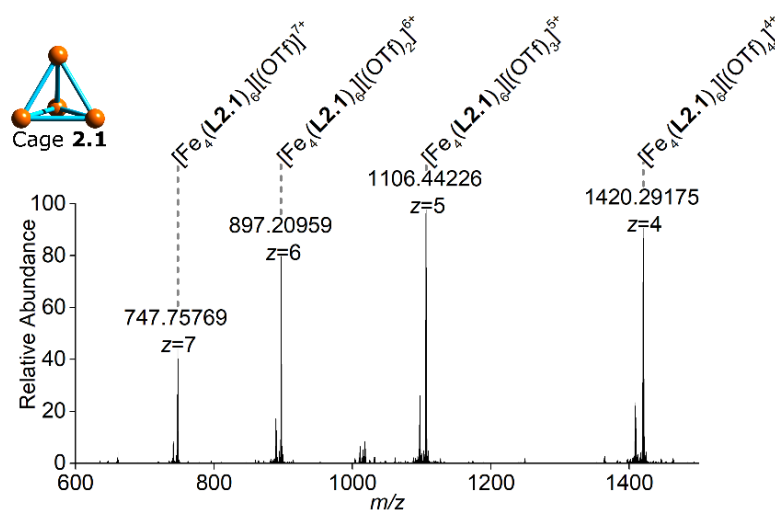


Figure 2.2. High resolution ESI-MS spectrum of the tetrahedral cage **2.1**.

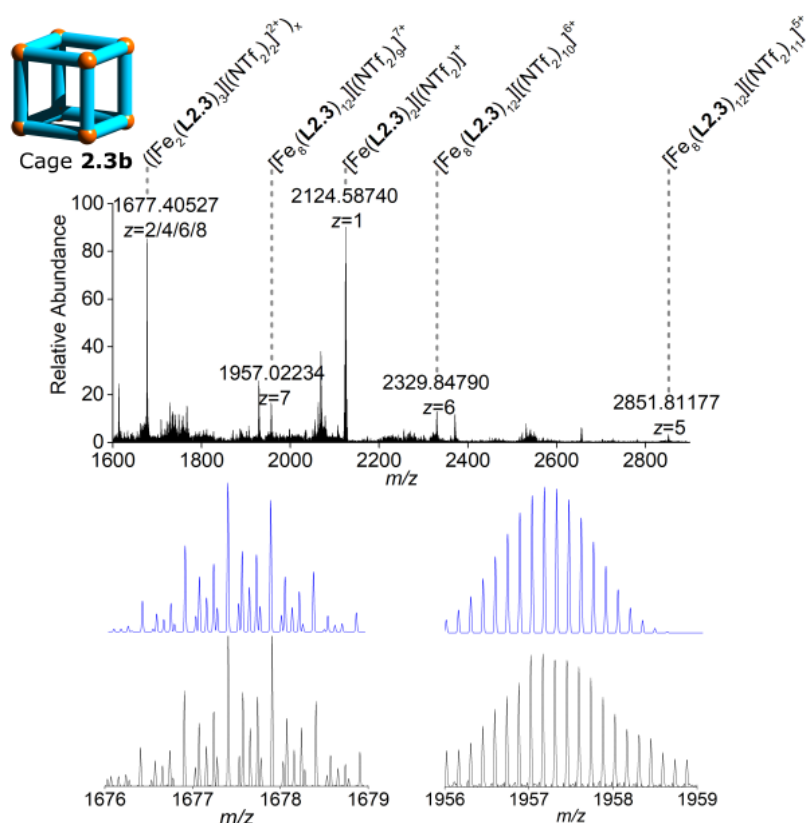
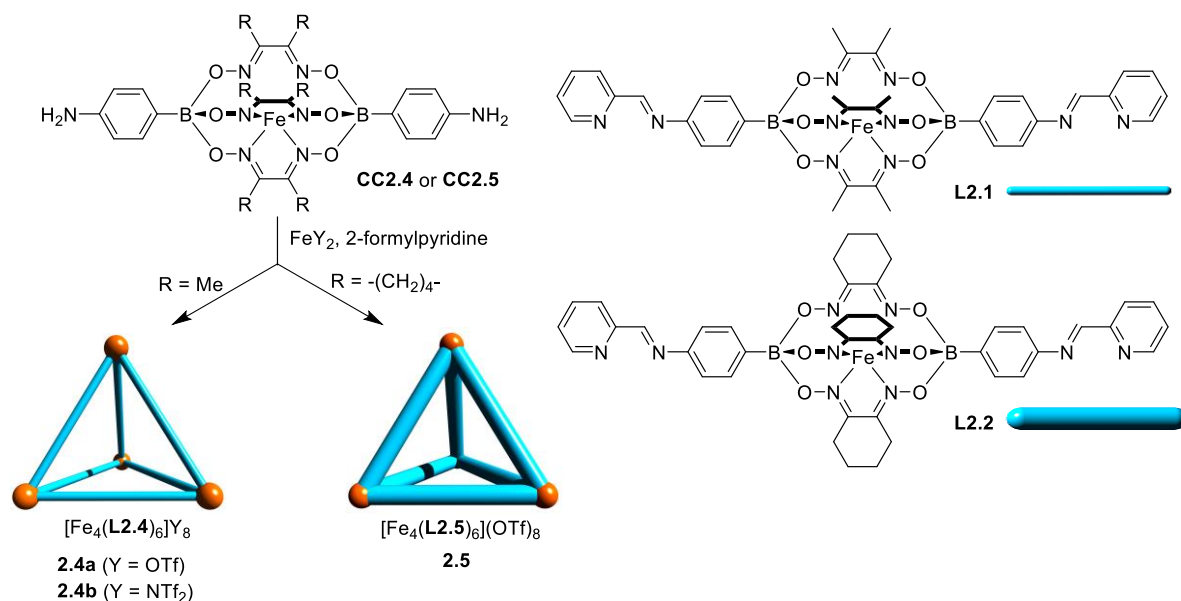


Figure 2.3. High resolution ESI-MS spectrum cubic cage **2.3b** (top), along with zoom-ins on the peaks at 1677 and 1957 m/z (bottom). The simulated spectra are in blue placed above the experimental data.

We infer **2.2** and **2.3** to possess an approximately cubic structure, with eight iron(II) centers at its vertices. Cubic coordination cages with $\text{Fe}^{\text{II}}(\text{N},\text{N}'\text{-chelate})_3$ complexes as vertices have already been described.^[90] These complexes are often based on fourfold-symmetric, face-capping ligands, and have an $\text{Fe}^{\text{II}}_8\text{L}_6$ stoichiometry. A cubic $\text{Fe}^{\text{II}}_8\text{L}_{12}$ cage has also been reported, but the coordinate vectors of its ligands are oriented at 120° with respect to each other,^[90a] in contrast with the parallel coordinate vectors of **L2.2** and **L2.3**. $\text{M}^{\text{II}}_8\text{L}_{12}$ cages with other metal ions in the vertices ($\text{M} = \text{Cu}^{\text{II}}, \text{Zn}^{\text{II}}, \text{Ni}^{\text{II}}, \text{Co}^{\text{II}}$) have also been studied.^[52a, 91] These cages were obtained using template effects,^[52a] or ligands with some conformational freedom, resulting in variable coordinate vectors. In our case, the coordinate vectors of **L2.2** and **L2.3** should favor the formation of a tetrahedral $\text{Fe}^{\text{II}}_4\text{L}_6$ cage. The fact that we observe an entropically disfavored $\text{Fe}^{\text{II}}_8\text{L}_{12}$ cage instead of a tetrahedron can be attributed to the small aspect ratio of ligands **L2.2** and **L2.3**. Their lateral size is significantly larger than that of **L2.1**, and a tetrahedral geometry would lead to unfavorable steric interactions between the lateral $-(\text{CH}_2)_4-$ or Et groups.

Next, we investigated the formation of coordination cages starting from the aniline-terminated clathrochelates **CC2.4** and **CC2.5**. The lateral size of these complexes is the same as for **CC2.1** and **CC2.2** (Me and $-(\text{CH}_2)_4$ -side-chains), but condensation with 2-formylpyridine results in ligands with an increased distance between the two N,N'-chelating sites (**Scheme 2.2**). The aspect ratio of the metalloligands is thus increased.

When **CC2.4** or **CC2.5** was combined with 2-formylpyridine and $\text{Fe}^{\text{II}}(\text{OTf})_2$ or $\text{Fe}^{\text{II}}(\text{NTf}_2)_2$, DOSY spectroscopy indicated all products to diffuse at indistinguishable rates. The ^1H NMR spectra of cages **2.4** and **2.5** showed several sets of signals, indicating the presence of diastereoisomers.^[10a, 10b, 85d, 89] Clear evidence for the stoichiometry of the cages was again obtained by high resolution mass spectrometry: both cages have the composition $\text{Fe}^{\text{II}}_4\text{L}_6$ (**Scheme 2.5**).



Scheme 2.5. Synthesis of the coordination cages **2.4** and **2.5**. Conditions: **CC2.4** or **CC2.5** (3 eq.), $\text{Fe}(\text{OTf})_2$ or $\text{Fe}(\text{NTf}_2)_2$ (2 eq.), 2-formylpyridine (6 eq.), CH_3CN , 50°C , 18 h.

The decanuclear cages **2.4b** and **2.5** were both analyzed by single crystal X-ray diffraction (**Figure 2.4**). Both cages crystallize as a racemic mixture of $\Delta\Delta\Delta\Delta$ and $\Lambda\Lambda\Lambda\Lambda$ isomers, with cage **2.4b** showing a pseudo C_3 symmetry axis, while cage **2.5** displays full crystallographic C_3 symmetry. The four $\text{Fe}^{\text{II}}(\text{N},\text{N}'\text{-chelatate})_3$ complexes in the vertices have an average distance of about 20 Å. The cavity of cage **2.4b** has a size of approximately 480 Å^3 as determined by VOIDOO calculations. For cage **2.5**, the cavity is considerably smaller (377 Å^3) because the lateral $-(\text{CH}_2)_4-$ groups block part of the space inside the cavity (**Figure 2.5**).

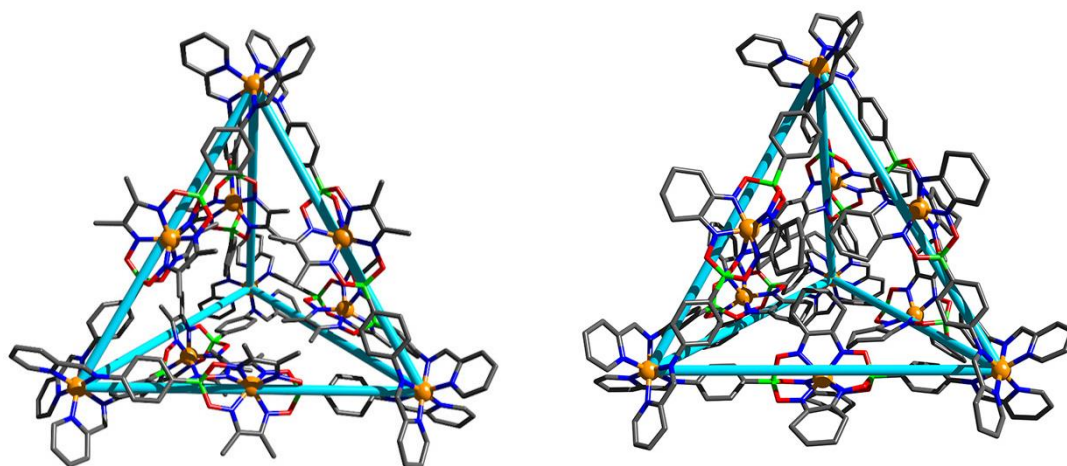


Figure 2.4: Molecular structures of the cages **2.4b** (left) and **2.5** (right) in the crystal. Hydrogen atoms, counter anions, and solvent molecules are omitted for clarity. Gray: C, dark blue: N, green: B, red: O and orange: Fe.

The formation of $\text{Fe}^{\text{II}}_4\text{L}_6$ cages with both aniline-terminated clathrochelates is consistent with the inference that aspect ratio and not the absolute width of the ligand is the decisive factor in controlling the geometry. In fact, ligand **L2.5** (the condensation product of **CC2.5** and 2 formylpyridine) and ligand **L2.2** have the same lateral size, but **L2.5** has an increased aspect ratio because the metal binding sites are farther apart. As a result of this difference, we observe an $\text{Fe}^{\text{II}}_8\text{L}_{12}$ cage with **L2.2** but an $\text{Fe}^{\text{II}}_4\text{L}_6$ cage with **L2.5**.

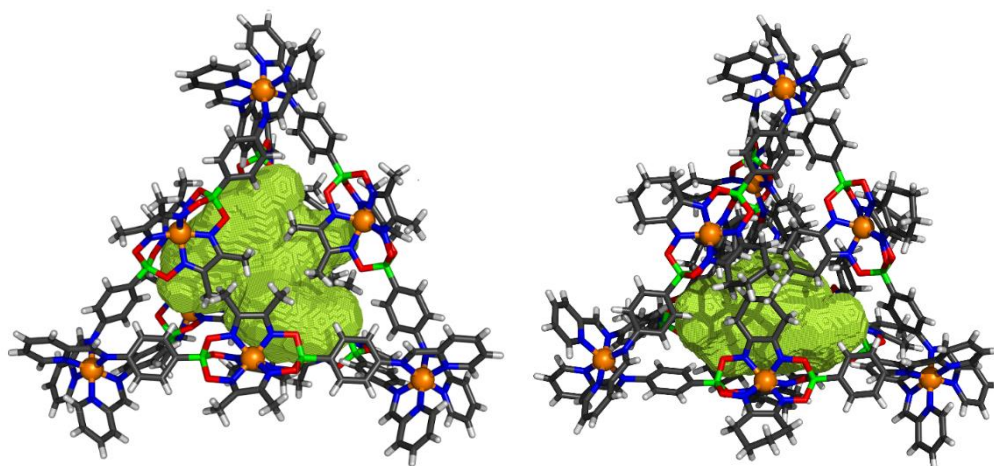


Figure 2.5. Graphical representation of the VOIDOO calculations on cages **2.4b** (left) and **2.5** (right), showing the detected void in the crystal structures. With the solvent molecules removed from the structure before calculation and the calculated void space indicated in yellow. C: Dark gray, N: dark blue, B: green, O: red, Fe: orange, H: white.

2.3 Conclusion

The size and the geometry of a ligand is of pivotal importance for metal-based self-assembly reactions. The ligand aspect ratio is a parameter which is rarely discussed in this context, however. We have shown that the aspect ratio can be used as an element of control during the formation of coordination cages. If we also consider the work of Giacomo Cecot on Pd^{II}-based cages, it has been shown for two different types of cages that there is a switch towards a higher nuclearity structure when the length-to-width ratio of the ligand was reduced. In the case of Fe^{II}-based cages, we have obtained an unusual cubic Fe^{II}₈L₁₂ structure instead of the common Fe^{II}₄L₆ tetrahedron when a ligand with a small aspect ratio was employed. In the case of Pd^{II}-based cages, it was shown that it is possible to form Pd^{II}₄L₈ or Pd^{II}₆L₁₂ cages, depending on the aspect ratio of the ligand. Intramolecular steric interactions between the ligands are likely responsible for these changes in geometry. The reduced intra-ligand interactions in the larger cages are enthalpically favorable, thereby compensating for the entropic penalty associated with the formation of assemblies of higher nuclearity.

Overall, our results provide clear evidence that the aspect ratio of a rigid rod-type ligand can be an important parameter for metal-based self-assembly reactions. In order to use this parameter as an element of control, it is desirable to employ a ligand which allows modulation of its aspect ratio without too much synthetic effort. Clathrochelate-based metalloligands appear ideally suited for this purpose, because their lengths, widths and functionalities can be varied easily.

Chapter 3 Pd^{II}₂L₄-type coordination cages up to three nanometers in size

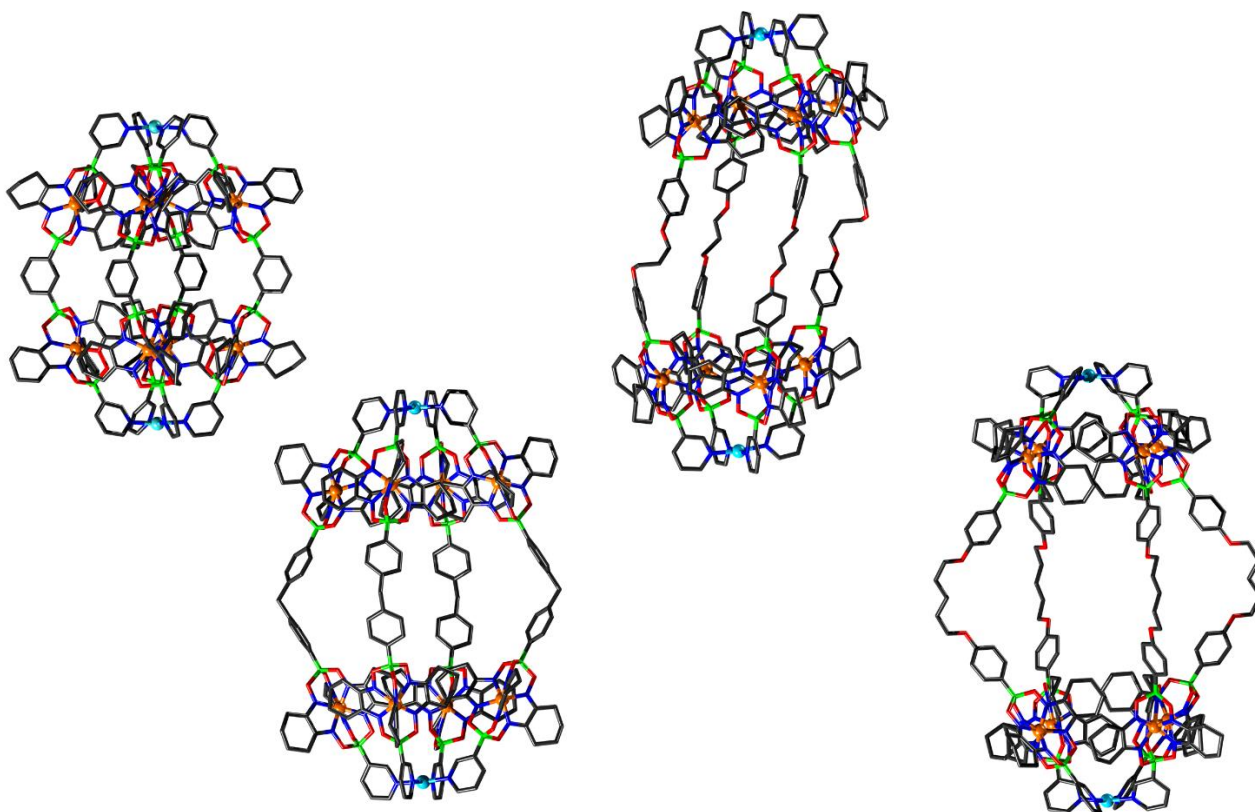
This chapter is based on published work:

"Pd^{II}₂L₄-type coordination cages up to three nanometers in size"^[80b]

S. M. Jansze, M. D. Wise, A. V. Vologzhanina, R. Scopelliti, K. Severin, *Chemical Science* **2017**, 8, 1901-1908.

Reprinted in an adapted version with permission from the Royal Society of Chemistry and all authors.

S. M. Jansze has contributed by designing and performing experiments, writing text and constructing figures for this publication.



3.1 Introduction

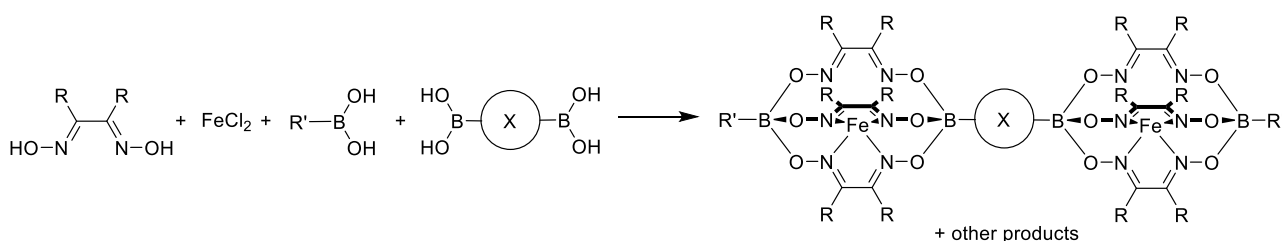
As described in Chapter 1 of this thesis, coordination-driven self-assembly provides a formidable means to construct molecularly defined nanostructures through a bottom-up approach.^[9b, 10a, 15, 17a, 18b, 29, 83c, 92] Ever larger and more complex metallasupramolecular structures have been reported in recent years, including topologically interesting architectures such as rotaxanes, catenanes, knots and links.^[12a, 53d, 93] Current efforts in this area are increasingly focused on creating metal-based nanostructures with novel functions – such as coordination cages that act as selective catalysts for organic reactions.^[5b, 10c, 85d, 94] However, addressing the ongoing structural challenges presented by coordination-driven self-assembly is similarly important, given the fundamental influence that the structure of a metallasupramolecular architecture exerts over its function. One such challenge is the creation of structurally defined assemblies of low symmetry starting from multiple chemically distinct building blocks (e.g. three different metal ions and three different ligands). Various strategies, such as orthogonal self-assembly,^[95] have been employed to tackle this problem, but there remains scope for further development. Another, deceptively simple, challenge is size. In order to create large (> 2 nm), molecularly defined nanostructures by self-assembly, one has two options: a) the assembly of a large number of small building blocks; or b) the assembly of a small number of large building blocks. Obviously, one could also use a large number of large building blocks, but this approach would suffer from the drawbacks of option a) and b).

Option a) is hampered by the fact that multicomponent metallasupramolecular assemblies are typically disfavored from an entropic point of view. Furthermore, intra- and intermolecular interactions must be precisely controlled in order to prepare an assembly of defined stoichiometry and geometry. The latter point is illustrated in works by the research group of Fujita, as described in Chapter 1 of this thesis. In order to avoid alternative structures and insoluble precipitates, they had to fine-tune the geometry, solubility and flexibility of the ligands they employed. The work of Fujita also highlights other difficulties in preparing large assemblies by coordination-driven self-assembly: the formation of kinetically trapped intermediates and the presence of large, solvent-filled voids.^[33] These voids are not only problematic for structural analysis by X-ray crystallography, but they can also affect the structural integrity of the assembly upon solvent removal during isolation.^[96] Related problems were also encountered for cages based on dynamic covalent chemistry.^[97]

Option b), the utilization of large building blocks, presents further challenges. First and foremost, the synthesis of such molecules can be highly demanding.^[98] With the development of clathrochelates as metalloligands (Chapter 1) we have begun to address this issue. Continuing these efforts, this chapter describes the preparation of a new set of bent metalloligands with terminal 3-pyridyl groups. These ligands were used to form Pd^{II}₂L₄ complexes, which are significantly larger than the Pd^{II}₂L₄ cages described to date. Structural and spectroscopic data suggest that some of the assemblies are stabilized by close intramolecular packing of lipophilic ligand side chains. Such packing effects may offer a general means for circumventing the 'void problem' outlined above, and to stabilize metallasupramolecular assemblies in highly polar solvents.

3.2 Results and discussion

An interesting aspect of the clathrochelate chemistry, as described in Chapter 1, is the fact that it is synthetically straightforward to prepare double clathrochelate complexes by using a mixture of a (functionalized) monoboronic acid and a diboronic acid (**Scheme 3.1**). Since the two boronic acids are incorporated in a statistical manner, the double clathrochelate complex is formed along with side products (e.g. the single clathrochelate complex with two capping groups B-R'). However, purification can be accomplished by chromatography or crystallization. We have previously used this synthetic approach to make linear metalloligands with terminal 4-pyridyl groups.^[66a] For the work presented in this chapter, we have focused on bent ligands.



Scheme 3.1. Synthesis of double clathrochelate complexes by combination of a monoboronic acid and a diboronic acid.

Bent, 'banana-shaped' ligands with terminal pyridyl groups are well suited for the construction of Pd^{II}₂L₄ coordination cages. In order to prepare cages with large cavities, relatively long and rigid ligands are required. Unsurprisingly, the synthesis of such ligands often requires substantial effort.^[17a, 18b] We hypothesized that the utilization of double clathrochelate complexes as ligands would allow Pd^{II}₂L₄ cages, with unprecedented size, to be accessed in a straightforward manner.

Using the approach outlined in **Scheme 3.1**, we have prepared the double clathrochelate complexes **L3.1–L3.4** (**Figure 3.1** right) by reaction of FeCl₂ with dimethylglyoxime or nioxime in the presence of 3-pyridylboronic acid and either 1,3-benzenediboronic acid or (methylenebis(1,4-phenylene))diboronic acid. In order to suppress the formation of longer oligomers, we have used substoichiometric amounts of the diboronic acid. The small amount of oligomeric material that is still formed was removed by purification over a short silica plug.

The main side product—the single clathrochelate complex with terminal 3-pyridyl groups—was separated out by size exclusion chromatography. This one-pot reaction protocol provides rapid access to the double clathrochelate metalloligands **L3.1 – L3.4** in yields between 39% and 59% (calculated based on the diboronic acid starting material). The new metalloligands were characterized by NMR spectroscopy and high-resolution mass spectrometry.^[80b] In addition, we have analyzed the solid state structures of **L3.1** and **L3.2** by single crystal X-ray crystallography (**Figure 3.1**, right) The ligands show the expected bent structure and the Fe^{II} complexes display the usual distorted trigonal prismatic coordination geometry.

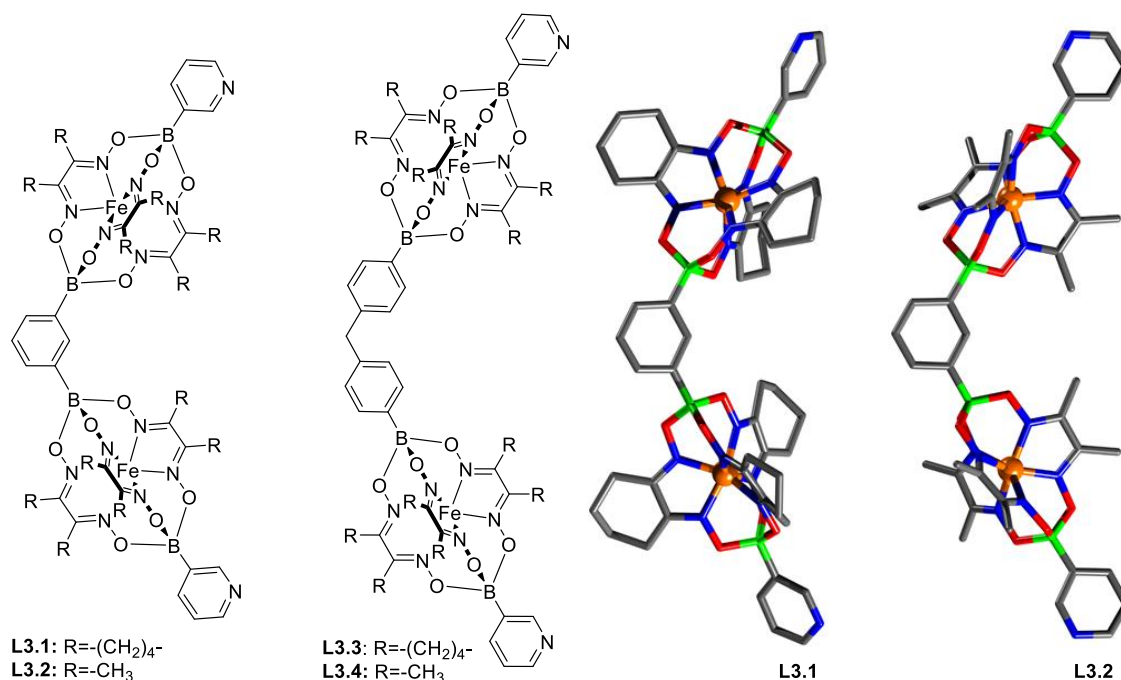
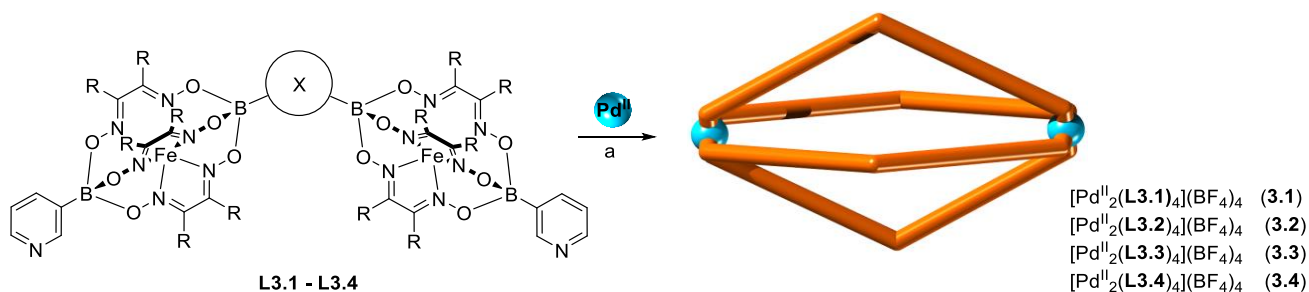


Figure 3.1. The metalloligands **L3.1–L3.4** (left) and the molecular structures of the double clathrochelates **L3.1** and **L3.2** as determined by single crystal X-ray diffraction (right). Hydrogen atoms and solvent molecules are omitted for clarity. Grey: C; blue: N; green: B; red: O; and orange: Fe.

The Pd^{II}₂L₄ cages **3.1–3.4** were prepared by addition of [Pd(CH₃CN)₄](BF₄)₂ to a suspension of the respective metalloligand in either CD₃CN or DMSO-*d*₆ (**Scheme 3.2**). The mixtures were then heated at 70 °C for 17 h, resulting in the formation of clear, deep orange solutions. The formation of Pd^{II}₂L₄ cages was evidenced by NMR spectroscopy and high-resolution mass spectrometry.^[80b] The ¹H NMR spectra of the solutions showed a single set of signals for the aromatic protons of the terminal 3-pyridyl groups. (**Figure 3.2**) The proton signals belonging to the dioximato ligands gave rise to more complex signal patterns, indicating restricted rotational freedom of the clathrochelate cores (for the free ligands, rotation around the B...Fe...B axis is fast on the NMR time scale). For solutions of complex **3.1** in CD₃CN (but not in DMSO-*d*₆), we also observed a reduced symmetry for the four central phenylene spacers (**Figure 3.2**, bottom). Broadening of the ¹H NMR signals of the -C₆H₄- group was observed at 328 K, indicating coalescence. These data provided initial evidence that the cages adopt a compact structure with close intraligand interactions.



Scheme 3.2. Synthesis of the coordination cages **3.1–3.4**. Conditions: [Pd(CH₃CN)₄](BF₄)₂ (0.5 eq.), CH₃CN or DMSO, 70 °C, 17 h.

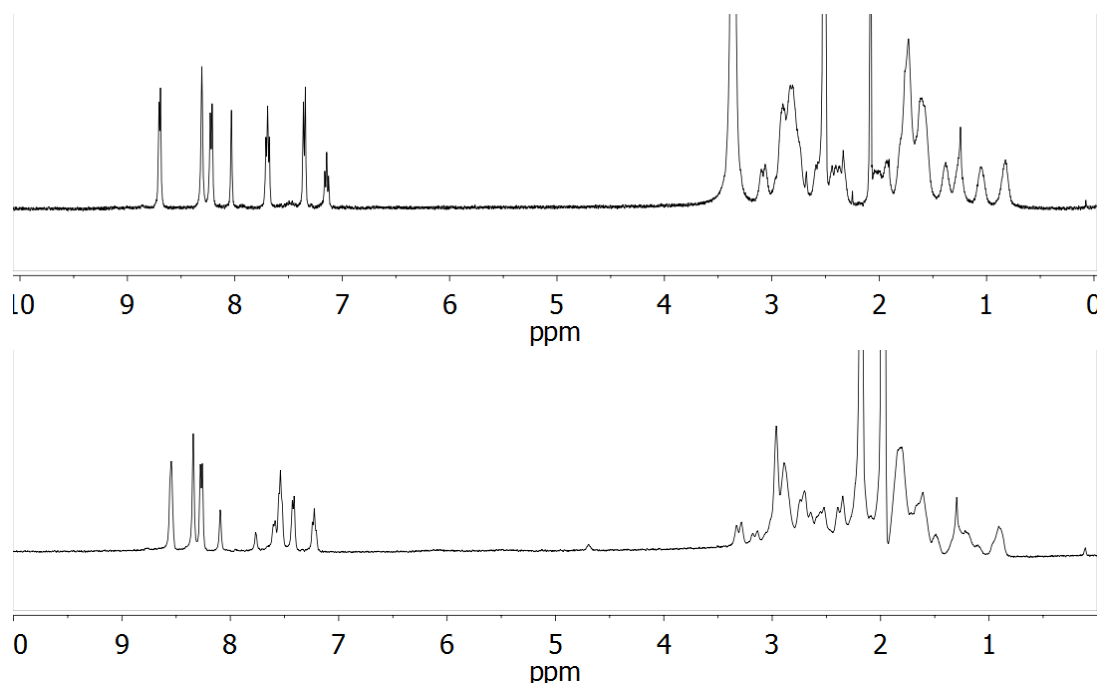


Figure 3.2. ¹H NMR spectra of coordination cage **3.1** in DMSO-d₆ (top) and CD₃CN (bottom).

DOSY NMR spectroscopy confirmed the formation of aggregates with a defined diffusion coefficient for all reactions. The high resolution ESI mass spectra of solutions of **3.2–3.4** showed dominant peaks for [Pd₂L₄]⁴⁺ complexes. For cage **3.1**, on the other hand, a strong peak corresponding to [Pd₂(**L3.1**)₄(BF₄)]³⁺ was observed, indicating that one of the four BF₄[−] anions is more tightly bound. The strong binding of one BF₄[−] was corroborated by ¹⁹F NMR spectroscopy. Two signals were observed, suggesting that the exchange of bound and unbound BF₄[−] anions is slow on the NMR time scale. (**Figure 3.3**)

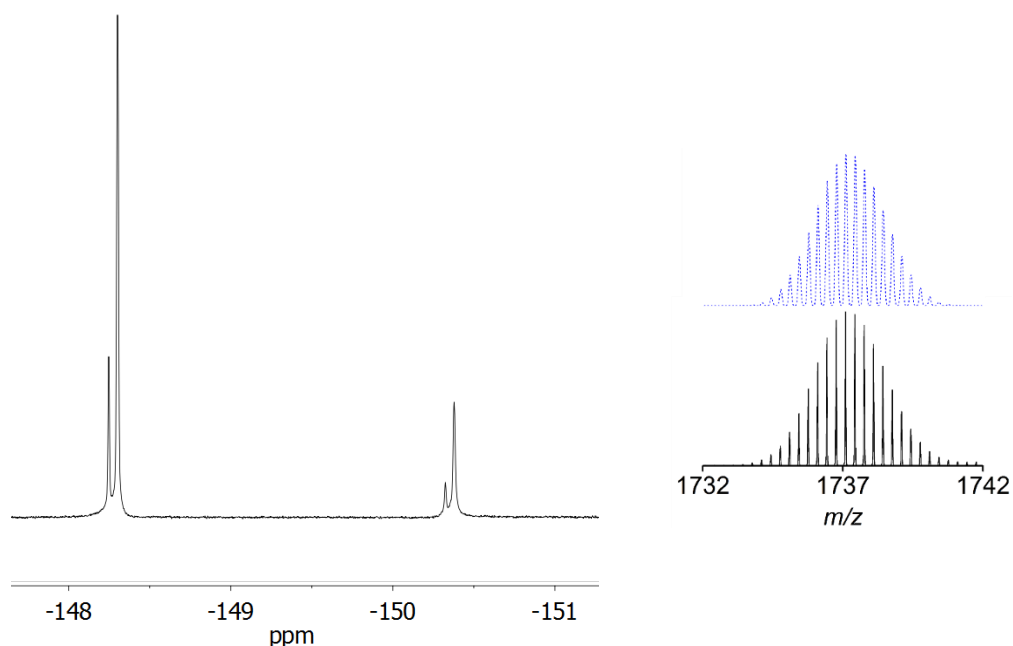


Figure 3.3. Left: ¹⁹F NMR spectrum of cage **3.1** in DMSO-d₆. Right: Zoom-in of the 3+ charged peak at 1737 *m/z* in the HRMS spectrum of coordination cage **3.1** in CH₃CN (bottom), with simulated spectrum shown in blue above.

Single crystal X-ray analyses were performed for cages **3.1**, **3.2** and **3.4** (**Figure 3.4**), revealing the expected Pd^{II}₂L₄ composition. These assemblies adopt a rugby ball-like, prolate-spheroid shape, with Pd(pyridyl)₄ complexes at the antipodes of the principal axis. With Pd...Pd distances of 2.1 nm (**3.1**), 2.0 nm (**3.2**), and 2.7 nm (**3.3**), the cages are very large compared to the Pd^{II}₂L₄ cages described so far (to the best of our knowledge, the largest crystallographically characterized Pd^{II}₂L₄ cage has a Pd...Pd distance of 1.7 nm).^[96a] Most of the anions and the co-crystallized solvent molecules in the structures of **3.1**, **3.2** and **3.4** are highly disordered, and the SQUEEZE algorithm was applied to solvent molecules during refinement. For complex **3.1**, however, we were able to locate one BF₄⁻ anion inside the cage. (**Figure 3.5**) The anion is tightly encapsulated within **3.1**, which is in line with the slow exchange kinetics observed by NMR spectroscopy and the MS data showing that one counter anion is retained. (**Figure 3.4**)

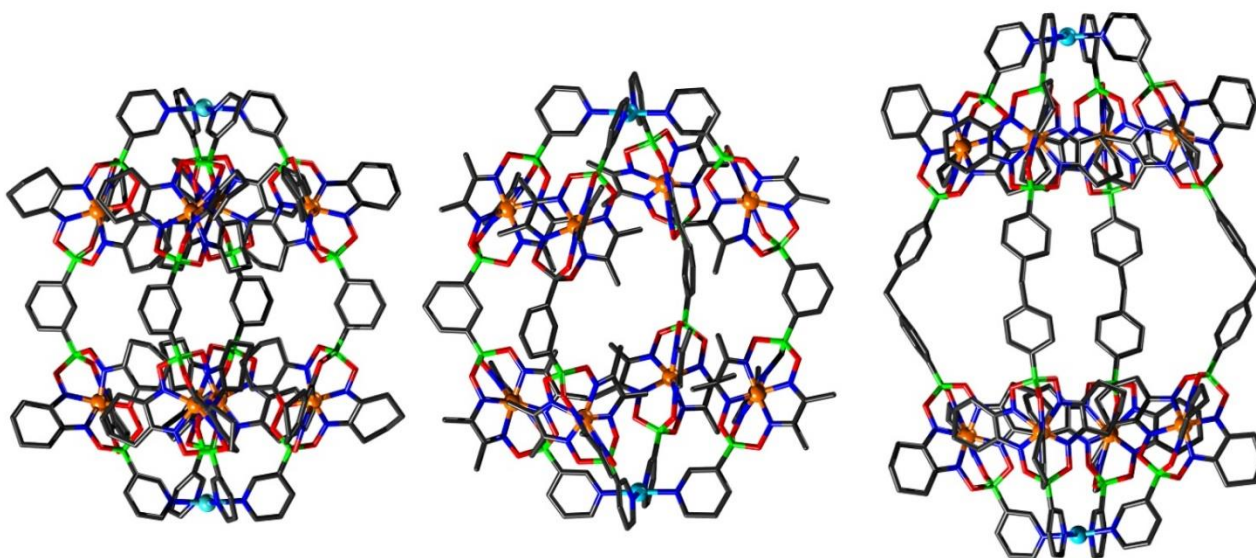


Figure 3.4. Molecular structures of cages **1** (left), **2** (middle), and **3** (right), as determined by single crystal X-ray diffraction. Hydrogen atoms, solvent molecules and anions are omitted for clarity. Grey: C; dark blue: N; green: B; red: O; cyan: Pd and orange: Fe.

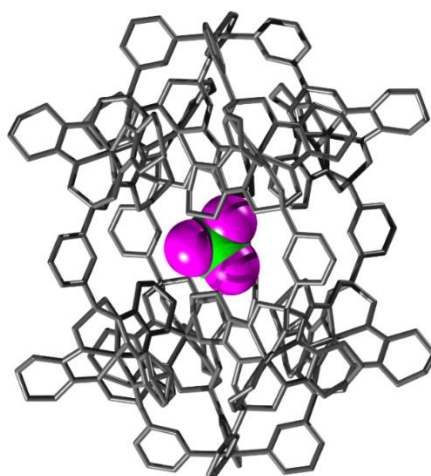


Figure 3.5. Molecular structures of cage **3.1** with space filling representation of the encapsulated BF₄⁻ anion. Hydrogen atoms are omitted for clarity. Green: B; pink: F; grey: all other atoms.

The structures of cages **3.1** and **3.3** show tight, interdigitated packing of the cyclohexyl side chains of the clathrochelate complexes (**Figure 3.4** and **3.6**, left). The close packing is likely responsible for the hindered rotation observed by NMR spectroscopy. For cage **3.2**, which has smaller methyl side chains, no such tight packing is observed (**Figure 3.6**, right). In the previous chapter we have shown that steric interactions between ligand side chains can thermodynamically destabilize a clathrochelate-based assembly^[79] and, in view of these earlier results, we suspected that the sterically less congested cages **3.2** and **3.4** would prove to be more stable than the tightly packed cages **3.1** and **3.3**. Surprisingly, the opposite is true.

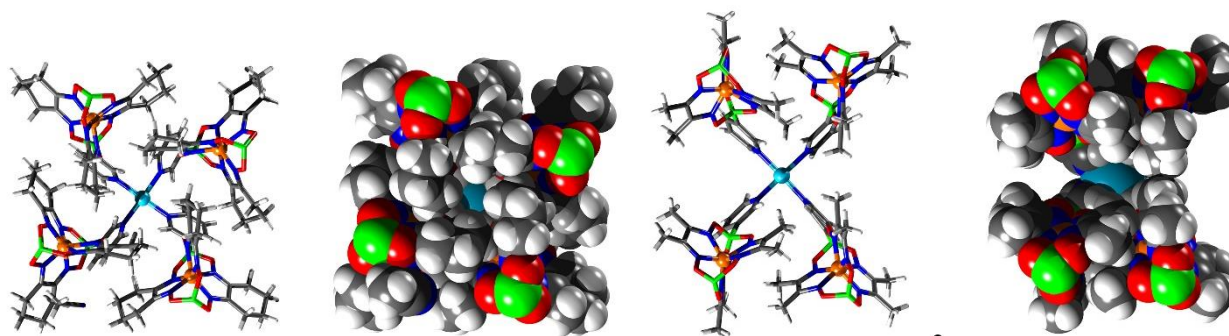
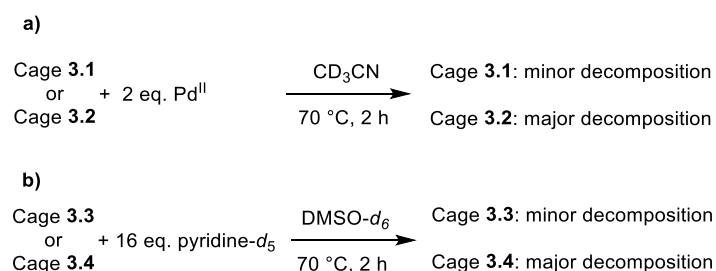


Figure 3.6. Parts of the structures of cage **3.1** (left) and cage **3.2** (right). The graphics depict the upper parts of the cages when viewed from the inside along the Pd...Pd axis, with wire representations on the left and space filling representations on the right. Solvent molecules and anions are omitted for clarity. Grey: C; dark blue: N; green: B; red: O; cyan: Pd and orange: Fe.

The relative thermodynamic stability of the smaller cages **3.1** and **3.2** in solution was examined by adding two equivalents of [Pd(CH₃CN)₄](BF₄)₂ to a solution of the cage in CD₃CN (**Scheme 3.3a**). After heating to 70°C for 2 h, the new equilibrium distribution was examined by ¹H NMR spectroscopy. In the case of cage **3.1**, only minor decomposition was observed. In the case of cage **3.2**, on the other hand, substantial ligand rearrangement and cage decomposition was detected.^[80b] These results indicate that cage **3.2** is less stable than cage **3.1** under these conditions. A stabilizing anionic template effect, resulting from the presence of a tightly encapsulated BF₄[−] anion in **3.1**, may offer an explanation for this trend.^[52a, 99]



Scheme 3.3. Decomposition experiments for evaluating the relative thermodynamic stability of the small cages **3.1** and **3.2** (a) as well as for the large cages **3.3** and **3.4** (b).

For the larger cages **3.3** and **3.4**, we used DMSO-*d*₆ as a solvent due to solubility problems in CD₃CN. Adding further equivalents of [Pd(CH₃CN)₄](BF₄)₂ to solutions of the cages did not result in detectable decomposition, presumably since Pd²⁺ ions are well solvated in DMSO and hence less efficient competition agents. We therefore used an excess of pyridine-*d*₅ to induce cage decomposition (**Scheme 3.3b**). The equilibrium composition was again determined by ¹H NMR spectroscopy after a heating period of 2 h at 70°C. Substantial decomposition was observed for cage **3.4**. In contrast, only low intensity new peaks were observed for cage **3.3**,

indicating a superior stability of the latter. For the larger cages **3.3** and **3.4**, stabilizing effects of the BF₄⁻ anions are unlikely to play an important role, as bound anions were observed neither by X-ray crystallography nor by NMR spectroscopy. Instead, we propose that the tightly packed cyclohexyl side chains are in fact a stabilizing factor for cage **3.3**. The packing of the lipophilic cyclohexyl groups buries a substantial amount of apolar surface area and, in a polar solvent such as DMSO, this clustering is expected to be energetically favorable.^[100]

We have also attempted to examine the relative stabilities of the smaller cages **3.1** and **3.2** in DMSO. Interestingly, we were not able to achieve quantitative assembly of cage **3.2** from ligand **L3.2** and [Pd(CH₃CN)₄](BF₄)₂, despite the unproblematic formation of cage **3.1** in DMSO. Apparently, **3.2** is not sufficiently stable to allow the assembly process to occur in a strongly coordinating solvent such as DMSO. As in the cases of **3.3** and **3.4**, we propose that solvophobic effects contribute to the higher stability of cage **3.1** (cyclohexyl side chains) when compared to cage **3.2** (methyl side chains).

The experiments described above suggest that clathrochelate-based metalloligands with cyclohexyl side chains are particularly suited for the construction of Pd^{II}₂L₄ cages in polar solvents because solvophobic effects impart an additional stability to the assemblies. Therefore, we synthesized even larger cages using the extended metalloligands **L3.5** and **L3.6** (Figure 3.7). The synthesis of these ligands was accomplished in a similar fashion as described for **L3.1** and **L3.3**, i.e. by using a mixture of 3-pyridylboronic acid and the corresponding diboronic acid along with nioxime and FeCl₂. Purification by size exclusion chromatography gave the ligands **L3.5** and **L3.6** in yields of 48% and 49%, respectively. It should be noted that both ligands are rather flexible due to the presence of O(CH₂)_nO linkers (*n* = 3 or 5). In principle, highly flexible bipyridyl ligands can give rise to mononuclear complexes of the formula Pd^{II}L₂.^[101] For **L3.5** and **L3.6**, the sterically demanding clathrochelate complexes were expected to prevent such 'back-biting' of the ligand.

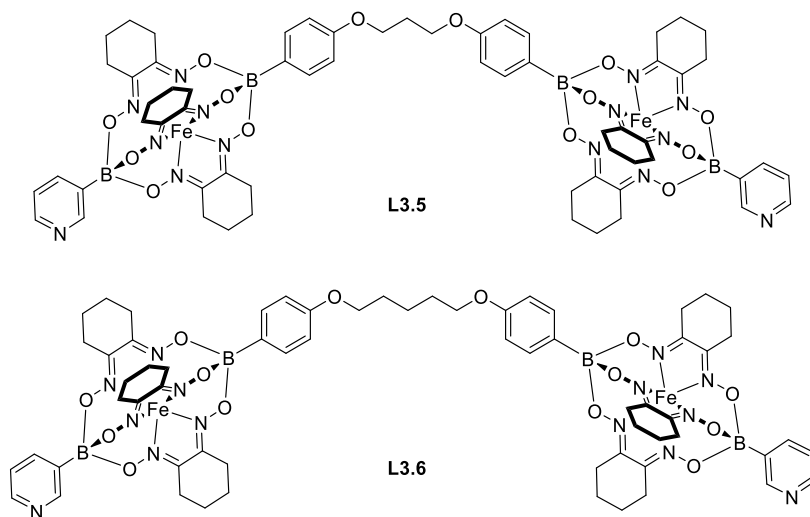
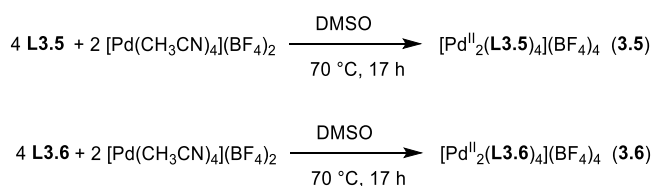


Figure 3.7 The metalloligands **L3.5** and **L3.6**.

Finding a suitable solvent for reactions of **L3.5** and **L3.6** with [Pd(CH₃CN)₄](BF₄)₂ turned out to be challenging due to solubility problems. The best compromise was achieved with DMSO. The ligands **L3.5** and **L3.6** display very poor solubility in DMSO, but the addition of [Pd(CH₃CN)₄](BF₄)₂ resulted in the formation of a light orange solution along with some solid (Scheme 3.4). Analysis of the solution by high resolution mass spectrometry provided clear evidence for the presence of Pd^{II}₂L₄ complexes.^[80b] Unfortunately, the low concentrations of the complexes in solution precludes analysis by NMR.



Scheme 4 Synthesis of the cages **3.5** and **3.6**.

Single crystals of **3.5** and **3.6** were obtained by slow diffusion of diisopropylether or diethyl ether into a solution of the cage in acetonitrile/DMSO (2:8). Crystallographic analyses show that Pd^{II}₂L₄-type complexes had formed in both cases (**Figure 3.9**). As observed for cages **3.1** and **3.3**, the assemblies feature tightly packed cyclohexyl side chains of the clathrochelate complexes adjacent to the palladium ions. The proximity of neighboring clathrochelate complexes is reflected by the average distance of the four adjacent Fe^{II} centers. The values observed for **3.5** (0.84 nm) and **3.6** (0.83 nm) are close to what was found for **3.1** (0.83 nm) and **3.3** (0.83 nm). Apparently, the presence of more flexible O(CH₂)_nO linkers in **3.5** and **3.6** does not result in a more relaxed arrangement of the clathrochelate complexes.

The O(CH₂)₅O linkers of cage **3.6** are bent outwards, whereas the O(CH₂)₃O groups of cage **3.5** are essentially straight. Consequently, the Pd...Pd distances of the two cages are similar (2.98 and 3.03 nm). The length of these cages is comparable to some of the longest cylindrical metallasupramolecular assemblies described to date.^[102]

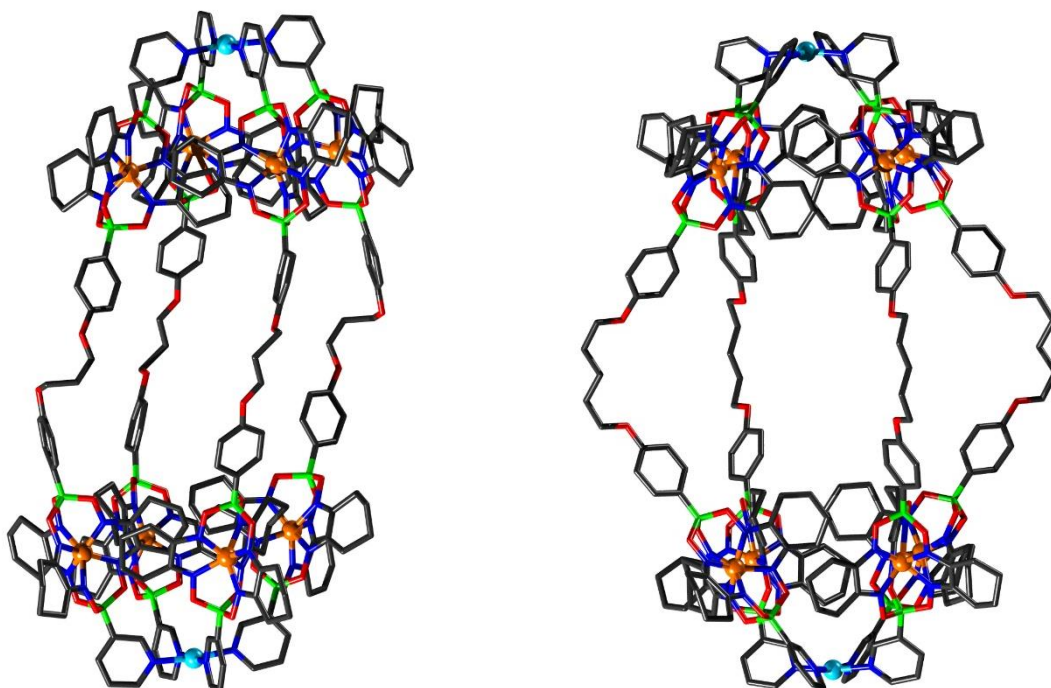


Figure 3.9 Molecular structures of the cages **3.5** (left) and **3.6** (right) as determined by single crystal X-ray diffraction. Hydrogen atoms, solvent molecules and anions are omitted for clarity. Grey: C; dark blue: N; green: B; red: O; cyan: Pd and orange: Fe.

3.3 Conclusion

We have synthesized and characterized novel, bent ditopic metalloligands with terminal 3-pyridyl groups. The preparation of these ligands is straightforward and relies on the Fe^{II}-templated formation of clathrochelate complexes. In order to access long metalloligands with two pyridyl-capped clathrochelate complexes, we have used a mixture of a diboronic acid and 3-pyridylboronic acid. This statistical synthesis gives rise to a mixture of products. However, purification by size exclusion chromatography is unproblematic. The ligands were used for the assembly of cage structures of the general formula (Pd^{II}₂L₄)(BF₄)₄. We characterized five of these assemblies by single crystal X-ray crystallography revealing remarkably large structures, spanning 2.0 nm to 3.0 nm. The thermodynamic stability of the cages was studied by competition experiments. These investigations revealed a surprising fact: cages based on ligands with sterically more demanding cyclohexyl side chains are more stable than cages based on ligands with smaller methyl side chains. We propose that the close packing of lipophilic cyclohexyl side chains contributes to the enhanced stability in polar solvents such as DMSO. Solvophobic effects of this kind are commonly observed for peptide or protein assemblies. For example, the aggregation of coiled-coil structures from amphiphilic α -helices is largely driven by the burial of hydrophobic surface area.^[103] However, in the area of metallasupramolecular chemistry, these effects are rarely used in a deliberate manner, and demonstrate exciting potential as a more general tool to stabilize large, hydrophobic assemblies in polar solvents.

Chapter 4 Inflating face-capped $\text{Pd}^{\text{II}}_6\text{L}_8$ coordination cages

This chapter is based on published work:

"Inflating face-capped Pd_6L_8 coordination cages"^[104]

S. M. Jansze, D. Ortiz, F. Fadaei Tirani, R. Scopelliti, L. Menin, K. Severin, *Chem. Commun.* **2018**, 54, 9529-9532.

Reprinted in an adapted version with permission from the Royal Society of Chemistry and all authors.

S. M. Jansze has contributed by designing and performing experiments, writing text and constructing figures for this publication.



4.1 Introduction

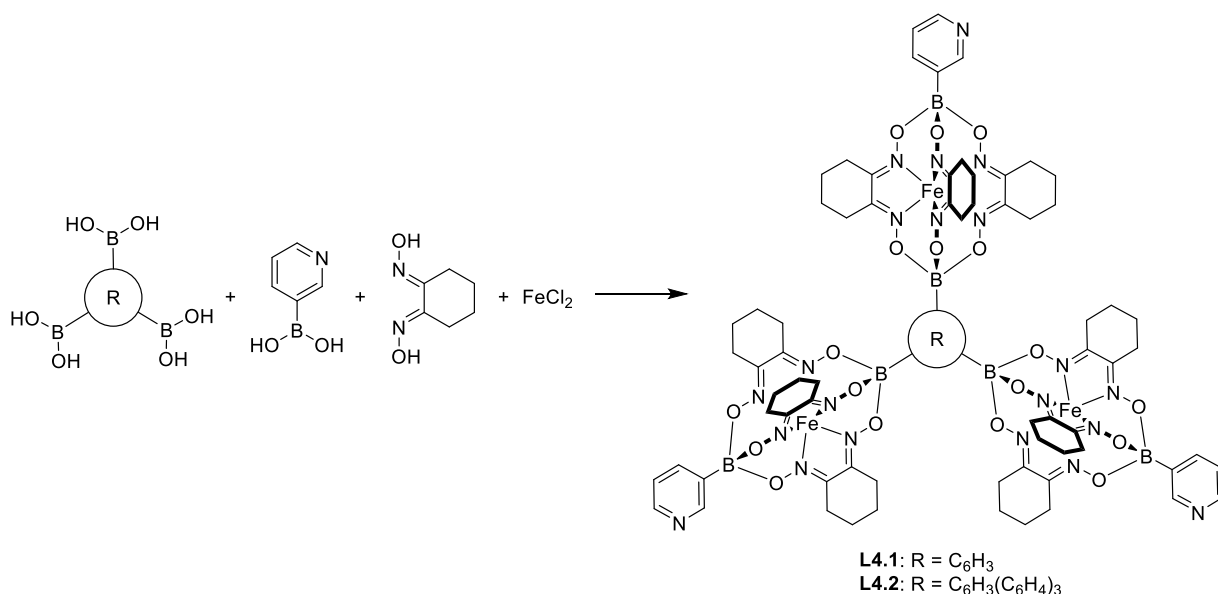
Geometrical considerations are of central importance in synthetic metallosupramolecular chemistry.^[9b, 10d, 22b, 92b, 105] Metal complexes are characterized by the number and the orientation of the available coordination sites, and ligands are categorized by the orientation of the coordinate vectors. Knowing these parameters, it is possible to make a prediction of what kind of structure will form during the self-assembly process. Besides geometry, there are other factors such as template effects^[40a, 106] or steric interactions,^[83c, 84, 79] which can influence the self-assembly process. However, geometrical analyses have been remarkably successful in predicting and rationalizing the outcome of metal-based self-assembly.

The absolute size of a ligand is irrelevant for a geometrical analysis. In principle, it should be possible to expand the size of a metallosupramolecular structure by increasing the size of the ligands, while keeping the number and orientation of the coordinate vectors constant. However, there is an obstacle. Larger ligands are typically more flexible, which makes the orientation of the coordinate vectors less defined. This flexibility could allow the formation of other assemblies along with – or instead of – the targeted structure. It should be noted that for some metal-ligand assemblies, ligand flexibility is more of an issue than for others, for example, in the case of the Pd^{II}_nL_{2n}-type coordination cages from Fujita and co-workers, as described in Chapter 1.

The combination of Pd^{II} ions with divergent, tritopic N-donor ligands is expected to give assemblies of the general formula Pd^{II}_{3n}L_{4n}. There are also examples where the donor atoms are arranged in a non-divergent manner^[101a, 102d, 107], but this is not further discussed. The assembly with the lowest number of building blocks, Pd^{II}₃L₄, can only form if some of the ligands act as chelates (two of the three N-donors bind to the same Pd^{II} ion).^[108] If the N-donor position does not allow the formation of a chelate, the resulting assembly will contain at least six Pd^{II} ions and eight ligands.^[45-47, 90d, 109] Since it is straightforward to design tritopic ligands which cannot form chelates, Pd^{II}_{3n}L_{4n} complexes appear to be a good starting point if the aim is to create particularly large assemblies based on ligands with nanoscale dimensions.

4.2 Results and discussion

For this study, we have used the tritopic ligands **L4.1** and **L4.2** (**Scheme 4.1**). These metalloligands contain three diamagnetic Fe^{II} clathrochelate complexes. We have previously shown that Fe^{II} clathrochelates are robust and versatile building blocks for supramolecular chemistry (Chapter 1). A key advantage of these complexes is the ease of synthesis, because clathrochelates are formed in metal-templated multicomponent reactions. This advantage is particularly evident for **L4.1** and **L4.2**, which were prepared by one-pot reactions using readily accessible or commercially available starting materials. Specifically, the synthesis is performed by heating a mixture of FeCl₂ (4 eq.), nioxime (12 eq.), 3-pyridylboronic acid (5 eq.) and a triboronic acid (1 eq.) in a solvent mixture of chloroform, methanol, and acetone (30:7:1) (**Scheme 4.1**). Substoichiometric amounts of the triboronic acid were used to limit the formation of oligomers. As a consequence, a mono clathrochelate complex with two pyridylboronate ester caps was the major product for this reaction. Since this complex is much smaller than **L4.1** and **L4.2**, it can be separated by size exclusion chromatography. The yields of the desired tritopic ligands are 57% (**L4.1**) and 49% (**L4.2**), respectively, when calculated based on the triboronic acid as limiting reagent.



Scheme 4.1. One-pot synthesis of the metalloligands **L4.1** and **L4.2**. The yields are calculated based on the triboronic acid as limiting reagent.

L4.1 and **L4.2** were characterized by NMR spectroscopy and high-resolution mass spectrometry.^[104] In addition, both compounds were analyzed by single crystal X-ray diffraction. The results show that the N-donor atoms of **L4.1** are approximately 2.2 nm apart (**Figure 4.1**). The presence of the additional phenyl spacers increases this value to 2.9 nm for ligand **L4.2**.

The coordination cages **4.1** and **4.2** were prepared by combining ligand **L4.1** or **L4.2** (4 eq.) with [Pd(CH₃CN)₄](BF₄)₂ (3 eq.) in DMSO-d₆ (**Scheme 4.2**). Since the ligands are poorly soluble in DMSO-d₆, suspensions were initially obtained, which turned into clear orange solutions after heating at 70 °C overnight. The ¹H NMR spectra of the solutions showed broad and not very well defined peaks, which is not unusual for large cage complexes in a viscous solvent.^[32, 33, 47, 110] Processing the data of the ¹H DOSY NMR also posed some problems related to the broad and overlapping peaks. Nonetheless, the DOSY spectra did confirm the formation of complexes with a uniform diffusion coefficient.

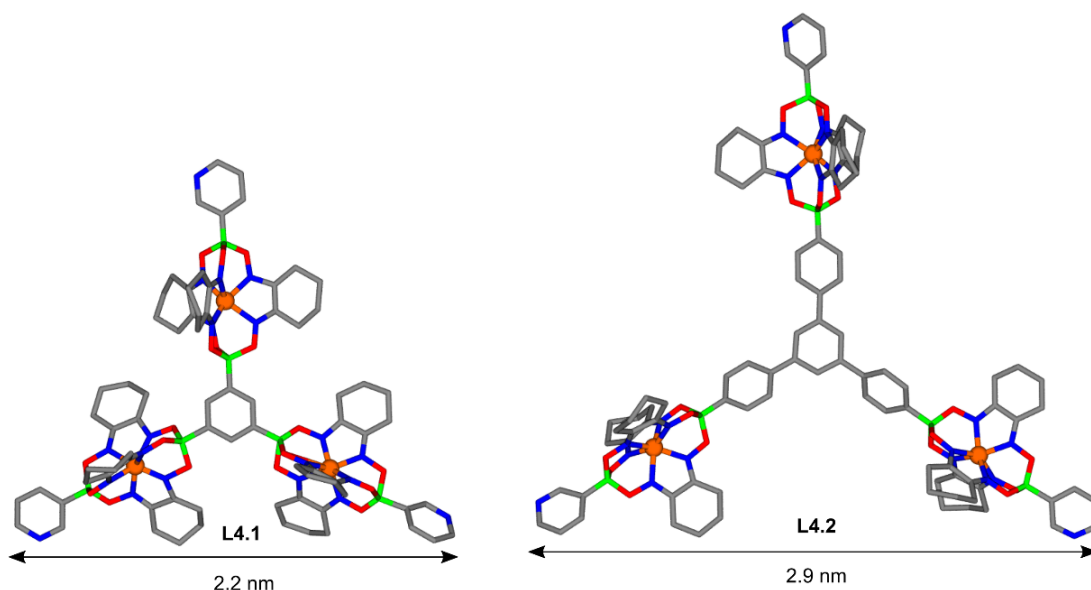
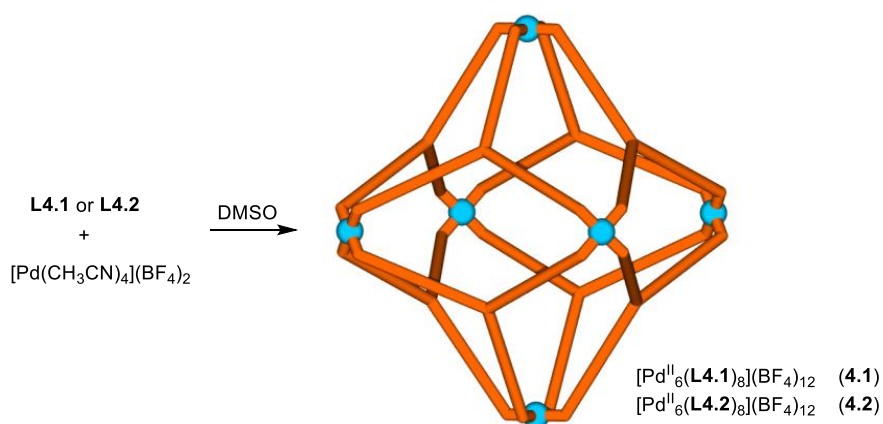


Figure 4.1. Molecular structures of the ligands **L4.1** (left) and **L4.2** (right) as determined by single crystal X-ray diffraction. Hydrogen atoms and solvent molecules are omitted for clarity. Grey: C; blue: N; green: B; red: O; and orange: Fe.



Scheme 4.2. Synthesis of the coordination cages **4.1** and **4.2**.

For both reactions, clear evidence for the formation of $\text{Pd}^{\text{II}}_6\text{L}_8$ -type complexes was obtained by mass spectrometry. The MS analyses were performed on a hybrid LTQ Orbitrap FTMS instrument operated in the positive ionization mode. The HESI-II probe in an Ion Max ion source was in-house modified in order to perform cold-spray ionization (CSI), a variant of electrospray ionization operated at low temperature.^[111] For more details about this method and the set-up can be found in the experimental section of this thesis. CSI-MS can be used to prevent decomposition of labile supramolecular structures and was shown to be crucial for such measurements. Using this methodology, the major peaks observed in the 1200–2600 m/z mass range were attributed to $[\text{Pd}^{\text{II}}_6\text{L}_8]^{12+}$ complexes with a variable number of BF_4^- anions (**Figure 4.2** and **4.3**).

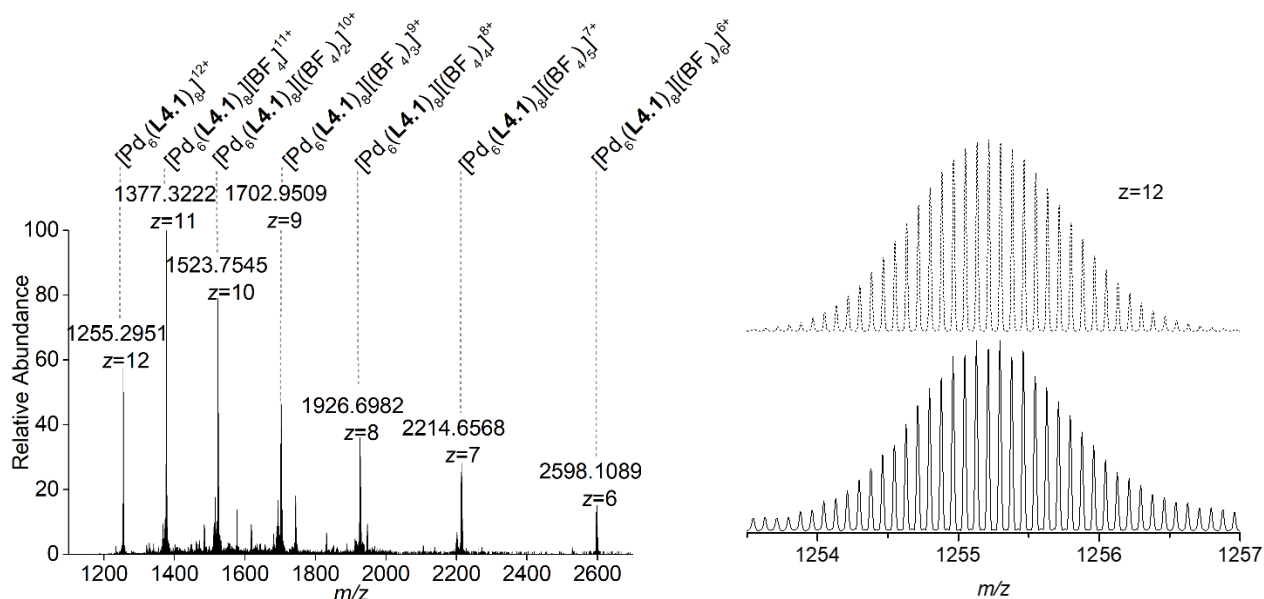


Figure 4.2. CSI-HRMS of cage **4.1** in 10% DMSO- d_6 in CH_3CN (left) and on the right a zoom-in of the 12+ charged peak around 1255 m/z in the HRMS spectrum of coordination cage **4.1** in CH_3CN (bottom), with simulated spectrum shown in dashed lines above.

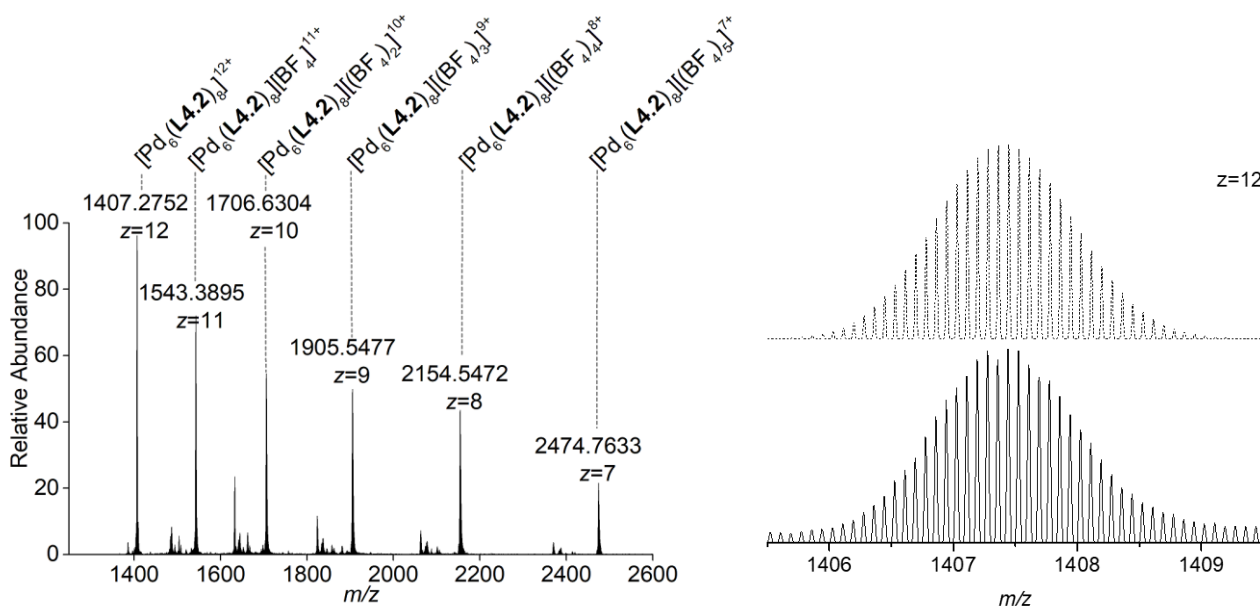


Figure 4.3. CSI-HRMS of cage **4.2** in 10% DMSO- d_6 in CH_3CN (left) and on the right a zoom-in of the 12+ charged peak around 1407 m/z in the HRMS spectrum of coordination cage **4.2** in CH_3CN (bottom), with simulated spectrum shown in dashed lines above.

Cage **4.1** was characterized by single crystal X-ray diffraction, and graphic representations of the cationic $[Pd^II_6(L4.1)_8]^{12+}$ complex are depicted in **Figure 4.4**. The location of most anions and solvent molecules is ill defined in the electron density map, and the solvent-masking program in OLEX2 was applied to treat this disorder.^[112]

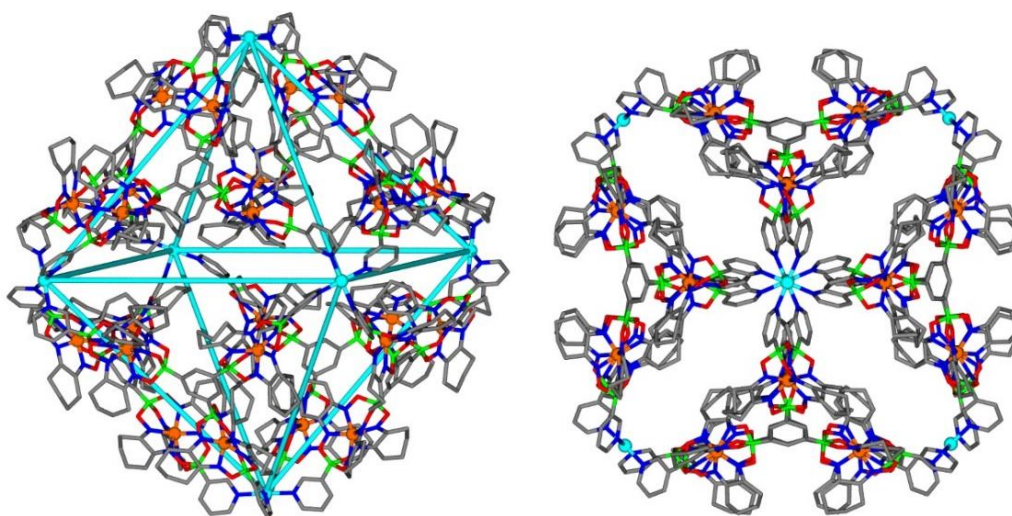


Figure 4.4. Molecular structure of cage **4.1** as determined by single crystal X-ray diffraction. Hydrogen atoms, BF_4^- anions, and solvent molecules are omitted for clarity. Grey: C; blue: N; green: B; red: O; cyan: Pd and orange: Fe.

The six Pd^{II} ions are positioned at the vertices of an octahedron, and the ligands panel the eight faces. The maximum $\text{Pd}\cdots\text{Pd}$ distance is 3.3 nm. This value is larger than what is found for other M_6L_n cages ($\text{M} = \text{Pd}^{\text{II}}, \text{Pt}^{\text{II}}$) reported in the Cambridge Crystallographic Data Center (CCDC). For an extensive search in the CCDC database, the software ConQuest was used with a CCDC database input which was updated on February 2018. The search query that was created was MN_4 (a metal center surrounded by 4 N-atoms) and MN_2P_2 (a metal center surrounded by 2 N-atoms and 2 P-atoms), with $\text{M} = \text{Pd}^{\text{II}}$ or Pt^{II} and requirements for the overall molecular formula $\text{M}>1$, $\text{N}>3$ and $\text{C}>40$. For all relevant crystal structures returned by this search (676 in total 138 with Pt vs 538 with Pd) the indication the max M-M distance was determined, which is indicated by "size" in **Figure 4.5**. The database analysis reveals that the majority of the structures have maximum $\text{Pd}\cdots\text{Pd}$ distances below 2 nm, (**Figure 4.5**, left) and only few assemblies (amongst which cage **4.1**) have a "size" of more than 3 nm.

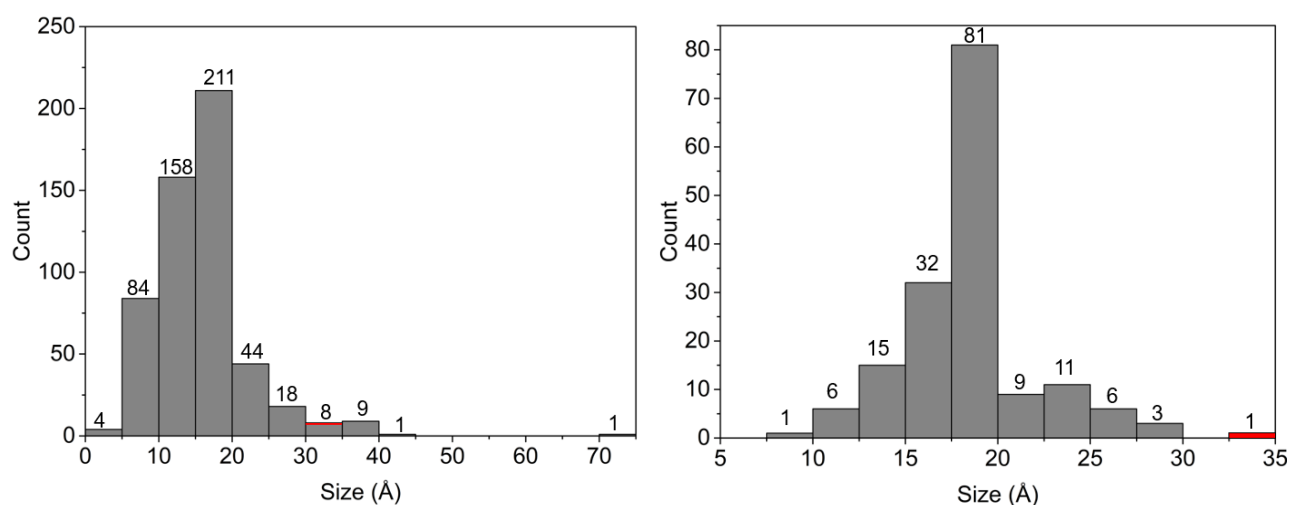


Figure 4.5. Graphical representations of a CCDC analysis of supramolecular complexes containing Pd^{II} . Left: all complexes with $\text{M}=\text{Pd}^{\text{II}}$. Right: all complexes with 6 metals (M) with $\text{M} = \text{Pd}^{\text{II}}$ or Pt^{II} . Cage **4.1** (maximum $\text{Pd}\cdots\text{Pd}$ distance of 3.3 nm) was included for the construction of the graphs in red.

Cage **4.1** features relatively small openings, because the bulky side chains of the clathrochelate complexes are in close proximity to each other. For the calculations of the size of the cavity, by the use of the VOIDOO software after removal of solvents and anions. A virtual probe with a radius of 3.0 Å, instead of the standard 1.4 Å probe size, was used, which is the smallest probe-size where the probe didn't fall out of the main cavity. The size of the cavity which is accessible by this probe, is estimated to be around $2.8 \times 10^3 \text{ Å}^3$ (**Figure 4.6**).

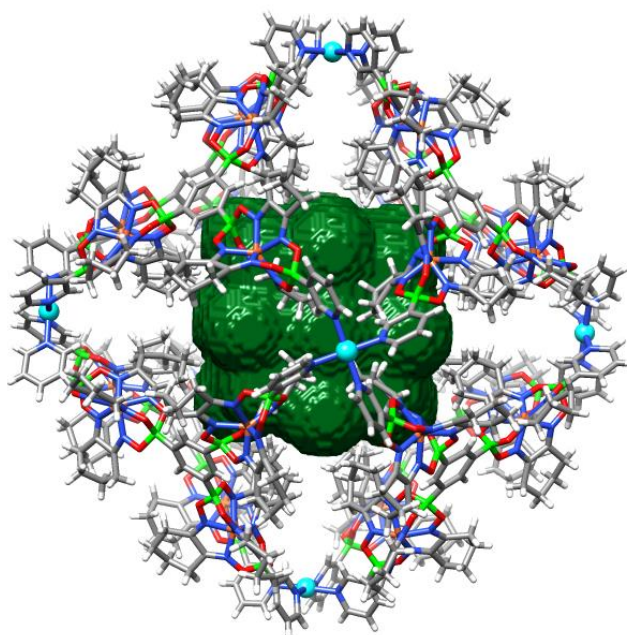


Figure 4.6. Graphical representation of the VOIDOO calculations on cages **4.1**, showing the detected void in the crystal structures. With the solvent molecules removed from the structure before calculation and the calculated void space indicated in green. Grey: C; blue: N; green: B; red: O; cyan: Pd and orange: Fe.

Single crystals for the larger cage **4.2** were also obtained. Unfortunately, we were not able to obtain diffraction data of good quality, despite testing different crystals and various experimental set-ups (including synchrotron radiation). On two occasions, it was possible to determine the size of the unit cell ($\sim 193'000 \text{ Å}^3$, see experimental section), but we were not able to solve the structure.

In order to estimate the size of cage **4.2**, we have constructed a molecular model using the Spartan software. The results show that the maximum Pd...Pd distance for this cage is around 4.2 nm. As expected, the cage shows much larger openings compared to what was found for **4.1** (**Figure 4.7**).

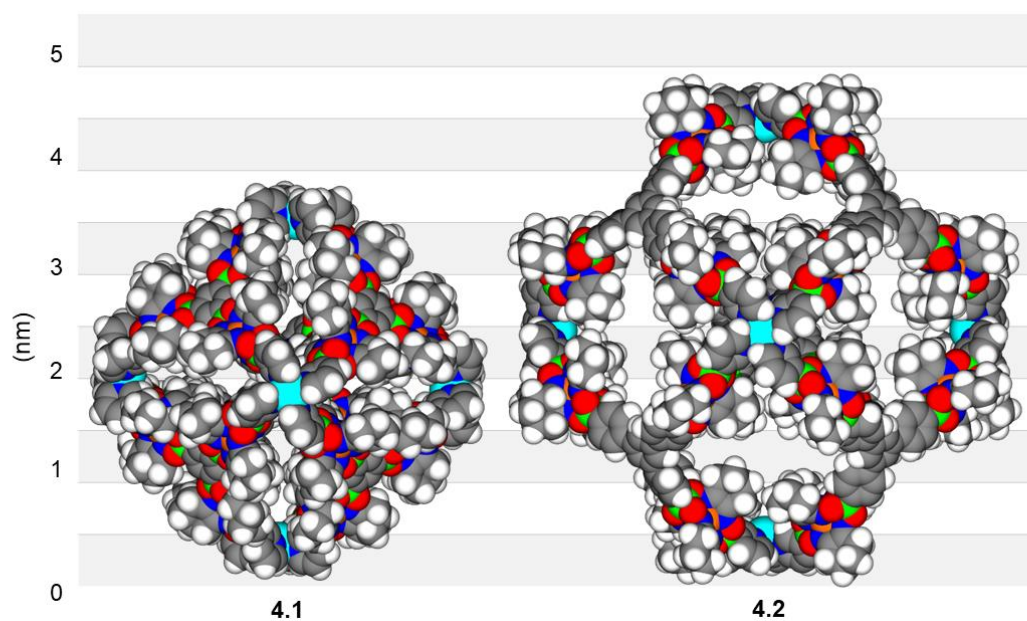


Figure 4.7. Space filling representation of cage **4.1** (left), as determined by X-ray diffraction, and of cage **4.2** (right), as obtained by molecular modelling. Solvent molecules are omitted for clarity. Grey: C; blue: N; green: B; red: O; cyan: Pd and orange: Fe.

4.3 Conclusion

To conclude, we have investigated if it is possible to inflate coordination cages by increasing the size of the ligand. On purpose, we have chosen Pd^{II}₆L₈-type cages for our study. Due to geometric constraints, these complexes are not likely to undergo a structural reorganization into smaller aggregates. We have synthesized two large, tritopic N-donor ligands by using clathrochelate complexes as key structural elements. Upon combination with Pd²⁺ ions, we were indeed able to form Pd^{II}₆L₈-type coordination cages. One cage was characterized by single crystal X-ray diffraction. With a maximum Pd...Pd distance of 3.3 nm, this complex represents the largest M₆L_n cage (M = Pd^{II}, Pt^{II}) in the CCDC database. The second cage is even larger (Pd...Pd_{max} ~ 4.2 nm), but unfortunately we were not able to obtain diffraction data of sufficient quality to solve the structure (despite using synchrotron radiation). This failure is indicative of one key challenge when working with metallocupramolecular structures of this size: the structural characterization becomes exceedingly difficult. For the present study, we have focused on structural aspects, but it is clear that very large cages offer interesting opportunities in terms of function (e.g. encapsulation of large guests).

Chapter 5 Palladium-based metal-ligand assemblies: the contrasting behavior upon addition of pyridine or acid

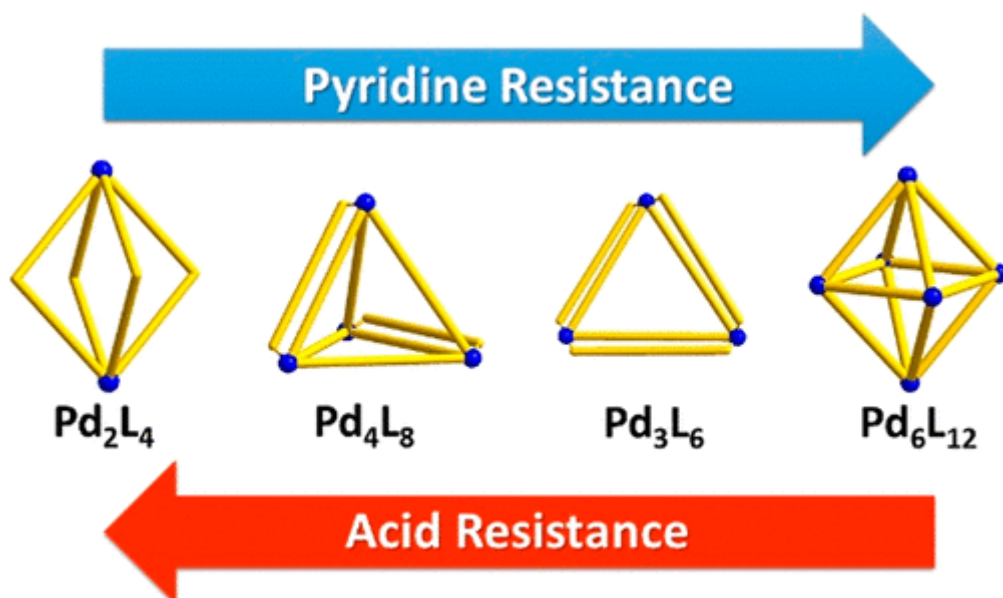
This chapter is based on published work:

"Palladium-Based Metal-Ligand Assemblies: The Contrasting Behavior Upon Addition of Pyridine or Acid"

S. M. Jansze, K. Severin, *J. Am. Chem. Soc.* **2019**, *141*, 815-819.^[113]

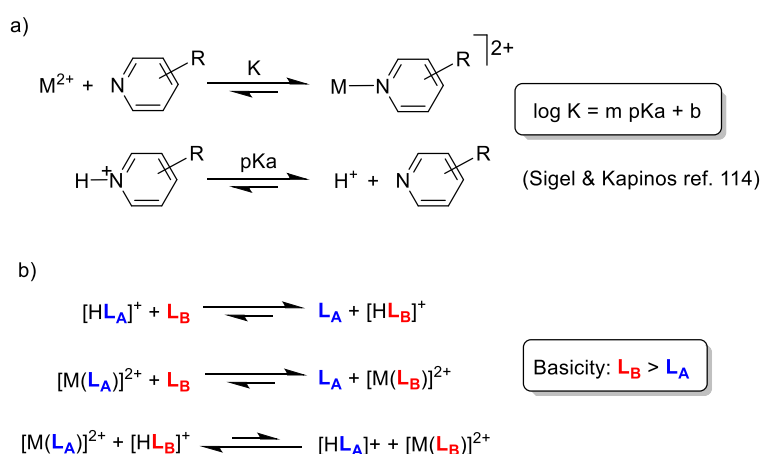
Reprinted in an adapted version with permission from the American Chemical Society and all authors.

S. M. Jansze has contributed by designing and performing experiments, writing text and constructing figures for this submitted manuscript.



5.1 Introduction

The relation between the basicity of a ligand and the stability of a metal complex has been investigated by Kapinos and Sigel for dicationic metal ions and a series of pyridine ligands.^[114] In aqueous solution (25 °C, $I = 0.5$ M NaNO₃), they observed that the logarithm of the association constant K is proportional to the pK_a value of the protonated pyridine ligand (**Scheme 5.1a**). For 3d transition metal ions and for sterically non-demanding pyridines (no *ortho* substituents), they found that the correlation factor m varies between 0.10 (Mn²⁺) and 0.42 (Cu²⁺). The fact that the correlation factor m is significantly smaller than 1 has an interesting consequence: Let's consider two ligands **L_A** and **L_B**, with **L_B** being more basic than **L_A** (**Scheme 5.1b**). Ligand **L_B** will form a more stable complex with M²⁺. When the two ligands compete for a limiting amount of M²⁺, complex [M^{II}(**L_B**)]²⁺ will be more abundant than [M^{II}(**L_A**)]²⁺. However, in the presence of an appropriate amount of acid, ligand **L_B** will be protonated first, and [M^{II}(**L_A**)]²⁺ will be the dominant metal complex in solution.



Scheme 5.1. Correlation between ligand basicity and complex stability.

We hypothesized that similar trends might be observed in non-aqueous solutions for more complex metallosupramolecular assemblies. If this would be the case, then one could use acid to switch between different metal-ligand assemblies, in a similar way as it is possible to perform an acid-induced switch from [M^{II}(**L_B**)]²⁺ to [M^{II}(**L_A**)]²⁺ (**Scheme 5.1b**).

5.2 Results and discussion

For our studies, we focused on supramolecular structures containing Pd^{2+} ions and polydentate N-donor ligands. As discussed in Chapter 1, these kinds of complexes have been studied extensively over the last years, and applications in the fields of catalysis,^[115] medicinal chemistry,^[19f-19h, 116] and materials science^[5f, 117] are currently being investigated.

There is evidence that the ligand basicity is an important factor for the stability of $[\text{Pd}^{\text{II}}_n(\text{N-donor})_m]^{2n+}$ assemblies. Mukherjee and co-workers have shown that a $[\text{Pd}^{\text{II}}_2\text{L}_4]^{4+}$ complex based on a ditopic pyridyl ligand can be converted into a macrocyclic $[\text{Pd}^{\text{II}}_3\text{L}'_6]^{4+}$ complex or a spherical $[\text{Pd}^{\text{II}}_6\text{L}''_8]^{12+}$ cage by addition of more basic imidazolyl ligands, which displace the pyridyl ligands.^[45] Furthermore, it was demonstrated by the groups of Hardie,^[109a] Chand,^[118] and Crowley^[19a] that 4-dimethylaminopyridine (DMAP) can be used to convert $[\text{Pd}_6\text{L}_8]^{12+}$ and $[\text{Pd}^{\text{II}}_2\text{L}_4]^{4+}$ structures into the more stable $[\text{Pd}^{\text{II}}(\text{DMAP})_4]^{2+}$, and that the disassembly process can be reversed by addition of *p*-toluenesulfonic acid. The latter reactions represent a more complex version of the system depicted in **Scheme 5.1b**. However, it should be noted DMAP is a highly basic N-donor ligand. In acetonitrile, the pK_a of the corresponding acid is more than 5 units higher than that of protonated pyridine (17.95 vs. 12.53, respectively).^[119] The ligands which are typically used for the construction of $[\text{Pd}^{\text{II}}_n(\text{N-donor})_m]^{2n+}$ assemblies are significantly less basic than DMAP, and it was not clear how the stability of Pd^{II} complexes is affected by more subtle changes in ligand basicity.

Figure 5.1a depicts the ditopic N-donor ligands which we have employed for our studies. The bent bipyridyl ligand **L5.1** is known to form $[\text{Pd}^{\text{II}}_2(\text{L5.1})_4]^{4+}$ complexes,^[120] whereas the linear ligand **L5.2** gives tetrahedral $[\text{Pd}_4(\text{L5.2})_8]^{8+}$ complexes^[24, 25c] upon combination with Pd^{2+} . The ligands **L5.3** and **L5.4** contain electron-donating methoxy groups in para position to the N-donor atom. Therefore, they represent more basic analogues of **L5.1** and **L5.2**. For comparison, the pK_a values of pyridine and *p*-methoxypyridine in acetonitrile differ by 1.7 units (12.53 vs 14.23, respectively).^[119] When mixed with $[\text{Pd}(\text{CH}_3\text{CN})_4](\text{BF}_4)_2$, ligand **L5.3** was found to give a dinuclear $[\text{Pd}^{\text{II}}_2(\text{L5.3})_4]^{4+}$ complex, similar to what was observed for **L5.1**. For the linear ligand **L5.4**, we observed the clean formation of a double-walled $[\text{Pd}^{\text{II}}_3(\text{L5.4})_6]^{6+}$ macrocycle instead of a tetrahedral cage as observed for **L5.2**. The reason for the preferential formation of a $[\text{Pd}^{\text{II}}_3\text{L}_6]^{6+}$ complex instead of a $[\text{Pd}^{\text{II}}_4\text{L}_8]^{8+}$ complex is presently not clear. However, it should be noted that $[\text{Pd}^{\text{II}}_3\text{L}_6]^{6+}$ and $[\text{Pd}^{\text{II}}_4\text{L}_8]^{8+}$ (tetrahedral or macrocyclic) complexes seem to be similar in energy, and small changes can trigger an interconversion as discussed in Chapter 1.

It is worth noting that trinuclear $[\text{Pd}^{\text{II}}_3\text{L}_6]^{6+}$ complexes and tetrahedral $[\text{Pd}^{\text{II}}_4\text{L}_8]^{8+}$ structures can easily be distinguished by NMR spectroscopy, because the latter have a reduced symmetry (double set of signals for the ligands). The new complexes $[\text{Pd}^{\text{II}}_2(\text{L5.3})_4]^{4+}$ and $[\text{Pd}^{\text{II}}_3(\text{L5.4})_6]^{6+}$ were also characterized by high-resolution mass spectrometry. The metalloligand **L5.5** contains a chemically inert Fe^{2+} clathrochelate complex.^[1] The reaction of **L5.5** with Pd^{2+} is known to give an octahedral $[\text{Pd}^{\text{II}}_6(\text{L5.5})_{12}]^{12+}$ complex.^[78]

The relative basicity of the ligands **L5.1–L5.5** was determined by NMR spectroscopy. For this purpose, we have performed titration experiments with pairs of ligands and trifluoroacetic acid (TFA) in either CD_3CN or a 1:1 mixture of CD_3CN and CD_2Cl_2 (**L5.4** and **L5.5** are poorly soluble in pure CD_3CN). Since it was not possible to use a common solvent for all ligands, we have not attempted to obtain quantitative values. The simple monodentate ligands DMAP, 4-methoxypyridine (MeOPy), pyridine (Py), and 3-chloropyridine (ClPy) were included as references (**Figure 5.1b**).

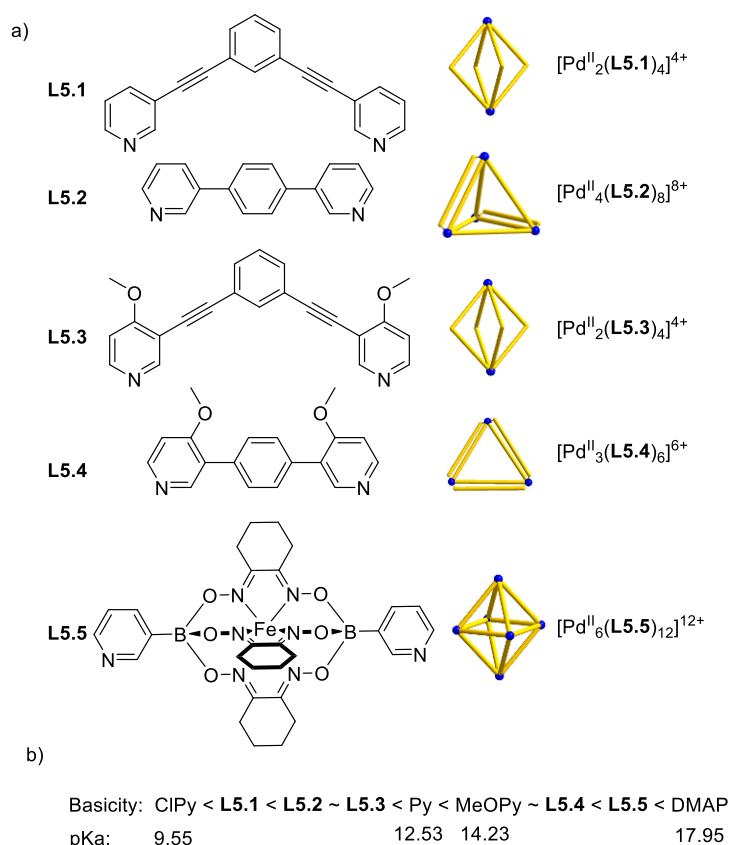
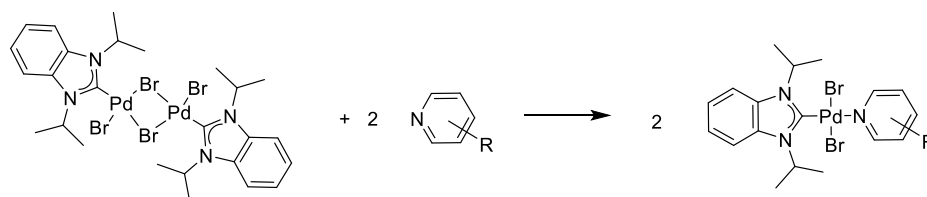


Figure 5.1. a) Structures of the N-donor ligands used in this study and the corresponding complexes with Pd^{2+} ; b) The relative basicity of the ligands. The pK_a values (acetonitrile) of the pyridine reference compounds are taken from reference 119.

The ligands **L5.1**–**L5.3** were found to be more basic than 3-chloropyridine but less basic than pyridine, with **L5.1** being the least basic of the three, and **L5.2** and **L5.3** displaying comparable basicity. Ligand **L5.4** has similar basicity to 4-methoxypyridine, but it is less basic than the metalloligand **L5.5**. The high basicity of the latter can be attributed to the presence of a tetra-coordinated boronate ester group.^[121] Still, **L5.5** was found to be significantly less basic than DMAP.

The donor strength of the ligands was evaluated by determining the Huynh Electronic Parameter (HEP).^[122] In order to do so, we have prepared Pd^{II} complexes featuring an N-heterocyclic carbene ligand in *trans* position to the N-donor (**Figure 5.2**). Solutions of the complexes in CDCl_3 were analyzed by ^{13}C NMR spectroscopy. The HEP corresponds to the chemical shift of the carbene C-atom. The value provides a quantitative measure for the σ -donor strength of a ligand, with higher numbers indicating a better donor capability. The values for **L5.1**–**L5.5** are given in **Table 5.1**. It is evident that there is a good match with the relative basicity of the ligands, with both the HEP values and the basicity increasing in the order **L5.1** < **L5.2** ~ **L5.3** < **L5.4** < **L5.5**. The HEPs of the reference compounds are aligned accordingly: the lowest value is found for 3-chloropyridine (158.7), followed by pyridine (160.1),^[123] 4-methoxypyridine (160.5), and finally DMAP (162.1).



Scheme 5.2. Reaction between the dimeric carbene complex and an N-donor ligand for determining the HEP.

Next, we have examined the relative stability of the Pd^{II} assemblies derived from **L5.1–L5.5** by performing competition experiments with pyridine. Solutions of the five complexes were prepared by dissolving an appropriate amount of [Pd(CH₃CN)₄](BF₄)₂ together with the corresponding ligand ([**L5.x**] = 9.0 mM) in a mixture of CD₃CN and CD₃NO₂ (8:2). Addition of one equivalent of pyridine-*d*₅, with respect to each N-donor atom in the assembly, resulted in partial destruction of the assembly. The extent of pyridine-induced disassembly after an equilibration time of 2 h at 60 °C was determined by ¹H NMR spectroscopy (**Table 5.1** and **Figure 5.2**).

Table 5.1. Disassembly of the Pd^{II} complexes upon addition of TFA (4 eq.) or pyridine-*d*₅ (1 eq.), and the HEP values of the ligands.^a

L#	Assembly	Disassembly (%)		HEP (ppm)
		TFA	pyridine- <i>d</i> ₅	
L5.1	[Pd ^{II} ₂ (L5.1) ₄] ⁴⁺	<5	68	159.4
L5.2	[Pd ^{II} ₄ (L5.2) ₈] ⁸⁺	44	20	159.8
L5.3	[Pd ^{II} ₂ (L5.3) ₄] ⁴⁺	49	29	159.8
L5.4	[Pd ^{II} ₃ (L5.4) ₆] ⁶⁺	65	<5	160.4
L5.5	[Pd ^{II} ₆ (L5.5) ₁₂] ¹²⁺	>90	<5	161.4

^a The disassembly experiments were performed in CD₃CN and CD₃NO₂ (8:2), whereas the HEP values were determined in CDCl₃.

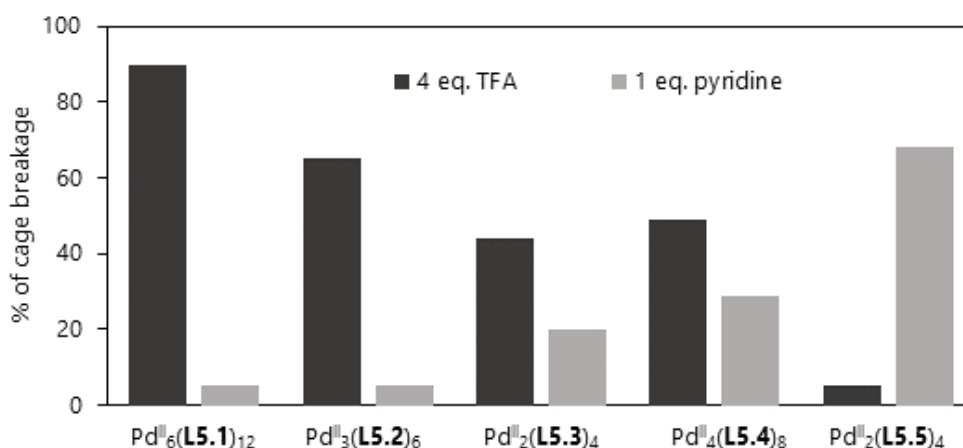
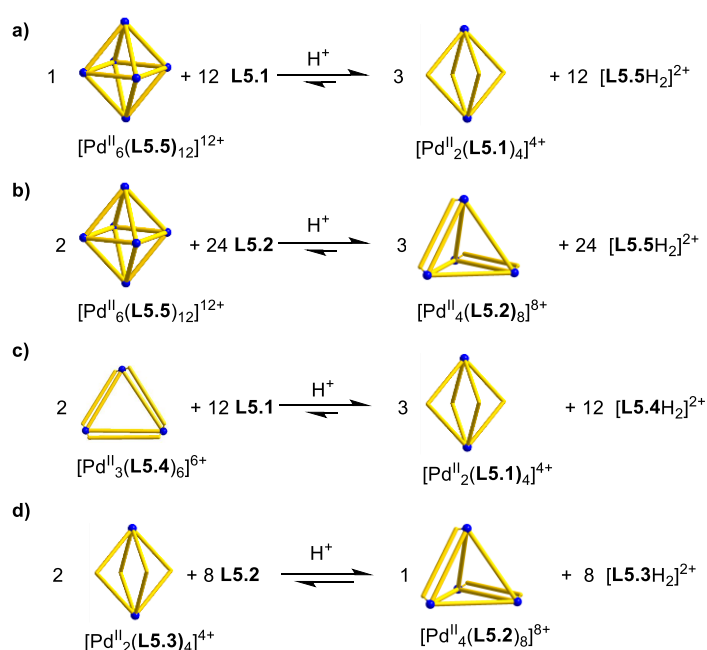


Figure 5.2. A graphical representation of the disassembly data represented in **Table 5.1**.

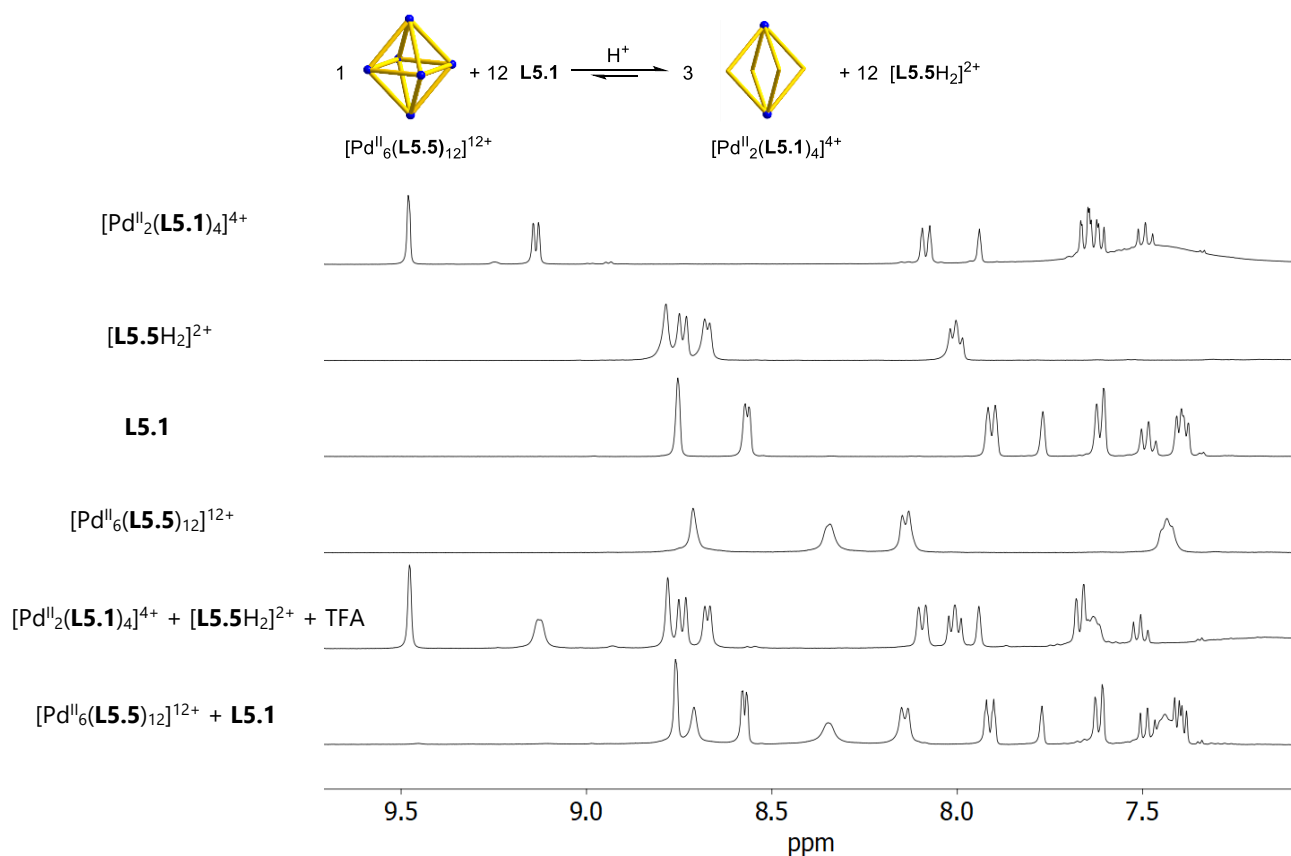
The addition of pyridine had the largest effect on the dinuclear complex $[\text{Pd}^{\text{II}}_2(\text{L5.1})_4]^{4+}$, with 68% of the assembly being broken, as determined by integration of the ^1H NMR cage signals with respect to an internal standard (TMS). Significantly smaller values of 20 and 29% were observed for $[\text{Pd}^{\text{II}}_4(\text{L5.2})_8]^{8+}$ and for $[\text{Pd}^{\text{II}}_2(\text{L5.3})_4]^{4+}$, and no significant disassembly was detected for $[\text{Pd}^{\text{II}}_3(\text{L5.4})_6]^{6+}$ and $[\text{Pd}^{\text{II}}_6(\text{L5.5})_{12}]^{12+}$ (below 5%). One can observe a correlation between the stability of the assembly and the basicity/ σ -donor strength of the N-donor, with more donating ligands leading to more stable assemblies. It is noteworthy that entropy is apparently a less important factor for the stability, because the hexanuclear complex $[\text{Pd}^{\text{II}}_6(\text{L5.5})_{12}]^{12+}$ is significantly more stable than the entropically favored dinuclear complexes $[\text{Pd}^{\text{II}}_2(\text{L5.1})_4]^{4+}$ and $[\text{Pd}^{\text{II}}_2(\text{L5.3})_4]^{4+}$.

The acid resistance of the Pd^{II} complexes was determined in a similar fashion using TFA (4 eq. with respect to the amount of N-donor atoms) instead of pyridine. Now, the correlation between stability and ligand basicity was inverted: the hexanuclear complex $[\text{Pd}_6(\text{L5.5})_{12}]^{12+}$ was found to be the most acid-sensitive assembly (nearly full disassembly), and extended acid resistance was observed for the dinuclear complex $[\text{Pd}^{\text{II}}_2(\text{L5.1})_4]^{4+}$ (**Table 5.1**).

The results of the competition experiments suggested that an acid-induced switch between different $[\text{Pd}^{\text{II}}_n\text{L}_{2n}]^{2n+}$ structures could be possible.^[9c, 82j, 124] First, we examined the conversion of the most acid-sensitive assembly $[\text{Pd}^{\text{II}}_6(\text{L5.5})_{12}]^{12+}$ into the most acid-resistant assembly $[\text{Pd}^{\text{II}}_2(\text{L5.1})_4]^{4+}$ (**Scheme 5.3a**). A prerequisite for such a switch is the structural integrity of $[\text{Pd}^{\text{II}}_6(\text{L5.5})_{12}]^{12+}$ in the presence of an excess of **L5.1**. The superior stability of $[\text{Pd}_6(\text{L5})_{12}]^{12+}$ suggested that the octahedral cage might be the preferred assembly in a competition situation with **L5.1**. When an equilibrated solution of **L5.1** (2 eq.), **L5.5** (2 eq.) and $[\text{Pd}(\text{CH}_3\text{CN})_4](\text{BF}_4)_2$ (1 eq.) in $\text{CD}_3\text{CN}/\text{CD}_3\text{NO}_2$ (8:2) was analyzed by ^1H NMR spectroscopy, we indeed observed the selective formation of $[\text{Pd}^{\text{II}}_6(\text{L5.5})_{12}]^{12+}$ along with 'free' ligand **L5.1** (**Scheme 5.4**). When TFA (4 eq.) was added to the mixture, we could observe the interconversion of the octahedral cage into the dinuclear complex $[\text{Pd}^{\text{II}}_2(\text{L5.1})_4]^{4+}$. After an equilibration time of 2 h at 60 °C, the transformation of $[\text{Pd}^{\text{II}}_6(\text{L5.5})_{12}]^{12+}$ into $[\text{Pd}^{\text{II}}_2(\text{L5.1})_4]^{4+}$ was complete (> 90% according to ^1H NMR, **Scheme 5.4**).

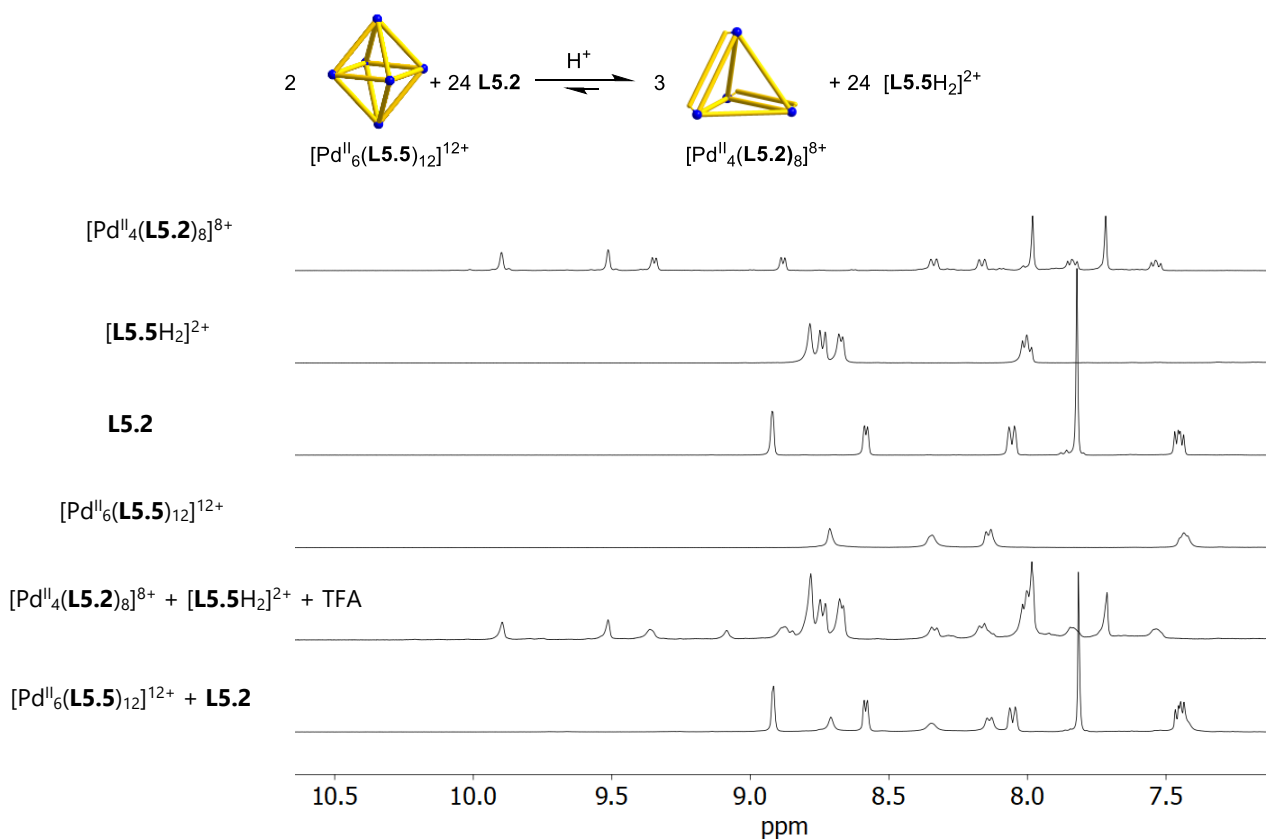


Scheme 5.3. Acid-induced interconversion of different $[\text{Pd}^{\text{II}}_n\text{L}_{2n}]^{2n+}$

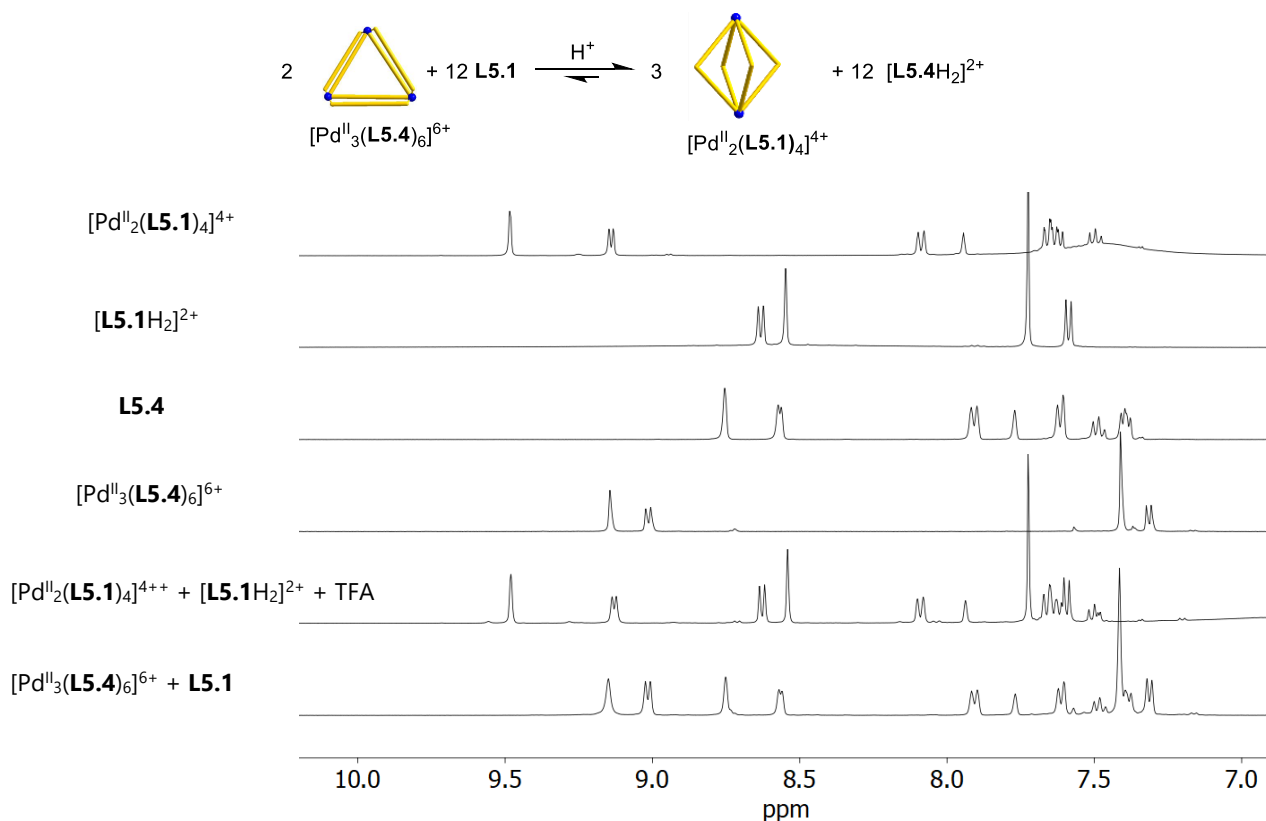


Scheme 5.4. Aromatic part of the ¹H NMR spectra (400 MHz, CD₃CN/CD₃NO₂ 8:2) of a mixture of [Pd(CH₃CN)₄](BF₄)₂ (1 eq.), ligand **L5.1** (2 eq.), and ligand **L5.5** (2 eq.) before (spectrum on the bottom) and after (spectrum directly above) addition of the TFA (2 eq. per pyridine group present). The relevant reference spectra are shown above.

An acid-induced interconversion of $[\text{Pd}^{\text{II}}_n\text{L}_{2n}]^{2n+}$ structures was also possible for the ligand pairs **L5.5/L5.2** and **L5.4/L5.1**. In the former case, ligand exchange transformed an octahedral cage into a tetrahedral cage (**Scheme 5.5**), whereas in the latter case, a double-walled triangle was converted into a dinuclear cage structure (**Scheme 5.6**).

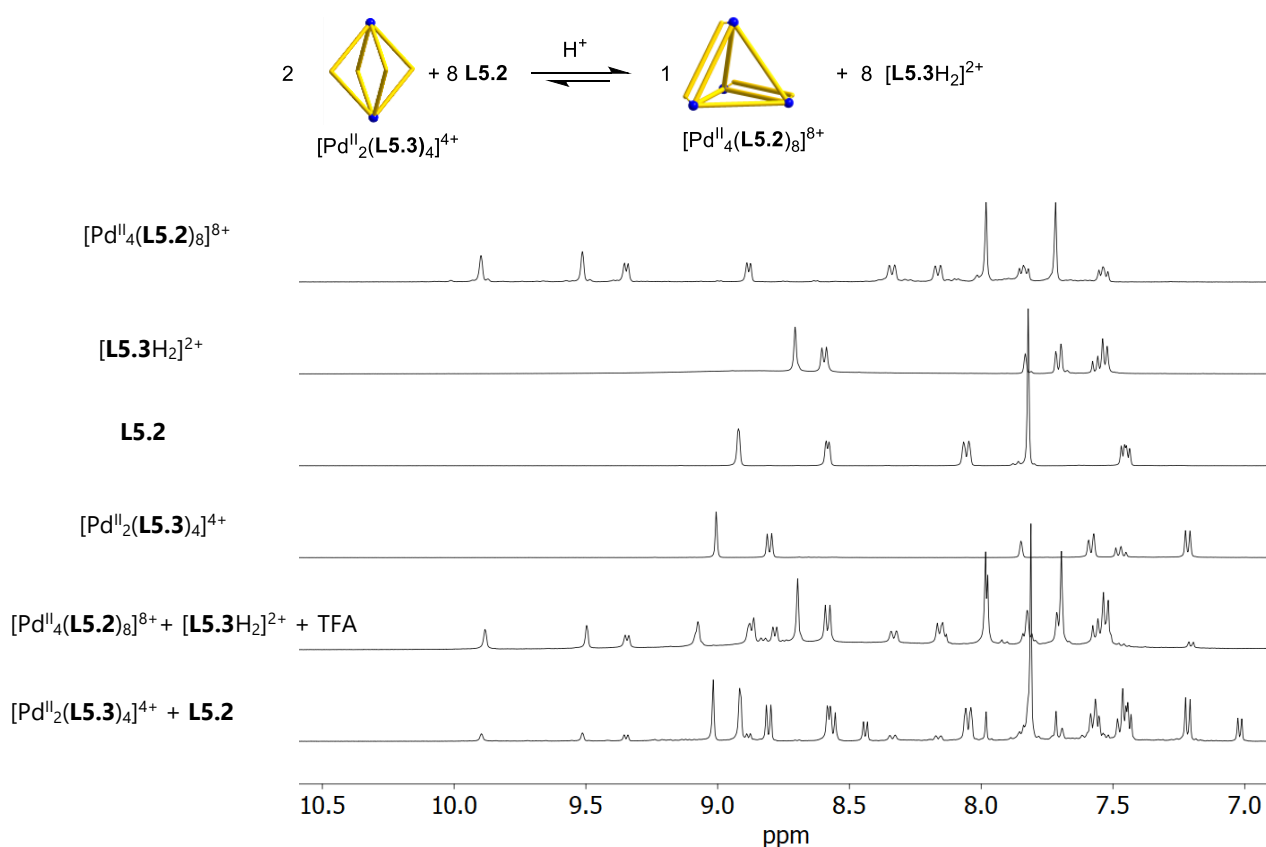


Scheme 5.5. Aromatic part of the ^1H NMR spectra (400 MHz, $\text{CD}_3\text{CN}/\text{CD}_3\text{NO}_2$ 8:2) of a mixture of $[\text{Pd}(\text{CH}_3\text{CN})_4](\text{BF}_4)_2$ (1 eq.), ligand **L5.2** (2 eq.), and ligand **L5.5** (2 eq.) before (spectrum on the bottom) and after (spectrum directly above) addition of the TFA (2 eq. per pyridine group present). The relevant reference spectra are shown above.



Scheme 5.6. Aromatic part of the ^1H NMR spectra (400 MHz, $\text{CD}_3\text{CN}/\text{CD}_3\text{NO}_2$ 8:2) of a mixture of $[\text{Pd}(\text{CH}_3\text{CN})_4](\text{BF}_4)_2$ (1 eq.), ligand **L5.1** (2 eq.), and ligand **L5.4** (2 eq.) before (spectrum on the bottom) and after (spectrum directly above) addition of the TFA (2 eq. per pyridine group present). The relevant reference spectra are shown above.

Furthermore, we examined the behavior of a mixture containing **L5.2** and **L5.3** (Scheme 5.3d). These ligands display a comparable basicity and, according to the HEP, the same σ -donor strength (Table 5.1). When combined with $[\text{Pd}(\text{CH}_3\text{CN})_4](\text{BF}_4)_2$, the ^1H NMR spectrum showed the preferential formation of the entropically favored dinuclear complex $[\text{Pd}^{\text{II}}_2(\text{L5.3})_4]^{4+}$, but small amounts of the tetramer $[\text{Pd}^{\text{II}}_4(\text{L5.2})_8]^{8+}$ could also be detected. No ligand scrambling was observed by ^1H NMR or MS. Upon addition of acid, the relative abundance was inverted, with $[\text{Pd}^{\text{II}}_4(\text{L5.2})_8]^{8+}$ being the dominant metal-ligand assembly in solution (Scheme 5.7). These results show that even small differences in ligand basicity can be exploited to generate a large bias in the structures expressed by self-assembly. Other ligand combinations like **L5.1/L3** and **L5.2/L5.4** were also tested, but ligand scrambling was observed, and more detailed investigations were therefore not performed.



Scheme 5.7. Aromatic part of the ^1H NMR spectra (400 MHz, $\text{CD}_3\text{CN}/\text{CD}_3\text{NO}_2$ 8:2) of a mixture of $[\text{Pd}(\text{CH}_3\text{CN})_4](\text{BF}_4)_2$ (1 eq.), ligand **L5.2** (2 eq.), and ligand **L5.3** (2 eq.) before (spectrum on the bottom) and after (spectrum directly above) addition of the TFA (2 eq. per pyridine group present). The relevant reference spectra are shown above. As can be observed there is no complete self-sorting or switching in this case; the description on the left side indicates the major species in solution.

5.3 Conclusion

In summary, we have investigated the stability of five different $[\text{Pd}^{\text{II}}_n(\text{N-donor})_{2n}]^{2n+}$ assemblies (four cages and one macrocycle) by performing disassembly experiments with pyridine and TFA. The susceptibility towards degradation by pyridine was found to be inversely correlated to the acid resistance. The most acid-resistant complex $[\text{Pd}^{\text{II}}_2(\text{L5.1})_4]^{4+}$ was disassembled to a large extent upon addition of pyridine (68%), whereas the most pyridine-resistant cage $[\text{Pd}^{\text{II}}_6(\text{L5.5})_{12}]^{12+}$ was very sensitive to acid. The contrasting behaviour upon addition of pyridine or TFA, can be linked to the basicity of the N-donor ligand. Interestingly, ligand basicity seems to be a more dominant factor for the stability of the assembly than entropy. For example, we observed the selective formation of the hexanuclear cage $[\text{Pd}^{\text{II}}_6(\text{L5.5})_{12}]^{12+}$ in the presence of **L5.1**, even though **L5.1** can form the entropically favored dinuclear $[\text{Pd}^{\text{II}}_2(\text{L5.1})_4]^{4+}$ complexes.

The context-dependent stability of Pd^{II} -based metal-ligand assemblies should be considered for applications of these complexes as drug delivery systems, as cages based on highly basic ligands are expected to be more resistant to detrimental ligand exchange reactions with competing bio-ligands. On the other hand, these cages would be more susceptible to releasing their 'cargo' under the more acidic conditions of a tumor cell.^[125] The possibility to use the pH for a (reversible) switch between different supramolecular structures could also be of interest for application in materials science.^[126] Evidently, the stability of metal-ligand assemblies is influenced by numerous factors, the ligand basicity/donor strength being just one of them. Therefore, it will be interesting to investigate if an inverse correlation between acid and pyridine resistance can be observed for metallosupramolecular structures other than $[\text{Pd}^{\text{II}}_n\text{L}_{2n}]^{2n+}$ complexes.

Chapter 6 Reversible disassembly of metallosupramolecular structures mediated by a metastable-state photoacid

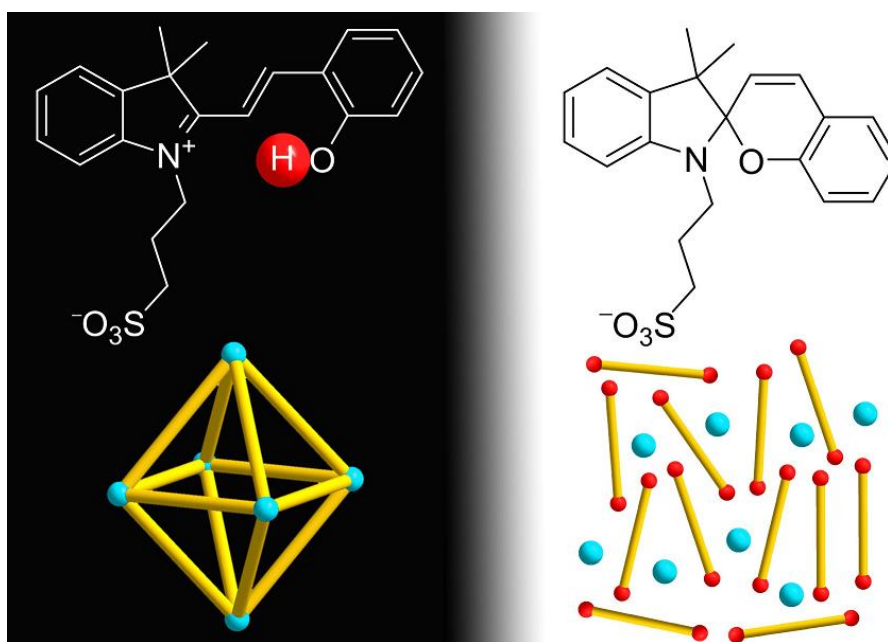
This chapter is based on published work:

"Reversible disassembly of metallosupramolecular structures mediated by a metastable-state photoacid"^[127]

S. M. Jansze, G. Cecot, K. Severin, *Chemical Science* **2018**, 9, 4253-4257.

Reprinted in an adapted version with permission from the Royal Society of Chemistry and all authors.

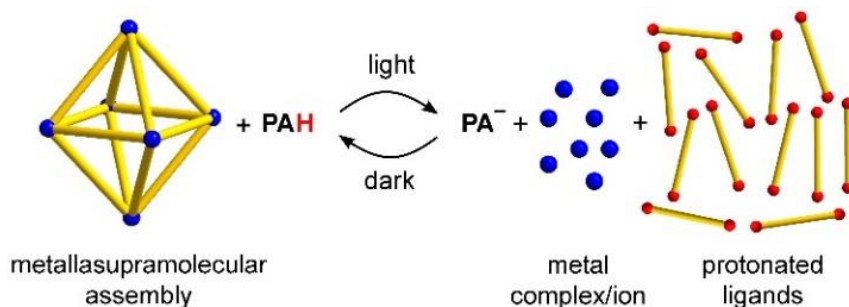
S. M. Jansze has contributed by designing and performing experiments, writing text and constructing figures for this publication.



6.1 Introduction

The controlled manipulation of supramolecular structures with light represents an interesting option to create functional nanoscale devices.^[124, 128] A common strategy to implement light-responsiveness in *metal-ligand assemblies* is the utilization of photochromic ligands. Light allows altering the geometry of the ligand, which in turn may result in a structural reconfiguration of the metallasupramolecular assembly.^[5c, 9c] For example, bipyridyl ligands containing dithienylethene units have been used for the light-induced conversion of a $\text{Pd}^{\text{II}}_{24}\text{L}_{48}$ capsule into small metallamacrocycles,^[129] to create $\text{Pd}^{\text{II}}_2\text{L}_4$ cages with light-dependent host-guest chemistry,^[21] and for the photo-induced sol-gel switching of a metallogel.^[130] Ligands containing the azobenzene motif were employed to modulate the host-guest chemistry of a spherical $\text{Pd}^{\text{II}}_{12}\text{L}_{24}$ complex,^[37] to alter the solubility of a coordination cage,^[131] and to control the catenation of a palladium metallacycle.^[132]

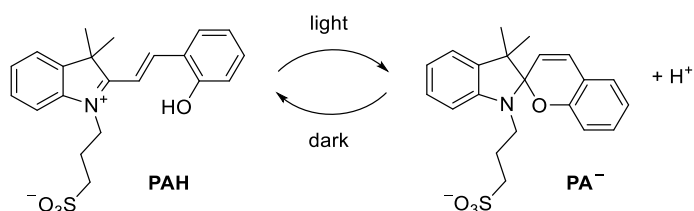
The construction of light-responsive metal-ligand assemblies with photochromic ligands is not straightforward. The design of suited ligands can be challenging, and the preparation of the ligands may involve substantial synthetic efforts. In this study, we describe an alternative and more general approach to render metal-ligand assemblies light-responsive: the addition of a metastable-state photoacid. Based on the knowledge presented in the previous chapter, we demonstrate that the acidification by the photoacid upon irradiation can be used for the disassembly of for the switching between metallasupramolecular structures.^[49, 133] The process is reversible, and the original metallasupramolecular structures form again in the dark at room temperature (**Scheme 6.1**).



Scheme 6.1. Reversible disassembly of metallasupramolecular structures by means of a metastable-state photoacid (PAH). The M_6L_{12} coordination cage is used as a representative example of a metal-ligand assembly

6.2 Results and Discussion

For our investigations, we decided to use the merocyanine photoacid **PAH**, the structure of which is depicted in **Scheme 6.2**. Upon exposure to violet light (425 nm), **PAH** undergoes a ring-closing reaction to give the spiropyran **PA⁻**, along with liberation of a proton (**Scheme 6.2**).^[134] The spiropyran form is metastable and accumulates under irradiation. As a result, a pH drop of more than 2 units can be achieved. When light irradiation is stopped, the merocyanine form **PAH** is regenerated.



Scheme 6.2. Irradiation with light converts the merocyanine **PAH** into the spiropyran **PA⁻**, with concomitant liberation of a proton.

The metastable-state photoacid **PAH** was introduced by Liao and co-workers in 2011.^[135] Since then, **PAH** and structurally related compounds have been used in the context of supramolecular chemistry. Applications include the light-induced complexation of a pyridinium salt by a macrocyclic receptor,^[136] the switching of a rotaxane-based molecular shuttle,^[137] the light-controlled reversible self-assembly of nanorods,^[138] the reversible chromism of guests in coordination cages,^[139] the modulation of a hydrazine switch,^[140] the reversible photo-induced gel-sol transition of a dipeptide gel,^[141] and the controlled aggregation of nanoparticles,^[142] among others.^[143, 134] We wanted to explore if **PAH** is also suited for controlling the structures of metal-ligand assemblies by light.

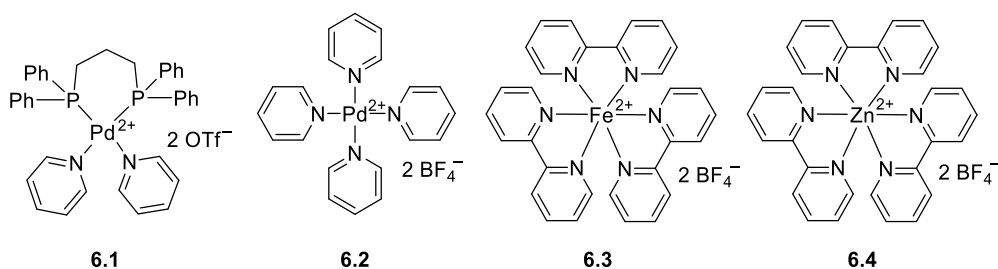
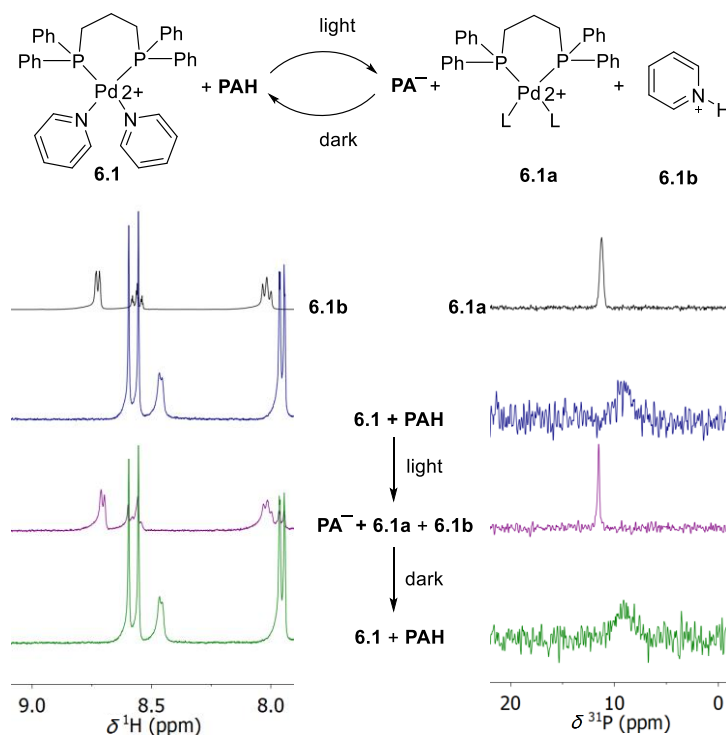


Figure 6.1. Chemical structures of model complexes **6.1–6.4**.

First, we performed test reactions with the Pd^{II} complex [(dppp)Pd(py)₂](OTf)₂ (**6.1**). Complex **6.1** features a strongly bonded 1,3-bis(diphenylphosphino)propane (dppp) ligand and two labile pyridine (py) ligands (**Figure 6.1**). We chose complex **6.1**, because Pd^{II} complexes with chelating diphosphine ligands are popular building blocks in metallasupramolecular chemistry.^[9a, 9b] As connecting units, polypyridyl ligands are often employed, and the pyridyl ligands in **6.1** are surrogates for more intricate ligands. A solution of complex **6.1** (125 μM) and **PAH** (8 equiv.) was prepared in the dark using a mixture of CD₃CN and D₂O (8:2) as the solvent. The solution was then irradiated for 20 minutes with violet light using a commercial LED panel (λ = 425 nm). After irradiation, the sample was immediately analyzed by ¹H and ³¹P NMR spectroscopy, and further NMR spectra were recorded after 8 hours in the dark (**Scheme 6.3**).

The ^1H NMR spectrum of the mixture before irradiation shows two doublets in the region between 7.5 and 9 ppm, which can be assigned to the photoacid **PAH** (Scheme 6.3, left side). In addition, one can observe a doublet at ~ 8.5 ppm, resulting from the pyridine NCH protons. Irradiation leads to the nearly complete disappearance of the two **PAH** signals. The NCH signal of the bound pyridine ligands is no longer observable. Instead, three new signals appear. These peaks can be attributed to the formation of protonated pyridine (**6.1b**), as evidenced by comparison with a reference sample of pyridinium chloride (Scheme 6.3, spectrum on the top left side). After 8 hours in the dark, the NMR spectrum of the sample is indistinguishable from that of the sample before irradiation. The ^{31}P NMR spectrum of the starting mixture shows a broad peak at ~ 9 ppm, which is converted to a sharper signal at ~ 12 ppm after irradiation (Scheme 6.3, right side). A similar signal is observed when complex $[(\text{dppp})\text{Pd}](\text{OTf})_2$ is dissolved in $\text{CD}_3\text{CN}/\text{D}_2\text{O}$. We attribute this signal to a complex $[(\text{dppp})\text{Pd}^{\text{II}}\text{L}_2]$ (**6.1a**), with L being either solvent and/or triflate. Again, the spectrum converts back to that of the starting mixture when the sample is kept in the dark. Taken together, the data are strong evidence for a light-induced displacement of the pyridine ligands, which is fully reversed in the dark.



Scheme 6.3. Irradiation of a mixture of complex **6.1** (125 μM) and the photoacid **PAH** (8 equiv.) in $\text{CD}_3\text{CN}/\text{D}_2\text{O}$ (8:2) by violet light results in the displacement of the pyridyl ligands as evidenced by the ^1H NMR (left side) and ^{31}P NMR spectra (right side). The triflate anions of **6.1** are not shown for clarity. L indicates solvent or OTf^- .

Similar test reactions were performed with the model complexes $[(\text{py})_4\text{Pd}^{\text{II}}](\text{BF}_4)_2$ (**6.2**), $[(\text{bipy})_3\text{Fe}^{\text{II}}](\text{BF}_4)_2$ (**6.3**), and $[(\text{bipy})_3\text{Zn}^{\text{II}}](\text{BF}_4)_2$ (**6.4**) (bipy = 2,2'-bipyridyl) (Figure 6.1). These kind of coordination motifs are also found in numerous metallasupramolecular assemblies.^[10d, 15, 17a, 144] As it was observed for **6.1**, it was possible to dissociate the N-donor ligands by irradiation with light, and re-complexation was observed in the dark.^[127] For the Pd^{II} complex **6.2** and the Zn^{II} complex **6.4**, the photo-induced conversion was very high ($> 80\%$), whereas for the Fe^{II} complex **6.3**, only partial disassembly was observed ($\sim 46\%$ of complex **6.3** remained intact). We have also attempted to break complex **6.3** with a Brønsted acid, namely trifluoroacetic acid (TFA, 4 equiv. with respect to the N-donor groups). As with **PAH**, only partial disassembly was observed, indicating that the Fe^{II} complex is less susceptible to an acid-induced ligand displacement.

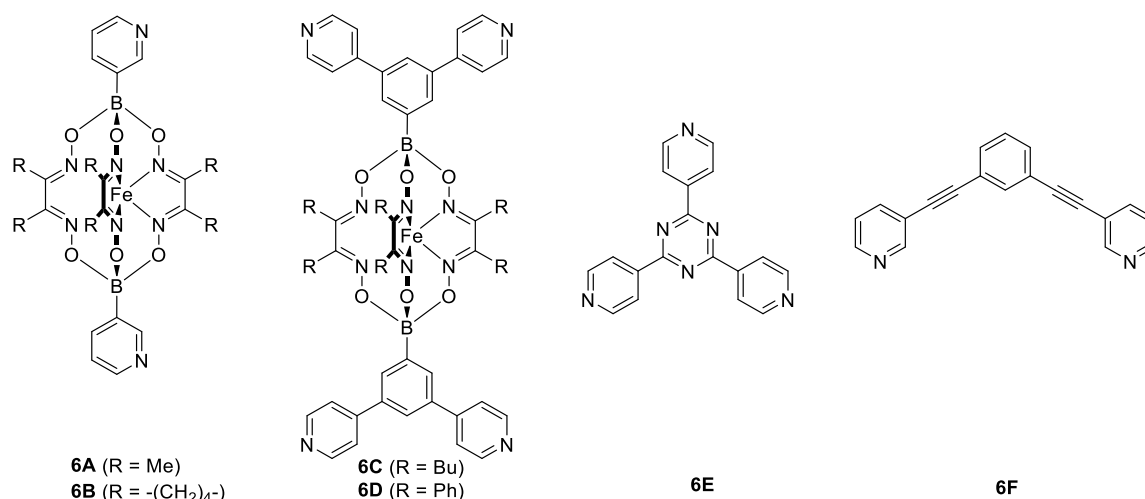


Figure 6.2. Structures of the pyridyl ligands **6A–6F**.

Encouraged by the results with the model complexes **6.1–6.4**, we next examined reactions with larger and structurally more complex metal-ligand assemblies. Six different metallasupramolecular structures were prepared using the pyridyl ligands depicted in **Figure 6.2**. More specifically, we have prepared an octahedral $Pd^{II}_6L_{12}$ cage with $[Pd^{II}(py^*)_4]^{2+}$ (py^* = substituted pyridine) complexes at the vertices, bridging ligands **6A**, and a $[B(p-C_6H_4F)_4]^-$ guest molecule (**6.5**),^[78] two $M^{II}_6L_4$ cages with gyrobifastigium-like geometry and $[(dppp)Pd^{II}(py^*)]^{2+}$ or $[(dcpm)Pt^{II}(py^*)]^{2+}$ complexes connecting the tetratopic ligand **6C** (**6.6** and **6.7**, $dcpm$ = bis(dicyclohexylphosphino)methane),^[66b, 80a] a coordination barrel containing $[(dcpm)Pt^{II}(py^*)]^{2+}$ complexes and ligand **6D** (**6.8**),^[80a] a trigonal prismatic Ru complex with trispyridyl ligand **6E** (**6.9**), and an $Pd^{II}_2L_4$ cage based on ligand **6F** with $[Pd^{II}(py^*)_4]^{2+}$ vertices (**6.10**)²⁶ (**Figure 6.3**).

First test reactions with complex **6.5** and TFA (2 equivalences to N-donor) showed that the complex can be fully disassembled by acid. We then set up an experiment similar to what has been described for the model complexes. Assembly **6.5** was dissolved together with an excess of the photoacid PAH in a mixture of CD_3CN and D_2O (8:2) in the dark. After irradiation with violet light, we immediately recorded 1H and ^{19}F NMR spectra, followed by additional spectra after a waiting period of 8 hours in the dark. Preliminary studies revealed that the addition of small amounts of NaCl facilitated the disassembly process, and all subsequent experiments with **6.5** were performed with six equivalents of NaCl. It is worth noting that chloride ions are known for their ability to decompose Pd^{II} cages.^[19a, 145, 42] For complex **6.5**, six equivalents of NaCl were not sufficient to induce detectable decomposition, even though we were able to disrupt the assembly at higher NaCl concentrations. The beneficial effect of small amounts of NaCl for the photoswitching process might be due to stabilization of the Pd^{II} ions after ligand displacement.

The 1H NMR spectrum after irradiation indicates the acid-induced de-complexation of the pyridyl ligands (**Scheme 6.4**, left side). Additional evidence for the disassembly of the octahedron was obtained by analyzing the ^{19}F NMR spectra (**Scheme 6.4**, right side). The initial spectrum shows two signals, one for the encapsulated $[B(p-C_6H_4F)_4]^-$ guest molecule, and one for non-bound $[B(p-C_6H_4F)_4]^-$. After irradiation, only 'free' $[B(p-C_6H_4F)_4]^-$ (**6.5c**) is observed. In the dark, the $Pd^{II}_6L_{12}$ cage is re-formed, as corroborated by the 1H NMR spectrum, and the ^{19}F NMR signal of the encapsulated borate anion. Overall, it is evident that light irradiation leads to a destruction of the metallasupramolecular structure and liberation of the guest. The process is reversible: in the dark, the cage with the encapsulated guest is formed again.

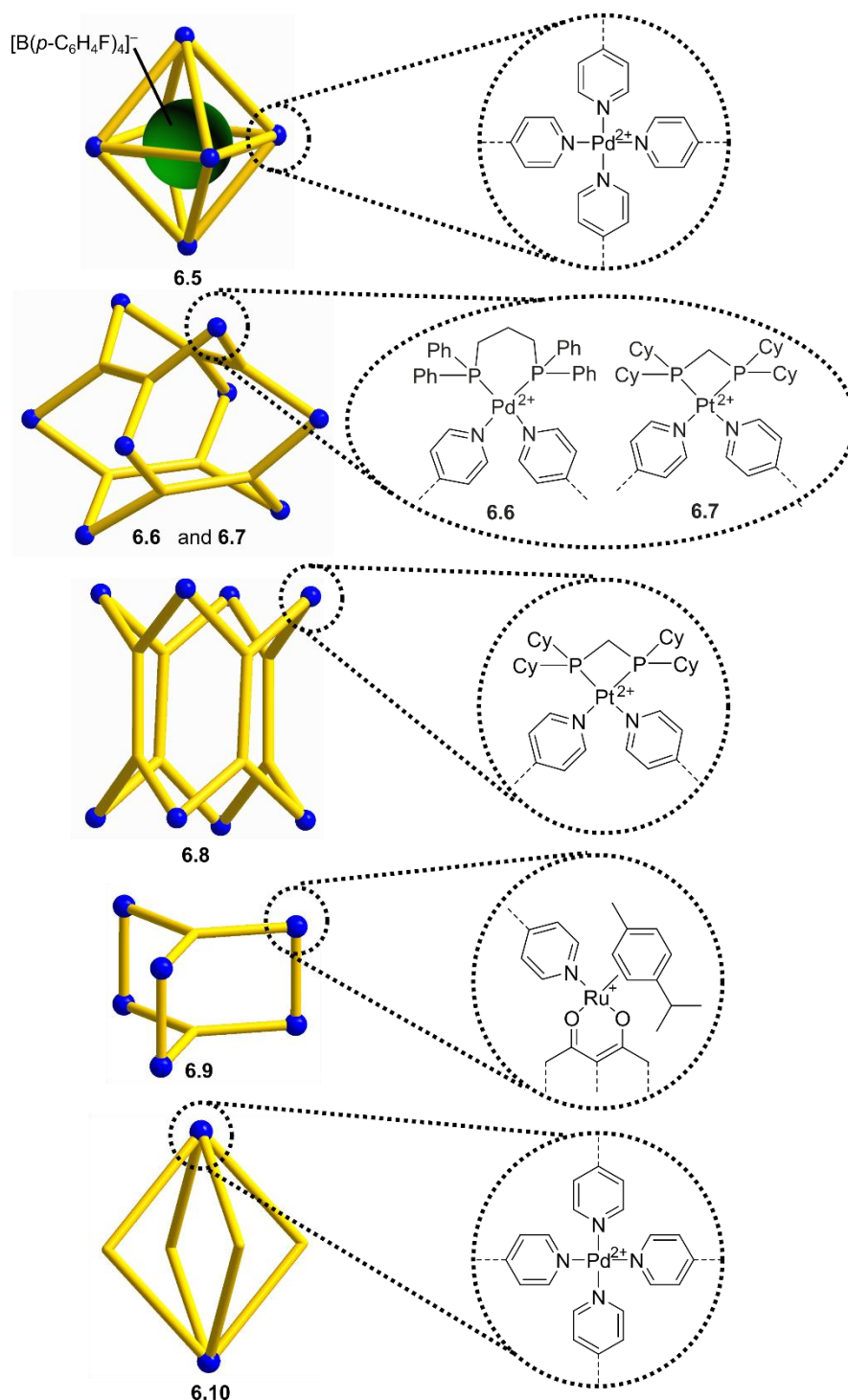
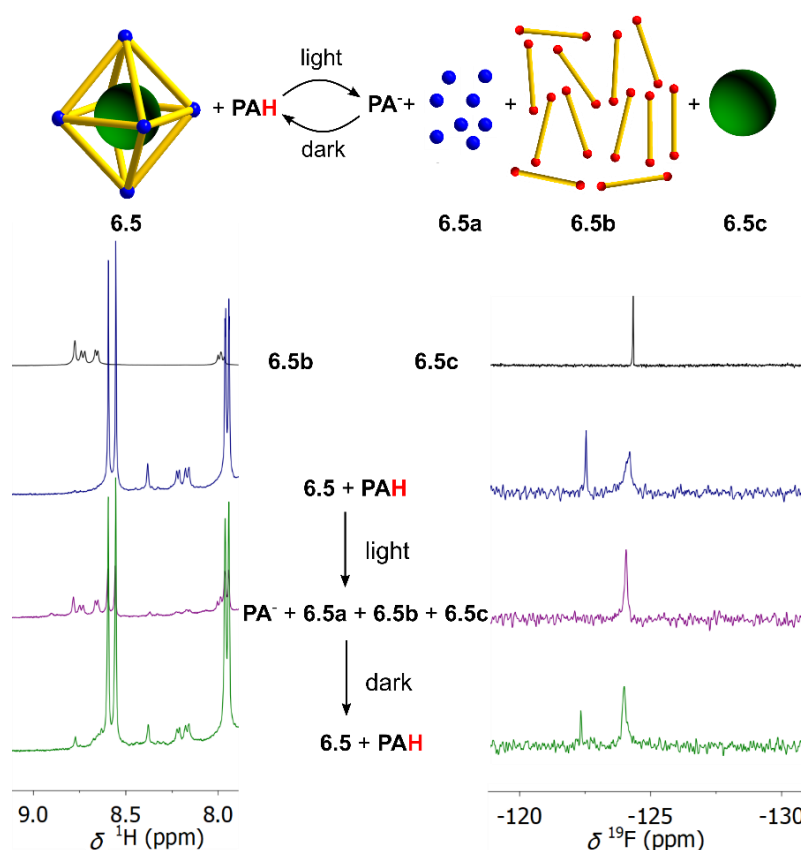


Figure 6.3. Schematic representation of the metallasupramolecular structures used in this study.

Experiments with the assemblies **6.6–6.10** gave similar results: a reversible, light-induced disassembly of the cage structures was observed by NMR spectroscopy in all cases.^[127] For **6.6**, **6.7**, and **6.8**, the switching efficiency was found to be very high, with at least 80% of the cages being disassembled by the photoacid. For **6.9** and **6.10**, the process was less efficient, with only 16% (**6.9**) and 45% (**6.10**) of the cage structures being disrupted.



Scheme 6.4. Irradiation of a mixture of cage **6.5** (10 μ M), NaCl (60 μ M), and the photoacid **PAH** (8 equiv. with respect to each bipyridyl ligand) in $\text{CD}_3\text{CN}/\text{D}_2\text{O}$ (8:2) by violet light results in disassembly of the cage and liberation of the $[\text{B}(p\text{-C}_6\text{H}_4\text{F})_4]^-$ guest (green ball) as evidenced by the ^1H NMR (left) and ^{19}F NMR spectra (right). Details about the bridging ligand (yellow) are given in the ESI.

The difference in switching efficiency between cage **6.5** (> 80%) and cage **6.10** (45%) is intriguing, given that both assemblies are based on $[\text{Pd}^{\text{II}}(\text{py}^*)_4]^{2+}$ complexes. We were able to identify two factors which contribute to the reduced switching efficiency observed for **6.10**: First, ^1H NMR spectrometry revealed the photoacid binds weakly to cage **6.10**,^[146, 18d, 127] and this interaction is expected to stabilize the assembly. Such an interaction was not observed for cage **5**. Second, as also described in the previous chapter, the pyridyl ligand **6A** used for cage **6.5** is more basic than the pyridyl ligand **6F** used for cage **6.10**. Consequently, acid-induced disassembly is favored for cage **6.5**.

The disassembly process was fully reversible in all cases. Kinetic investigations at 298 K showed that all assemblies are re-formed with half-lives between 20 and 70 minutes. For comparison: the photoacid alone switches back with $t_{1/2}$ of 2.4 minutes under these conditions ($\text{CH}_3\text{CN}/\text{H}_2\text{O}$, 8:2), indicating that the re-formation of the coordination complex is the rate-limiting step. The re-assembly of the complexes **6.5** and **6.8** was also followed at 50 $^\circ\text{C}$. As expected, the reactions were faster, and complete re-assembly was observed after 30 minutes (**6.5**) or 10 minutes (**6.8**), respectively.

The robustness of the photoswitching process was demonstrated by repeated disassembly-assembly cycles using the coordination barrel **6.8** (Figure 6.4). A mixture of the barrel and **PAH** was irradiated for 20 minutes, and then ^1H NMR and ^{31}P NMR spectra were recorded. After 2.5 hours in the dark, additional spectra were measured. This procedure was repeated another four times. The ^1H and ^{31}P NMR spectra show barrel destruction and re-assembly over all cycles. The relative amount of the protonated ligand **6.8b**, as determined by ^1H NMR spectroscopy, was used as an indication of the switching efficiency. The process displayed good stability over the five cycles (Figure 6.4). Ultimately, the sensitivity of **PAH** towards hydrolytic degradation represents a limit,^[135-136] but within the timeframe of our experiment, hydrolysis was not observed.

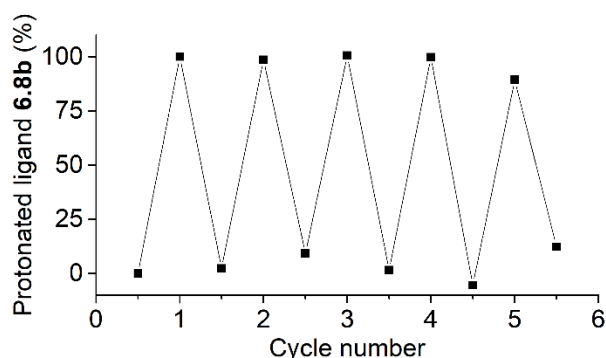
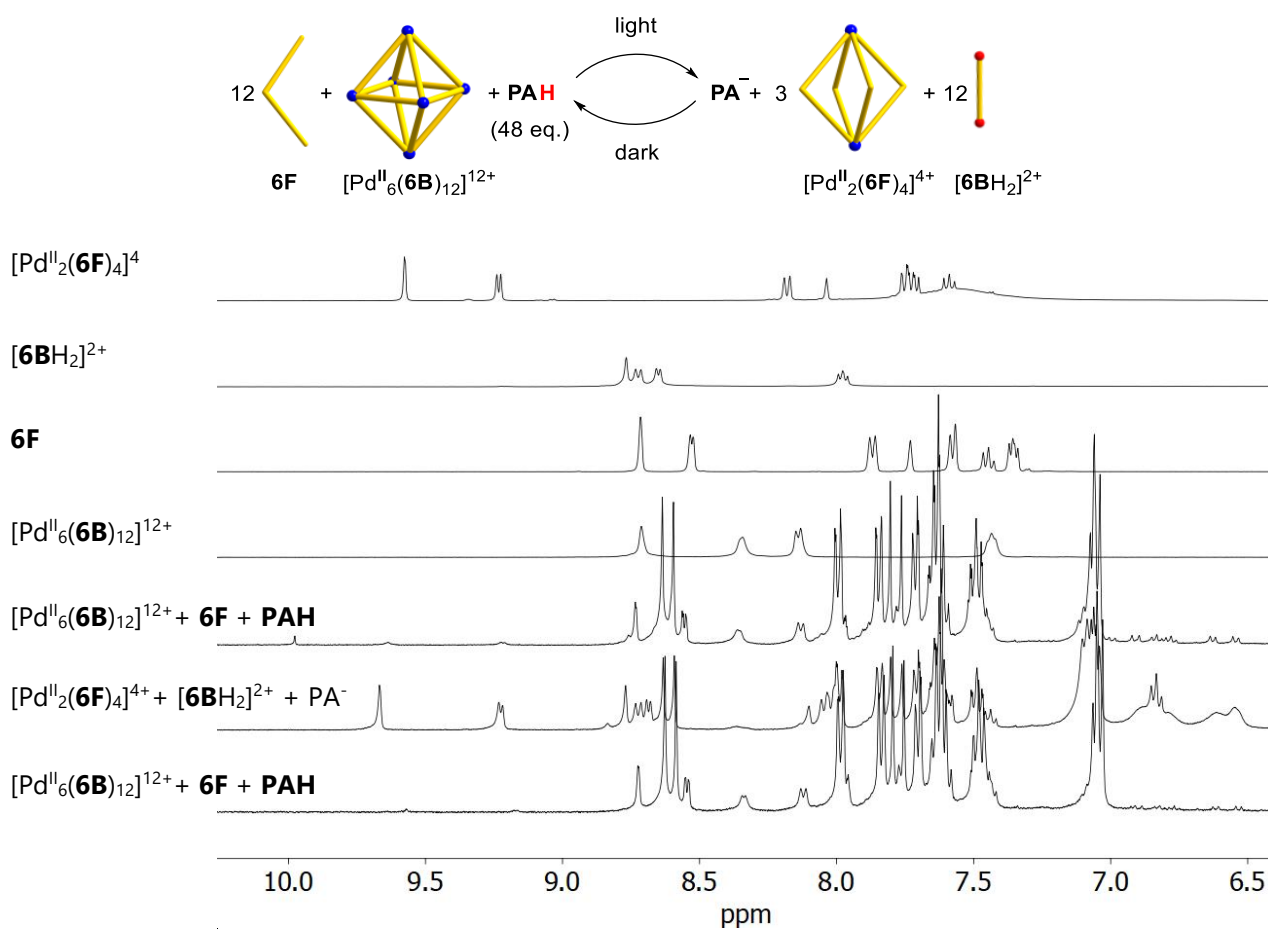


Figure 6.4. Repeated photoswitching between the coordination barrel **6.8** and its disassembled state. The relative amount of the protonated ligand **6.8b** was used as an indication of the switching efficiency. For the first cycle, the amount of **6.8b** was normalized to 0 and 100%, respectively.

In view of the results summarized above and in the previous chapter, we were also interested to explore if **PAH** can also be employed to switch between different $[\text{Pd}^{\text{II}}_n\text{L}_{2n}]^{2n+}$ structures.

As a test reaction, we have examined the acid-induced conversion of $[\text{Pd}_6(\mathbf{6B})_{12}]^{12+}$ into $[\text{Pd}_2(\mathbf{6F})_4]^{4+}$.^[113] A solution containing **6B** (2 eq.), **6F** (2 eq.) and $[\text{Pd}^{\text{II}}(\text{CH}_3\text{CN})_4](\text{BF}_4)_2$ (1 eq.) in $\text{CD}_3\text{CN}/\text{D}_2\text{O}$ (8:2) was prepared. The photoacid **PAH** (2 eq. per N-donor) was added in the dark, and the mixture was analyzed by ^1H NMR spectroscopy. Exposing the sample to violet light at room temperature for 11 h lead to conversion of $[\text{Pd}_6(\mathbf{6B})_{12}]^{12+}$ into $[\text{Pd}_2(\mathbf{6F})_4]^{4+}$ (Scheme 6.5). The reaction could be reversed by keeping the sample in the dark at 60 °C for 6 h. Over the course of the reaction, the photoacid is hydrolyzed to a small extent. Therefore, this methodology is not suited to repetitive switching between different structures. Nevertheless, it shows that the interconversions of $[\text{Pd}^{\text{II}}_n\text{L}_{2n}]^{2n+}$ complexes can be triggered by light.



Scheme 6.5. ^1H NMR (400 MHz) spectra of the switching between $[\text{Pd}^{\text{II}}_6(\text{6B})_{12}]^{12+}$ (bottom) and $[\text{Pd}^{\text{II}}_2(\text{6F})_4]^{4+}$ (one up from the bottom) and back (two up from the bottom) by the addition of 2 eq. of PA in a mixture of CD_3CN and D_2O (8:2) and the reference spectra.

6.3 Conclusion

We have demonstrated that the addition of a metastable-state photoacid to solutions of metallasupramolecular assemblies renders the systems photo-responsive. Irradiation with violet light leads to proton transfer from the photoacid to the ligands, resulting in partial or full disassembly of the metal-ligand structure. The process is in all cases reversed in the dark. In principle, similar changes could be induced by addition of acids and bases, as described in the previous chapter. However, the utilization of light is not effecting the overall composition of the system (e.g. no accumulation of salts), and light can be used with good spatial and temporal control. Compared to the utilization of photochromic ligands, our approach offers the advantage of being more general and easier to implement. For the present study, we have focused on metallasupramolecular structures based on polypyridyl ligands, but it is expected that the methodology can be extended to assemblies with other ligands, given that the basicity of the system is within the pH range of the photoacid. We have already shown that the approach is suited for the light-induced release of guest molecules, but other applications can be envisioned as well. For example, it could be possible to control catalytic reactions with light, since some coordination cages are able to act as catalytic nanoreactors.^[94c, 94d] Furthermore, it should be possible to use a related approach for photoswitching of metallasupramolecular polymers and metallogels.

Chapter 7 Conclusions and outlook

To conclude, this thesis has shown the applicability of clathrochelate metalloligands in structural supramolecular chemistry. The study of these coordination structures, has given three new insight into structural supramolecular chemistry, namely: 1) the importance of ligand size ratio on cage architecture and stability, 2) clathrochelates metalloligands are particularly suitable for the formation of large supramolecular structures and 3) knowledge into the context-dependent stability of coordination structures.

The first three research chapters of this thesis describe mainly the results that lead to the first two insights. When the aspect ratio of a ligand is reduced, by either decreasing the length or increasing the width of the ligand, a structure of higher nuclearity is obtained. These results indicate that the aspect ratio of rigid rod-type ligands can be used as a decisive factor in metal-based self-assembly reactions. The employment of large and easily accessible double clathrochelate ligands affords $\text{Pd}^{\text{II}}_2\text{L}_4$ -type cages of unprecedented size. Competition experiments to study the stability of these cages indicated that the close packing of the lipophilic side chains led to increased stability. Finally, triple clathrochelate metalloligands were employed to construct $\text{Pd}^{\text{II}}_6\text{L}_8$ -type coordination cages, again unprecedented in size.

The fifth and sixth chapters of this thesis describe the results that lead to the third insight. A detailed study into the basicity and stability of a range of ligands, and the $[\text{Pd}^{\text{II}}_n(\text{N-donor})_{2n}]^{2n}$ coordination structures that form from these ligands, shows that more basic ligands give coordination complexes which are more resistant against pyridine disassembly. In contrast, the nanostructures based on more basic ligands were more sensitive to disassembly upon the addition of acid. This context-dependent stability was used to switch between different $[\text{Pd}^{\text{II}}_n(\text{N-donor})_{2n}]^{2n}$ coordination complexes. A metastable-state photoacid was then employed to reversibly disassemble a range of supramolecular cage structures.

Clathrochelate metalloligands were ideally suited for these studies due to the straightforward adaptation of length, width and functional groups on the ligands. The clathrochelate metalloligands are prepared in a one-pot synthesis from readily accessible starting materials. Besides, studies have shown that clathrochelate ligands are particularly basic, and are therefore forming more thermodynamically stable structures.

By gaining these three insights into structural supramolecular chemistry, it has become possible to better understand and predict the coordination complexes that form from ligands with specific properties. This implies that the design of even more complex functional nanostructures is within reach. By having the possibility to carefully design structures with a certain shape, size or stability, functions like selective encapsulation and release of guests can be introduced in a targeted manner.

Experimental section

General

All chemicals were obtained from commercial sources (see below, per chapter) and used without further purification unless stated otherwise. Solvents were dried using a solvent purification system from Innovative Technologies, Inc.. Reactions were carried out under an atmosphere of dry N₂ using standard Schlenk techniques.

NMR spectra were obtained on a Bruker DRX (¹H: 400 MHz) equipped with a BBO 5 mm probe, a Bruker Avance III spectrometer (¹H: 600 MHz) equipped with a 5 mm CPTClz cryo-probe, a Bruker Avance II (¹H: 800 MHz) equipped with a 5 mm CPTClz cryo-probe, a Bruker DRX (¹H: 400 MHz) equipped with a BBO 5 mm probe and a Bruker Avance III spectrometer (¹H: 400 MHz) equipped with a 5 mm BBFO-Plus probe. The chemical shifts are reported in parts per million δ (ppm) referenced to the residual solvent signal or an internal standard. All spectra were recorded at 298 K, unless stated otherwise. The analysis of NMR spectra was performed with MestreNova and for the DOSY analysis the Bayesian DOSY transform from MestreNova was used.

Routine ESI-MS data were acquired on a Q-TOF Ultima mass spectrometer (Waters) operated in the positive ionization mode and fitted with a standard Z-spray ion source equipped with the Lock-Spray interface. Data were processed using the MassLynx 4.1 software.

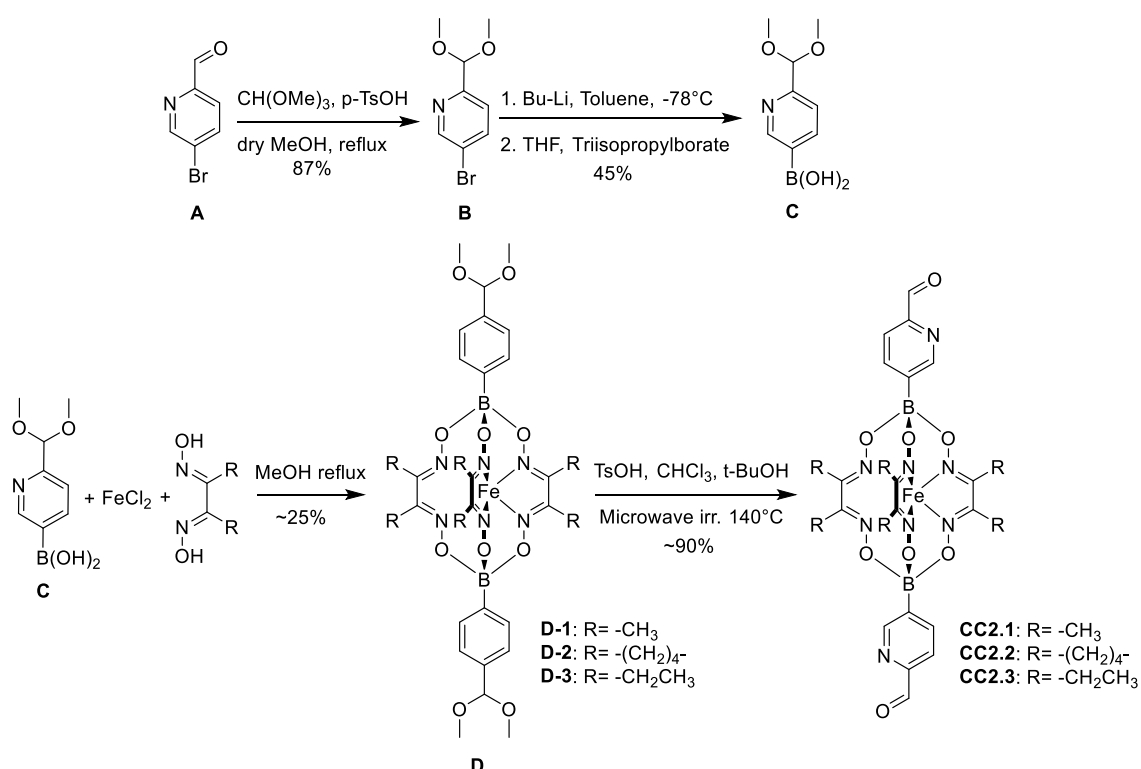
Unless stated otherwise, high resolution mass spectra were acquired for pure, pre-synthesized samples of all cages and cage mixtures. The analytes were dissolved in methanol or acetonitrile to a final concentration of ~10-20 μ M. The machine used was a linear trap quadrupole Fourier transform ion cyclotron resonance mass spectrometer, 10T LTQ FT-ICR MS (Thermo Scientific), equipped with a 2X NADEL cell.^[147] Analytes were ionized via HESI source in Ion Max housing (Thermo Scientific); heater temperature was set to 0 °C (effective temperature 30–50 °C), and the typical flow rate was 10 μ L/min. Mass spectra were acquired with a minimum resolution setting of 100,000 at 400 *m/z*. Or hybrid ion trap-Orbitrap Fourier transform mass spectrometer, Orbitrap Elite (Thermo Scientific) equipped with a TriVersa Nanomate (Advion) nano-electrospray ionization source. Mass spectra were acquired with a minimum resolution setting of 120,000 at 400 *m/z*. To reduce the degree of analyte gas phase reactions leading to side products unrelated to solution phase, the transfer capillary temperature was lowered to 50 °C in both instruments. Experimental parameters were controlled via standard and advanced data acquisition software. Post-acquisition analysis was performed using vendor software, Xcalibur (Thermo Scientific), and ChemCalc (<http://www.chemcalc.org/>) web tool.^[148]

Experimental section Chapter 2

Commercial sources: 5-bromo-pyridine-2-carbaldehyde (**A**) – Fluorochem, 4-bromoaniline (**E**) – Fluorochem, pyridine-3-boronic acid – Fluorochem, anhydrous iron(II) chloride – Acros, dimethylglyoxime – Apollo Scientific, nioxime – ABCR, $[\text{Pd}(\text{CH}_3\text{CN})_4](\text{BF}_4)_2$ – Sigma Aldrich and $\text{Fe}(\text{OTf})_2$ – Sigma Aldrich

Synthetic procedures

Diethyldioxime^[149], boronic acids **C**^[87] and **G**^[88] and the iron(II)triflimide (NTf_2) salt^[150] were prepared according to literature procedures.



Scheme ES1. Synthesis of the pyridine carboxaldehyde-terminated clathrochelates **CC2.1–CC2.3**. (**B**) $\text{CH}(\text{OMe})_3$ (3 eq.), p-TsOH (0.02 eq.), dry MeOH, reflux 3h; (**C**) 1. dry toluene at -78°C , BuLi 2.4 M in hexanes (1.5 eq.); 2. dry THF, triisopropylborate (1.2 eq.) at -78°C .

CC2.1: Anhydrous FeCl_2 (97 mg, 0.76 mmol, 1 eq.), dimethylglyoxime (265 mg, 2.28 mmol, 3 eq.) and boronic acid **C** (300 mg, 1.52 mmol, 2 eq.) were dissolved in degassed MeOH (50 mL). The mixture was heated under reflux for 4 h. Subsequently, the solvent was removed under reduced pressure. CHCl_3 (20 mL) was added, filtered, washed with saturated aqueous NaHCO_3 (2x 20 mL) and brine (1x 20 mL) and dried (MgSO_4), after which the solution was concentrated again under reduced pressure. Purification by silica flash chromatography (30 x 5 cm, EtOAc, 40–65 μm , 230–400 mesh) gave clathrochelate **D-1** (118 mg, 0.16 mmol, 21%).

^1H NMR (400 MHz, CDCl_3) δ 8.85 (s, 2H), 7.95 (dd, $J = 7.7, 1.7$ Hz, 2H), 7.42 (d, $J = 7.6$ Hz, 2H), 5.41 (s, 2H) 3.33 (s, 12H), 2.32 (s, 18H). ^{13}C NMR (101 MHz, CDCl_3) δ 156.11, 152.52, 152.51, 140.20, 120.27, 104.50, 53.75, 13.46, (C-B not detected). HRMS (ESI): m/z calculated for $\text{C}_{28}\text{H}_{38}\text{B}_2\text{FeN}_8\text{O}_{10}$ $[\text{M}+\text{H}]^+$ 725.2335, found 725.2346.

D-1 was divided over six 5 mL microwave vials in small portions (18 mg, 0.03 mmol). To each of the vials, TsOH (0.5 mg, 3 μ mol, 0.1 eq.), CHCl₃ (3.2 mL) and *t*-BuOH (0.8 mL) was added. The vials were heated by microwave irradiation at 140 °C for 4 h. Afterwards, the combined reaction mixtures were washed with sat. NaHCO₃ (3 \times 15 mL), dried (MgSO₄), and the solvent was removed under reduced pressure. The product was purified by silica flash chromatography (30 \times 5 cm, EtOAc, 40-65 μ m, 230-400 mesh) to give clathrochelate **CC2.1** as a red powder (from combined six vials: 87 mg, 0.14 mmol, 92%).

¹H NMR (400 MHz, CDCl₃) δ 10.12 (s, 2H), 9.07 (s, 2H), 8.17 (d, *J* = 7.8 Hz, 2H), 7.96 (d, *J* = 7.6 Hz, 2H), 2.45 (s, 16H). ¹³C NMR (101 MHz, CDCl₃) δ 194.51, 153.73, 153.0, 152.44, 140.52, 121.13, 13.642, (C-B not detected). HRMS (ESI): *m/z* calculated for C₂₄H₂₇B₂FeN₈O₈ [M+H]⁺ 633.1487, found 633.1497.

CC2.2: Anhydrous FeCl₂ (97 mg, 0.76 mmol, 1 eq.), nioxime (325 mg, 2.28 mmol, 3 eq.) and boronic acid **C** (300 mg, 1.52 mmol, 2 eq.) were dissolved in degassed MeOH (50 mL). The mixture was heated under reflux at 80 °C for 4 h. Subsequently, the solvent was removed under reduced pressure. CHCl₃ (20 mL) was added, the mixture was filtered, washed with saturated aqueous NaHCO₃ (2 \times 20 mL) and brine (1 \times 20 mL), and dried (MgSO₄), after which the solvent was removed under reduced pressure. Purification by silica flash chromatography (30 \times 5 cm, EtOAc, 40-65 μ m, 230-400 mesh) gave clathrochelate **D-2** (198 mg, 0.25 mmol, 33%).

¹H NMR (400 MHz, CDCl₃) δ 8.87 (s, 2H), 8.00 (dd, *J* = 7.7, 1.8 Hz, 2H), 7.49 (dd, *J* = 7.7, 1.0 Hz, 2H), 5.39 (s, 2H), 3.42 (s, 12H), 2.92 (s, 12H), 1.81 (s, 12H). ¹³C NMR (101 MHz, CDCl₃) δ 156.51, 153.05, 152.71, 140.51, 120.60, 104.95, 54.11, 26.69, 22.01, (C-B not detected). HRMS (ESI): *m/z* calculated for C₃₄H₄₄B₂FeN₈O₁₀ [M+H]⁺ 803.2806, found 803.2805.

D-2 was divided over five 5 mL microwave vials in small portions (20 mg, 0.03 mmol). To each of the vials, TsOH (0.5 mg, 3 μ mol, 0.1 eq.), CHCl₃ (3.2 mL) and *t*-BuOH (0.8 mL) was added. The vials were heated by microwave irradiation at 140 °C for 4 h. Afterwards, the combined reaction mixtures were washed with sat. NaHCO₃ (3 \times 15 mL), dried (MgSO₄), and the solvent was removed under reduced pressure. Purification by silica flash chromatography (30 \times 5 cm, EtOAc, 40-65 μ m, 230-400 mesh) gave clathrochelate **CC2.2** as a red powder (from combined five vials: 83 mg, 0.12 mmol, 93%).

¹H NMR (400 MHz, CDCl₃) δ 10.05 (s, 2H), 8.96 (s, 2H), 8.06 (d, *J* = 7.6 Hz, 2H), 7.86 (d, *J* = 8.3 Hz, 2H), 2.88 (s, 12H), 1.77 (s, 12H). ¹³C NMR (101 MHz, CDCl₃) δ 193.32, 152.61, 151.63, 151.2, 139.44, 119.92, 25.34, 20.52, (C-B not detected). HRMS (ESI): *m/z* calculated for C₃₀H₃₃B₂FeN₈O₈ [M+H]⁺ 711.1957, found 711.1968.

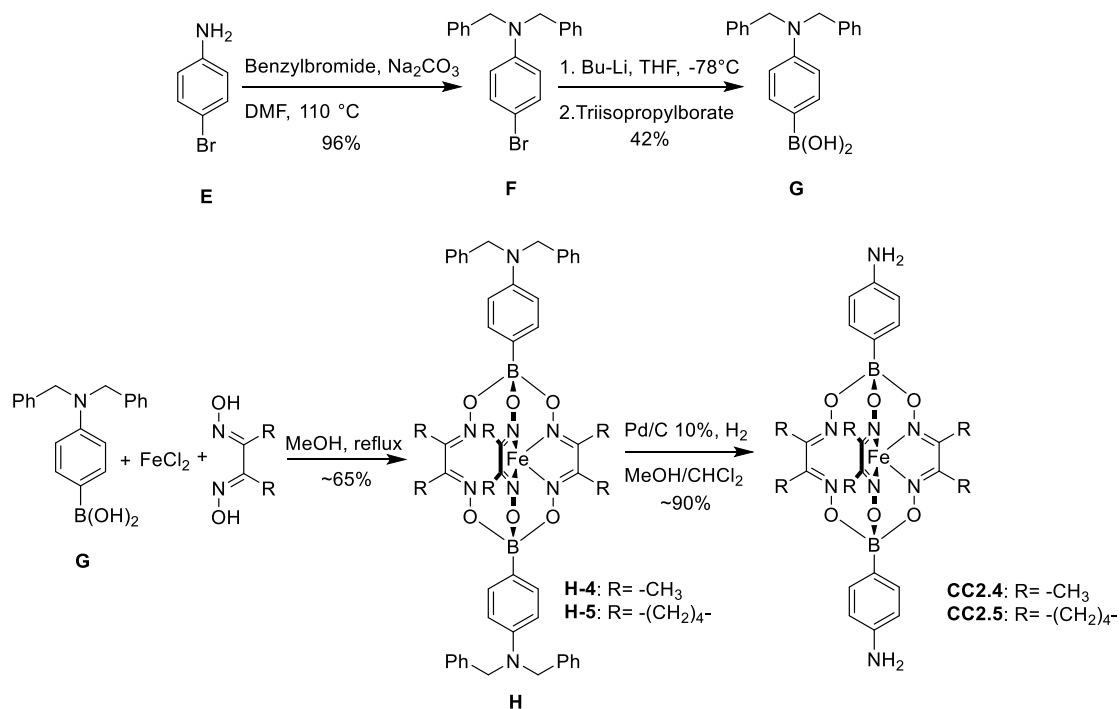
CC2.3: Anhydrous FeCl₂ (97 mg, 0.76 mmol, 1 eq.), ethyldioxime (329 mg, 2.28 mmol, 3 eq.) and boronic acid **C** (300 mg, 1.52 mmol, 2 eq.) were dissolved in degassed MeOH (50 mL). The mixture was heated under reflux at 80 °C for 4 h. Subsequently, the solvent was removed under reduced pressure. CHCl₃ (20 mL) was added, the mixture was filtered, washed with saturated aqueous NaHCO₃ (2 \times 20 mL) and brine (1 \times 20 mL), and dried (MgSO₄), after which the solvent was removed under reduced pressure. Purification by silica flash chromatography (30 \times 5 cm, EtOAc, 40-65 μ m, 230-400 mesh) gave clathrochelate **D-3** (176 mg, 0.22 mmol, 29%).

¹H NMR (400 MHz, CDCl₃) δ 8.93 (s, 2H), 8.02 (dd, *J* = 7.7, 1.7 Hz, 2H), 7.52 (d, *J* = 8.2 Hz, 2H), 5.40 (s, 2H), 3.46 (s, 12H), 2.83 (q, *J* = 7.5 Hz, 12H), 1.17 (t, *J* = 7.5 Hz, 18H). ¹³C NMR (101 MHz, CDCl₃) δ 158.02, 155.95, 152.64, 140.02, 120.11, 104.80, 53.87, 20.91, 11.46, (C-B not detected). HRMS (ESI): *m/z* calculated for C₃₄H₅₁B₂FeN₈O₁₀ [M+H]⁺ 809.3276, found 809.3281.

D-3 was divided over seven 5 mL microwave vials in small portions (20 mg, 0.02 mmol). To each of the vials, TsOH (0.5 mg, 3 μ mol, 0.1 eq.), CHCl_3 (3.2 mL) and *t*-BuOH (0.8 mL) was added. The vials were heated by microwave irradiation at 140 $^{\circ}\text{C}$ for 4 h. Afterwards, the combined reaction mixtures were washed with sat. NaHCO_3 (3 \times 15 mL), dried (MgSO_4), and the solvent was removed under reduced pressure. Purification by silica flash chromatography (30 \times 5 cm, EtOAc, 40-65 μm , 230-400 mesh) gave clathrochelate **CC2.3** as a red powder (from combined five vials: 115 mg, 0.16 mmol, 95%).

^1H NMR (400 MHz, Chloroform-*d*) δ 10.13 (s, 2H), 9.08 (s, 2H), 8.15 (d, J = 7.6 Hz, 2H), 7.97 (d, J = 7.6 Hz, 2H), 2.85 (q, J = 7.5 Hz, 12H), 1.19 (t, J = 7.5 Hz, 18H). ^{13}C NMR (101 MHz, CDCl_3) δ 194.45, 158.59, 153.71, 152.31, 140.45, 121.16, 21.13, 11.63, 1.17. (C-B not detected). HRMS (ESI): m/z calculated for $\text{C}_{30}\text{H}_{38}\text{B}_2\text{FeN}_8\text{O}_8$ $[\text{M}+\text{H}]^+$ 717.2438, found 717.2434

The NMR spectra for these clathrochelates are included in the supporting information of the publication cited under reference 79.



Scheme ES2. Synthesis of the amine-terminated clathrochelates **CC2.4** and **CC2.5**. (**F**) Benzylbromide (2.1 eq.), Na_2CO_3 (1.5 eq.), DMF at 110 $^{\circ}\text{C}$ overnight;^[24] (**G**) dry THF at $-78\text{ }^{\circ}\text{C}$, BuLi 2.4 M in hexanes (1.2 eq.), triisopropylborate (1.8 eq.).^[88]

CC2.4: Anhydrous FeCl_2 (60 mg, 0.32 mmol, 1 eq.), dimethylglyoxime (165 mg, 0.94 mmol, 3 eq.) and boronic acid **G** (300 mg, 0.63 mmol, 2 eq.) were dissolved in degassed MeOH (50 mL) and heated under reflux at 80 $^{\circ}\text{C}$ for 5 h. The reaction mixture was cooled to r.t. and the precipitate was collected after centrifugation (10 min. at 4000 rpm), washed with MeOH (15 mL) and dried to give clathrochelate **H-4** (186 mg, 0.19 mmol, 60%).

^1H NMR (400 MHz, CD_2Cl_2) δ 7.59 (d, J = 8.6 Hz, 4H), 7.35 – 7.25 (m, 20H), 6.81 (d, J = 8.7 Hz, 4H), 4.69 (s, 8H), 2.40 (s, 18H). ^{13}C NMR (101 MHz, CD_2Cl_2) δ 152.25, 149.14, 139.85, 133.11, 129.04, 127.30, 127.27, 112.46, 55.11, 13.61, (C-B not detected). HRMS (ESI): m/z calculated for $\text{C}_{52}\text{H}_{54}\text{B}_2\text{FeN}_8\text{O}_6$ $[\text{M}+\text{H}]^+$ 965.3798, found 965.3779.

For the deprotection step, the clathrochelate **H-4** (162 mg, 0.17 mmol) was combined with 20% Pd/C (17 mg) in MeOH (25 mL) and CHCl₃ (10 mL), and placed under an atmosphere of H₂ and heated to 50 °C for 4 h. The reaction mixture was filtered, washed with MeOH (10 mL), and the solvent was removed under reduced pressure. CHCl₃ (20 mL) was added, filtered, washed with saturated aqueous NaHCO₃ (2 × 20 mL) and brine (1 × 20 mL), dried over MgSO₄. The volume of the solution was reduced to 2 mL under reduced pressure, and the solution was mixed with pentane (13 mL). The precipitate was collected and washed with diethyl ether (2 × 15 mL) to give clathrochelate **CC2.4** as a red solid (98 mg, 0.16 mmol, 89%).

¹H NMR (400 MHz, CDCl₃) δ 7.56 (d, *J* = 8.1 Hz, 4H), 6.73 (d, *J* = 8.2 Hz, 4H), 2.41 (s, 18H). ¹³C NMR (101 MHz, CDCl₃) δ 151.81, 146.32, 132.94, 114.83, 13.52, (C-B not detected). HRMS (ESI): *m/z* calculated for C₂₄H₃₁B₂FeN₈O₆ [M+H]⁺ 605.1902, found 605.1909.

CC2.5: Anhydrous FeCl₂ (100 mg, 0.789 mmol, 1 eq.), nioxime (336 mg, 2.36 mmol, 3 eq.) and boronic acid **G** (500 mg, 1.58 mmol, 2 eq.) were dissolved in degassed MeOH (100 mL). The mixture was heated under reflux at 80 °C for 5 h. The reaction mixture was cooled to r.t. and the precipitate was collected after centrifugation (10 min. at 4000 rpm), washed with MeOH (15 mL) and dried to give clathrochelate **H-5** (607 mg, 0.58 mmol, 74%).

¹H NMR (400 MHz, CD₂Cl₂) δ 7.41 (d, *J* = 7.7 Hz, 4H), 7.37 – 7.15 (m, 20H), 6.69 (d, *J* = 7.8 Hz, 4H), 4.68 (s, 8H), 2.85 (s, 12H), 1.76 (s, 12H). ¹³C NMR (101 MHz, CD₂Cl₂) δ 152.01, 149.19, 139.86, 133.10, 129.05, 127.31, 127.26, 112.44, 55.08, 26.71, 22.20, (C-B not detected). HRMS (ESI): *m/z* calculated for C₅₈H₆₀B₂FeN₈O₆ [M+H]⁺ 1043.4269, found 1043.4249.

For the deprotection step, the clathrochelate **H-5** (565 mg, 0.542 mmol) was combined with 20% Pd/C (80 mg) in MeOH (35 mL) and CHCl₃ (20 mL), placed under an atmosphere of H₂ and heated to 50 °C for 4 h. The reaction mixture was filtered, washed with MeOH (20 mL), and the solvent was removed under reduced pressure. CHCl₃ (50 mL) was added, filtered, washed with saturated aqueous NaHCO₃ (2 × 50 mL) and brine (1 × 50 mL), dried over MgSO₄. The volume of the solution was reduced to 2 mL under reduced pressure, and the solution was mixed with pentane (13 mL). The precipitate was collected and washed with diethyl ether (2 × 15 mL) to give clathrochelate **CC2.5** as a red solid (365 mg, 0.537 mmol, 99%).

¹H NMR (400 MHz, CDCl₃) δ 7.51 (d, *J* = 8.3 Hz, 4H), 6.68 (d, *J* = 8.3 Hz, 4H), 2.93 (s, 12H), 1.77 (s, 12H). ¹³C NMR (101 MHz, CDCl₃) δ 151.62, 146.23, 132.82, 114.72, 26.33, 21.74, (C-B not detected). HRMS (ESI): *m/z* calculated for C₃₀H₃₇B₂FeN₈O₆ [M+H]⁺ 683.2372, found 683.2383.

The NMR spectra for these clathrochelates are included in the supporting information of the publication cited under reference 79.

Cages 2.1–2.5

The respective clathrochelate complex (**CC2.1**, **2**, **3**, **4**, or **5**; 3 eq.) and the iron salt ($\text{Fe}(\text{OTf})_2$ or $\text{Fe}(\text{NTf}_2)_2$) (2 eq.) were dissolved in acetonitrile (20 mL). The complementary small molecule (6 eq. *p*-toluidine for **CC2.1**–**CC2.3**, or 6 eq. 2-formylpyridine for **CC2.4** and **CC2.5**) was added and the reaction mixture was stirred at 50 °C overnight. The solvent was removed under reduced pressure, and the residue was re-dissolved in acetonitrile (5 mL) and precipitated with diethyl ether containing 10% pentane (10 mL). The resulting solid was washed once with a mixture of diethyl ether and pentane (1:1, 15 mL), and once with CHCl_3 (15 mL). Drying under vacuum gave the respective coordination cage in high yield. Further details about the syntheses can be found in **Table ES1** and analytical data of the cages are listed below.

		3 eq. Ligand		2 eq. $\text{Fe}(\text{OTf})_2$		6 eq. <i>p</i> -toluidine		6 eq. 2-formyl- pyridine		Yield cage		
Ligand #	Cage #	mg	μmol	mg	μmol	mg	μmol	mg	μmol	mg	μmol	%
CC2.1	2.1	40	63	15	42	14	126	-	-	64	10	98
CC2.2	2.2a	40	56	13	38	12	113	-	-	59	4	93
CC2.3	2.3a	40	56	13	37	12	112	-	-	60	4	95
CC2.4	2.4a	40	66	16	44	-	-	14	132	65	11	97
CC2.5	2.5	40	58	14	39	-	-	13	117	59	9	92
		3 eq. Ligand		2 eq. $\text{Fe}(\text{NTf}_2)_2$		6 eq. <i>p</i> -toluidine		6 eq. 2-formyl- pyridine		Yield cage		
CC2.2	2.2b	40	56	24	38	12	113	-	-	70	5	93
CC2.3	2.3b	40	56	24	37	12	112	-	-	68	4	93
CC2.4	2.4b	40	66	28	44	-	-	14	132	72	10	97

Table ES1. Details for the synthesis of the cages **2.1–2.5**.

The full characterisation data for these complexes are included in the supporting information of the publication cited under reference 79.

Single crystal X-ray analysis

Intensity data for the clathrochelates **CC2.1** was measured at low temperature [120(2) K or 100(2) K] using Mo K_{α} radiation on a Bruker APEX II CCD diffractometer equipped with a kappa geometry goniometer. The dataset was reduced by EvalCCD^[151] and then corrected for absorption.^[152] Molecular graphics and publication material were produced with Olex2.^[112]

Intensity data for building blocks **CC2.4**, **CC2.5** and cage **2.4b**, were collected at the Swiss Norwegian beamline BM01A at the ESRF in Grenoble (France) equipped with a Pilatus2M pixel detector from Dectris Ltd. Data collection was performed at low temperature [120 K] using a Cryostream 700 Series from Oxford Cryosystems Ltd. Data integration was carried out using CrysAlis Pro. Multi-scan empirical absorption corrections were applied to the data using CrysAlis Pro. Despite the use of synchrotron radiation, few reflections at greater than 1.1 Å resolution were observed for **2.4b**. Nevertheless, the quality of the data is far more than sufficient to establish the connectivity of the structures.

Intensity data for cage **2.5** were collected using a Bruker D8 VENTURE equipped with high-brilliance μ S Cu- K_{α} radiation (1.54178 Å) with ω and ψ scans at low temperature [135(2) K]. Data integration and reduction were undertaken with SAINT. A multi-scan empirical absorption correction was applied to the data using SADABS. Despite the use of a high-intensity laboratory source, few reflections at greater than 1.1 Å resolution were observed. Nevertheless, the quality of the data is clearly sufficient to establish the connectivity of the structure.

All the structures were solved and refined with SHELX.^[153] Fourier map of compounds **CC2.1**, **2.4b** and **2.5** were treated by the SQUEEZE algorithm of PLATON.^[154] Disorder was modeled using standard crystallographic methods including constraints and restraints where necessary. Thermal parameter restraints (SIMU, DELU and/or RIGU) were applied to the anisotropic displacement parameters of anions and solvent molecules (MeCN, DMF, Me₂CO and Et₂O) and to all non-metal atoms in the structures of cage **2.4b**. Geometrical restraints (SADI or DFIX) were also applied to the anions and solvent molecules, as well to some bond distances within the cages to ensure a reasonable refinement. For **2.4b** bond lengths and angles within pairs of organic ligands were restrained to be similar to each other. Several anions in the structures of the cages were modeled as disordered over two or three locations and/or with fractional occupancy. Some disordered anions and solvent molecules were modeled with isotropic thermal parameters. Carbon-bound hydrogen atoms were included in idealized positions and refined using a riding model. The contribution of the electron density associated with disordered counter anions and solvent molecules, which could not be modeled with discrete atomic positions were handled using the SQUEEZE routine in PLATON to generate solvent masks (.fab files) which were included in the SHELX refinement via the ABIN instruction leaving the original structure factors untouched.

Crystallographic data have been deposited to the CCDC and correspond to the following codes: **CC2.1** (1442394), **CC2.4** (1442248), **CC2.5** (1442090), **2.4b** (1442396) and **2.5** (1442397). Copies of the data can be obtained free of charge on application to the CCDC, 12 Union Road, Cambridge, CB2 1EZ, U.K. (fax, (internat.) +44-1223-336033; E-mail, deposit@ccdc.cam.ac.uk).

Single crystals of sufficient quality for X-ray analysis were obtained by using the following methods:

CC2.1: Slow diffusion of hexane into a solution of the clathrochelate in DCM.

CC2.4: Slow diffusion of diethylether into a solution of the HCl salt of the clathrochelate in MeOH.

CC2.5: Slow diffusion of diethylether into a solution of the HCl salt of the clathrochelate ligand in MeOH.

2.4b: Slow diffusion of diethylether into a solution of the NTf₂ salt of the cage in CH₃CN.

2.5: Slow diffusion of hexane into a solution of the OTf salt of the cage in acetone with the addition of a drop of concentrated solution of KSbF₆.

VOIDOO calculations on **2.4b** and **2.5**

The available void space in cages **2.4b** and **2.5** was determined by VOIDOO calculations.¹⁵ Based on the crystal structures of these cages (anions and solvent molecules are removed from the structure for the calculations), the calculations were performed with standard parameters, with the exception of the following parameters:

Maximum number of volume refinement cycles:	30
Minimum size of secondary grid:	3
Grid for plot files:	0.2
Primary grid spacing:	0.1
Plot grid spacing:	0.1

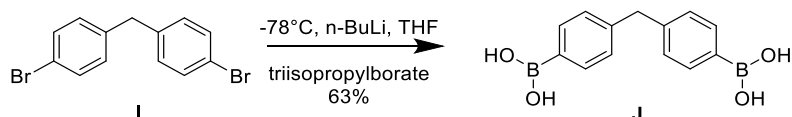
It is observed that cage **2.4** has a significantly bigger cavity than cage **2.5**, namely 480 Å³ vs. 377 Å³, on average. As shown in the **Figure 2.5**, the cavity in cage **2.5** (right) is partly blocked due to the bulky side groups of clathrochelate ligand **CC2.5**.

Experimental section Chapter 3

Commercial sources: 1,3-dibromopropane – AlfaAesar, 1,3-phenylenediboronic acid – FluoroChem, 1,4-dibromobenzene – VWR International SA, 1,5 dibromopentane – TCI, 4-bromobenzaldehyde – Maybridge, 4-bromophenol – Sigma Aldrich, dimethylglyoxime – Apollo Scientific, iron(II)chloride anhydrous – VWR International SA, nioxime – TCI, *p*-tolylboronic acid – Sigma Aldrich, pyridine-3-boronic acid – FluoroChem and $[\text{Pd}(\text{CH}_3\text{CN})_4](\text{BF}_4)_2$ – ABCR

Synthetic procedures

Bis(bromophenyl)methane (**I**) was synthesized following a literature procedure.^[155]

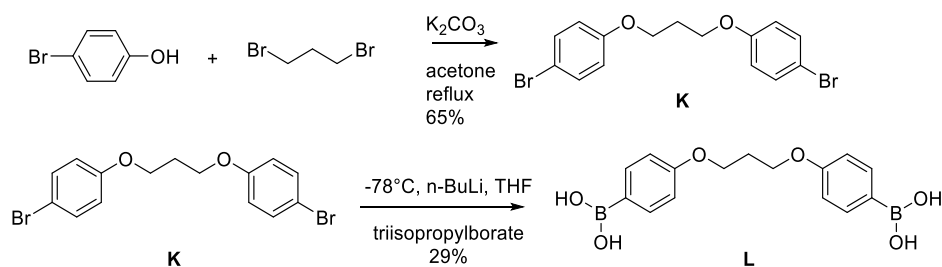


Scheme ES3: Synthesis of diboronic acid **J** from bis(4-bromophenyl)methane (**I**).

A solution of bis(4-bromophenyl)methane (**I**) (3.0 g, 9.2 mmol) in THF (40 mL) was cooled to -78°C . *N*-butyllithium in hexane (2.5 M, 8.1 mL, 20.2 mmol, 2.2 eq.) was slowly added and stirred for an additional 30 min before triisopropylborate (3.8 g, 4.7 mL, 20.2 mmol, 2.2 eq.) was added. The reaction mixture was then left to warm up to r.t. overnight. Aqueous HCl (1 M, 20 mL) was added to quench the reaction and the solvent was removed under reduced pressure. A solid was collected, which was washed with water (3×50 mL) and with a 1:1 pentane/DCM mixture (2×50 mL) and dried by air. Diboronic acid **J** was obtained in the form of a white powder (1.9 g, 5.8 mmol, 63%).

^1H NMR (400 MHz, DMSO-d_6) δ 7.91 (s, 4H), 7.66 (d, $J = 7.5$ Hz, 4H), 7.14 (d, $J = 7.6$ Hz, 4H), 3.89 (s, 2H). ^{13}C NMR (101 MHz, DMSO-d_6) δ 143.06, 134.31, 127.81, 40.15, (C-B not detected). HRMS (ESI): m/z calculated for $\text{C}_{17}\text{H}_{22}\text{B}_2\text{NaO}_4$ [$\text{M} + 4 \text{CH}_2 + \text{Na}$] $^+$ ($4 \times$ methoxy adduct, from methanol as solvent) 335.1602, found 335.1609.

The NMR spectra for this dioboronic acid are included in the supporting information of the publication cited under reference 80b.



Scheme ES4: Synthesis of diboronic acid **L**.

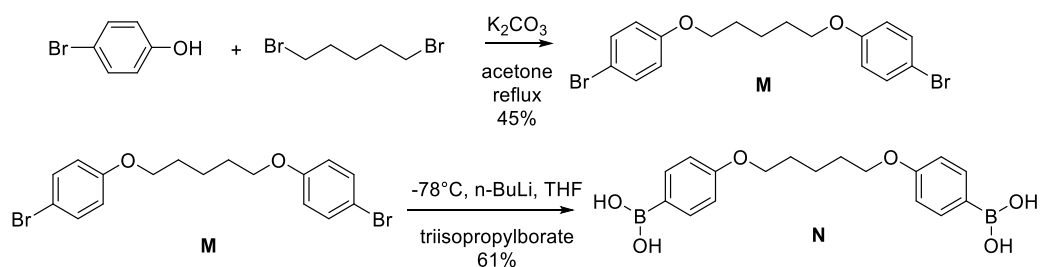
4-Bromophenol (10 g, 57.8 mmol, 2 eq.), 1,3-dibromopropane (5.8 g, 28.9 mmol 1 eq.) and K_2CO_3 (60 g, 780 mmol 7.5 eq.) were added to acetone (250 mL) and the mixture was heated under reflux overnight. The reaction mixture was cooled to r.t. and the white solid was filtered and washed with acetone (200 mL) and DCM (100 mL). The organic layer was evaporated under reduced pressure to obtain the dibromo compound **K** as a white powder (7.2 g, 18.7 mmol, 65%).

^1H NMR (400 MHz, CD_2Cl_2) δ 7.37 (d, J = 8.9 Hz, 4H), 6.81 (d, J = 8.9 Hz, 4H), 4.11 (t, J = 6.1 Hz, 4H), 2.23 (p, J = 6.1 Hz, 2H). ^{13}C NMR (101 MHz, CD_2Cl_2) δ 158.66, 132.76, 116.88, 113.22, 65.21, 29.67. HRMS (APCI): m/z calculated for $\text{C}_{15}\text{H}_{15}\text{Br}_2\text{O}_2$ $[\text{M}+\text{H}]^+$ 385.9341, found 385.9327.

A solution of the dibromo starting material **K** (5.0 g, 13.0 mmol) in THF (40 mL) was cooled to -78°C . N-butyllithium in hexane (2.5 M, 11.4 mL, 28.59 mmol, 2.2 eq.) was slowly added and stirred for an additional 30 min before triisopropylborate (5.4 g, 6.6 mL, 28.5 mmol, 2.2 eq.) was added. The reaction mixture was then left to warm up to r.t. overnight. Aqueous HCl (1 M, 10 mL) was added to quench the reaction and the solvent was removed under reduced pressure. A solid was collected, which was washed with water (3×50 mL) and with a 1:1 DCM/MeOH mixture (2×50 mL) and dried by air. The diboronic acid **L** was obtained in the form of a white powder (1.2 g, 3.8 mmol, 29%).

^1H NMR (400 MHz, $\text{DMSO}-d_6$) δ 7.83 (s, 4H), 7.73 (d, J = 8.3 Hz, 4H), 6.91 (d, J = 8.4 Hz, 4H), 4.15 (t, J = 6.1 Hz, 4H), 2.18 (p, J = 5.9 Hz, 2H). ^{13}C NMR (101 MHz, $\text{DMSO}-d_6$) δ 160.15, 135.85, 113.42, 63.93, 28.63, (C-B not detected). HRMS (ESI): m/z calculated for $\text{C}_{19}\text{H}_{26}\text{B}_2\text{NaO}_6$ $[\text{M}+4\text{CH}_2+\text{Na}]^+$ (4 \times methoxy adduct, from methanol solvent) 395.1813, found 395.1811.

The NMR spectra for this dioboronic acid are included in the supporting information of the publication cited under reference 80b.



Scheme ES5: Synthesis of diboronic acid **M**.

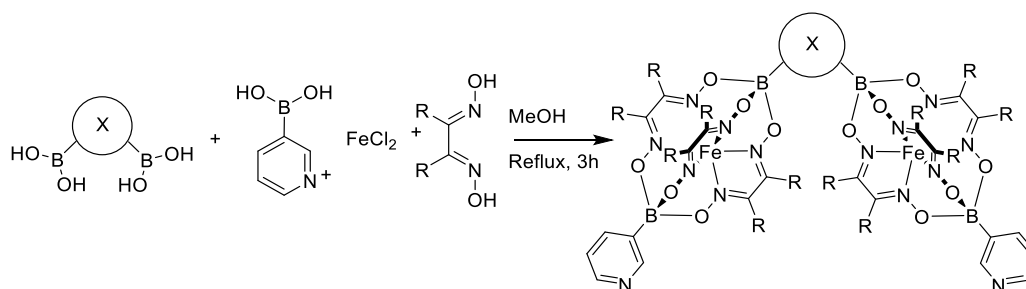
4-Bromophenol (10 g, 57.8 mmol, 2 eq.), 1,5-dibromopentane (6.7 g, 28.9 mmol 1 eq.) and K_2CO_3 (60 g, 780 mmol 7.5 eq.) were added to acetone (250 mL) and the mixture was heated under reflux overnight. The reaction mixture was cooled to r.t. and the white solid was filtered off and washed with acetone (200 mL). The organic layer was evaporated under reduced pressure and the remaining solid was washed with hexane (50 mL) and dried to obtain the dibromo compound **M** as a white powder (5.1 g, 12.4 mmol, 45%).

^1H NMR (400 MHz, CD_2Cl_2) δ 7.37 (d, J = 8.9 Hz, 4H), 6.79 (d, J = 8.9 Hz, 4H), 3.95 (t, J = 6.4 Hz, 4H), 1.83 (p, J = 6.6 Hz, 4H), 1.62 (p, J = 7.7, 7.1 Hz, 2H). ^{13}C NMR (101 MHz, CD_2Cl_2) δ 158.87, 132.71, 116.86, 112.96, 68.63, 29.46, 23.16. HRMS (APCI): m/z calculated for $\text{C}_{17}\text{H}_{19}\text{Br}_2\text{O}_2$ $[\text{M}+\text{H}]^+$ 414.9732, found 414.9724

A solution of the dibromo starting material **M** (3.0 g, 7.2 mmol) in THF (40 mL) was cooled to -78°C . *N*-butyllithium in hexane (2.5 M, 6.4 mL, 15.9 mmol, 2.2 eq.) was slowly added and stirred for an additional 30 min before triisopropylborate (3.0 g, 3.7 mL, 15.9 mmol, 2.2 eq.) was added. The reaction mixture was then left to warm up to r.t. overnight. Aqueous HCl (1 M, 20 mL) was added to quench the reaction and the solvent was removed under reduced pressure. A solid was collected, which is washed with water (3×50 mL) and with a 1:1 pentane/DCM mixture (2×50 mL) and dried by air. The diboronic acid **N** was obtained in the form of a white powder (1.8 g, 4.3 mmol, 61%).

^1H NMR (400 MHz, $\text{DMSO}-d_6$) δ 7.82 (s, 4H), 7.70 (d, J = 7.5 Hz, 4H), 6.86 (d, J = 7.5 Hz, 4H), 3.98 (t, J = 6.0 Hz, 4H), 1.86 – 1.69 (m, 4H), 1.69 – 1.40 (m, 2H). ^{13}C NMR (101 MHz, $\text{DMSO}-d_6$) δ 174.83, 150.31, 127.88, 81.57, 42.93, 36.76, (C-B not detected). HRMS (ESI): m/z calculated for $\text{C}_{21}\text{H}_{30}\text{B}_2\text{NaO}_6$ $[\text{M}+4\text{CH}_2+\text{Na}]^+$ (4 \times methoxy adduct, from methanol solvent) 423.2126, found 423.2140.

The NMR spectra for this dioboronic acid are included in the supporting information of the publication cited under reference 80b.



Scheme ES6. Synthesis of double clathrochelate **L3.1–L3.6**

Anhydrous FeCl_2 (4 eq.) and the respective dioxime (12 eq.) were dissolved in MeOH (15 mL). In a separate flask, the respective diboronic acid (100 mg, 1 eq.) and 3-pyridine boronic acid (6 eq.) were dissolved in methanol (130 mL), acetone (5 mL), and water (2 mL) and heated to reflux and stirred for 30 min. The pre-prepared mixture of dioxime and FeCl_2 , was added to the boronic acid mixture, the mixture was heated to reflux for an additional 2 h, before the solvent was removed under reduced pressure. The remaining solid was dissolved in CHCl_3 (100 mL), filtered and washed with a saturated aqueous solution of sodium EDTA and 5% ammonia (100 mL). The organic phase was dried over MgSO_4 , and evaporated under reduced pressure. The solid was pre-purified by a short silica column (150 g silica, 10% MeOH in DCM) to remove any polymeric material. The dark red fractions were evaporated under reduced pressure, the solid was dissolved in DCM (10 mL), filtered over H-PTFE 20/25 syringe filters and separated on a size exclusion column (200 g, dry weight, Bio-Beads S-X3 in DCM). The pure fractions (checked by MS, positive mode), were combined and washed with saturated NaHCO_3 solution, dried over MgSO_4 and the solvent was removed under reduced pressure to yield a red powder as the double clathrochelate.

Tables ES2: Amounts used for the synthesis of double clathrochelates **L3.1–L3.6**. BA is boronic acid, CC is clathrochelate. In the places where there is no specific diboronic acid stated (**L3.1** and **L3.2**) the starting material was 1,3-phenylboronic acid.

Double CC	Di-BA	4 eq. FeCl_2		12 eq. nioxime		1 eq. Di BA		6 eq. 3-pyridineBA		Yield double clathrochelate		
#	#	mg	mmol	mg	mmol	mg	mmol	mg	μmol	mg	mmol	%
L3.1	-	306	2.4	1029	7.2	100	0.60	445	3.6	435	0.35	59
L3.3	J	198	1.6	667	4.7	100	0.39	288	2.3	262	0.20	51

Double CC	Di-BA	4 eq. FeCl_2		12 eq. dimethyl-glyoxime		1 eq. Di BA		6 eq. 3-pyridineBA		Yield double clathrochelate		
#	#	mg	mmol	mg	mmol	mg	mmol	mg	μmol	mg	mmol	%
L3.2	-	306	2.4	841	7.2	100	0.60	445	3.6	264	0.25	41
L3.4	J	198	1.6	545	4.7	100	0.39	288	2.3	177	0.15	39
Double CC	Di-BA	4 eq. FeCl_2		12 eq. nioxime		1 eq. Di BA		6 eq. 3-pyridineBA		Yield double clathrochelate		
#	#	mg	mmol	mg	mmol	mg	mmol	mg	μmol	mg	mmol	%
L3.5	L	160	1.3	540	3.8	100	0.32	233	1.9	326	0.24	48
L3.6	N	147	1.2	496	3.5	100	0.29	214	1.7	200	0.14	49

L3.1: ^1H NMR (400 MHz, CD_2Cl_2) δ 8.72 (s, 2H), 8.43 (d, J = 3.5 Hz, 2H), 7.88 (d, J = 6.4 Hz, 3H), 7.51 (d, J = 7.3 Hz, 2H), 7.21 - 7.16 (m, 3H), 2.85 (d, J = 13.4 Hz, 24H), 1.74 (s, 24H). ^{13}C NMR (101 MHz, CD_2Cl_2) δ 152.98, 152.74, 152.32, 148.90, 140.22, 135.74, 131.72, 126.81, 123.50, 26.81, 26.75, 22.20, (C-B not detected). HRMS (ESI): m/z calculated for $\text{C}_{52}\text{H}_{62}\text{B}_4\text{Fe}_2\text{N}_{14}\text{O}_{12}$ $[\text{M}+2\text{H}]^{2+}$ 615.1888, found 615.1895.

L3.2: ^1H NMR (CD_2Cl_2) δ 8.91 (s, 2H), 8.58 (broad d, 2H), 8.11 (s, 1H), 8.03 (d, J = 7.3 Hz, 2H), 7.72 (d, J = 7.3 Hz, 2H), 7.38 (t, J = 7.3 Hz, 1H), 7.36 – 7.27 (m, 2H), 2.50 (s, 18H), 2.47 (s, 18H). ^{13}C NMR (^{13}C NMR (101 MHz, CD_2Cl_2) δ 152.92, 152.41, 152.00, 148.82, 139.19, 135.04, 131.25, 126.31, 122.81, 13.10, (C-B not detected). HRMS (ESI): m/z calculated for $\text{C}_{40}\text{H}_{50}\text{B}_4\text{Fe}_2\text{N}_{14}\text{O}_{12}$ $[\text{M}+2\text{H}]^{2+}$ 537.1407, found 537.1396.

L3.3: ^1H NMR (400 MHz, CD_2Cl_2) δ 8.80 (s, 2H), 8.50 (broad d, 2H), 7.92 (d, J = 7.1 Hz, 2H), 7.57 (d, J = 7.5 Hz, 4H), 7.25 – 7.17 (m, 6H), 3.98 (s, 2H), 2.91 (s, 24H), 1.81 (s, 24H). ^{13}C NMR (101 MHz, CD_2Cl_2) δ 153.48, 152.74, 152.46, 149.41, 141.77, 139.75, 132.29, 128.45, 123.34, 42.61, 26.77, 22.16, (C-B not detected). HRMS (ESI): m/z calculated for $\text{C}_{59}\text{H}_{68}\text{B}_4\text{Fe}_2\text{N}_{14}\text{O}_{12}$ $[\text{M}+2\text{H}]^{2+}$ 660.2124, found 660.2134.

L3.4: ^1H NMR (400 MHz, CD_2Cl_2) δ 8.89 (s, 2H), 8.57 (broad d, 2H), 8.02 (d, J = 6.5 Hz, 2H), 7.67 (d, J = 6.9 Hz, 4H), 7.38 – 7.05 (m, 6H), 4.05 (s, 2H), 2.46 (s, 36H). ^{13}C NMR (101 MHz, CD_2Cl_2) δ 152.92, 152.43, 152.15, 148.84, 141.23, 139.19, 131.76, 127.87, 122.79, 42.07, 13.13, 13.10, (C-B not detected). HRMS (ESI): m/z calculated for $\text{C}_{47}\text{H}_{56}\text{B}_4\text{Fe}_2\text{N}_{14}\text{O}_{12}$ $[\text{M}+2\text{H}]^{2+}$ 582.1640, found 582.1631.

L3.5: ^1H NMR (400 MHz, CD_2Cl_2) δ 8.81 (s, 2H), 8.51 (broad d, 2H), 7.97 (d, J = 7.1 Hz, 2H), 7.57 (d, J = 8.1 Hz, 4H), 7.27 (t, J = 8.0 Hz, 2H), 6.89 (d, J = 8.1 Hz, 4H), 4.18 (t, J = 5.9 Hz, 4H), 2.91 (s, 24H), 2.27 (t, J = 8.0 Hz, 2H), 1.81 (s, 24H). ^{13}C NMR (101 MHz, CD_2Cl_2) δ 159.48, 152.85, 152.77, 152.41, 148.78, 140.34, 133.40, 123.53, 114.11, 65.02, 30.04, 26.78, 22.15, (C-B not detected). HRMS (ESI): m/z calculated for $\text{C}_{61}\text{H}_{72}\text{B}_4\text{Fe}_2\text{N}_{14}\text{O}_{14}$ $[\text{M}+2\text{H}]^{2+}$ 690.2230, found 690.2236.

L3.6: ^1H NMR (400 MHz, CD_2Cl_2) δ 8.80 (s, 2H), 8.51 (s, 2H), 7.93 (d, J = 6.1 Hz, 2H), 7.56 (d, J = 7.3 Hz, 4H), 7.24 (s, 2H), 6.87 (d, J = 6.9 Hz, 4H), 4.02 (broad t, 4H), 2.91 (s, 24H), 1.92-1.75 (m, 28H), 1.68 (broad t, 2H). ^{13}C NMR (101 MHz, CD_2Cl_2) δ 159.66, 153.35, 152.40, 149.29, 139.88, 133.37, 123.38, 114.09, 68.18, 29.78, 26.78, 23.33, 22.16, (C-B not detected). HRMS (ESI): m/z calculated for $\text{C}_{63}\text{H}_{76}\text{B}_4\text{Fe}_2\text{N}_{14}\text{O}_{14}$ $[\text{M}+2\text{H}]^{2+}$ 704.2387, found 704.2383.

The NMR spectra for these ligands are included in the supporting information of the publication cited under reference 80b.

Cages 3.1–3.6

To the double clathrochelate ligand (see **Table ES3** for amounts, 2.2 μmol , 2 eq.) and $[\text{Pd}(\text{CH}_3\text{CN})_4](\text{BF}_4)_2$ (0.5 mg, 1.1 μmol , 1 eq.) 0.6 mL of solvent (CD_3CN or DMSO-d_6) was added. The solution was heated at 70 °C for 17 h, in which the solution went from turbid to a clear red solution with everything dissolved. NMR shows full conversion to yield the Pd_2L_4 coordination cages. (except in the cases of double clathrochelate (**L3.5**) and (**L3.6**) where there was a small amount of precipitate).

Table ES3: The amounts of the double clathrochelates used for the synthesis of the Pd_2L_4 coordination cages.

Double clathrochelate #	Amount used (mg)
L3.1	2.8
L3.2	2.4
L3.3	3.0
L3.4	2.6
L3.5	3.1
L3.6	3.2

The full characterisation data for these complexes are included in the supporting information of the publication cited under reference 80b.

Destruction experiments

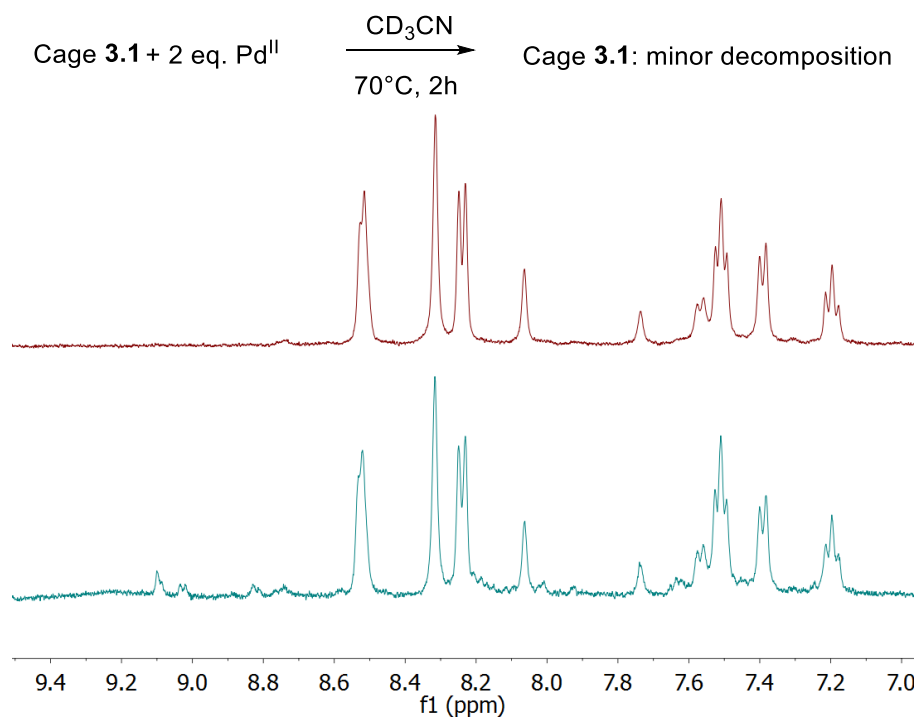


Figure ES1. ¹H NMR spectrum of cage **3.1** in CD₃CN (top) and after the addition of 2 eq. of [Pd(CH₃CN)₄](BF₄)₂ and heating at 70 °C for 2 h to fully equilibrate the sample.

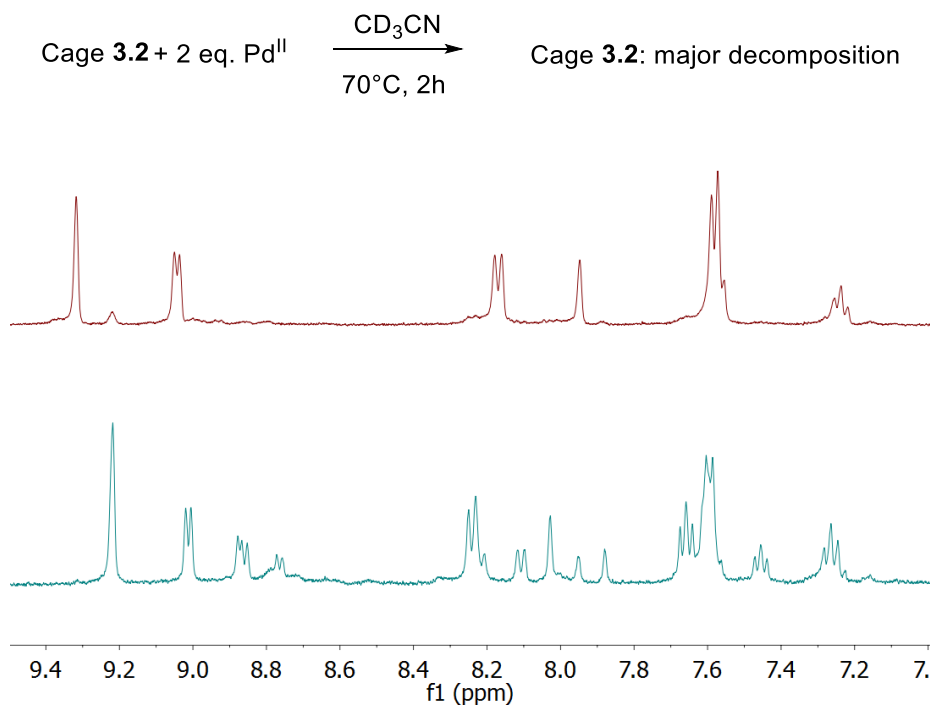


Figure ES2. ¹H NMR spectrum of cage **3.2** in CD₃CN (top) and after the addition of 2 eq. of [Pd(CH₃CN)₄](BF₄)₂ and heating at 70 °C for 2 h to fully equilibrate the sample.

Cage **3.3** + 16 eq. pyridine- d_5 $\xrightarrow[70^\circ\text{C}, 2\text{h}]{\text{DMSO-}d_6}$ Cage **3.3**: minor decomposition

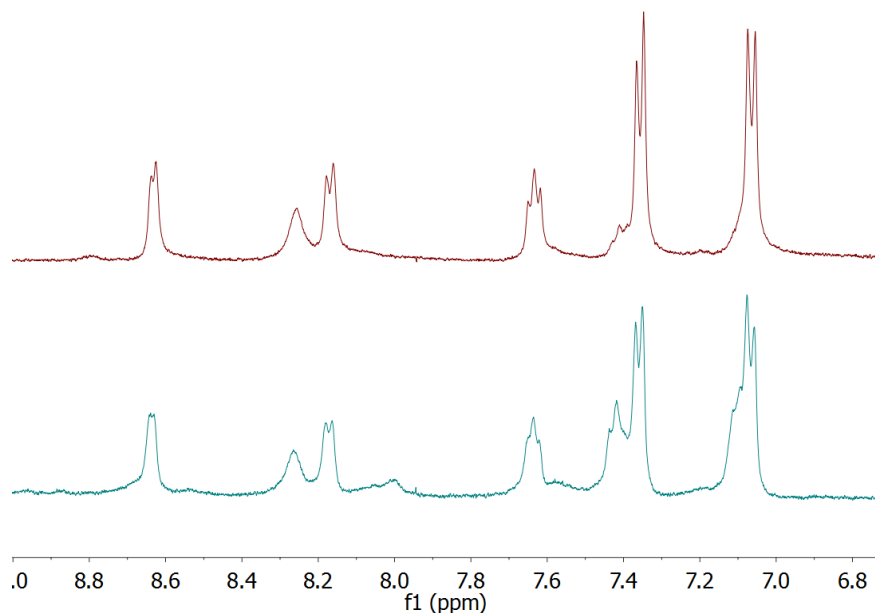


Figure ES3. ^1H NMR spectrum of cage **3.3** in $\text{DMSO-}d_6$ (top) and after the addition of 16 eq. of pyridine- d_5 and heating at 70°C for 2 h to fully equilibrate the sample.

Cage **3.4** + 16 eq. pyridine- d_5 $\xrightarrow[70^\circ\text{C}, 2\text{h}]{\text{DMSO-}d_6}$ Cage **3.4**: major decomposition

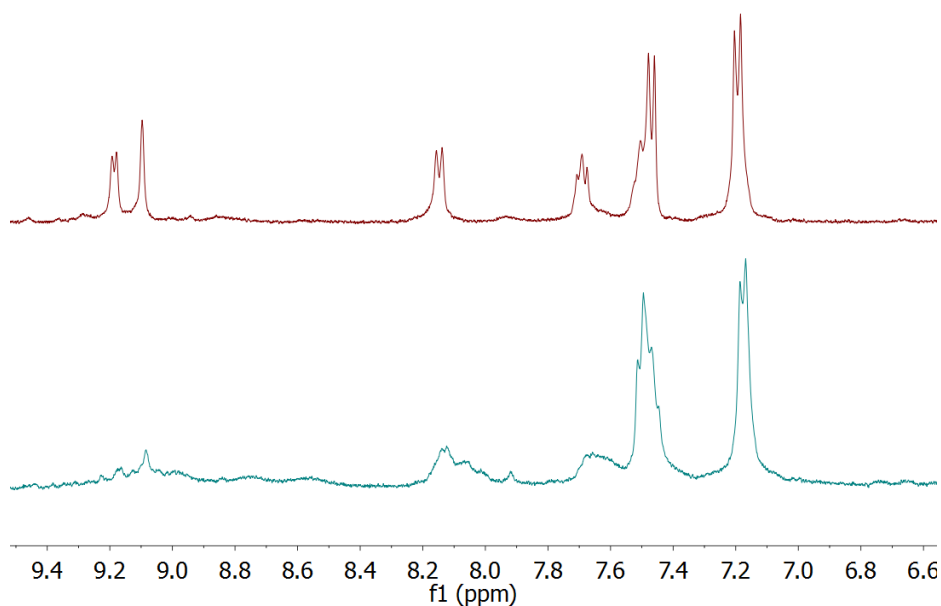


Figure ES4. ^1H NMR spectrum of cage **3.4** in $\text{DMSO-}d_6$ (top) and after the addition of 16 eq. of pyridine- d_5 and heating at 70°C for 2 h to fully equilibrate the sample.

Single crystal X-ray analysis

Intensity data for all ligands and cages were collected on a Rigaku SuperNova dual system in combination with an Atlas CCD detector using Cu- K_{α} radiation ($\lambda = 1.54178 \text{ \AA}$) at 140.0(2) K. The solutions were obtained by *SHELXT*; and the refinements were carried out by *SHELXL-2014*^[153] and *OLEX2*^[112] programs. The crystal structures were refined using full-matrix least-squares based on F^2 with anisotropically refined non-hydrogen atoms (except some disordered -nioxime fragments and solvent molecules which were refined in isotropic approximation). The anions in cages (all disordered and some ordered ones) were refined isotropically with U_{iso} and B-F and B...B distances fixed. Hydrogen atoms were placed in calculated positions by means of the "riding" model. Additional electron density found in the difference Fourier map of cage **3.1-3.3**, **3.5**, **3.6** was treated by the SQUEEZE algorithm of *PLATON* and refined using ABIN instruction because of presence of a twinned component. Unfortunately, weak reflection ability and presence of a twinned component resulted in poor convergence factors for **3.2** and **3.5**. Nevertheless, the quality of the data is clearly sufficient to establish the connectivity of these structures. Intense disorder affected solvent molecules of **L3.1**, **L3.2**, **3.1**, **3.3**, **3.6** and several moieties of crystal structures **3.1**, **3.2** and **3.5** tough restraints/constraints (involving SHELX commands: DFIX, SADI, SIMU, RIGU, EADP and ISOR) were used to handle it.

Crystallographic data have been deposited with the CCDC no. 1511090–1511096. Copies of the data can be obtained free of charge on application to the CCDC, 12 Union Road, Cambridge, CB2 1EZ, U.K. (fax, (internat.) +44-1223-336033; E-mail, deposit@ccdc.cam.ac.uk).

Single crystals of sufficient quality for X-ray analysis were obtained by using slow diffusion with the following solvents:

L3.1 and **L3.2** DCM and diethyl ether

Cage **3.1** CH₃CN and diethyl ether

Cage **3.2** 20% CH₃CN in DMSO and diethylether

Cage **3.3** 20% CH₃CN in DMSO and isopropylether

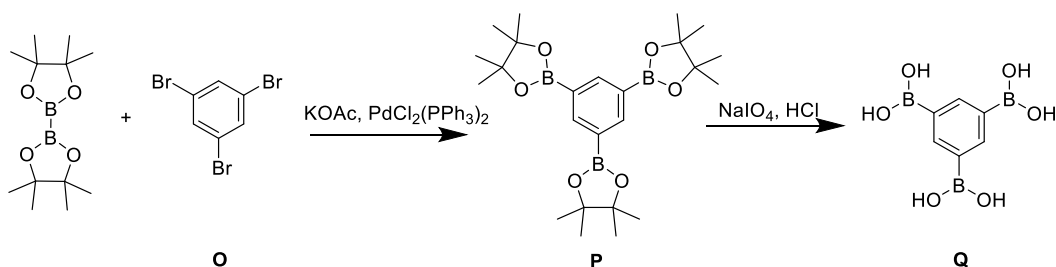
Cage **3.5** 20% CH₃CN in DMSO and isopropylether

Cage **3.6** 20% CH₃CN in DMSO and diethylether

Experimental section Chapter 4

Commercial sources: anhydrous iron(II) chloride – Acros, nioxime – ABCR, bis(triphenylphosphine)palladium(II) dichloride – Sigma Aldrich, 1,3,5-tribromobenzene – Apollo Scientific, 1,3,5-tris(4-bromophenyl)benzene – TCI, bis(pinacolato)diboron – FluoroChem, sodium (meta)periodate – Sigma Aldrich, pyridine-3-boronic acid – FluoroChem, $[\text{Pd}(\text{CH}_3\text{CN})_4](\text{BF}_4)_2$ – ABCR

Synthetic procedures



Scheme ES7. Synthesis of triboronic acid **Q**.

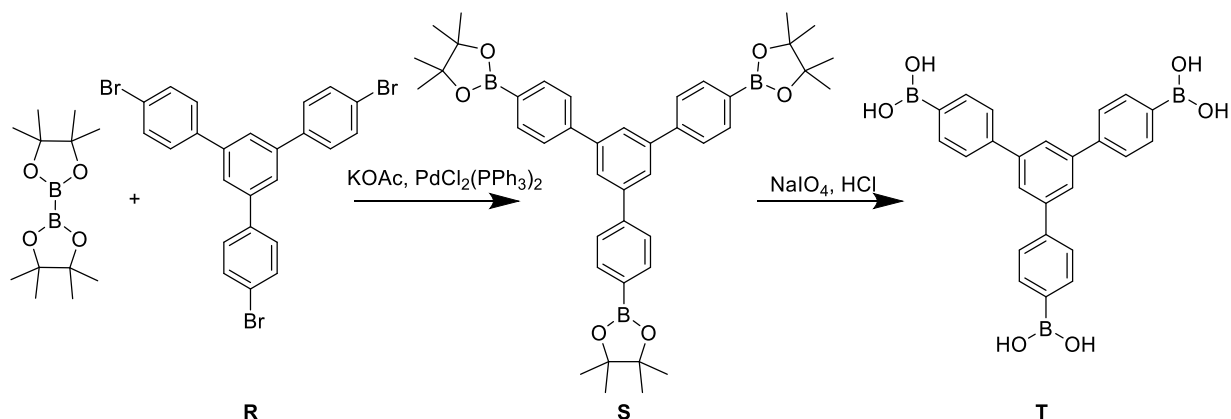
1,3,5-Tribromobenzene **O** (10.0 g, 32 mmol), bis(pinacolato)diboron (26.6 g, 105 mmol, 3.3 eq.), KOAc (10.3 g, 105 mmol, 3.3 eq.), and $\text{PdCl}_2(\text{PPh}_3)_2$ (1.3 g, 1.9 mmol, 0.06 eq.) were combined in a round bottom flask. Degassed dioxane (250 mL) was added and the reaction was stirred at 120 °C overnight. The reaction is cooled to r.t., filtered, dried under reduced pressure and purified by silica column chromatography (gradient of 20% to 50% EtOAc in Hexane). The pure fractions were dried under reduced pressure, which yielded a white powder which was verified by ^1H NMR to be the triboronate ester **P** (9.8 g, 21.5 mmol, 67%). The latter was used directly for the deprotection reaction described below.

^1H NMR (400 MHz, CDCl_3) δ 8.36 (s, 3H), 1.33 (s, 36H).

The deprotection reaction was carried out by a modified method of a published procedure.^[97b] The triboronate ester **P** (9.8 g, 21.5 mmol) and sodium (meta)periodate (41.3 g, 194 mmol, 9 eq.) were suspended in a mixture of THF (240 mL) and H_2O (60 mL) and stirred at r.t. overnight. Aqueous HCl (2 M, 5 mL) were added and the reaction mixture was stirred for 24 h. Methanol (600 mL) was added, the mixture was filtered and concentrated under reduced pressure. Aqueous HCl (1M, 300 mL) was added and the mixture was left to stir for 2 h at r.t.. The white solid was collected by filtration and dried by air to yield the triboronic acid **Q** (3.8 g, 18.3 mmol, 85%).

^1H NMR (600 MHz, $\text{DMSO}-d_6$) δ 8.15 (s, 3H), 7.81 (s, 6H). ^{13}C NMR (151 MHz, $\text{DMSO}-d_6$) δ 141.98, 131.61 (weak, C-B). HRMS (ESI): m/z calculated for $\text{C}_{11}\text{H}_{19}\text{B}_3\text{NaO}_6^+$, (Cationized with Na and 5 × methoxy adducts, from methanol as solvent) 303.1358, found 303.1368 (3.1 ppm).

The NMR data for this triboronic acid are included in the supporting information of the publication cited under reference 104.



Scheme ES8. Synthesis of triboronic acid **T**.

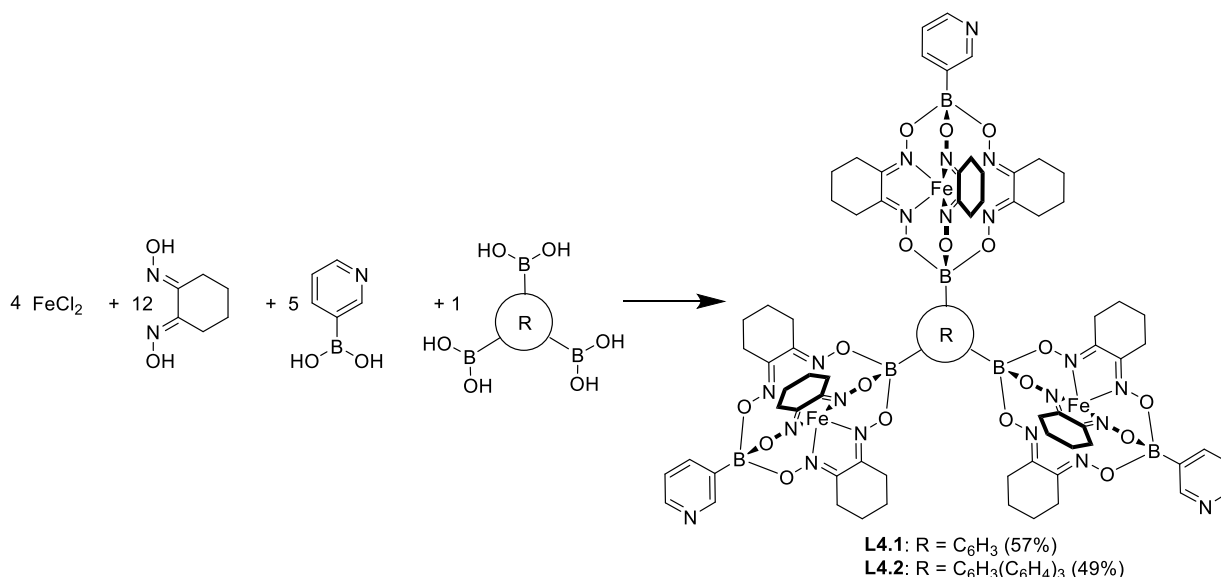
1,3,5-Tris(4-bromophenyl)benzene **R** (5.0 g, 9.2 mmol), bis(pinacolato)diboron (7.7 g, 30.4 mmol, 3.3 eq.), KOAc (3.0 g, 30.4 mmol, 3.3 eq.), and PdCl₂(PPh₃)₂ (0.39 g, 0.18 mmol, 0.06 eq.) were combined in a round bottom flask. Degassed dioxane (100 mL) was added and the reaction was stirred at 120 °C overnight. The reaction was cooled to r.t., filtered, dried under reduced pressure, and purified by silica column chromatography (gradient of 20% to 50% EtOAc in Hexane). The pure fractions were dried under reduced pressure, which yielded a white powder which was verified by ¹H NMR to be the triboronate ester **S** (5.3 g, 7.7 mmol, 84%). The latter was used directly for the deprotection reaction described below.

¹H NMR (400 MHz, CDCl₃) δ 7.93 (d, *J* = 7.6 Hz, 6H), 7.82 (s, 3H), 7.71 (d, *J* = 7.5 Hz, 6H), 1.38 (s, 36H).

The deprotection reaction was carried out by a modified method of a published procedure.^{[97b]S1} The triboronate ester **S** (5.3 g, 7.7 mmol) and sodium (meta)periodate (14.7 g, 69 mmol, 9 eq.) were suspended in a mixture of THF (100 mL) and H₂O (25 mL) and stirred at r.t. overnight. Aqueous HCl (2 M, 2 mL) were added and the reaction mixture was stirred for 24 h. Methanol (400 mL) was added, the mixture was filtered and concentrated under reduced pressure. Aqueous HCl (1M, 120 mL) was added and the mixture was left to stir for 2 h at r.t.. The white solid was collected by filtration and dried by air to yield the triboronic acid **T** (3.2 g, 7.3 mmol, 95%).

¹H NMR (400 MHz, DMSO-*d*₆) δ 8.11 (s, 6H), 7.93 (d with s overlapping, 9H), 7.85 (d, *J* = 7.7 Hz, 6H). ¹³C NMR (101 MHz, DMSO-*d*₆) δ 141.58, 141.50, 134.78, 126.15, (C-B not detected). HRMS (ESI): *m/z* calculated for C₂₉H₃₀B₃NaO₆⁺, (Cationized with Na and 5 × methoxy adducts, from methanol as solvent) 531.2317, found 531.2313 (0.8 ppm).

The NMR data for this triboronic acid are included in the supporting information of the publication cited under reference 104.



Scheme ES9. Synthesis of the metalloligands **L4.1** and **L4.2**.

Anhydrous FeCl₂ (4 eq.) and the respective dioxime (12 eq.) were dissolved in MeOH (15 mL). In a separate flask, the respective triboronic acid (100 mg, 1 eq.) and 3-pyridine boronic acid (5 eq.) were dissolved in methanol (20 mL), acetone (5 mL), and chloroform (150 mL) and heated to reflux and stirred for 30 min. The pre-prepared mixture of dioxime and FeCl₂, was added to the boronic acid mixture, the mixture was heated to reflux for an additional 3 h, before the solvent was removed under reduced pressure. The remaining solid was dissolved in CHCl₃ (100 mL), filtered and washed with a saturated aqueous solution of sodium EDTA and 5% ammonia (100 mL). The organic phase was dried over MgSO₄, and evaporated under reduced pressure. The solid was pre-purified by a short silica column (150 g silica, 10% MeOH in DCM) to remove any polymeric material. The dark red fractions were evaporated under reduced pressure, the solid was dissolved in DCM (10 mL), filtered over H-PTFE 20/25 syringe filters and separated on a size exclusion column (200 g, dry weight, Bio-Beads S-X3 in DCM). The pure fractions (checked by MS, pos. mode), were combined and washed with saturated NaHCO₃ solution, dried over MgSO₄, and the solvent was removed under reduced pressure to yield a red powder.

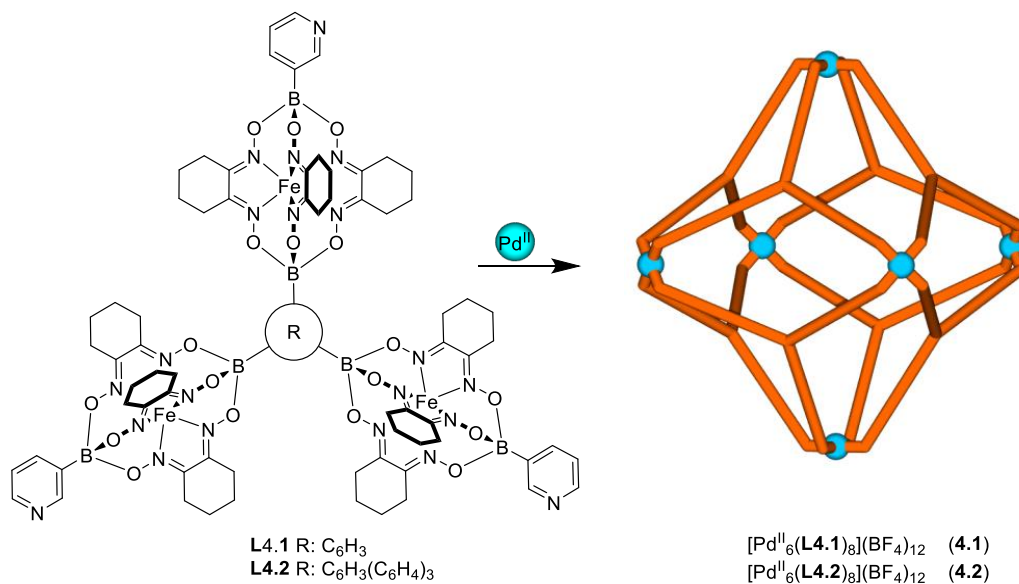
Table ES4. Amounts used for the synthesis of the metalloligands **L4.1** and **L4.2**. BA is boronic acid, CC is clathrocholate.

Ligand	tri-BA	4 eq. FeCl ₂		12 eq. nioxime		1 eq. tri-BA		5 eq. 3-pyridine BA		Yield		
#	#	mg	mmol	mg	mmol	mg	mmol	mg	mmol	mg	mmol	%
L4.1	Q	290	2.3	977	6.9	120	0.60	352	2.9	435	0.35	57
L4.2	T	198	1.6	667	4.7	100	0.39	288	2.3	262	0.20	49

L4.1: ¹H NMR (400 MHz, CD₂Cl₂) δ 8.81 (s, 3H), 8.51 (d, *J* = 3.5 Hz, 3H), 7.99 – 7.84 (m, 6H), 7.29 – 7.16 (m, 3H), 2.95 (2 s, 36H), 1.83 (s, 36H). ¹³C NMR (151 MHz, CD₂Cl₂) δ 153.49, 152.61, 152.06, 151.81, 149.42, 139.72, 123.33, 26.79, 26.70, 22.23, 22.19, (C-B not detected). HRMS (ESI): *m/z* calculated for C₇₅H₉₀B₆Fe₃N₂₁O₁₈ [M+3H]³⁺ 602.1813, found 602.1818 (0.8 ppm).

L4.2: ^1H NMR (400 MHz, CD_2Cl_2) δ 8.81 (s, 3H), 8.51 (d, J = 4.8 Hz, 3H), 7.98 – 7.70 (m, 21H), 7.32 – 7.16 (m, 3H), 2.95 (2 s, 36H), 1.84 (s, 36H). ^{13}C NMR (151 MHz, CD_2Cl_2) δ 153.48, 152.80, 152.61, 149.45, 143.23, 141.12, 139.72, 132.73, 125.32, 123.35, 26.82, 26.77, 22.14, (C-B not detected). HRMS (ESI): m/z calculated for $\text{C}_{93}\text{H}_{102}\text{B}_6\text{Fe}_3\text{N}_{21}\text{O}_{18}$ $[\text{M}+3\text{H}]^{3+}$ is 678.2128, found 678.2145 (2.5 ppm).

The NMR data for the ligands are included in the supporting information of the publication cited under reference 104.



Scheme ES10. Synthesis of the Pd_6L_8 coordination cages **4.1** and **4.2** from **L4.1** and **L4.2**

To the metalloligand (see **Table ES5** for amounts, 1.5 μmol , 4 eq.) and $[\text{Pd}(\text{CH}_3\text{CN})_4](\text{BF}_4)_2$ (0.5 mg, 1.1 μmol , 3 eq.) 0.6 mL of DMSO-d_6 was added. The solution was heated at 70 $^\circ\text{C}$ for 17 h, in which the solution went from turbid to a clear red solution with everything dissolved. NMR shows full conversion to yield the $\text{Pd}^{\text{II}}_6\text{L}_8$ coordination cages.

Table ES5. The amounts of the double clathrochelates used for the synthesis of the M_6L_8 coordination cages.

Metalloligand #	Amount used (mg)
L4.1	2.7
L4.2	3.0

The full characterisation data for these two complexes are included in the supporting information of the publication cited under reference 104.

Cold-spray ionisation

Cold-spray ionisation (CSI) MS was performed on a hybrid linear ion trap (LTQ) Orbitrap Elite mass spectrometer (Thermo Scientific, Bremen, Germany) equipped with a modified HESI-II probe in an Ion Max ion source. In order to perform CSI-MS experiments, the commercial sheath (blue in **Figure ES5**) and auxiliary (green in **Figure ES5**) gas lines were modified and redirected towards a liquid nitrogen cooling device (black in **Figure ES5**).

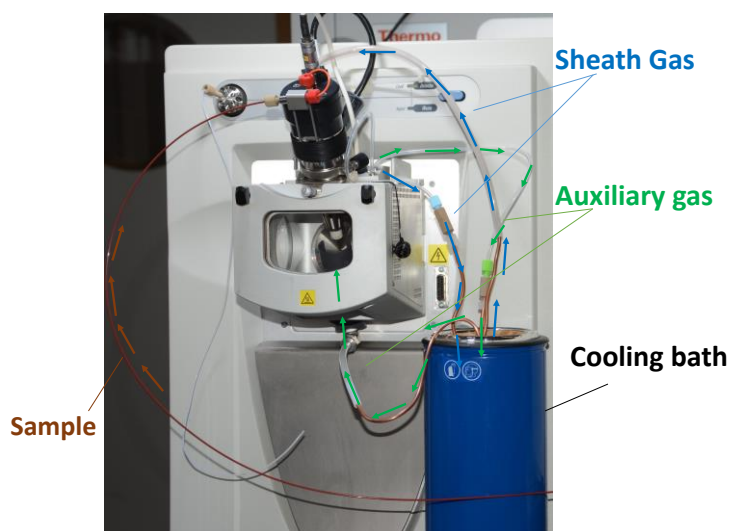


Figure ES5. Modified HESI-II probe in an Ion Max ion Source (Thermo Scientific). The sheath gas pathway is represented in blue whereas the auxiliary gas line is in green. Both lines are modified and redirected through the cooling bath.

In the probe body, the sheath gas (inner coaxial N_2) emerging from the metal needle sprays the sample after being redirected through the cooling bath. The auxiliary gas is redirected to the same cooling bath before entering a homemade PVC chamber located at the bottom of the source and helping in stabilizing the temperature as well as the spray (**Figure ES6**).

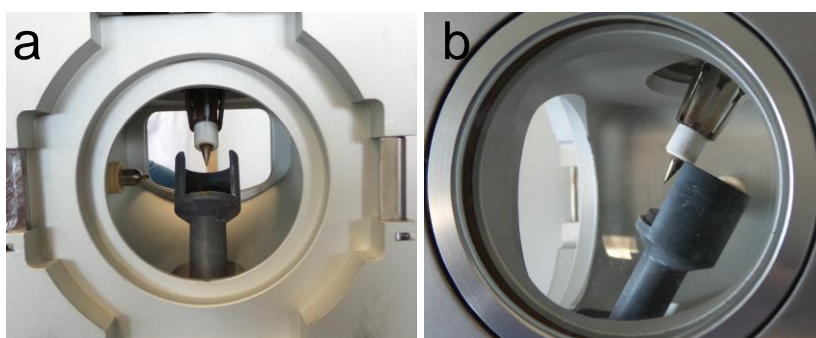


Figure ES6. a) Left side and b) Front/back view of the HESI-II probe with the homemade PVC piece placed at the bottom of the Ion Max ion source.

The PVC piece used to redirect the auxiliary gas is composed of three different parts. The main PVC body (**Figure ES7a**) drives the cooled gas towards the entrance of the Orbitrap. A perforated disk (**Figure ES7b**)

diffuses the auxiliary gas and is crucial to give a stable signal. Both pieces are attached to the HESI-II probe using a third PVC clamp (**Figure ES7c**).

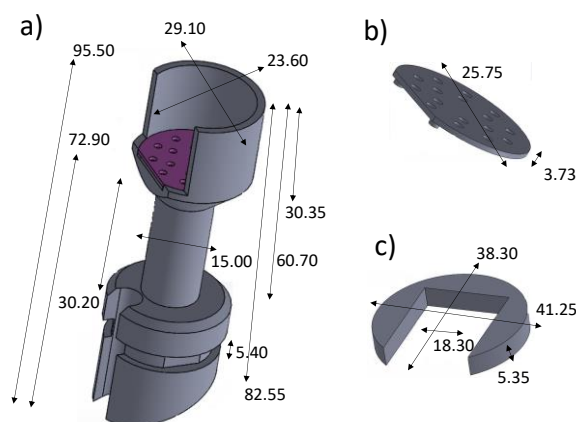


Figure ES7. Measurements and design of the homemade PVC pieces contained in the CSI source; a) main body, b) gas diffuser and c) attachment piece. Values are in mm.

The spray temperature is dependent on the cooling bath composition and therefore temperature, the length of the tubing (inside and outside the bath), the materials chosen for the lines as well as the gas flow rates. Therefore, calibration curves were made by placing a thermocouple near the spray, in order to know the instant spray temperature under different conditions of gas flow rates. The liquid nitrogen was used as refrigerant in the cooling bath, the spray temperature was manually controlled by adjusting both the sheath and the auxiliary gas flows, allowing a range of temperature from 20 °C to –50 °C (**Figure ES8**). For this particular setup applied to the mass spectrum measurement of coordination cages, the sheath and auxiliary gas flows were fixed at 6 and 4, respectively, to obtain a spray temperature around –10 °C. This temperature was shown to be the best to both preserve the integrity of coordination cages and obtain sufficient number of ions in the gas phase.

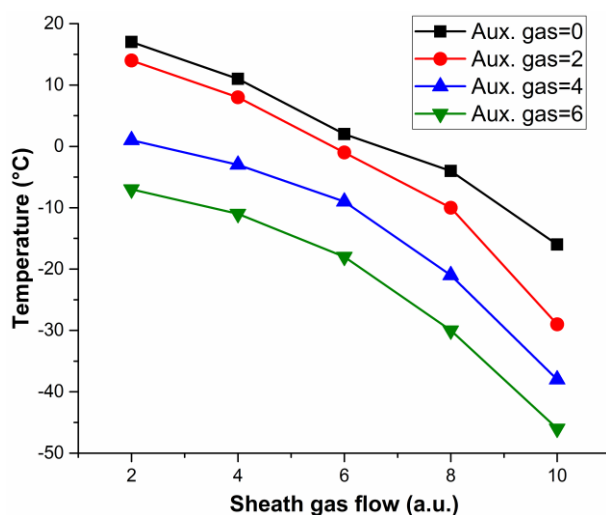


Figure ES8. Measured spray temperatures depending on both sheath and the auxiliary gas flows.

High resolution mass spectra were acquired for pure, pre-synthesized samples of the cages. The analytes were diluted in acetonitrile to a final concentration of ~10-20 µM. The standard XCalibur 2.2 data acquisition and instrument control system was utilized (Thermo Scientific). Samples were introduced at a flow rate of 20 µL/min and sprayed using an ionization voltage of +1.2 kV and an ion transfer capillary temperature of 80 °C. FT-MS

spectra were acquired using the high mass range (between 400–4000 m/z) in the reduced profile mode with a resolution set to 120'000 at 400 m/z and a target value of charges of 1 million. All Orbitrap FTMS scans were recorded averaging 10 microscans to improve the SNR and setting a maximum injection time value at 1000 ms.

Spartan model cage **4.2**

A model of cage **4.2** was constructed using Spartan and it's MMF energy minimisation.

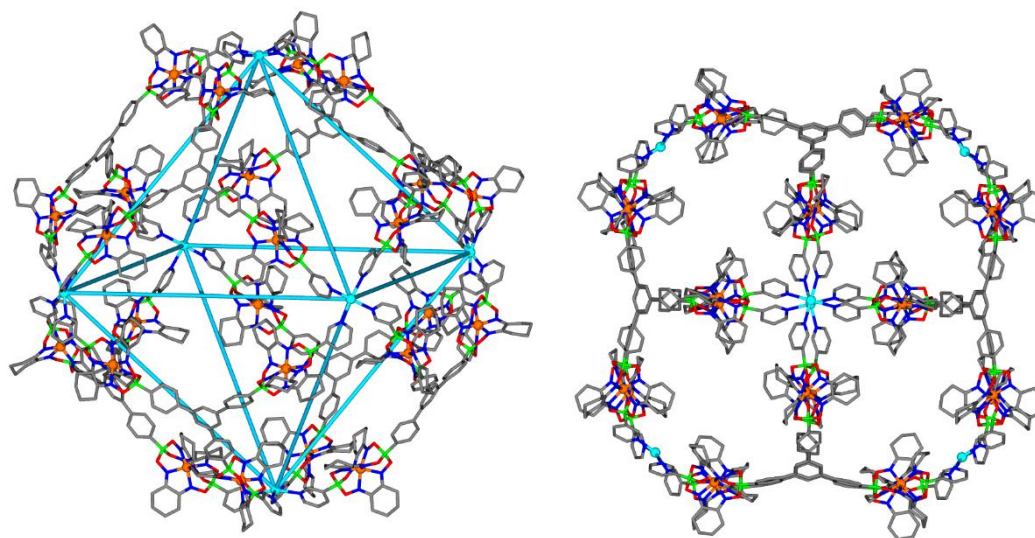


Figure ES9. Graphical representation of the structure of cage **4.2** from the Spartan model. Hydrogen atoms are omitted for clarity. Grey: C; blue: N; green: B; red: O; cyan: Pd and orange: Fe.

Crystallographic data

Bragg-intensities of **L4.1**, **L4.2** and the cage **4.1** were measured at low temperature using Cu $K\alpha$ radiation on a Rigaku SuperNova dual system diffractometer equipped with an Atlas CCD detector for the compounds **L4.1** and the cage **4.1** and one equipped with an Atlas S2 CCD detector for the compound **L4.2**. The datasets were reduced and then corrected for absorption, with the help of a set of faces enclosing the crystals as snugly as possible, with CrysAlis^{Pro}.

The solutions and refinements for the structures were performed by SHELXT and SHELXL-2018 (release 3),^[153] respectively. All non-hydrogen atoms were refined anisotropically using full-matrix least-squares based on $|F|^2$. All hydrogen atoms were placed in geometrically calculated positions and refined using a riding model where each H-atom was assigned a fixed isotropic displacement parameter with a value equal to 1.2 U_{eq} of its parent C-atom.

The structure of **L4.1** was refined as a two-component inversion twin yielding a BASF parameter of 0.48(2). The distance similarity restraint (SADI) was needed for the refinement of the cyclohexyl rings. SIMU and RIGU restraints were also applied on the displacement parameters of the light atoms. Almost, four highly disordered dichloromethane solvent molecules were removed from the model by the SQUEEZE algorithm of PLATON.^[154]

In the case of **L4.2**, two cyclohexyl moieties and one pyridine ring were disordered over two orientations. The atoms of each orientation were located in a difference Fourier map for each disordered ring. The major and minor parts were refined anisotropically, but distance and similarity restraints (SADI and SIMU) were applied for a convergent least-squares refinement. RIGU restraint was also applied on the displacement parameters of the atoms. Highly disordered solvent molecules were removed with the help of the solvent-masking program in OLEX2.^[112]

The structure of cage **4.1** was refined as a two-component inversion twin yielding a BASF parameter of 0.50(4). RIGU and SIMU restraints were applied on the displacement parameters of all the atoms and the light atoms, respectively. Aromatic groups were restrained to have an ideal hexagonal geometry, using the card AFIX 66. Some distance similarity restraints (SADI and DFIX) were applied to the cyclohexyl moieties. Additional counter ions and solvent molecules, too disordered to be located in the electron density map, were taken into account using the solvent-masking program in OLEX2.^[112]

Crystallographic data have been deposited to the CCDC and correspond to the following codes: **L4.1** (CCDC1849686), **L4.2** (1849685), Cage **4.1** (1849687). Copies of the data can be obtained free of charge on application to the CCDC, 12 Union Road, Cambridge, CB2 1EZ, U.K. (fax, (internat.) +44-1223-336033; E-mail, deposit@ccdc.cam.ac.uk).

Table ES6. Determined unit cell dimensions from two differently grown crystals of cage **4.2**.

	SJ131 - DMSO	SJ125 – DMSO-d₆
cell_length_a	64.286(8)	64.465(8)
cell_length_b	43.795(3)	43.629(3)
cell_length_c	76.413(7)	76.113(11)
cell_volume	193902(30)	192730(30)
cell_angle_alpha	90.0	90.0
cell_angle_beta	115.668(14)	115.802(16)
cell_angle_gamma	90.0	90.0

Single crystals of sufficient quality for X-ray analysis were obtained by using slow diffusion with the following solvents:

L4.1: Slow diffusion of pentane into a solution of **L4.1** in DCM.

L4.2: Slow diffusion of pentane into a solution of **L4.2** in DCM.

4.1: Slow diffusion of isopropyl acetate into a solution of **4.1** in DMSO with the addition of 24 eq. of NaClO₄, over the time of several months.

4.2: Slow diffusion of toluene into a solution of **4.2** in DMSO or DMSO-d₆, over the time of several months.

VOIDOO calculations cage **4.1**

In order to determine the available void space (probe-occupied volume) within complex **4.1**, VOIDOO calculations^[156] based on the crystal structure were performed. A virtual probe with a radius of 3.0 Å (smallest probe-size where the probe didn't fall out of the cavity) was employed, and the standard parameters were used, unless noted below.

- Maximum number of volume-refinement cycles: 30
- Minimum size of secondary grid: 3
- Grid for plot files: 0.3
- Primary grid spacing: 0.1
- Plot grid spacing: 0.1

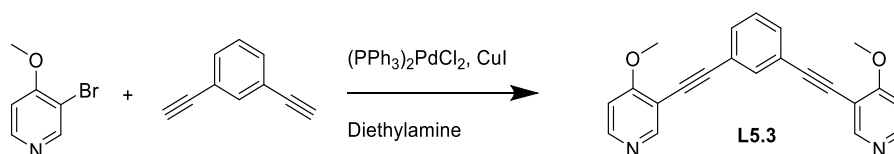
For complex **1**, the following values were found: Volume: $2.79 \times 10^3 \text{ Å}^3$ (standard deviation 0.87 Å^3), which would correspond to a sphere with a radius of 8.74 Å.

Experimental section Chapter 5

Commercial sources: $[\text{Pd}(\text{CH}_3\text{CN})_4](\text{BF}_4)_2$ – ABCR, 1,3-diethynylbenzene – TCI, 3-bromo-4-methoxypyridine – Fluorochem, $(\text{PPh}_3)_2\text{PdCl}_2$ – Sigma Aldrich, CuI – Sial, Diethylamine – Acros, 1,4-Phenylenediboronic acid – Sigma Aldrich, $\text{Pd}_2(\text{dba})_3$ – TCI, Triphenylphosphine – Roth AG, TFA – Acros, 4-methoxypyridine – TCI, pyridine – Fluorochem, DMAP – Fluka, 3-chloropyridine – Apollo, NaTFA – Fluorochem.

Synthetic procedures

The ligands **L5.1**,^[120] **L5.4**,^[157] **L5.5**^[66a] and the carbene complex $[\text{PdBr}_2(\text{iPr}_2\text{-bimy})]_2$ for the HEP,^[158] were prepared according to literature procedures.



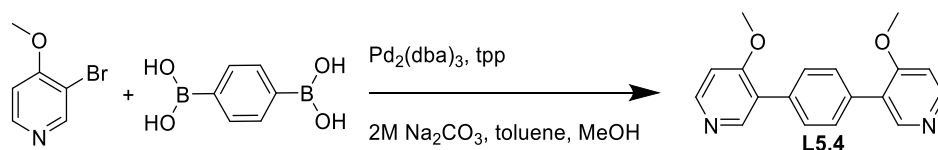
Scheme ES11. Synthesis of **L5.3**.

Derived from a literature procedure,^[120] ligand **L5.3** was synthesized as follows:

1,3-Diethynylbenzene (0.66 mL, 5.0 mmol), 3-bromo-4-methoxypyridine (1.25 mL, 10.3 mmol, 2.1 eq.), $(\text{PPh}_3)_2\text{PdCl}_2$ (80 mg, 0.11 mmol), and CuI (15 mg, 0.08 mmol) were combined in a round-bottomed flask and degassed. Degassed diethylamine (15 mL) was added and the reaction was heated at 60 °C under nitrogen for 18 h. Ethyl acetate (100 mL) was added and the mixture was filtered. Water (100 mL) was added to the filtrate, the organic layer was separated and the water layer was washed with ethylacetate (2 × 100 mL). The organic layers were combined, dried over MgSO_4 , evaporated under reduced pressure and purified by column chromatography (silica, 2-5% MeOH in DCM) to yield ligand **L5.3** (351 mg, 1.03 mmol, 21%) as a pale yellow solid.

^1H NMR (600 MHz, CD_2Cl_2) δ = 8.57 (s, 2H), 8.43 (d, J = 5.8, 2H), 7.74 (s, 1H), 7.54 (dd, J = 7.8, 1.6, 2H), 7.39 (t, J = 7.8, 1H), 6.87 (d, J = 5.8, 2H), 3.97 (s, 6H). ^{13}C NMR (151 MHz, CD_2Cl_2) δ = 166.07, 154.24, 151.43, 134.97, 132.07, 129.26, 123.93, 110.07, 94.99, 83.83, 56.41. HRMS (ESI): m/z calculated for $\text{C}_{22}\text{H}_{17}\text{N}_2\text{O}_2$ $[\text{M}+\text{H}]^+$ 341.1285, found 341.1296.

The NMR spectra are included in the supporting information of the publication cited under reference 113.



Scheme ES12. Synthesis of **L5.4**.

Derived from a literature procedure,^[157] ligand **L5.4** was synthesized as follows:

1,4-Phenylenediboronic acid (0.7 g, 4.2 mmol), 3-bromo-4-methoxypyridine (1.54 mL, 12.7 mmol, 3 eq.), Pd₂(dba)₃ (100 mg, 0.11 mmol), and triphenylphosphine (232 mg, 0.89 mmol) were combined in a round bottom flask and degassed. To the mixture degassed toluene (125 mL), methanol (20 mL) and 2 M Na₂CO₃ (20 mL) was added and the reaction was heated at 70 °C under nitrogen for 18 h. Afterwards, the organic layer was separated and the water layer was washed with DCM (3 × 50 mL). The organic layers were combined and dried over MgSO₄, evaporated under reduced pressure and purified by column chromatography (silica, 2-5% MeOH in DCM) to yield ligand **L5.4** (264 mg, 1.3 mmol, 27%) as a white solid.

¹H NMR (600 MHz, CD₂Cl₂) δ = 8.47 (d, *J* = 5.7, 2H), 8.45 (s, 2H), 7.59 (s, 4H), 6.94 (d, *J* = 5.7, 2H), 3.90 (s, 6H).

¹³C NMR (151 MHz, CD₂Cl₂) δ = 163.09, 151.15, 134.88, 129.89, 126.46, 107.05, 55.95. HRMS (ESI): *m/z* calculated for C₁₈H₁₆N₂O₂ [M+H]⁺ 293.1285, found 293.1285.

The NMR spectra are included in the supporting information of the publication cited under reference 113.

Complexes from **L5.1** – **L5.5**

The ligand (see **Table ES7** for amounts, 4.50 μmol, 2 eq.) was added to [Pd(CH₃CN)₄](BF₄)₂ (1.0 mg, 2.25 μmol, 1 eq.) in a mixture of CD₃CN and CD₃NO₂ (8:2) (0.5 mL). The solution was heated at 60 °C for 17 h. During this time, the solution went from turbid (in the case of **L5.4** and **L5.5**) to clear. The NMR spectra indicated full conversion to the respective assemblies.

Table ES7. The amounts of the ligands (**L5.1** – **L5.5**) used for the synthesis of the coordination complexes.

Ligand #	Coordination complex	Amount used (mg)	Final concentration complex (mM)
L5.1	[Pd ^{II} ₂ (L5.1) ₄] ⁴⁺	1.26	2.25
L5.2	[Pd ^{II} ₄ (L5.2) ₈] ⁸⁺	1.04	1.13
L5.3	[Pd ^{II} ₂ (L5.3) ₄] ⁴⁺	1.53	2.25
L5.4	[Pd ^{II} ₃ (L5.4) ₆] ⁶⁺	1.31	1.50
L5.5	[Pd ^{II} ₆ (L5.5) ₁₂] ¹²⁺	2.94	0.75

The analytical data of the new complexes resulting from **L5.3** and **L5.4** are given below. For the characterization of the complexes resulting from **L5.1**^[120], **L5.2**^[24] and **L5.5**,^[66a] we would like to refer to the previously published results.

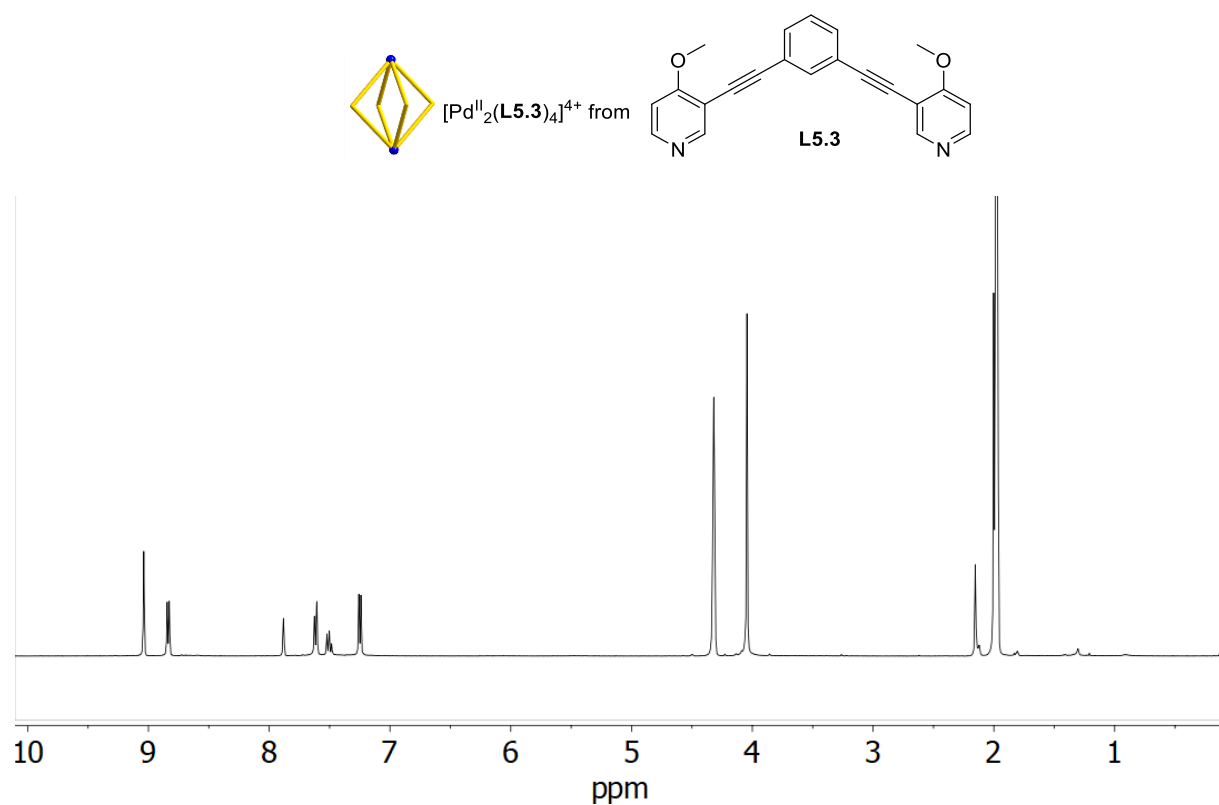


Figure ES10. ^1H NMR (400 MHz) spectrum (400 MHz) of $[\text{Pd}^{\text{II}}_2(\text{L5.3})_4]^{4+}$ in a mixture of CD_3CN and CD_3NO_2 (8:2).

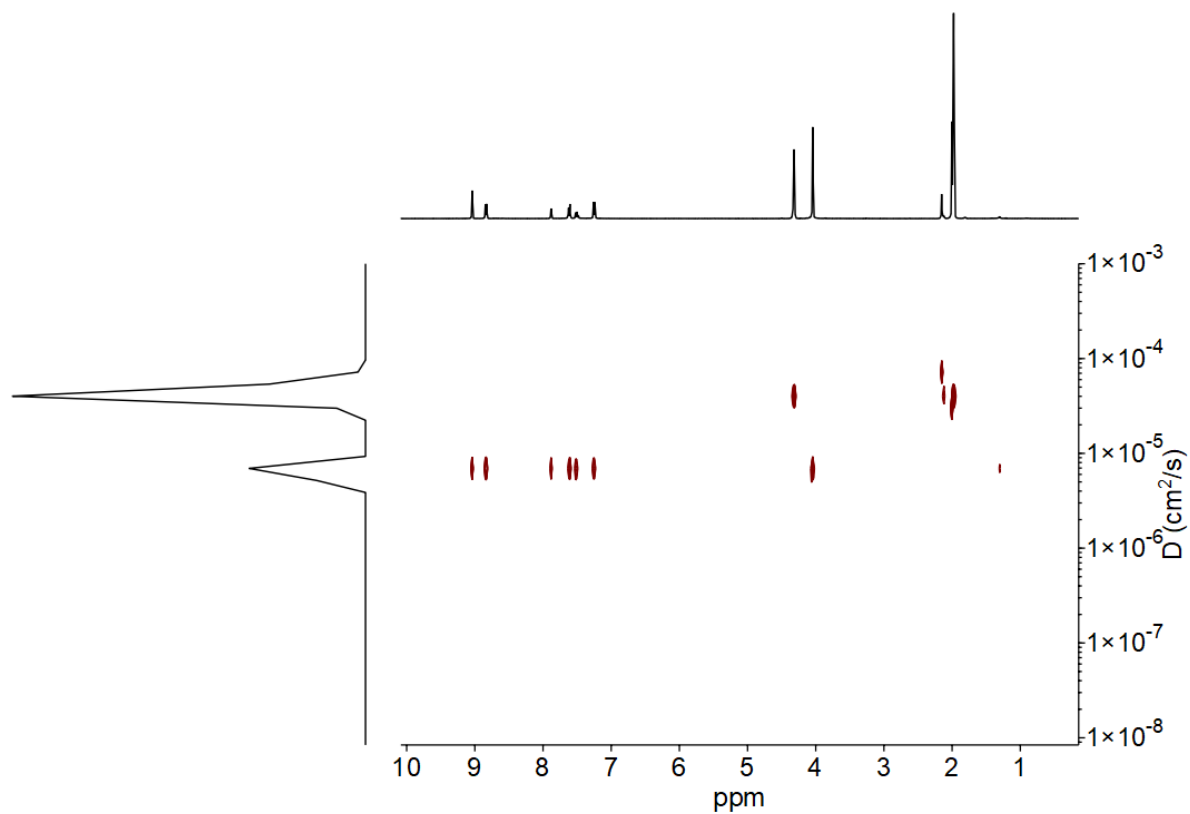


Figure ES11. ^1H DOSY NMR (400 MHz) spectrum of $[\text{Pd}^{\text{II}}_2(\text{L5.3})_4]^{4+}$ in a mixture of CD_3CN and CD_3NO_2 (8:2).

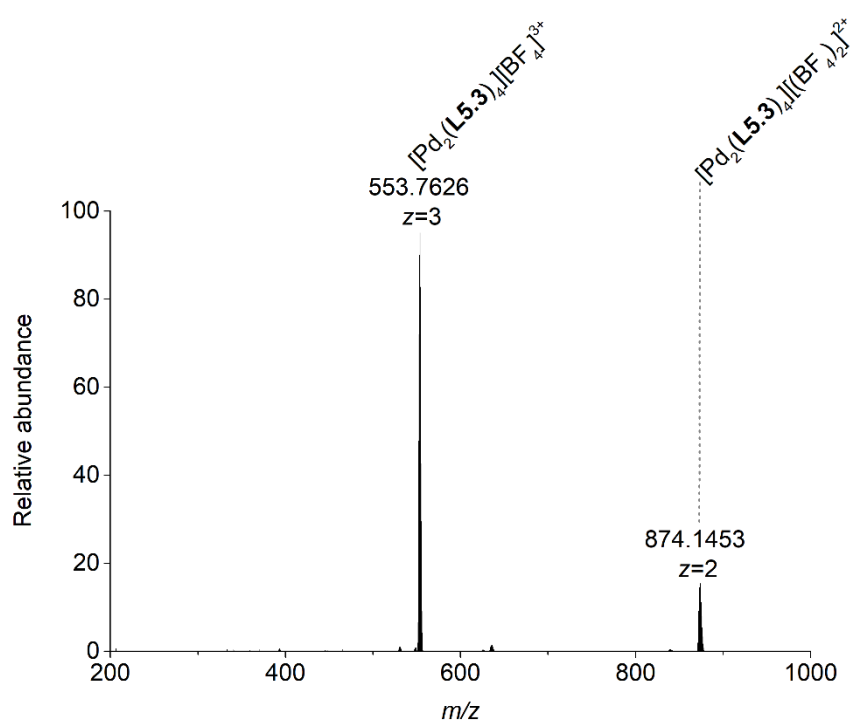


Figure ES12. HRMS of coordination cage $[\text{Pd}^{\text{II}}_2(\text{L5.3})_4]^{4+}$ in a mixture of CH_3CN and CD_3NO_2 (95:5).

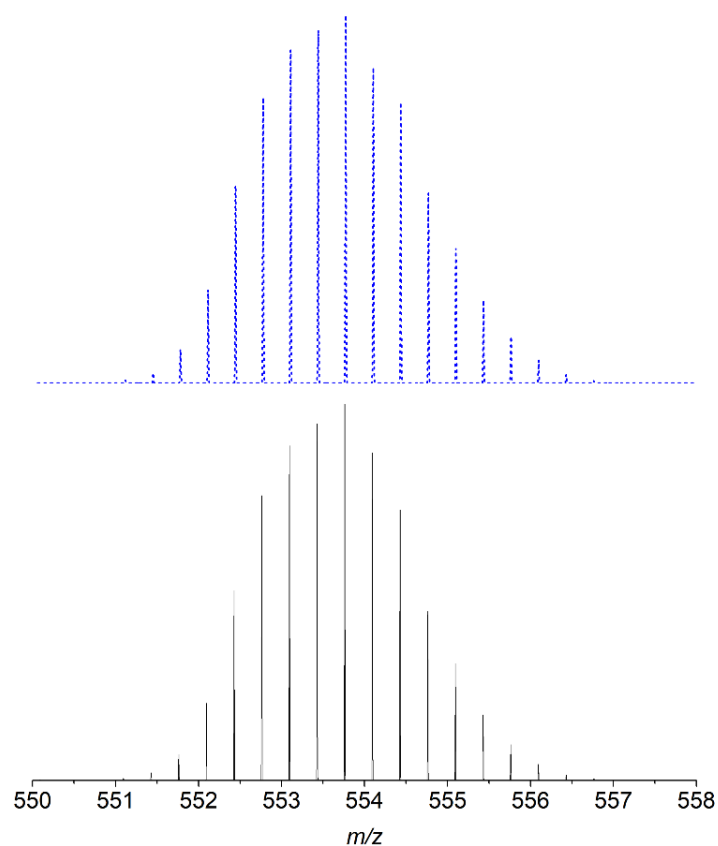


Figure ES13. HRMS of coordination cage $[\text{Pd}^{\text{II}}_2(\text{L5.3})_4]^{4+}$ in a mixture of CH_3CN and CD_3NO_2 (95:5). Zoom-in around the 554 m/z region (bottom). Simulated mass spectrum of the +3 charge species of the complex $[\text{Pd}_2(\text{L3})_4][\text{BF}_4]^{3+}$ (top).

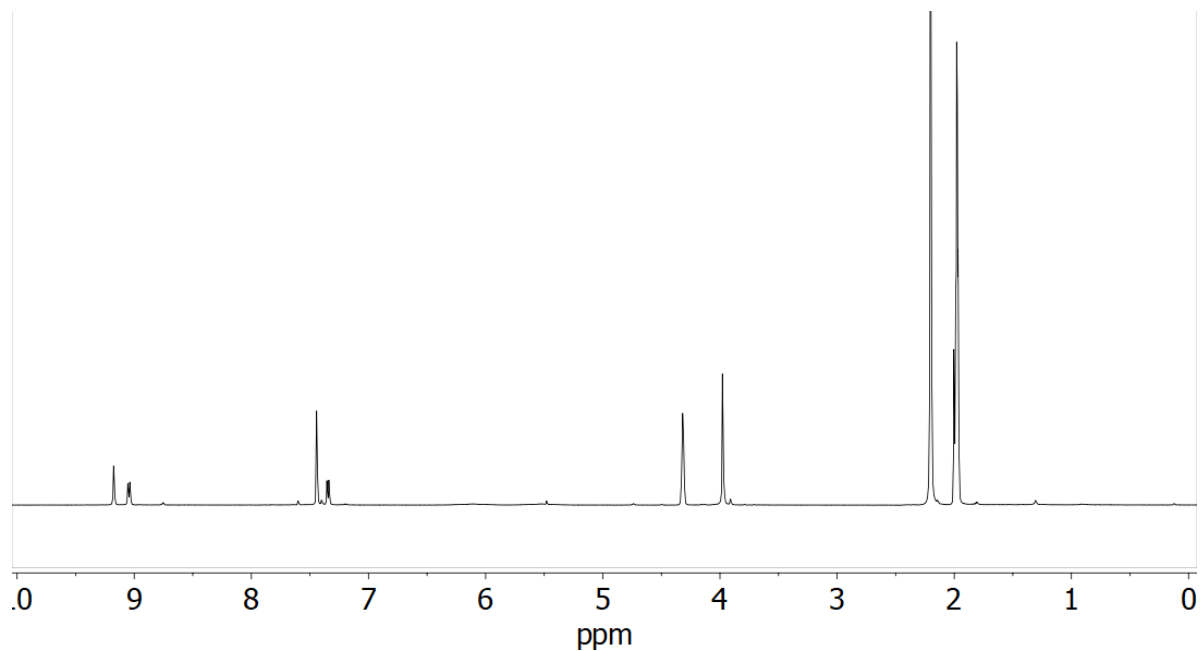
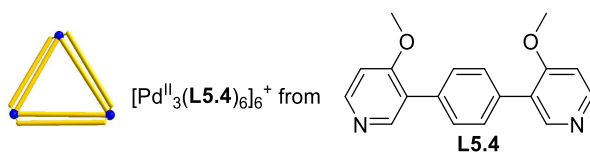


Figure ES14. ^1H NMR (400 MHz) spectrum of $[\text{Pd}^{\text{II}}_3(\text{L5.4})_6]^{6+}$ in a mixture of CD_3CN and CD_3NO_2 (8:2).

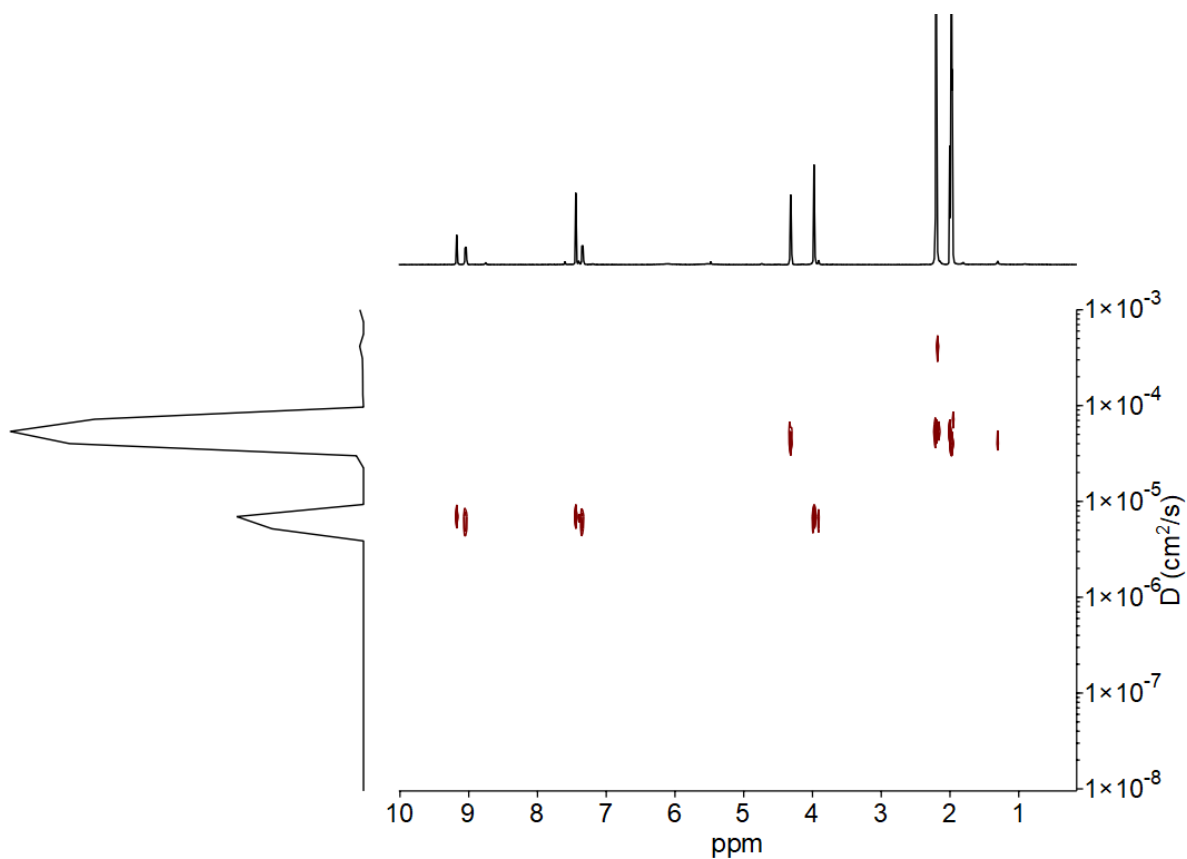


Figure ES15. ^1H DOSY NMR (400 MHz) spectrum of $[\text{Pd}^{\text{II}}_3(\text{L5.4})_6]^{6+}$ in a mixture of CD_3CN and CD_3NO_2 (8:2).

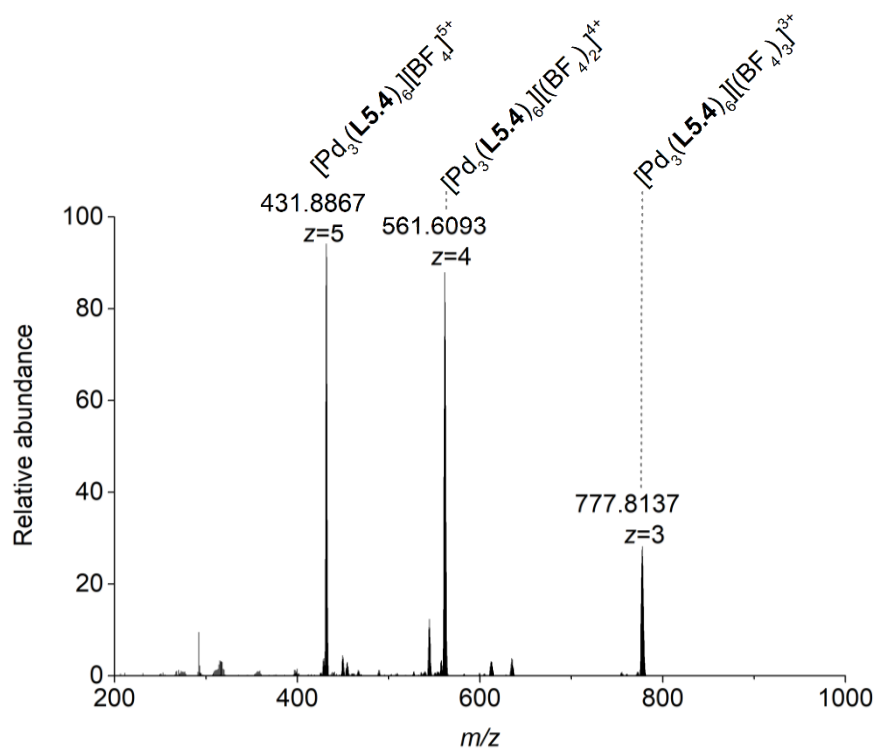


Figure ES16. HRMS of coordination complex $[\text{Pd}^{\text{II}}_3(\text{L5.4})_6]^{6+}$ in a mixture of CH_3CN and CD_3NO_2 (95:5).

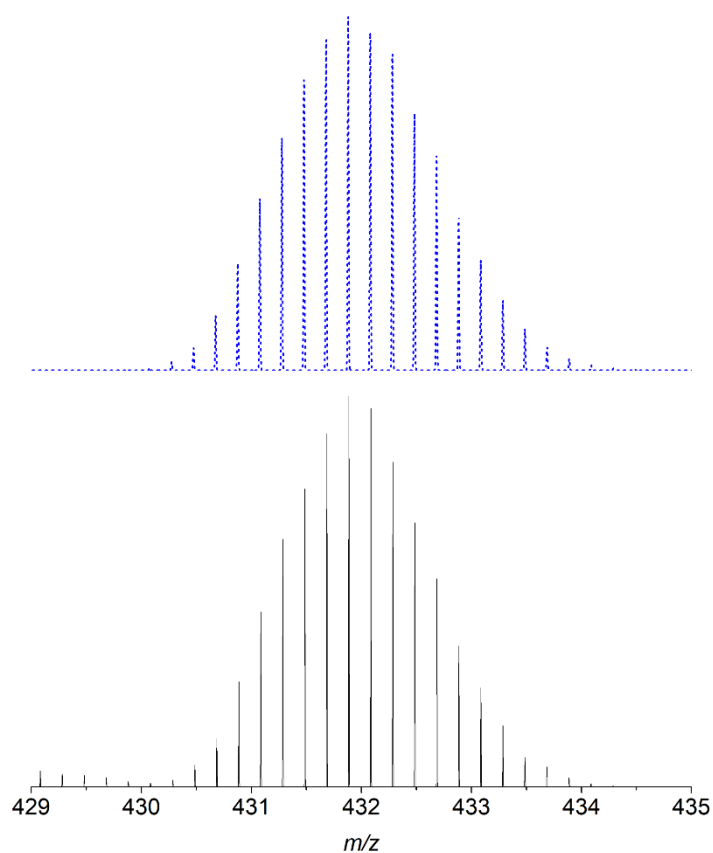


Figure ES17. HRMS of coordination complex $[\text{Pd}^{\text{II}}_3(\text{L5.4})_6]^{6+}$ in a mixture of CH_3CN and CD_3NO_2 (95:5). Zoom-in around the 432 m/z region (bottom). Simulated mass spectrum of the +5 charge species of the complex $[\text{Pd}_3(\text{L4})_6][\text{BF}_4]^{5+}$ (top).

Determination of the ΔpK_a

Two ligands (4.5 μ mol, 9 mM for the ligands or 9.0 μ mol, 18 mM for the reference compounds) were combined in CD_3CN or a mixture of CD_3CN : CD_2Cl_2 1:1 (0.5 mL). A stock solution of TFA (57.4 μ L in 1 mL CD_3CN , 750 mM) was prepared to contain 4.5 μ mol per 6 μ L stock solution. Per sample there was 2 x 4.5 μ mol of ditopic ligands (36 mM of pyridine groups) present. With the addition of 6 μ L TFA stock solution (9 mM), 0.25 eq. of the total amount of pyridine groups were protonated.

For every combination, there were 6 points recorded, with the last point being 1.25 eq. of acid (45 mM) per pyridine group (36 mM) present in solution. The plots below show the average chemical shifts of multiple selected signals for each ligand in the mixture with respect to the normalized chemical shift at 1.25 eq. of acid (normalized to 100%).

ΔpK_a : ClPy < **L5.1** < **L5.2** ~ **L5.3** < Py < MeOPy ~ **L5.4** < **L5.5** < DMAP

A graphical representation of the data for the ΔpK_a determination are included in the supporting information of the publication cited under reference 113.

Determination of the HEP

One of the ditopic ligands (4.5 μ mol, 9 mM) or reference compounds (9.0 μ mol, 18 mM) and the dimeric carbene complex (4.2 mg, 4.5 μ mol, 9 mM) were combined in $CDCl_3$ (0.5 mL) and after mixing, the 1H and ^{13}C spectra were directly recorded. The residual solvent signals from $CDCl_3$ are referenced to 77.7 ppm^[122] and the ^{13}C chemical shift of the carbene signal was reported in ppm in **Table 5.1**.

The NMR spectra for the determination of the HEP are included in the supporting information of the publication cited under reference 113.

Disassembly of the complexes

Solutions of the cages were prepared as described above (section 2.2.). Stock solutions of respectively TFA (57.4 μ L in 1 mL CD_3CN , 750 mM) and pyridine- d_5 (60.1 μ L in 1 mL CD_3CN , 750 mM) were prepared to contain 4.5 μ mol TFA per 6 μ L stock solution. Per sample, there was a final concentration of 9 mM of ditopic ligands and 72 mM of acid or 18 mM of pyridine- d_5 .

There is one broad peak visible in the 1H NMR spectra, which is believed to belong to the residual H_2O . Due to the acidity of the samples, this peak can shift all the way up in the aromatic region in some cases.

The NMR spectra of the disassembly of the complexes are included in the supporting information of the publication cited under reference 113.

Acid-mediated switching between different assemblies

The two respective ligands (4.50 μmol , 9 mM each) were combined and a sub-stoichiometric amount of $[\text{Pd}(\text{CH}_3\text{CN})_4](\text{BF}_4)_2$ (1.0 mg, 2.25 μmol , 4.5 mM) and a mixture of CD_3CN and CD_3NO_2 (8:2) (0.5 mL) was added. The solution was heated at 60 $^\circ\text{C}$ for 17 h. During this time the solution went from turbid (in the case of **L5.4** and **L5.5**) to clear.

It was observed that the complex of the most basic ligand was preferentially formed. After addition of acid from the TFA stock solution (resulting in an acid concentration of 72 mM, 2 eq. of acid per pyridine group present), as described in section 3 and 5, the solution was heated at 60 $^\circ\text{C}$ for 2 h to reach the new thermodynamic equilibrium, before being measured again.

There is one broad peak visible in the ^1H NMR spectra, which is believed to belong to the residual H_2O . Due to the acidity of the samples, this peak can shift all the way up in the aromatic region in some cases. The aromatic regions of these NMR spectra are shown in Chapter 5 (**Scheme 5.4 – 5.7**).

The MS sample was taken at the beginning (before addition of acid) of every reaction and diluted with CH_3CN , before being measured.

The MS spectra of the acid-mediated switching between different assemblies are included in the supporting information of the publication cited under reference 113.

Experimental section Chapter 6

Commercial sources: 2,2'-dipyridyl – TCI, 2,4,6-tri(4-pyridyl)-1,3,5-triazine – ABCR, iron(II) tetrafluoroborate hexahydrate – Sigma Aldrich, pyridine – Sigma Aldrich, sodium tetrakis(4-fluorophenyl)borate hydrate – TCI, $\text{Pd}(\text{CH}_3\text{CN})_4(\text{BF}_4)_2$ – ABCR and zinc tetrafluoroborate hydrate – ABCR

Synthetic procedures

The Pd^{II} complex $[(\text{dppp})\text{Pd}(\text{OTf})_2]$,^[66b] and the metallasupramolecular structures **6.5**,^[66a] **6.7**,^[80a] **6.8**,^[80a] **6.9**,^[159] and **6.10**^[160] were prepared according to literature procedures.

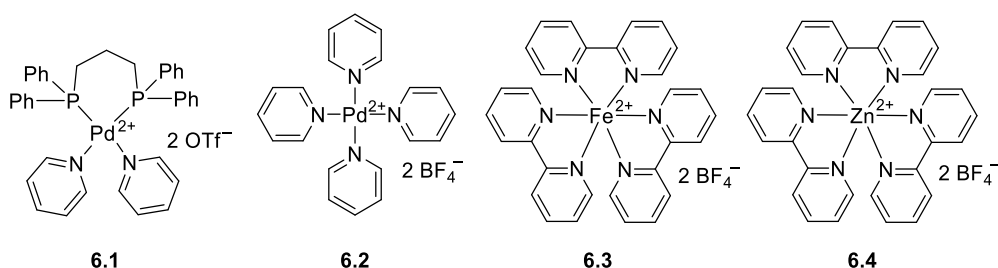


Figure ES18. Chemical structures of model complexes **6.1–6.4**.

General procedure for the synthesis of model complexes (**6.1–6.4**). For the amounts and metal (complex) source used, see the table below.

Pyridine (5 mg, 0.06 mmol) (for **6.1** and **6.2**) or 2,2'-bipyridine (30 mg, 0.19 mmol) (for **6.3** and **6.4**) was combined with the corresponding metal (complex) in degassed acetonitrile (5 mL). The mixture was stirred at r.t. for 18 h, after which diethyl ether (10 mL) was added to precipitate the complex. The solid was collected by centrifugation and washed with diethyl ether (10 mL) to obtain the complexes **6.1–6.4**.

Model complex #	Metal complex	Equivalents of ligand to metal	mg	Yield
6.1	$(\text{dppp})\text{Pd}(\text{OTf})_2$	2	15.3	18.2 mg, 60%
6.2	$\text{Pd}(\text{CH}_3\text{CN})_4(\text{BF}_4)_2$	4	7.0	8.3 mg, 88%
6.3	$\text{Fe}(\text{BF}_4)_2 \cdot 6\text{H}_2\text{O}$	3	14.7	42.2 mg, 93%
6.4	$\text{Zn}(\text{BF}_4)_2 \cdot 6\text{H}_2\text{O}$	3	20.0	34.4 mg, 91%

Table ES8. Amounts used, and yield for the synthesis of model complexes **6.1–6.4**.

Characterization of model complexes **6.1–6.4**.

6.1: ^1H NMR (400 MHz, $\text{CD}_3\text{CN}:\text{D}_2\text{O}$ 4:1) δ = 8.42 (d, J =5.3, 4H), 7.69 – 7.07 (m, 26H), 2.92 (broad s, 2H), 2.16 (tr, J =18, 4H). ^{13}C NMR (151 MHz, $\text{CD}_3\text{CN}:\text{D}_2\text{O}$ 4:1) δ 150.62, 140.23, 133.83, 133.77, 133.63, 130.53, 130.45, 127.17, 122.42, 22.29, 18.45. ^{31}P NMR (162 MHz, $\text{CD}_3\text{CN}:\text{D}_2\text{O}$ 4:1) δ 8.2. HRMS (ESI): m/z calculated for $\text{C}_{37}\text{H}_{36}\text{N}_2\text{P}_2\text{Pd} [\text{M}-2\text{OTf}]^{2+}$ 338.0689, found 338.0696

6.2: ^1H NMR (600 MHz, $\text{CD}_3\text{CN}:\text{D}_2\text{O}$ 4:1) δ = 8.80 (d, J =5.1, 8H), 7.95 (t, J =9.0, 4H), 7.51 (d, J =6.6, 8H). ^{13}C NMR (151 MHz, $\text{CD}_3\text{CN}:\text{D}_2\text{O}$ 4:1) δ = 152.00, 142.07, 128.39. HRMS (ESI): m/z calculated for $\text{C}_{20}\text{H}_{20}\text{N}_4\text{Pd}$ $[\text{M}-2\text{BF}_4]^{2+}$ 211.0356, found 211.0360.

6.3: ^1H NMR (600 MHz, $\text{CD}_3\text{CN}:\text{D}_2\text{O}$ 4:1) δ = 8.52 (d, J =6.0, 6H), 8.07 (t, J =6.0, 6H), 7.36 (m, 12H). ^{13}C NMR (151 MHz, $\text{CD}_3\text{CN}:\text{D}_2\text{O}$ 4:1) δ 160.04, 154.97, 139.67, 128.34, 124.86. HRMS (ESI): m/z calculated for $\text{C}_{30}\text{H}_{24}\text{N}_6\text{Fe}$ $[\text{M}-2\text{BF}_4]^{2+}$ 262.0700, found 262.0700.

6.4: ^1H NMR at 275K (400 MHz, $\text{CD}_3\text{CN}:\text{D}_2\text{O}$ 4:1, 275 K) δ = 8.51 (d, J =8.1, 6H), 8.21 (t, J =7.8, 6H), 7.90 (d, J =2.4, 6H), 7.53 (t, J =8.1, 6H). ^{13}C NMR (151 MHz, $\text{CD}_3\text{CN}:\text{D}_2\text{O}$ 4:1) δ = 150.10, 148.97, 142.80, 128.39, 124.24. HRMS (ESI): m/z calculated for $\text{C}_{30}\text{H}_{24}\text{N}_6\text{Zn}$ $[\text{M}-2\text{BF}_4]^{2+}$ 266.0671, found 266.0674.

The NMR spectra of these complexes are included in the supporting information of the publication cited under reference 127.

General experimental set-up for the photoswitching experiments

The photoswitching experiments were performed with the use of a Topled (MDE Display + Electronics GmbH) SET5050-5M-RGB wrapped around a glass container (see image below). To activate the photoacid, the samples were placed in the container and irradiated with violet light (425 nm) for 20 minutes at r.t., unless stated otherwise. The samples are then left at r.t. in the dark for the indicated time.



Figure ES19. Experimental set-up for the activation of the photoacid. On the photo on the left side, the LEDs are turned off, and on the photo on the right side, they are turned on with the same violet light that was used for these experiments.

The $\text{CD}_3\text{CN}/\text{D}_2\text{O}$ (8:2) solvent mixture was suited to solubilize the photoacid and a range of metallasupramolecular structures. All samples were prepared using 2 mg of photoacid (5 μmol in 0.5 mL, 1 mM). The amount of the metallasupramolecular assembly was adjusted to the amount of the photoacid. We used 4 equivalents of photoacid per functional group that can be protonated (so in most cases, per pyridine group). For example: the octahedral cage **6.5** has 12 ligands, with 2 pyridine groups per ligand, so $(2 \times 12 =)$ 24 times 4, comes to 96 equivalents of photoacid with respect to the amount of **6.5**. The samples were prepared and handled in the dark unless stated otherwise.

The samples were first measured, then irradiated for 20 minutes (indicated by "light"), then measured again, and left in the dark for 8 hours (indicated by "dark"), followed by a final measurement. Based on the integration of selected signals, the amount of disassembled structure was estimated. When this estimate falls between 80-100 %, it is indicated with >80%.

NMR spectra of the protonated ligands were obtained from samples containing the ligand and an excess of HCl (pH around 1).

The NMR spectra of the reversible disassembly of all complexes **6.1** – **6.10** are included in the supporting information of the publication cited under reference 127.

Repetitive disassembly of barrel **6.8**

The coordination barrel **6.8** was disassembled and re-assembled over 5 cycles. One cycle consists of 20 min light exposure, followed by 2.5 h in the dark. The sample contained DCM as an internal standard, and the change in integration of three separate signals of the protonated ligand **6D** were monitored.

The NMR spectra of the repetitive reversible disassembly of complex **6.8** are included in the supporting information of the publication cited under reference 127.

Kinetic study of the re-assembly processes

Samples containing the photoacid and the respective metal complex were irradiated for 20 minutes. ¹H NMR spectra were then recorded after 0, 10, 20, and 30 min (for $t = 0$ the amount of protonated ligand was normalized to 100%). All measurements were performed at 298 K. The signals of the protonated ligand were integrated (DCM was used as internal standard) to give the data depicted below. The amount of the protonated ligand is expected to be indirectly proportional to the amount of re-assembled metal complex. A direct integration of the signals of the supramolecular complexes was hampered by signal overlap with the signals of the photoacid.

A graphical representation of the data from the kinetic study is included in the supporting information of the publication cited under reference 127.

Photoacid-induced switching between $[\text{Pd}_6(\mathbf{6B})_{12}]^{12+}$ and $[\text{Pd}_2(\mathbf{6F})_4]^{4+}$

A stock solution was prepared containing **6F** (0.9 mg, 3.2 μmol , 2 eq., 1.3 mM) and **6B** (2.1 mg, 3.2 μmol , 2 eq., 1.3 mM) with a sub-stoichiometric amount of $[\text{Pd}(\text{CH}_3\text{CN})_4](\text{BF}_4)_2$ (0.7 mg, 1.6 μmol , 1 eq., 3.2 mM, 0.6 mM) in CD_3CN and D_2O (8:2) (2.5 mL). One fifth of this solution (0.5 mL, with 0.6 μmol , 0.26 mM of each ligand) was added to the photoacid (2 mg, 5.2 μmol , 2 eq. of acid per pyridine group in solution, 2.1 mM) in the dark. The sample was measured, irradiated with violet light at r.t. for 11 h, measured and kept in the dark at 60 °C for 6 h before being measured again (**Scheme 6.5**). Over the course of the reaction, the photoacid is hydrolyzed to a small extent. Therefore, this methodology is not suited to repetitive switching between different structures.

References

- [1] S. M. Jansze, K. Severin, *Acc. Chem. Res.* **2018**, *51*, 2139-2147.
- [2] D. A. Leigh, *Angew. Chem. Int. Ed.* **2016**, *55*, 14506-14508.
- [3] J.-M. Lehn, *Angew. Chem. Int. Ed.* **1988**, *27*, 89-112.
- [4] J.-M. Lehn, *Angew. Chem. Int. Ed.* **1990**, *29*, 1304-1319.
- [5] a) J. W. Steel, J. L. Atwood, *Supramolecular Chemistry*, 2nd ed., Wiley, Chichester, UK, **2009**; b) M. D. Ward, P. R. Raithby, *Chem. Soc. Rev.* **2013**, *42*, 1619-1636; c) A. J. McConnell, C. S. Wood, P. P. Neelakandan, J. R. Nitschke, *Chem. Rev.* **2015**, *115*, 7729-7793; d) M. J. Webber, R. Langer, *Chem. Soc. Rev.* **2017**, *46*, 6600-6620; e) M. Baroncini, M. Canton, L. Casimiro, S. Corra, J. Groppi, M. La Rosa, S. Silvi, A. Credi, *Eur. J. Inorg. Chem.* **2018**, *2018*, 4589-4603; f) S. Datta, M. L. Saha, P. J. Stang, *Acc. Chem. Res.* **2018**, *51*, 2047-2063; g) D. A. Roberts, B. S. Pilgrim, J. R. Nitschke, *Chem. Soc. Rev.* **2018**, *47*, 626-644.
- [6] F. Biedermann, H.-J. Schneider, *Chem. Rev.* **2016**, *116*, 5216-5300.
- [7] L. Li, D. J. Fanna, N. D. Shepherd, L. F. Lindoy, F. Li, *J. Incl. Phenom. Macrocycl. Chem.* **2015**, *82*, 3-12.
- [8] a) W. Lu, Z. Wei, Z.-Y. Gu, T.-F. Liu, J. Park, J. Park, J. Tian, M. Zhang, Q. Zhang, T. Gentle Iii, M. Bosch, H.-C. Zhou, *Chem. Soc. Rev.* **2014**, *43*, 5561-5593; b) S. Saha, I. Regeni, G. H. Clever, *Coord. Chem. Rev.* **2018**, *374*, 1-14.
- [9] a) R. Chakrabarty, P. S. Mukherjee, P. J. Stang, *Chem. Rev.* **2011**, *111*, 6810-6918; b) T. R. Cook, P. J. Stang, *Chem. Rev.* **2015**, *115*, 7001-7045; c) W. Wang, Y.-X. Wang, H.-B. Yang, *Chem. Soc. Rev.* **2016**, *45*, 2656-2693.
- [10] a) T. K. Ronson, S. Zarra, S. P. Black, J. R. Nitschke, *Chem. Commun.* **2013**, *49*, 2476-2490; b) M. M. J. Smulders, I. A. Riddell, C. Browne, J. R. Nitschke, *Chem. Soc. Rev.* **2013**, *42*, 1728-1754; c) C. J. Brown, F. D. Toste, R. G. Bergman, K. N. Raymond, *Chem. Rev.* **2015**, *115*, 3012-3035; d) Z. Wu, K. Zhou, A. V. Ivanov, M. Yusobov, F. Verpoort, *Coord. Chem. Rev.* **2017**, *353*, 180-200; e) D. Zhang, T. K. Ronson, J. R. Nitschke, *Acc. Chem. Res.* **2018**, *51*, 2423-2436.
- [11] a) S.-L. Huang, T. S. A. Hor, G.-X. Jin, *Coord. Chem. Rev.* **2017**, *333*, 1-26; b) G.-Y. Wu, L.-J. Chen, L. Xu, X.-L. Zhao, H.-B. Yang, *Coord. Chem. Rev.* **2018**, *369*, 39-75.
- [12] a) J.-F. Ayme, J. E. Beves, C. J. Campbell, D. A. Leigh, *Chem. Soc. Rev.* **2013**, *42*, 1700-1712; b) S. F. M. van Dongen, S. Cantekin, J. A. A. W. Elemans, A. E. Rowan, R. J. M. Nolte, *Chem. Soc. Rev.* **2014**, *43*, 99-122; c) S. D. P. Fielden, D. A. Leigh, S. L. Woltering, *Angew. Chem. Int. Ed.* **2017**, *56*, 11166-11194.
- [13] a) T. R. Cook, Y.-R. Zheng, P. J. Stang, *Chem. Rev.* **2012**, *113*, 734-777; b) H. Furukawa, K. E. Cordova, M. O'Keeffe, O. M. Yaghi, *Science* **2013**, *341*, 974-986; c) C. Wang, D. Liu, W. Lin, *J. Am. Chem. Soc.* **2013**, *135*, 13222-13234; d) J. Liu, L. Chen, H. Cui, J. Zhang, L. Zhang, C.-Y. Su, *Chem. Soc. Rev.* **2014**, *43*, 6011-6061; e) M. Eddaoudi, D. F. Sava, J. F. Eubank, K. Adil, V. Guillerme, *Chem. Soc. Rev.* **2015**, *44*, 228-249; f) T. Drake, P. Ji, W. Lin, *Acc. Chem. Res.* **2018**, *51*, 2129-2138.
- [14] a) S. Bhattacharya, S. K. Samanta, *Chem. Rev.* **2016**, *116*, 11967-12028; b) A. Karoyo, L. Wilson, *Gels* **2017**, *3*, 1; c) N. Falcone, H.-B. Kraatz, *Chem. Eur. J.* **2018**, *24*, 14316-14328; d) J. L. Mann, A. C. Yu, G. Agmon, E. A. Appel, *Biomater. Sci.* **2018**, *6*, 10-37.
- [15] S. Mukherjee, P. S. Mukherjee, *Chem. Commun.* **2014**, *50*, 2239-2248.
- [16] a) A. K. Bar, G. Mostafa, P. S. Mukherjee, *Inorg. Chem.* **2010**, *49*, 7647-7649; b) Z. Zhao, Y.-R. Zheng, M. Wang, J. B. Pollock, P. J. Stang, *Inorg. Chem.* **2010**, *49*, 8653-8655; c) Y.-R. Zheng, Z. Zhao, M. Wang, K. Ghosh, J. B. Pollock, T. R. Cook, P. J. Stang, *J. Am. Chem. Soc.* **2010**, *132*, 16873-16882; d) A. K. Bar, S. Raghothama, D. Moon, P. S. Mukherjee, *Chem. - Eur. J.* **2012**, *18*, 3199-3209.
- [17] a) M. Han, D. M. Engelhard, G. H. Clever, *Chem. Soc. Rev.* **2014**, *43*, 1848-1860; b) G. H. Clever, P. Punt, *Acc. Chem. Res.* **2017**, *50*, 2233-2243.

- [18] a) J. E. M. Lewis, J. D. Crowley, *Supramol. Chem.* **2014**, *26*, 173-181; b) A. Schmidt, A. Casini, F. E. Kühn, *Coord. Chem. Rev.* **2014**, *275*, 19-36; c) M. D. Johnstone, E. K. Schwarze, J. Ahrens, D. Schwarzer, J. J. Holstein, B. Dittrich, F. M. Pfeffer, G. H. Clever, *Chem. - Eur. J.* **2016**, *22*, 10791-10795; d) S. Löffler, J. Lübken, A. Wuttke, R. A. Mata, M. John, B. Dittrich, G. H. Clever, *Chem. Sci.* **2016**, *7*, 4676-4684.
- [19] a) J. E. M. Lewis, E. L. Gavey, S. A. Cameron, J. D. Crowley, *Chem. Sci.* **2012**, *3*, 778-784; b) T. Y. Kim, N. T. Lucas, J. D. Crowley, *Supramol. Chem.* **2015**, *27*, 734-745; c) S. M. McNeill, D. Preston, J. E. M. Lewis, A. Robert, K. Knerr-Rupp, D. O. Graham, J. R. Wright, G. I. Giles, J. D. Crowley, *Dalton Trans.* **2015**, *44*, 11129-11136; d) A. Ahmedova, R. Mihaylova, D. Momekova, P. Shestakova, S. Stoykova, J. Zaharieva, M. Yamashina, G. Momekov, M. Akita, M. Yoshizawa, *Dalton Trans.* **2016**, *45*, 13214-13221; e) A. Ahmedova, D. Momekova, M. Yamashina, P. Shestakova, G. Momekov, M. Akita, M. Yoshizawa, *Chem. - Asian J.* **2016**, *11*, 474-477; f) F. Kaiser, A. Schmidt, W. Heydenreuter, P. J. Altmann, A. Casini, S. A. Sieber, F. E. Kühn, *Eur. J. Inorg. Chem.* **2016**, *2016*, 5189-5196; g) A. Schmidt, M. Hollering, M. Drees, A. Casini, F. E. Kühn, *Dalton Trans.* **2016**, *45*, 8556-8565; h) A. Schmidt, V. Molano, M. Hollering, A. Pöthig, A. Casini, F. E. Kühn, *Chem. - Eur. J.* **2016**, *22*, 2253-2256.
- [20] V. Martí-Centelles, A. L. Lawrence, P. J. Lusby, *J. Am. Chem. Soc.* **2018**, *140*, 2862-2868.
- [21] M. Han, R. Michel, B. He, Y.-S. Chen, D. Stalke, M. John, G. H. Clever, *Angew. Chem. Int. Ed.* **2013**, *52*, 1319-1323.
- [22] a) A. B. S. Elliott, J. E. M. Lewis, H. van der Salm, C. J. McAdam, J. D. Crowley, K. C. Gordon, *Inorg. Chem.* **2016**, *55*, 3440-3447; b) R. A. S. Vasdev, D. Preston, J. D. Crowley, *Dalton Trans.* **2017**, *46*, 2402-2414.
- [23] T. Y. Kim, R. A. S. Vasdev, D. Preston, J. D. Crowley, *Chem. - Eur. J.* **2018**, *24*, 14878-14890.
- [24] D. K. Chand, K. Biradha, M. Kawano, S. Sakamoto, K. Yamaguchi, M. Fujita, *Chem. - Asian J.* **2006**, *1*, 82-90.
- [25] a) S. Kai, T. Tateishi, T. Kojima, S. Takahashi, S. Hiraoka, *Inorg. Chem.* **2018**, *57*, 13083-13086; b) T. Tateishi, S. Kai, Y. Sasaki, T. Kojima, S. Takahashi, S. Hiraoka, *Chem. Commun.* **2018**, *54*, 7758-7761; c) T. Tateishi, T. Kojima, S. Hiraoka, *Inorg. Chem.* **2018**, *57*, 2686-2694.
- [26] a) K. Suzuki, M. Kawano, M. Fujita, *Angew. Chem. Int. Ed.* **2007**, *46*, 2819-2822; b) B. Brusilowskij, S. Neubacher, C. A. Schalley, *Chem. Commun.* **2009**, 785-787; c) S. Ganta, D. K. Chand, *Dalton Trans.* **2015**, *44*, 15181-15188.
- [27] T. Zhang, L.-P. Zhou, X.-Q. Guo, L.-X. Cai, Q.-F. Sun, *Nat. Commun.* **2017**, *8*, 15898.
- [28] S. Prusty, K. Yazaki, M. Yoshizawa, D. K. Chand, *Chem. - Eur. J.* **2017**, *23*, 12456-12461.
- [29] K. Harris, D. Fujita, M. Fujita, *Chem. Commun.* **2013**, *49*, 6703-6712.
- [30] K. Suzuki, M. Tominaga, M. Kawano, M. Fujita, *Chem. Commun.* **2009**, 1638-1640.
- [31] M. Tominaga, K. Suzuki, M. Kawano, T. Kusukawa, T. Ozeki, S. Sakamoto, K. Yamaguchi, M. Fujita, *Angew. Chem. Int. Ed.* **2004**, *43*, 5621-5625.
- [32] Q.-F. Sun, J. Iwasa, D. Ogawa, Y. Ishido, S. Sato, T. Ozeki, Y. Sei, K. Yamaguchi, M. Fujita, *Science* **2010**, *328*, 1144-1147.
- [33] D. Fujita, Y. Ueda, S. Sato, H. Yokoyama, N. Mizuno, T. Kumasaka, M. Fujita, *Chem* **2016**, *1*, 91-101.
- [34] Q.-F. Sun, T. Murase, S. Sato, M. Fujita, *Angew. Chem. Int. Ed.* **2011**, *50*, 10318-10321.
- [35] N. Kamiya, M. Tominaga, S. Sato, M. Fujita, *J. Am. Chem. Soc.* **2007**, *129*, 3816-3817.
- [36] T. Kikuchi, S. Sato, M. Fujita, *J. Am. Chem. Soc.* **2010**, *132*, 15930-15932.
- [37] T. Murase, S. Sato, M. Fujita, *Angew. Chem. Int. Ed.* **2007**, *46*, 5133-5136.
- [38] T. Murase, S. Sato, M. Fujita, *Angew. Chem. Int. Ed.* **2007**, *46*, 1083-1085.
- [39] K. Suzuki, S. Sato, M. Fujita, *Nat. Chem.* **2009**, *2*, 25.
- [40] a) M. Frank, M. D. Johnstone, G. H. Clever, *Chem. - Eur. J.* **2016**, *22*, 14104-14125; b) W. M. Bloch, J. J. Holstein, B. Dittrich, W. Hiller, G. H. Clever, *Angew. Chem. Int. Ed.* **2018**, *57*, 5534-5538.
- [41] a) S. Freye, D. M. Engelhard, M. John, G. H. Clever, *Chem. - Eur. J.* **2013**, *19*, 2114-2121; b) S. Freye, R. Michel, D. Stalke, M. Pawliczek, H. Frauendorf, G. H. Clever, *J. Am. Chem. Soc.* **2013**, *135*, 8476-8479; c) M. Frank, J. Ahrens, I. Bejenke, M. Krick, D. Schwarzer, G. H. Clever, *J. Am. Chem. Soc.* **2016**, *138*, 8279-8287; d) Y.-H. Li, J.-J. Jiang, Y.-Z. Fan, Z.-W. Wei, C.-X. Chen, H.-J. Yu, S.-P. Zheng, D. Fenske, C.-Y. Su, M. Barboiu, *Chem. Commun.* **2016**, *52*, 8745-8748.
- [42] R. Zhu, J. Lübken, B. Dittrich, G. H. Clever, *Angew. Chem. Int. Ed.* **2015**, *54*, 2796-2800.

- [43] a) S. Löffler, J. Lübben, L. Krause, D. Stalke, B. Dittrich, G. H. Clever, *J. Am. Chem. Soc.* **2015**, *137*, 1060-1063; b) S. Löffler, A. Wuttke, B. Zhang, J. J. Holstein, R. A. Mata, G. H. Clever, *Chem. Commun.* **2017**, 53, 11933-11936.
- [44] T. K. Ronson, J. Fisher, L. P. Harding, M. J. Hardie, *Angew. Chem. Int. Ed.* **2007**, *46*, 9086-9088.
- [45] D. Samanta, P. S. Mukherjee, *Chem. - Eur. J.* **2014**, *20*, 12483-12492.
- [46] B. Roy, E. Zangrando, P. S. Mukherjee, *Chem. Commun.* **2016**, 52, 4489-4492.
- [47] T. Y. Kim, L. Digal, M. G. Gardiner, N. T. Lucas, J. D. Crowley, *Chem. - Eur. J.* **2017**, *23*, 15089-15097.
- [48] J. R. Nitschke, *Angew. Chem. Int. Ed.* **2004**, *43*, 3073-3075.
- [49] P. Mal, D. Schultz, K. Beyeh, K. Rissanen, J. R. Nitschke, *Angew. Chem. Int. Ed.* **2008**, *47*, 8297-8301.
- [50] P. Mal, B. Breiner, K. Rissanen, J. R. Nitschke, *Science* **2009**, *324*, 1697-1699.
- [51] I. A. Riddell, M. M. J. Smulders, J. K. Clegg, J. R. Nitschke, *Chem. Commun.* **2011**, 47, 457-459.
- [52] a) I. A. Riddell, Y. R. Hristova, J. K. Clegg, C. S. Wood, B. Breiner, J. R. Nitschke, *J. Am. Chem. Soc.* **2013**, *135*, 2723-2733; b) I. A. Riddell, T. K. Ronson, J. K. Clegg, C. S. Wood, R. A. Bilbeisi, J. R. Nitschke, *J. Am. Chem. Soc.* **2014**, *136*, 9491-9498.
- [53] a) H.-B. Wu, Q.-M. Wang, *Angew. Chem. Int. Ed.* **2009**, *48*, 7343-7345; b) M. C. Das, S. Xiang, Z. Zhang, B. Chen, *Angew. Chem. Int. Ed.* **2011**, *50*, 10510-10520; c) G. Kumar, R. Gupta, *Chem. Soc. Rev.* **2013**, *42*, 9403-9453; d) L. F. Lindoy, K.-M. Park, S. S. Lee, *Chem. Soc. Rev.* **2013**, *42*, 1713-1727; e) S. Srivastava, R. Gupta, *CrystEngComm* **2016**, *18*, 9185-9208.
- [54] D. H. Busch, *Rec. Chem. Prog.* **1964**, *25*, 107-126.
- [55] Y. Z. Voloshin, I. G. Belaya, R. K. Krämer, *Cage Metal Complexes; Clathrochelates Revisited*, Springer International Publishing, New York, United States, **2017**.
- [56] J. M. Lehn, *Acc. Chem. Res.* **1978**, *11*, 49-57.
- [57] D. R. Boston, N. J. Rose, *J. Am. Chem. Soc.* **1968**, *90*, 6859-6860.
- [58] J. E. Parks, B. E. Wagner, R. H. Holm, *J. Am. Chem. Soc.* **1970**, *92*, 3500-3502.
- [59] V. L. Goedken, S.-M. Peng, *J. Chem. Soc., Chem. Commun.* **1973**, 62-63.
- [60] I. I. Creaser, J. M. Harrowfield, A. J. Herlt, A. M. Sargeson, J. Springborg, R. J. Geue, M. R. Snow, *J. Am. Chem. Soc.* **1977**, *99*, 3181-3182.
- [61] Y. Z. Voloshin, N. A. Kostromina, R. K. Kramer, *Clathrochelates: Synthesis, Structure and Properties*, Elsevier Science, Amsterdam, The Netherlands, **2002**.
- [62] Y. Z. Voloshin, V. V. Novikov, Y. V. Nelyubina, *RSC Advances* **2015**, *5*, 72621-72637.
- [63] J. G. Muller, J. J. Grzybowski, K. J. Takeuchi, *Inorg. Chem.* **1986**, *25*, 2665-2667.
- [64] a) Y. Z. Voloshin, O. A. Varzatskii, I. I. Vorontsov, M. Y. Antipin, *Angew. Chem. Int. Ed.* **2005**, *44*, 3400-3402; b) Y. Z. Voloshin, Varzatskii, O. A., Novikov, V. V., Strizhakova, N. G., Vorontsov, I. I., Vologzhanina, A. V., Lyssenko, K. A., Romanenko, G. V., Fedin, M. V., Ovcharenko, V. I. and Bubnov, Y. N., *Eur. J. Inorg. Chem.* **2010**, *2010*, 5401-5415.
- [65] Y. Z. Voloshin, V. V. Novikov, Y. V. Nelyubina, A. S. Belov, D. M. Roitershtein, A. Savitsky, A. Mokhir, J. Sutter, M. E. Miehl, K. Meyer, *Chem. Commun.* **2018**, 54, 3436-3439.
- [66] a) M. D. Wise, A. Ruggi, M. Pasqu, R. Scopelliti, K. Severin, *Chem. Sci.* **2013**, *4*, 1658-1662; b) G. Cecot, B. Alameddine, S. Prior, R. D. Zorzi, S. Geremia, R. Scopelliti, F. T. Fadaei, E. Solari, K. Severin, *Chem. Commun.* **2016**, 52, 11243-11246; c) I. N. Denisenko, O. A. Varzatskii, R. A. Selin, A. S. Belov, E. G. Lebed, A. V. Vologzhanina, Y. V. Zubavichus, Y. Z. Voloshin, *RSC Advances* **2018**, *8*, 13578-13587.
- [67] S. Khanra, T. Weyhermüller, E. Bill, P. Chaudhuri, *Inorg. Chem.* **2006**, *45*, 5911-5923.
- [68] M. Pasqu, M. Marmier, C. Schouwey, R. Scopelliti, J. J. Holstein, G. Bricogne, K. Severin, *Chem. - Eur. J.* **2014**, *20*, 5592-5600.
- [69] J. L. Bila, M. Marmier, K. O. Zhurov, R. Scopelliti, I. Živković, H. M. Rønnow, N. E. Shaik, A. Sienkiewicz, C. Fink, K. Severin, *Eur. J. Inorg. Chem.* **2018**, *2018*, 3118-3125.
- [70] M. Marmier, M. D. Wise, J. J. Holstein, P. Pattison, K. Schenk, E. Solari, R. Scopelliti, K. Severin, *Inorg. Chem.* **2016**, *55*, 4006-4015.
- [71] C. Ge, J. Zhang, Z. Qin, P. Zhang, R. Zhang, H. Zhao, Y. Wang, X. Zhang, *Inorg. Chim. Acta* **2017**, *463*, 134-141.

- [72] a) M. Marmier, G. Cecot, B. F. E. Curchod, P. Pattison, E. Solari, R. Scopelliti, K. Severin, *Dalton Trans.* **2016**, 45, 8422-8427; b) M. Marmier, G. Cecot, A. V. Vologzhanina, J. L. Bila, I. Zivkovic, H. M. Ronnow, B. Nafradi, E. Solari, P. Pattison, R. Scopelliti, K. Severin, *Dalton Trans.* **2016**, 45, 15507-15516.
- [73] a) T. Imamura, K. Fukushima, *Coord. Chem. Rev.* **2000**, 198, 133-156; b) S. Huh, S.-J. Kim, Y. Kim, *CrystEngComm* **2016**, 18, 345-368.
- [74] Y.-Y. Zhang, Y.-J. Lin, G.-X. Jin, *Chem. Commun.* **2014**, 50, 2327-2329.
- [75] S. El Ghachtouli, R. Guillot, W. Leibl, A. Aukauloo, *J. Porphyrins Phthalocyanines* **2014**, 18, 1125-1130.
- [76] A. Ardavan, A. M. Bowen, A. Fernandez, A. J. Fielding, D. Kaminski, F. Moro, C. A. Muryn, M. D. Wise, A. Ruggi, E. J. L. McInnes, K. Severin, G. A. Timco, C. R. Timmel, F. Tuna, G. F. S. Whitehead, R. E. P. Winpenny, *Npj Quantum Information* **2015**, 1, 15012.
- [77] C. D. K., B. Kumar, K. Masaki, S. Shigeru, Y. Kentaro, F. Makoto, *Chem. – Asian J.* **2006**, 1, 82-90.
- [78] M. D. Wise, J. J. Holstein, P. Pattison, C. Besnard, E. Solari, R. Scopelliti, G. Bricogne, K. Severin, *Chem. Sci.* **2015**, 6, 1004-1010.
- [79] S. M. Jansze, G. Cecot, M. D. Wise, K. O. Zhurov, T. K. Ronson, A. M. Castilla, A. Finelli, P. Pattison, E. Solari, R. Scopelliti, G. E. Zelinskii, A. V. Vologzhanina, Y. Z. Voloshin, J. R. Nitschke, K. Severin, *J. Am. Chem. Soc.* **2016**, 138, 2046-2054.
- [80] a) G. Cecot, M. Marmier, S. Geremia, R. De Zorzi, A. V. Vologzhanina, P. Pattison, E. Solari, F. Fadaei Tirani, R. Scopelliti, K. Severin, *J. Am. Chem. Soc.* **2017**, 139, 8371-8381; b) S. M. Jansze, M. D. Wise, A. V. Vologzhanina, R. Scopelliti, K. Severin, *Chem. Sci.* **2017**, 8, 1901-1908.
- [81] a) W. Liu, W. Huang, M. Pink, D. Lee, *J. Am. Chem. Soc.* **2010**, 132, 11844-11846; b) W. Liu, W. Huang, C.-H. Chen, M. Pink, D. Lee, *Chem. Mater.* **2012**, 24, 3650-3658; c) B. Alameddine, S. Shetty, N. Baig, S. Al-Mousawi, F. Al-Sagheer, *Polymer* **2017**, 122, 200-207.
- [82] a) S. J. Dalgarno, N. P. Power, J. L. Atwood, *Coord. Chem. Rev.* **2008**, 252, 825-841; b) R. W. Saalfrank, H. Maid, A. Scheurer, *Angew. Chem. Int. Ed.* **2008**, 47, 8794-8824; c) D. J. Tranchemontagne, Z. Ni, M. O'Keeffe, O. M. Yaghi, *Angew. Chem. Int. Ed.* **2008**, 47, 5136-5147; d) B. Therrien, *Eur. J. Inorg. Chem.* **2009**, 2009, 2445-2453; e) P. Jin, S. J. Dalgarno, J. L. Atwood, *Coord. Chem. Rev.* **2010**, 254, 1760-1768; f) M. J. Wiester, P. A. Ulmann, C. A. Mirkin, *Angew. Chem. Int. Ed.* **2011**, 50, 114-137; g) H. Amouri, C. Desmarests, J. Moussa, *Chem. Rev.* **2012**, 112, 2015-2041; h) N. J. Young, B. P. Hay, *Chem. Commun.* **2013**, 49, 1354-1379; i) Y.-F. Han, G.-X. Jin, *Acc. Chem. Res.* **2014**, 47, 3571-3579; j) A. M. Lifschitz, M. S. Rosen, C. M. McGuirk, C. A. Mirkin, *J. Am. Chem. Soc.* **2015**, 137, 7252-7261.
- [83] a) M. Yoshizawa, J. Nakagawa, K. Kumazawa, M. Nagao, M. Kawano, T. Ozeki, M. Fujita, *Angew. Chem. Int. Ed.* **2005**, 44, 1810-1813; b) L. Zhao, B. H. Northrop, Y.-R. Zheng, H.-B. Yang, H. J. Lee, Y. M. Lee, J. Y. Park, K.-W. Chi, P. J. Stang, *J. Org. Chem.* **2008**, 73, 6580-6586; c) M. L. Saha, S. Neogi, M. Schmittel, *Dalton Trans.* **2014**, 43, 3815-3834.
- [84] A. M. Johnson, C. A. Wiley, M. C. Young, X. Zhang, Y. Lyon, R. R. Julian, R. J. Hooley, *Angew. Chem. Int. Ed.* **2015**, 54, 5641-5645.
- [85] a) I. A. Riddell, T. K. Ronson, J. R. Nitschke, *Chem. Sci.* **2015**, 6, 3533-3537; b) D. A. Roberts, B. S. Pilgrim, J. D. Cooper, T. K. Ronson, S. Zarra, J. R. Nitschke, *J. Am. Chem. Soc.* **2015**, 137, 10068-10071; c) C. S. Wood, T. K. Ronson, A. M. Belenguer, J. J. Holstein, J. R. Nitschke, *Nat. Chem.* **2015**, 7, 354-358; d) S. Zarra, D. M. Wood, D. A. Roberts, J. R. Nitschke, *Chem. Soc. Rev.* **2015**, 44, 419-432.
- [86] a) T. K. Ronson, A. B. League, L. Gagliardi, C. J. Cramer, J. R. Nitschke, *J. Am. Chem. Soc.* **2014**, 136, 15615-15624; b) J. A. Foster, R. M. Parker, A. M. Belenguer, N. Kishi, S. Sutton, C. Abell, J. R. Nitschke, *J. Am. Chem. Soc.* **2015**, 137, 9722-9729; c) T. K. Ronson, D. A. Roberts, S. P. Black, J. R. Nitschke, *J. Am. Chem. Soc.* **2015**, 137, 14502-14512; d) D. M. Wood, W. Meng, T. K. Ronson, A. R. Stefankiewicz, J. K. M. Sanders, J. R. Nitschke, *Angew. Chem. Int. Ed.* **2015**, 54, 3988-3992.
- [87] A. Sørensen, A. M. Castilla, T. K. Ronson, M. Pittelkow, J. R. Nitschke, *Angew. Chem. Int. Ed.* **2013**, 52, 11273-11277.
- [88] A. Meudt, B. Lehnemann, S. Scherer, A. Kalinin, V. Snieckus, Clariant GmbH, Germany; Archimica GmbH, **2004**.
- [89] a) A. M. Castilla, W. J. Ramsay, J. R. Nitschke, *Acc. Chem. Res.* **2014**, 47, 2063-2073; b) A. M. Castilla, W. J. Ramsay, J. R. Nitschke, *Chem. Lett.* **2014**, 43, 256-263.

- [90] a) W. Meng, B. Breiner, K. Rissanen, J. D. Thoburn, J. K. Clegg, J. R. Nitschke, *Angew. Chem. Int. Ed.* **2011**, *50*, 3479-3483; b) M. Otte, P. F. Kuijpers, O. Troeppner, I. Ivanović-Burmazović, J. N. H. Reek, B. de Bruin, *Chem. - Eur. J.* **2013**, *19*, 10170-10178; c) W. J. Ramsay, T. K. Ronson, J. K. Clegg, J. R. Nitschke, *Angew. Chem. Int. Ed.* **2013**, *52*, 13439-13443; d) W. J. Ramsay, F. T. Szczypiński, H. Weissman, T. K. Ronson, M. M. J. Smulders, B. Rybtchinski, J. R. Nitschke, *Angew. Chem. Int. Ed.* **2015**, *54*, 5636-5640.
- [91] a) Z. R. Bell, L. P. Harding, M. D. Ward, *Chem. Commun.* **2003**, 2432-2433; b) S. P. Argent, H. Adams, L. P. Harding, M. D. Ward, *Dalton Trans.* **2006**, 542-544; c) A. M. Najar, I. S. Tidmarsh, H. Adams, M. D. Ward, *Inorg. Chem.* **2009**, *48*, 11871-11881; d) M. D. Ward, *Chem. Commun.* **2009**, 4487-4499; e) A. Stephenson, M. D. Ward, *Dalton Trans.* **2011**, *40*, 10360-10369.
- [92] a) J. G. Hardy, *Chem. Soc. Rev.* **2013**, *42*, 7881-7899; b) L. Chen, Q. Chen, M. Wu, F. Jiang, M. Hong, *Acc. Chem. Res.* **2015**, *48*, 201-210; c) V. Croue, S. Goeb, M. Salle, *Chem. Commun.* **2015**, *51*, 7275-7289; d) E. J. L. McInnes, G. A. Timco, G. F. S. Whitehead, R. E. P. Winpenny, *Angew. Chem. Int. Ed.* **2015**, *54*, 14244-14269.
- [93] a) Q. Chen, F. Jiang, D. Yuan, G. Lyu, L. Chen, M. Hong, *Chem. Sci.* **2014**, *5*, 483-488; b) Q. Chen, L. Chen, F. Jiang, M. Hong, *Chem. Rec.* **2015**, *15*, 711-727; c) G. Gil-Ramírez, D. A. Leigh, A. J. Stephens, *Angew. Chem. Int. Ed.* **2015**, *54*, 6110-6150; d) K. E. Horner, M. A. Miller, J. W. Steed, P. M. Sutcliffe, *Chem. Soc. Rev.* **2016**, *45*, 6432-6448.
- [94] a) S. H. A. M. Leenders, R. Gramage-Doria, B. de Bruin, J. N. H. Reek, *Chem. Soc. Rev.* **2015**, *44*, 433-448; b) H. Vardhan, F. Verpoort, *Adv. Synth. Catal.* **2015**, *357*, 1351-1368; c) L. Catti, Q. Zhang, K. Tiefenbacher, *Chem. - Eur. J.* **2016**, *22*, 9060-9066; d) M. Otte, *ACS Catal.* **2016**, *6*, 6491-6510.
- [95] a) M. L. Saha, S. De, S. Pramanik, M. Schmittel, *Chem. Soc. Rev.* **2013**, *42*, 6860-6909; b) C.-H. Wong, S. C. Zimmerman, *Chem. Commun.* **2013**, *49*, 1679-1695; c) X.-Y. Hu, T. Xiao, C. Lin, F. Huang, L. Wang, *Acc. Chem. Res.* **2014**, *47*, 2041-2051; d) Z. He, W. Jiang, C. A. Schalley, *Chem. Soc. Rev.* **2015**, *44*, 779-789; e) M. Schmittel, *Chem. Commun.* **2015**, *51*, 14956-14968; f) P. Wei, X. Yan, F. Huang, *Chem. Soc. Rev.* **2015**, *44*, 815-832.
- [96] a) G. H. Clever, S. Tashiro, M. Shionoya, *Angew. Chem. Int. Ed.* **2009**, *48*, 7010-7012; b) L.-F. Ma, Q.-L. Meng, C.-P. Li, B. Li, L.-Y. Wang, M. Du, F.-P. Liang, *Cryst. Growth Des.* **2010**, *10*, 3036-3043; c) D. M. Engelhard, S. Freye, K. Grohe, M. John, G. H. Clever, *Angew. Chem. Int. Ed.* **2012**, *51*, 4747-4750.
- [97] a) M. E. Briggs, K. E. Jelfs, S. Y. Chong, C. Lester, M. Schmidtman, D. J. Adams, A. I. Cooper, *Cryst. Growth Des.* **2013**, *13*, 4993-5000; b) G. Zhang, O. Presly, F. White, I. M. Oppel, M. Mastalerz, *Angew. Chem. Int. Ed.* **2014**, *53*, 5126-5130; c) M. E. Briggs, A. I. Cooper, *Chem. Mater.* **2016**, *29*, 149-157; d) P. S. Reiss, M. A. Little, V. Santolini, S. Y. Chong, T. Hasell, K. E. Jelfs, M. E. Briggs, A. I. Cooper, *Chem. - Eur. J.* **2016**, *22*, 16547-16553.
- [98] a) S. K. Samanta, M. Schmittel, *J. Am. Chem. Soc.* **2013**, *135*, 18794-18797; b) D. A. Leigh, R. G. Pritchard, A. J. Stephens, *Nat. Chem.* **2014**, *6*, 978; c) M. Wang, C. Wang, X.-Q. Hao, J. Liu, X. Li, C. Xu, A. Lopez, L. Sun, M.-P. Song, H.-B. Yang, X. Li, *J. Am. Chem. Soc.* **2014**, *136*, 6664-6671; d) P. P. Neelakandan, A. Jiménez, J. D. Thoburn, J. R. Nitschke, *Angew. Chem.* **2015**, *127*, 14586-14590.
- [99] a) X. Fang, L. Hansen, F. Haso, P. Yin, A. Pandey, L. Engelhardt, I. Slowing, T. Li, T. Liu, M. Luban, D. C. Johnston, *Angew. Chem. Int. Ed.* **2013**, *52*, 10500-10504; b) G. T. Spence, P. D. Beer, *Acc. Chem. Res.* **2013**, *46*, 571-586; c) R. Custelcean, *Chem. Soc. Rev.* **2014**, *43*, 1813-1824.
- [100] a) I. A. Sedov, M. A. Stolov, B. N. Solomonov, *J. Phys. Org. Chem.* **2011**, *24*, 1088-1094; b) L. Yang, C. Adam, S. L. Cockroft, *J. Am. Chem. Soc.* **2015**, *137*, 10084-10087; c) D. Preston, S. M. McNeill, J. E. M. Lewis, G. I. Giles, J. D. Crowley, *Dalton Trans.* **2016**, *45*, 8050-8060.
- [101] a) S. Bandi, S. Samantray, R. D. Chakravarthy, A. K. Pal, G. S. Hanan, D. K. Chand, *Eur. J. Inorg. Chem.* **2016**, *2016*, 2816-2827; b) N. L. S. Yue, M. C. Jennings, R. J. Puddephatt, *Inorg. Chim. Acta* **2016**, *445*, 37-45.
- [102] a) C.-Y. Gao, L. Zhao, M.-X. Wang, *J. Am. Chem. Soc.* **2011**, *133*, 8448-8451; b) A. Granzhan, C. Schouwey, T. Riis-Johannessen, R. Scopelliti, K. Severin, *J. Am. Chem. Soc.* **2011**, *133*, 7106-7115; c) R. Djeda, C. Desmarests, L.-M. Chamoreau, Y. Li, Y. Journaux, G. Gontard, H. Amouri, *Inorg. Chem.* **2013**, *52*, 13042-13047; d) M. D. Johnstone, E. K. Schwarze, G. H. Clever, F. M. Pfeffer, *Chem. - Eur. J.* **2015**, *21*, 3948-3955; e) C. S. Wood, T. K. Ronson, A. J. McConnell, D. A. Roberts, J. R. Nitschke, *Chem. Sci.* **2016**, *7*, 1702-1706.

- [103] a) P. Burkhard, J. Stetefeld, S. V. Strelkov, *Trends Cell Biol.* **2001**, *11*, 82-88; b) A. N. Lupas, M. Gruber, in *Adv. Protein Chem.*, Vol. 70, Academic Press, **2005**, pp. 37-38; c) D. N. Woolfson, *Adv. Protein Chem.* **2005**, *70*, 79-112.
- [104] S. M. Jansze, D. Ortiz, F. Fadaei Tirani, R. Scopelliti, L. Menin, K. Severin, *Chem. Commun.* **2018**, *54*, 9529-9532.
- [105] a) S. Chakraborty, G. R. Newkome, *Chem. Soc. Rev.* **2018**, *47*, 3991-4016; b) M. Pan, K. Wu, J.-H. Zhang, C.-Y. Su, *Coord. Chem. Rev.* **2019**, *378*, 333-349.
- [106] a) C. Browne, W. J. Ramsay, T. K. Ronson, J. Medley-Hallam, J. R. Nitschke, *Angew. Chem. Int. Ed.* **2015**, *54*, 11122-11127; b) L.-Y. Sun, N. Sinha, T. Yan, Y.-S. Wang, T. T. Y. Tan, L. Yu, Y.-F. Han, F. E. Hahn, *Angew. Chem. Int. Ed.* **2018**, *57*, 5161-5165; c) H. J. Yu, Z. M. Liu, M. Pan, K. Wu, Z. W. Wei, Y. W. Xu, Y. N. Fan, H. P. Wang, C. Y. Su, *Eur. J. Inorg. Chem.* **2018**, *2018*, 80-85.
- [107] a) S. Bandi, A. K. Pal, G. S. Hanan, D. K. Chand, *Chem. - Eur. J.* **2014**, *20*, 13122-13126; b) D. Preston, J. E. M. Lewis, J. D. Crowley, *J. Am. Chem. Soc.* **2017**, *139*, 2379-2386.
- [108] T. K. Ronson, C. Carruthers, J. Fisher, T. Brotin, L. P. Harding, P. J. Rizkallah, M. J. Hardie, *Inorg. Chem.* **2010**, *49*, 675-685.
- [109] a) J. J. Henkelis, J. Fisher, S. L. Warriner, M. J. Hardie, *Chem. - Eur. J.* **2014**, *20*, 4117-4125; b) K. Li, L.-Y. Zhang, C. Yan, S.-C. Wei, M. Pan, L. Zhang, C.-Y. Su, *J. Am. Chem. Soc.* **2014**, *136*, 4456-4459; c) T. H. Noh, W. Hong, H. Lee, O.-S. Jung, *Dalton Trans.* **2015**, *44*, 787-794; d) Y. Yang, J.-H. Jia, X.-L. Pei, H. Zheng, Z.-A. Nan, Q.-M. Wang, *Chem. Commun.* **2015**, *51*, 3804-3807; e) K. Wu, K. Li, Y.-J. Hou, M. Pan, L.-Y. Zhang, L. Chen, C.-Y. Su, *Nat. Commun.* **2016**, *7*, 10487; f) S. Sanz, H. M. O'Connor, P. Comar, A. Baldansuren, M. B. Pitak, S. J. Coles, H. Weihe, N. F. Chilton, E. J. L. McInnes, P. J. Lusby, S. Piligkos, E. K. Brechin, *Inorg. Chem.* **2018**, *57*, 3500-3506.
- [110] G.-Q. Yin, H. Wang, X.-Q. Wang, B. Song, L.-J. Chen, L. Wang, X.-Q. Hao, H.-B. Yang, X. Li, *Nat. Commun.* **2018**, *9*, 567.
- [111] K. Yamaguchi, *Mass Spectrometry* **2013**, *2*, S0012.
- [112] O. V. Dolomanov, L. J. Bourhis, R. J. Gildea, J. A. K. Howard, H. Puschmann, *J. Appl. Crystallogr.* **2009**, *42*, 339-341.
- [113] S. M. Jansze, K. Severin, *J. Am. Chem. Soc.* **2019**, *141*, 815-819.
- [114] L. E. Kapinos, H. Sigel, *Inorg. Chim. Acta* **2002**, *337*, 131-142.
- [115] a) L. J. Jongkind, X. Caumes, A. P. T. Hartendorp, J. N. H. Reek, *Acc. Chem. Res.* **2018**, *51*, 2115-2128; b) I. Sinha, P. S. Mukherjee, *Inorg. Chem.* **2018**, *57*, 4205-4221.
- [116] A. Casini, B. Woods, M. Wenzel, *Inorg. Chem.* **2017**, *56*, 14715-14729.
- [117] a) Y. Wang, Y. Gu, E. G. Keeler, J. V. Park, R. G. Griffin, J. A. Johnson, *Angew. Chem. Int. Ed.* **2017**, *56*, 188-192; b) K. C. Bentz, S. M. Cohen, *Angew. Chem. Int. Ed.* **2018**, *57*, 14992-15001; c) Y. Gu, E. A. Alt, H. Wang, X. Li, A. P. Willard, J. A. Johnson, *Nature* **2018**, *560*, 65-69.
- [118] S. Ganta, D. K. Chand, *Inorg. Chem.* **2018**, *57*, 3634-3645.
- [119] I. Kaljurand, A. Kütt, L. Sooväli, T. Rodima, V. Mäemets, I. Leito, I. A. Koppel, *J. Org. Chem.* **2005**, *70*, 1019-1028.
- [120] P. Liao, B. W. Langloss, A. M. Johnson, E. R. Knudsen, F. S. Tham, R. R. Julian, R. J. Hooley, *Chem. Commun.* **2010**, *46*, 4932-4934.
- [121] N. M. C. Schmidlin, M. Lökov, I. Leito, T. Böttcher, *Chem. - Eur. J.* **2018**, *0*.
- [122] Q. Teng, H. V. Huynh, *Dalton Trans.* **2017**, *46*, 614-627.
- [123] D. Aulakh, H. K. Bilan, M. Wriedt, *CrystEngComm* **2018**, *20*, 1011-1030.
- [124] A. Díaz-Moscoso, P. Ballester, *Chem. Commun.* **2017**, *53*, 4635-4652.
- [125] G. Hao, Z. P. Xu, L. Li, *RSC Advances* **2018**, *8*, 22182-22192.
- [126] a) A. V. Zhukhovitskiy, M. Zhong, E. G. Keeler, V. K. Michaelis, J. E. P. Sun, M. J. A. Hore, D. J. Pochan, R. G. Griffin, A. P. Willard, J. A. Johnson, *Nat. Chem.* **2015**, *8*, 33; b) A. V. Zhukhovitskiy, J. Zhao, M. Zhong, E. G. Keeler, E. A. Alt, P. Teichen, R. G. Griffin, M. J. A. Hore, A. P. Willard, J. A. Johnson, *Macromolecules* **2016**, *49*, 6896-6902.
- [127] S. M. Jansze, G. Cecot, K. Severin, *Chem. Sci.* **2018**, *9*, 4253-4257.

- [128] a) S. Yagai, A. Kitamura, *Chem. Soc. Rev.* **2008**, 37, 1520-1529; b) D.-H. Qu, Q.-C. Wang, Q.-W. Zhang, X. Ma, H. Tian, *Chem. Rev.* **2015**, 115, 7543-7588; c) X. Yao, T. Li, J. Wang, X. Ma, H. Tian, *Adv. Opt. Mater.* **2016**, 4, 1322-1349; d) M. Kathan, S. Hecht, *Chem. Soc. Rev.* **2017**, 46, 5536-5550.
- [129] M. Han, Y. Luo, B. Damaschke, L. Gómez, X. Ribas, A. Jose, P. Peretzki, M. Seibt, G. H. Clever, *Angew. Chem. Int. Ed.* **2016**, 55, 445-449.
- [130] S.-C. Wei, M. Pan, Y.-Z. Fan, H. Liu, J. Zhang, C.-Y. Su, *Chem. - Eur. J.* **2015**, 21, 7418-7427.
- [131] a) G. H. Clever, S. Tashiro, M. Shionoya, *J. Am. Chem. Soc.* **2010**, 132, 9973-9975; b) J. Park, L.-B. Sun, Y.-P. Chen, Z. Perry, H.-C. Zhou, *Angew. Chem. Int. Ed.* **2014**, 53, 5842-5846.
- [132] D. Zhang, Y. Nie, M. L. Saha, Z. He, L. Jiang, Z. Zhou, P. J. Stang, *Inorg. Chem.* **2015**, 54, 11807-11812.
- [133] a) S. Hiraoka, Y. Sakata, M. Shionoya, *J. Am. Chem. Soc.* **2008**, 130, 10058-10059; b) S. Yi, V. Brega, B. Captain, A. E. Kaifer, *Chem. Commun.* **2012**, 48, 10295-10297; c) P. J. Altmann, A. Pöthig, *Angew. Chem. Int. Ed.* **2017**, 56, 15733-15736.
- [134] Y. Liao, *Acc. Chem. Res.* **2017**, 50, 1956-1964.
- [135] Z. Shi, P. Peng, D. Strohecker, Y. Liao, *J. Am. Chem. Soc.* **2011**, 133, 14699-14703.
- [136] Q. Shi, C.-F. Chen, *Org. Lett.* **2017**, 19, 3175-3178.
- [137] L.-P. Yang, F. Jia, J.-S. Cui, S.-B. Lu, W. Jiang, *Org. Lett.* **2017**, 19, 2945-2948.
- [138] J. Guo, H.-Y. Zhang, Y. Zhou, Y. Liu, *Chem. Commun.* **2017**, 53, 6089-6092.
- [139] D. Samanta, D. Galaktionova, J. Gemen, L. J. W. Shimon, Y. Diskin-Posner, L. Avram, P. Král, R. Klajn, *Nat. Commun.* **2018**, 9, 641.
- [140] L. A. Tatum, J. T. Foy, I. Aprahamian, *J. Am. Chem. Soc.* **2014**, 136, 17438-17441.
- [141] X. Li, J. Fei, Y. Xu, D. Li, T. Yuan, G. Li, C. Wang, J. Li, *Angew. Chem.* **2018**, 130, 1921-1925.
- [142] P. K. Kundu, D. Samanta, R. Leizrowice, B. Margulis, H. Zhao, M. Börner, T. Udayabhaskararao, D. Manna, R. Klajn, *Nat. Chem.* **2015**, 7, 646-652.
- [143] S. Silvi, A. Arduini, A. Pochini, A. Secchi, M. Tomasulo, F. M. Raymo, M. Baroncini, A. Credi, *J. Am. Chem. Soc.* **2007**, 129, 13378-13379.
- [144] a) W. M. Bloch, G. H. Clever, *Chem. Commun.* **2017**, 53, 8506-8516; b) L.-J. Chen, H.-B. Yang, M. Shionoya, *Chem. Soc. Rev.* **2017**, 46, 2555-2576.
- [145] D. Preston, A. Fox-Charles, W. K. C. Lo, J. D. Crowley, *Chem. Commun.* **2015**, 51, 9042-9045.
- [146] a) G. H. Clever, M. Shionoya, *Chem. - Eur. J.* **2010**, 16, 11792-11796; b) S. Hiraoka, M. Kiyokawa, S. Hashida, M. Shionoya, *Angew. Chem. Int. Ed.* **2010**, 49, 138-143.
- [147] K. Nagornov, A. Kozhinov, O. Tsybin, Y. Tsybin, *J. Am. Soc. Mass. Spectrom.* **2015**, 26, 741-751.
- [148] L. Patiny, A. Borel, *J. Chem. Inf. Model.* **2013**, 53, 1223-1228.
- [149] A. B. Zaitsev, E. Y. Schmidt, A. M. Vasil'tsov, A. I. Mikhaleva, O. V. Petrova, A. V. Afonin, N. V. Zorina, *Chem. Heterocyc. Compd.* **2006**, 42, 34-41.
- [150] M. Earle, B. J. McAuley, A. Ramani, K. Seddon, J. Thompson, M. Earle, B. J. McAuley, A. Ramani, K. Seddon, J. Thompson, **2002**.
- [151] A. J. M. Duisenberg, L. M. J. Kroon-Batenburg, A. M. M. Schreurs, *J. Appl. Crystallogr.* **2003**, 36, 220-229.
- [152] R. H. Blessing, *Acta Crystallogr. A* **1995**, 51, 33-38.
- [153] G. Sheldrick, *Acta Crystallogr. C* **2015**, 71, 3-8.
- [154] A. Spek, *Acta Crystallogr. D* **2009**, 65, 148-155.
- [155] J. M. Tour, A. M. Rawlett, M. Kozaki, Y. Yao, R. C. Jagessar, S. M. Dirk, D. W. Price, M. A. Reed, C.-W. Zhou, J. Chen, W. Wang, I. Campbell, *Chem. - Eur. J.* **2001**, 7, 5118-5134.
- [156] G. J. Kleywegt, T. A. Jones, *Acta Crystallogr.* **1994**, D50, 178.
- [157] M. Schulze, V. Kunz, P. D. Frischmann, F. Würthner, *Nat. Chem.* **2016**, 8, 576.
- [158] H. V. Huynh, Y. Han, J. H. H. Ho, G. K. Tan, *Organometallics* **2006**, 25, 3267-3274.
- [159] N. P. E. Barry, B. Therrien, *Eur. J. Inorg. Chem.* **2009**, 2009, 4695-4700.
- [160] D. P. August, G. S. Nichol, P. J. Lusby, *Angew. Chem. Int. Ed.* **2016**, 55, 15022-15026.

Curriculum Vitae

Personal information

Full Name: Suzanne Maria Jansze

Place of birth: Nieuwendijk, The Netherlands



@S_Jansze



[linkedin.com/in/SMJansze](https://www.linkedin.com/in/SMJansze)



ORCID ID: 0000-0003-2979-2630



ResearcherID: A-7771-2015

Education & Research experiences

Feb 2015 – May 2019 (expected)

PhD in Chemistry at the École Polytechnique Fédérale de Lausanne (EPFL), CH

“Molecular nanostructures based on polyfunctional clathrochelate complexes”

- Research program in the Laboratory of Supramolecular Chemistry under the supervision of Prof. Kay Severin. Topic: Design, synthesis and characterization of small molecule building blocks for the formation of clathrochelate metalloligands and further study of the self-assembly processes and supramolecular complexes.
- Research project is part of the Marie Curie Horizon 2020 ResMoSys ITN network in collaboration with amongst others: Prof. Jonathan Nitschke, University of Cambridge, UK; Prof. Milko van der Boom, Weizmann Institute, ISR; Prof. Aldrik Velders, Wageningen UR, NL.

Sept 2012 – Aug 2014

MSc Molecular Life Sciences at Wageningen UR, NL

- Continuation of the BSc Molecular Life Sciences (see below). With a specialisation in Organic and Physical chemistry.
- **“Design and synthesis of azobenzene ligands for responsive coordination polymers”**
MSc Thesis (7 months) on synthesis, analyses and self-assembly behavior of photo-responsive lanthanide-coordination polymers in a collaboration between the laboratories of BioNanoTechnology (Prof. Aldrik Velders), Organic Chemistry (Prof. Han Zuilhof) and Physical Chemistry (Prof. Jasper van der Gucht) at Wageningen UR, NL.
- **“Liquid crystal dimers and the twist-bend nematic phase”**
MSc international internship (6 months) at the University of Aberdeen, UK, concerning the design, synthesis and phase behavior of twist-bend nematic liquid crystals. Research conducted under the supervision of Prof. Corrie Imrie, a leading expert in the field of liquid crystals.

Sept 2009 – Aug 2012

BSc Molecular Life Sciences at Wageningen UR, NL

- Interdisciplinary undergraduate program, combining a strong foundation in chemistry with biology and physics to prepare students for research at the forefront of science.
- **“Synthesising linkers involved in the development of a biosensor for the diagnosis of depression”**
BSc Thesis (6 months) at the Laboratory of Organic Chemistry at Wageningen UR, the Netherlands under supervision of Dr. Ton Marcelis, Prof. Han Zuilhof and Prof. Teris van Beek. A project on developing synthesis protocols for a two-step and a five-step synthesis of boronic acid linkers.
- Minor in Neurobiology and Neuropsychology (6 months) at the Radboud University, NL.

Employment history

Sept 2014 – Jan 2015

Teaching and Research Assistant at Wageningen UR, NL

Continuation of projects from my MSc thesis research at the Laboratory of BioNanoTechnology of Prof. Aldrik Velders (see above). During this time, I gained advanced synthetic training (synthesis of various organic ligands and inorganic complexes) and teaching experience, as we were developing and assisting during the practical lab sessions for two new courses for 3rd and 4th year (end BSc or MSc) students.

Sept 2014 – Oct 2014 and Sept 2013 – Nov 2013

Teaching Assistant at Wageningen UR, NL

Teaching assistant for the practical course "Bio-organic chemistry for Lifesciences" aimed at first year students with the subject of basics of organic chemistry, in the group of Prof. Han Zuilhof.

Institutional responsibilities

- EPFL: Responsible for the safety and organization of two lab-spaces (~8 people) and size-exclusion chromatography equipment.
- Wageningen UR: Responsible for scheduling, booking rooms and designing course materials for two undergraduate courses.

Prizes, awards, fellowships

- December 2018 SNSF Early Postdoc.Mobility fellowship to work at UC Berkeley, USA.
- July 2017 Oral presentation at the ISMSC Cambridge, UK.
- March 2017 Poster prize at the RCS Twitter Poster conference in the category of Inorganic chemistry.
- Sept 2016 Best oral presentation runner up at the SCS Fall Meeting in the category of Inorganic & Coordination Chemistry
- Aug 2016 SciFinder Future Leader Program.
- Jan 2014 Travel grant from the organic chemistry section of the KNCV to support my international internship at the University of Aberdeen, UK.

Personal skills

- Languages: Dutch and English ILR Level 5 – Native or bilingual proficiency
German and French ILR Level 2 – Limited working proficiency
- Software: Good competence in Microsoft Office, ChemDraw, MestreNova, Diamond, Spartan Molecular Modelling, CCDC software package (Mercury, ConQuest, etc.), Origin and Inkscape.
- Science Comm.: To share the ups and downs (serious and not so serious parts) of my life as a chemist, and interesting research, I regularly place posts on [Twitter \(@S_Jansze\)](#). I use my Twitter account exclusively for chemistry and research related content.
- With the ITN ResMoSys Marie Curie research network, we manage a [Facebook](#) and [YouTube](#) page to present our research to a broad audience, by posting short movies and other messages.
- Volunteer work: **Samaritain Lausanne-mixte, Lausanne, Switzerland Aug 2017 – present**
- Emergency medical responder. Obtained all the required certificates to participate as an emergency medical responder. As an organization we assist during big events in the city of Lausanne and surroundings, like the marathon (15 000 participants).
- Youth Association Unitas, Wageningen the Netherlands Sept 2009 – Jan 2015**
- Chair of several committees in the associations. Tasks included: Representing the association in discussions with professionals (municipal officials, lawyers, court judges, real estate agents, etc.), giving bimonthly presentations to the members (>150 people) of the association, making work-schedules, leading discussions & coordinating groups of up to 60 volunteer staff at large (80 000 guests) multi-day music festival events.
- Pop Stage XiniX Nieuwendijk, the Netherlands Sept 2006 – Jan 2015**
- Responsible for running of the venue (up to 700 paying guests). Tasks included: instructing and coordinating of a group of around 20 volunteer staff, instructing security professionals and performing regular security checks.

Scientific Peer-Reviewed Publications

Palladium-Based Metal-Ligand Assemblies: The Contrasting Behavior Upon Addition of Pyridine or Acid

S. M. Jansze and K. Severin

Journal of the American Chemistry Society, **2019**, 141, 815-819

Clathrochelate-Based Metalloligands: Applications in Supramolecular Chemistry and Materials Science

S. M. Jansze and K. Severin

Accounts of Chemical Research, **2018**, 51, 9, 2139-2147

Inflating Face-Capped Pd₆L₈ Coordination Cages

S. M. Jansze, D. Ortiz, F. Fadaei Tirani, R. Scopelliti, L. Menin and K. Severin

Chemical Communications, **2018**, 54, 9529-9532

Reversible Disassembly of Metallasupramolecular Structures Mediated by a Metastable-State Photoacid

S. M. Jansze, G. Cecot and K. Severin

Chemical Science, **2018**, 9, 4253-4257

Pd^{II}₂L₄-type coordination cages up to three nanometers in size

S. M. Jansze, M. D. Wise, A. V. Vologzhanina, R. Scopelliti and K. Severin

Chemical Science, **2017**, 8, 1901-1908

Structure–property relationships in twist-bend nematogens: the influence of terminal groups

J.P. Abberley, S. M. Jansze, R. Walker, D. A. Paterson, P. A. Henderson, A. T. M. Marcelis, J. M. D. Storey and C. T. Imrie

Liquid Crystals, **2017**, 44, 68-83

Ligand Aspect Ratio as a Decisive Factor for the Self-Assembly of Coordination Cages

S. M. Jansze, G. Cecot, M. D. Wise, K.O. Zhurov, T. K. Ronson, A. M. Castilla, A. Finelli, P. Pattison, E. Solari, R. Scopelliti, G. E. Zelinskii, A. V. Vologzhanina, Y. Z. Voloshin, J. R. Nitschke and K. Severin

Journal of the American Chemistry Society, **2016**, 138, 2046–2054

New insights into the liquid crystal behaviour of hydrogen-bonded mixtures provided by temperature-dependent FTIR spectroscopy

D. A. Paterson, A. Martínez-Felipe, S.M. Jansze, A. T. M. Marcelis, J. M. D. Storey and C. T. Imrie

Liquid Crystals, **2015**, 42, 928-939

2-Amino-4 α ,7-dimethyl-4,4 α -dihydro-3H-phenoxazin-3-one as an unexpected product from reduction of 5-methyl-2-nitrophenol

S.M. Jansze, V. Saggiomo, A. T. M. Marcelis, M. Lutz and A. H. Velders

Tetrahedron Letters, **2015**, 9, 1060–1062

A Twist-Bend Nematic Phase Driven by Hydrogen Bonding

S. M. Jansze, A. Martínez-Felipe, J. M. D. Storey, A. T. M. Marcelis and C. T. Imrie

Angewandte Chemie, International Edition, **2015**, 54, 643–646

